Carbon-based polymer nanocomposites with enhanced conductive properties

Doctoral Dissertation
Doctoral Program in Materials Science and Technology (30th Cycle)

Carbon-based polymer nanocomposites with enhanced conductive properties

By

Andrea Caradonna

******

Supervisor:
Prof. Claudio Francesco, Badini

Doctoral Examination Committee:
Prof. De Nardo Luigi, Referee, Politecnico di Milano
Prof. Paganini Maria Cristina, Referee, Università degli Studi di Torino
Prof. Mensitieri Giuseppe, Università degli Studi di Napoli Federico II
Prof. Bonelli Barbara , Politecnico di Torino
Prof. Tagliaferro Alberto, Politecnico di Torino

Politecnico di Torino
2017

Declaration

I hereby declare that, the contents and organization of this dissertation constitute my own original work and does not compromise in any way the rights of third parties, including those relating to the security of personal data.

Andrea Caradonna

2017

* This dissertation is presented in partial fulfillment of the requirements for **Ph.D. degree** in the Graduate School of Politecnico di Torino (ScuDo).

Ma s' io avessi previsto tutto questo,
dati causa e pretesto, le attuali conclusioni
[...] forse farei lo stesso.

Acknowledgment

Firstly, I would like to express my sincere gratitude to my supervisor Prof. Claudio Francesco Badini and to all the professors and researchers involved in this Ph.D. thesis.

I would like to thank the referees and the rest of the thesis examination committee.

Finally a special thanks to all my colleagues, friends, parents and you.

Abstract

Nowadays the development of new technologies requires materials with unconventional combination of properties. Polymers are classified as electrical and thermal insulating materials, which limits their use for several important technological applications. However, conductive polymers could be used in order to overcame drawbacks in the use of metals, metal alloys and ceramic materials as conductive media. Thermal conductive polymers could be profitably exploited in heat management applications (e.g. heat sink, heat exchangers), while electrical conductive polymers could be used in different fields depending on their electrical conductive values. To enhance the conductive properties of polymers, several approaches has been reported in literature. However, the most established way to achieve this goal consists in the development of suitable composite materials by means of the incorporation of conductive fillers within the polymeric matrix. The choice of the conductive filler is a crucial point in the development of the final material. Due to their extremely high thermal and electrical conductivity, coupled with the low density, the nano-metric scale and the outstanding mechanical properties, carbon-based nanomaterials are the most promising fillers suitable for processing conductive polymers. Since graphene nanoplatelets (GNPs) are considered young materials with potentials not yet fully exploited, multiwall carbon nanotubes (MWCNTs) are nowadays the most established materials used as conductive filler.

In this thesis work thermally and electrically conductive polymer composites, filled with carbon-based nanomaterials were investigated.

In the first part of the experimental work, particular attention was devoted to the development of GNPs-based thermally conductive polymers. By properly selecting several polymeric matrices and comparing several available processing techniques it was possible to outline a guideline in the use of GNPs as thermally conductive fillers. A strong filler characterization reveals that, in spite to the

amount of defects and to the filler purity, the main GNPs properties able to enhance the thermal conductivity of polymers is the lateral dimension.

With the aim of developing metal-free circuits integrated in nanocomposite, a laser printing process was successfully exploited in order to obtain electrical conductive paths on the surface of a polymeric materials containing MWCNTs. Starting from the literature knowhow and new experimental results, a complete comprehension of the parameters that affect the laser printing process was achieved by applying a statistical approach. By analysing the experimental outcomes with a statistical approach, it was possible to focus the attention on the main laser parameters that govern the process, thus obtaining multifunctional and multidirectional conductive materials with surface electrical resistance per unit length (inside the tracks) lower than 1 kΩ/cm at 0.5 wt.% of MWCNTs loading content.

Finally, by combining outcomes obtained as described above, hybrid carbon-based nanocomposites were developed, with the purpose of enhancing contemporaneously thermal and electrical conductivity. Hybrid materials, obtained starting from a commercial masterbatch containing MWCNTs, demonstrated the possibility to partially replace the high amounts of carbon nanotubes with low cost carbon based materials without worsening the good conductive properties.

Not only conductive properties were investigated, but all the studied materials were also characterized by means of mechanical and thermal stability tests, thus demonstrating the possibility of adopting carbon-based polymer nanocomposites as multifunctional materials.

Sommario

List of Figures

List of Tables

AIM

The main aim of this thesis is the study and the development of thermally and electrically conductive polymers that can be used in the automotive and/or electronic sectors, at both academic and industrial levels. Graphene nanoplatelets (GNPs), natural flakes graphite and multiwall carbon nanotubes (MWCNTs) were used as conductive media.

With the aim to develop a general guideline in the use of graphene nanoplatelets as thermally conductive fillers, different matrices (both thermoplastics and thermoset) were filled with commercially available graphene-like nanomaterials. Starting from a strong fillers characterization, three thermoplastic-based nanocomposites were developed by using the same amount of several commercially available GNPs and processed by means of the same dispersion technique. Moreover, to evaluate the dependence between the dispersion technique and the filler loading, a commercially available epoxy resin was further processed by means of several dispersion methods.

With the aim to create electrical conductive paths on the surface of a polymer containing MWCNTs, a new laser printing technology was adopted. By properly combine the different set of parameters from a statistical point of views (design of experiment) the full potential of the laser functionalization was exploited.

Finally, with the aim to develop polymers with enhanced thermal and electrical conductivity the synergism of hybrid GNPs-MWCNTs system was exploited. Moreover, with the aim of reduce the cost of the final materials, natural flakes graphite was used in order to substitute the most expensive nanofillers.

Chapter 1

Introduction

1.1 Polymeric composite materials

With the term “polymer” it is possible to indicate a particular class of materials, based on Carbon, Hydrogen and few other elements, made up of repeated subunits. In fact, the word polymer is a compound word derived from ancient Greek that means “many part”. They are prepared by a process known as polymerization in which a large number of identical subunits, called monomers, react in order to form long-chain macromolecules. A schematic representation of a polymer structure is reported in **Figure 1** . [1] Since the mid-19th century, with the development of the vulcanization process by Charles Goodyear, researchers (both at academic or industrial levels) focused their attention on the polymer science and technology. Nowadays polymers are present and used in all daily life areas, ranging from no technological applications up to automotive, aerospace and micro-electronics sectors. [2] This is due to the possibility to modulate, by means of organic chemistry modifications, the monomers characteristics getting to a specific and ad hoc material. In **Table 1** a list of the most commonly used polymers is reported. As observable, starting from the easiest polyethylene structure, up to the most complex ones such as, poly(ethylene terephthalate), polycarbonate, nylon 6,6etc., the polymer compositions can be very different, leading to a large variety of materials. Commonly speaking it is possible to classify polymers in two main groups. A polymer able to melt when heated is called thermoplastic. By the combined effect of heat and pressure, is possible to process it into desired form. In contrast a thermoset polymer is a cross linked resin

in which the effect of the heat source leads to a material degradation instead of melting. Moreover, it is insoluble in organic solvents and cannot be thermally process. Additional classifications could be done on the basis of chain structure (linear, branched, cross-linked or network) or on the basis of the isomeric states.

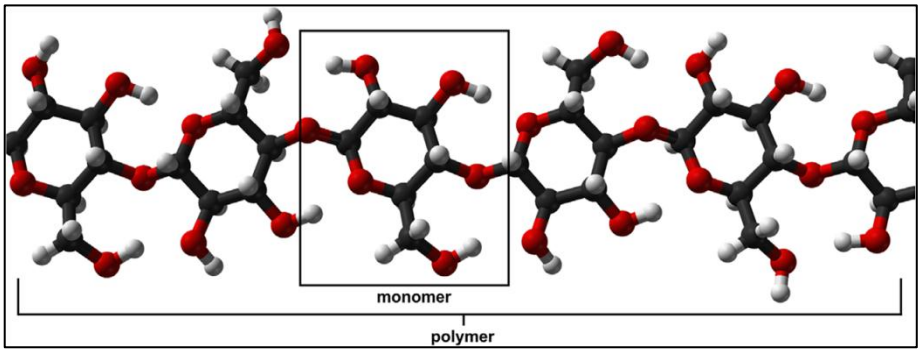

Figure 1 Schematic representation of polymer chain. [1]

In spite of the chemical structure involving chain conformation, molecular groups, degree of crystallinity, presence of heavy atoms, side chains and/or pendant groups, most of them exhibit similar characteristics, in particular if compared with other class of materials, such as metals, metal alloys and ceramics. Polymers are not stiff and rigid materials. From mechanical point of views they show a Young's modulus in the range between 7 MPa (for highly elastic materials) and 4GPa, while metal modulus is in the range of hundreds of GPa. Again maximum tensile strength is about 100 MPa, one order of magnitude lower with respect to metal alloys. In contrast, metals rarely elongate plastically to more than 100% as occurs for elastic polymers. Furthermore they are electrically and thermally insulators. [3] In some instances, these properties limited their use with respect to the metallic or ceramic counterparts especially in technological applications. Beyond those drawbacks, polymers show off interesting advantages in their use. First of all, most of them are chemically inert with respect to solvent as well as to oxidative process. Furthermore they possess a density value lower than those of the lightest metals which result in a comparable strength per unit of weight value. In addiction they are easy to form in complex shape.[4] [5] In light of this scenario, it is obviously that for different applicative areas, the possibility to replace metals or ceramic materials with lighter and/or chemically inert materials is nowadays an important issues. Polymeric composite materials, could be used in order to achieve this goal.

Polymer	Short name	Repeat Unit
Polyethylene	PE	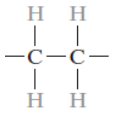
Poly(vinyl chloride)	PVC	
Polytetrafluoroethylene	PTFE	
Polypropylene	PP	
Polystyrene	PS	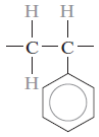
Poly(methyl methacrylate)	PMMA	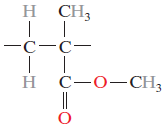
Poly(hexamethyleneadipamide)	Nylon 6,6	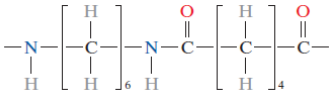
Poly(ethylene terephthalate)	PET	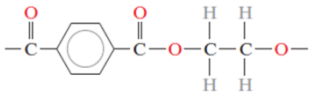
Polycarbonate	PC	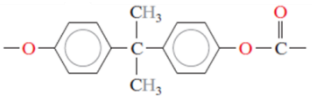

Table 1 List of repeat units for the most commonly used polymers.

The development of new technologies require materials with unconventional combination of properties. A composite materials is a system composed of two or more insoluble constituents, that differ in chemical compositions and shape. The final system can take advantages from the properties of all the constituents. It is clear that from the technological point of view, the possibility to modulate materials properties by means of constituent combinations, is an attractive field of research as demonstrated by the increase of the total amount of scientific publications in the last years, **Figure 2**.

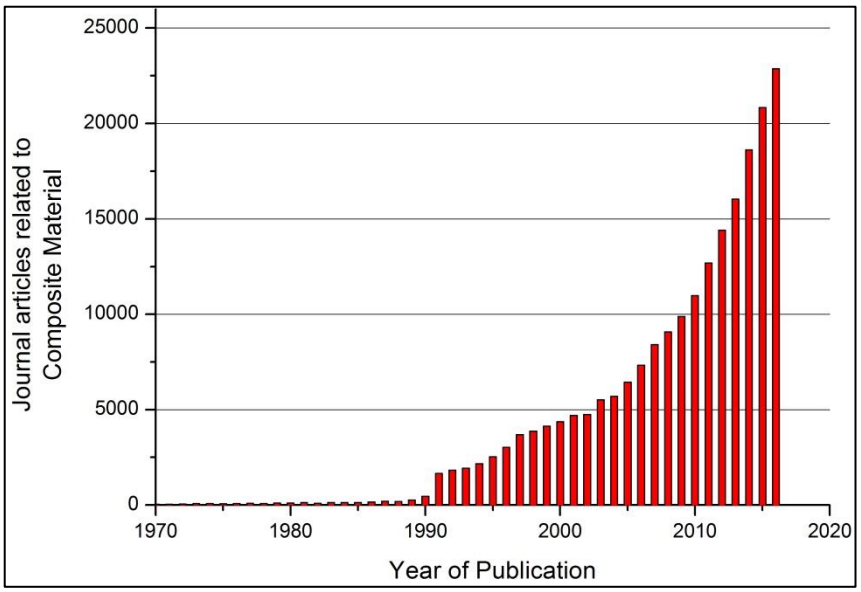

Figure 2 Number of publication per year regarding "Composite Material". Results from “Web of Science Core Collection” database.

A composite material is composed by three parts: matrix, filler and interface. The matrix is the main constituent, it is the continuous phase that surround the other ones. It has the main purpose of transferring stress to other phases, protect them from the environment and/or confer its specific properties to the final materials. The dispersed phase, also named as filler, is the second component of a composite material. Composite can take advantages from the intrinsic filler characteristic. However, the final enhancement could be affected by a poor matrix-filler interaction trough the interface. [3] [5] It is possible to classify composites materials in three different categories according to the matrix nature: metal matrix [6], ceramic matrix [7] and polymer matrix [8] composites. From the filler point of view they are classified as fiber-reinforced, particle-reinforced and structural. [3] Due to the extremely low density, low cost raw material associated to a low

manufacturing cost and easy processability (also in complex shape), high corrosion and chemical resistance, the field of polymeric composite materials is probably the most important and attractive composite research area.

It is possible to classify polymer composites in two main groups: structural or functional materials. In structural materials, mechanical properties are exploited while in functional materials polymers take advantages from the intrinsic filler characteristics. [9] While the reinforcement aspect of polymers is a primary area of interest, nowadays the attentions is focused to the design of polymer with specific intrinsic characteristics. This include conductive properties, [10] [11] flammability resistance, [12] optical properties, [13] batteries, [14] membrane [15] etc. for different application areas ranging from automotive and aerospace [16] industries up to microelectronics system, passing through medical and biomedical fields. [17] The improvement of the final properties depends on several parameters, including physics filler characteristic, filler-matrix interaction controlled by chemical filler compositions, particle dimensions, their aspect ratio and of course on the amount of filler and from its dispersion degree. [18] It is obvious that the filler properties plays an active role on the enhancement of polymer properties. It is possible to divide the fillers in 4 main groups, as reported in **Figure 3**.

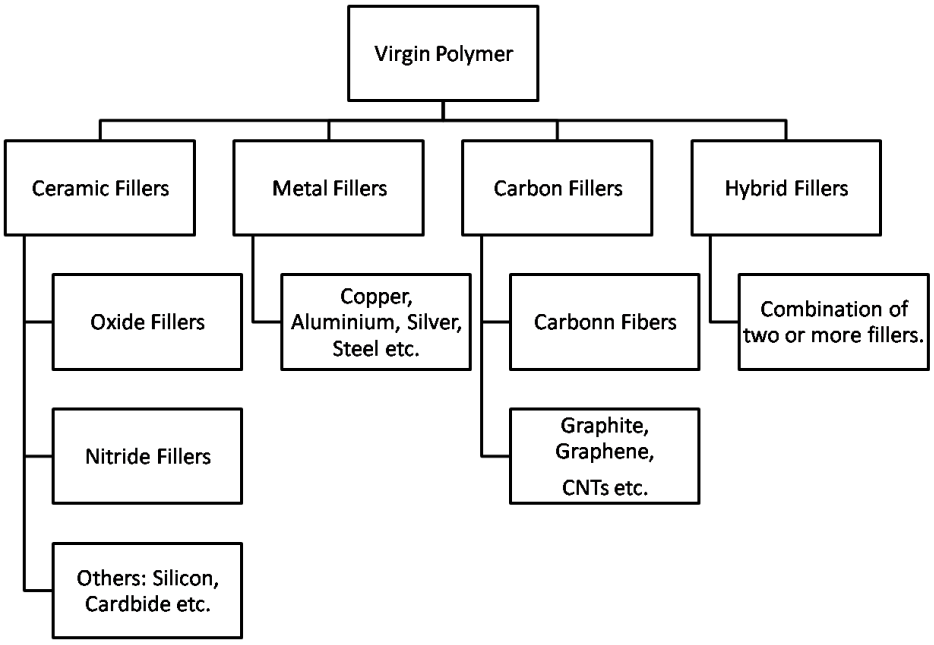

Figure 3 Schematic representation of fillers used in polymers composites materials.

Metal particles made of iron, copper, nickel [19] but also noble metals [20] have been used as fillers. Metals possess excellent mechanical and conductive properties combined with a good thermal stability. However, the addition of metallic particles to polymers also causes an increase of the material density limiting their use in lightweight applications. Moreover, it is very difficult to get a good filler-matrix interaction, in spite of filler functionalization. In contrast, chemically modified ceramic particles, such as inorganic clays, [16] [21], [22] were widely investigate with the aim to increase the filler compatibilization leading to a better filler dispersions and better final properties. Metal oxide or metal nitride ceramic materials, were also used as thermal and/or electrical conductive fillers. [23]–[26] Ceramics are known for their high compression resistance, excellent thermal stability and high corrosion resistance. However also in this case, the high density coupled with a low tensile strength and high brittleness limited their use as fillers. [17] Carbon based material, is the third class of materials used as fillers. Starting from carbon fibers up to graphite, carbon black and, most recently, carbon nanotubes and graphene, they show extraordinary mechanical and conductive properties, both electrical and thermal. Moreover due to the low density, with respect to other counterparts, carbon based fillers are the most promising materials, able to enhance the intrinsic polymers properties. [27]–[30] Finally, by using a hybrid fillers system, for instance a ceramic material coupled with a metallic ones, it is possible to take advantage from all the constituent properties. [1]

As mentioned before, polymers are classified as insulating materials, from both electrical and thermal conductivity limiting their use in different and important technological applications. Due to the extremely high conductive properties of carbon based materials, such as graphite, carbon nanotubes (CNT) and graphene and graphene nanoplatelets (GNP), researchers focused their attention on carbon based conductive polymeric composite materials. [31]

The main aim of this thesis, is to exploit the field of conductive polymers filled with carbon based materials from both thermal and electrical point of view. In the next sections, thermal and electrical conductivity will be discussed from a theoretical point of view, followed by a theoretical fillers presentation. State of the art will be exploited in order to assess the actual scenario to each result and discussion topics.

1.2 Thermal conductivity in polymer

Before starting to talk about thermal conductivity in polymers, we need to define thermal conductivity and its basic equations.

Per definition, heat is atoms or molecules in motion. In solids the atoms vibrate near their mean position. Higher the temperature is, higher the amplitude of the vibration is. In solid state, atoms can't vibrate independently, because they are coupled by their inter-atomic bonds. As reported in **Figure 4** an atom can vibrate in three different modes: one longitudinal and two transverse to the plane. The atom vibrations involve the propagation of elastic waves. These elastic waves, called phonons, can propagate through the entire material. At each of them is associated an energy related to its wavelength. Higher the wavelength is, lower the energy associated to it is. The minimum wavelength value is twice the atomic distance. In a materials composed by N atoms, that can vibrate in three different modes, there are 3N discrete wavelengths and each has energy k_BT, where k_B is the Boltzmann's constant ($1.38*10^{-23}$ J/K). The amount of energy required by 1 kg of materials to be heat of 1 K, at atmospheric pressure, is defined as heat capacity or specific heat, C_p. Since the volume occupied by an atom is Ω, the number of atoms per unit volume is represented by $N=1/\Omega$ meaning that the heat capacity per unit volume is ρC_p.

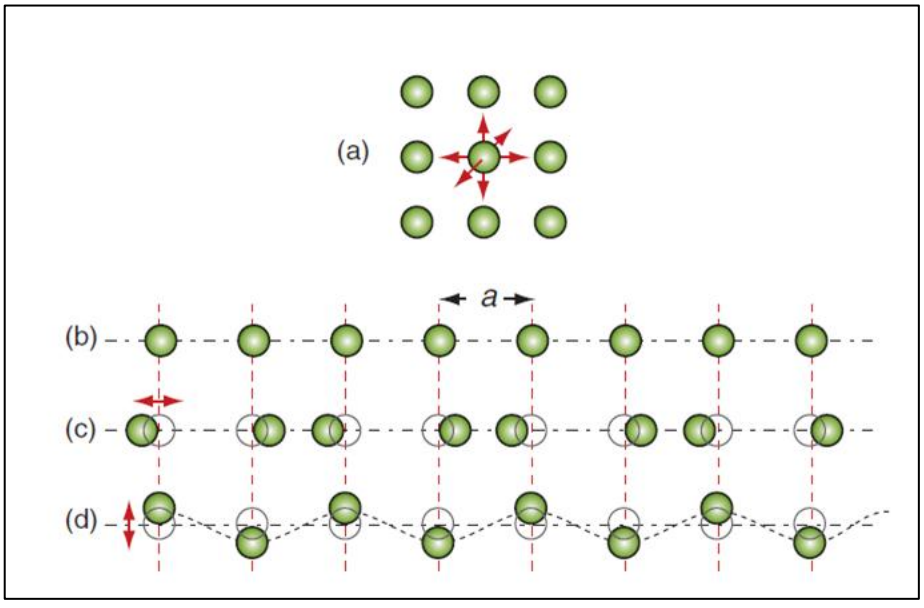

Figure 4 (a) Three atomic vibration modes. (b) A row of atoms placed at their fixed positions. (c) Longitudinal vibration. (d) One of the two transverse vibration mode.[5]

In solid state, heat is transmitted in three different ways: by thermal vibrations, by the movement of free electrons (in metals) or by radiation (in the case of transparent materials). Thermal conductivity is the measure of the capability of a material to conduct heat, and it is expressed as a power divided by a distance per unit of temperature (k, or in certain case λ, defined as W/m*K). [5] Considering the thermal conductivity as a transport property, it can be defined as the ratio between a flux and the directional driving force. In the case of thermal conductivity, the flux is represented by the heat flux q (that is the rate of heat flow Q across an area A) while the directional driving force is the thermal gradient between two material surfaces fixed at $T_1 \neq T_0$. [32] Mathematically speaking conductivity is represented by the following equation:

$$k = q/(dT/dx) = (Q/A)/(\Delta T/x_0) \quad (1)$$

As for any elastic waves, also phonon, move with the speed of sound. The phonon can propagate trough entire material as function of a thermal gradient ΔT. However due to scattering process that occurs between each of them, and between phonon-lattice impurities or phonon-lattice imperfections, the covered distance (l_m, also called mean free path) is typically in the order of few nanometers (0.01 μm) resulting in a lower speed propagation. Phonon conduction can be understood by using a net flux model. In **Figure 5** a schematic representation of the phonon conduction is reported.

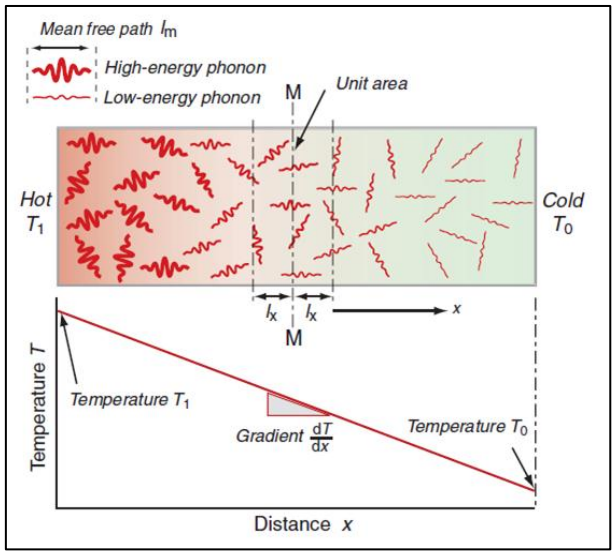

Figure 5 Heat transmission by phonons motion[5]

Phonon possess three degrees of freedom in *x*, *y*, and *z* directions. Focusing the attentions only on the *x* axis, on average, one-sixth of phonons travel in the *+x* direction (from hot to cold zone), while one-sixth move from the right to the left zone (*-x*). The energy associated to each of them is $\rho C_p(T+\Delta T)$ and $\rho C_p(T-\Delta T)$ respectively, where *T* is the temperature in their positions, $\Delta T=(dT/dx)l_m$ and the energy flux *q* across unit of area *M-M* per second is:

$$q = -\frac{1}{6}\rho C_p c_o \left(T + \frac{dT}{dx} l_m\right) + \frac{1}{6}\rho C_p c_o \left(T - \frac{dT}{dx} l_m\right) \tag{2}$$

$$q = -\frac{1}{3}\rho C_p c_o l_m \frac{dT}{dx} \tag{3}$$

By combining equation (3) with equation (1) is possible to define thermal conductivity as:

$$k = \frac{1}{3}\rho C_p c_o l_m \tag{4}$$

The same explanation could be done for electrons. In that case, c_0 and l_m become the velocity and the mean free path of the electrons. Thermal conductivity is the sum of the phonons and the electrons contribution as:

$$K = k_e + k_p \tag{5}$$

In metals, k_e is dominant due to the presence of large concentration of free carries (electrons sea) while the phonon contribution is irrelevant. In fact, it was demonstrated that the phonon contribution in copper (T.C.~ 400 W/mK) is limited to 1-2% of the total. [33] In contrast, due to the presence of covalent bonds, in polymeric materials, the effect of the electron is negligible leading to a thermal conductivity that is affected only by k_p. Independently from the carriers, as can be seen from equation 4, thermal conductivity depends on several parameters. Is possible to demonstrate, that the volumetric heat capacity (ρC_p) is still the same for all the materials (~$2*10^6$ J/m^3K) [5] and also the propagation velocity is a constant parameter, meaning that the parameter that affect the thermal conductivity is the phonon or electron mean free path l_m. Focusing the attention on phonon transportations, phonon mean free path is related to its relaxation time expressed as $l_m=\tau v$ where τ is the phonon relaxation time and *v* is the phonon

group velocity (in principle c_0). In the relaxation time approximation, various scattering mechanism are additive, limiting the phonon mean free path. Acoustic phonons, are scattered by other phonons, lattice impurities, lattice defect and interfaces. [33], [34] In this scenario is possible to distinguish two different phonon-transport regimes. Thermal transport is called diffusive when the size of the sample, L, is much larger than the phonon mean free path. In this case, phonon undergo many scattering events. In contrast, when $L \leq l_m$ thermal transport is called ballistic. In the approximation of infinite crystal, without any defect or impurities, only phonon to phonon scattering occurs reaching the so called intrinsic thermal conductivity. In contrast conductivity is called extrinsic when it is mostly limited by extrinsic effects such as phonon-boundary or phonon-defect or phonon-impurities scattering. When the phonon-boundary scattering is dominant, thermal conductivity is strongly dependent from L as $k_p \propto L$. [33]

A macromolecules chain can be descripted as a zigzag arrangement of the backbone atoms in which single chain bonds are capable of rotating and bending in three dimensions resulting in a macromolecule characterized by the presence of a multitude of bends, twist and kinks, as schematically represented in **Figure 6**.

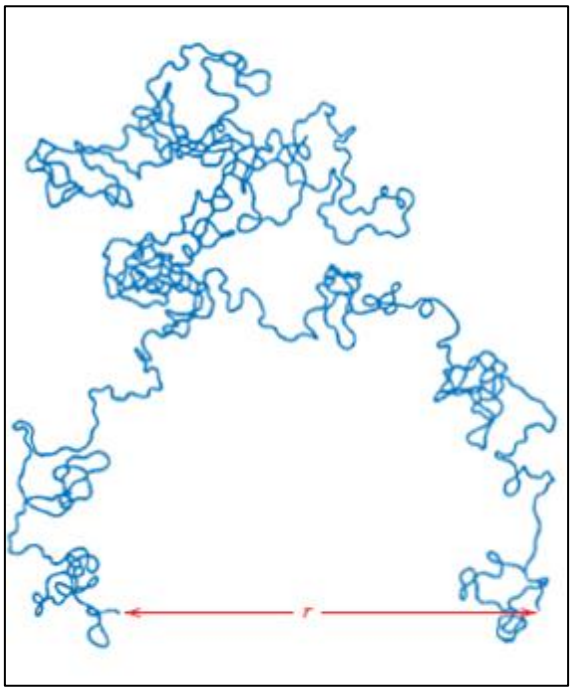

Figure 6 Schematic representation of single polymer chain molecule. [3]

In a bulk polymer, each chain is in the state of twisted random oriented molecule, coupled by weak intermolecular bonds such as van der Walls, dipole-dipole and hydrogen bonds (also covalent bond in crosslinked polymer). This means that in polymers, atoms and molecules, are not in an oriented configuration as happen in the case of ordered structures (metal, alloys or ceramic). This amorphous phase, is something that is very far from the theoretical perfect crystal, and this result in a thermal conduction that is extremely affected by extrinsic effect. Mean free path in amorphous polymers is in the range of few angstroms [35] leading to a poor thermal conductivity. From the theoretical point of view it was demonstrated, by using molecular dynamics simulation approach, that single molecular chain can in principle have rather high thermal conductivity with respect to bulk polymer. Henry and Chen, [36] found that thermal conductivity of a single polyethylene chain, with length over 100 nm, could be higher than 350 W/mK. Single PDMS (Polydimethylsiloxane) chain still has a thermal conductivity of 7 W/mK. [37] It is obviously that single polymer chain has much higher thermal conductivity with respect to the corresponding bulk materials. Both heat capacity C_p and phonon group velocity v of bulk polymer are almost the same as those of individual single chain. It is known that phonon mean free path along a chain is much larger then in transverse directions since covalent bond lattice vibrations are less anharmonic with respect to those associated to secondary bonds. Moreover, in bulk polymers the presence of defect, such as voids, impurities, polymer chain ends and entanglements further reduce the phonon mean free path resulting in a lower thermal conductivity. [38]

A list of the commonly used polymer and their related thermal conductivity values is reported in **Table 2**. As observable thermal conductivity is in the values range of 0.1 up to 0.5 W/mK. Thermal conductivity is affected by different parameters. The chain structure (including molecular composition as well as molecular conformation) is probably the most important one. It was demonstrated, by using large scale molecular dynamic simulations that higher thermal conductivity can be achieved in π-conjugate polymers. This is due to the rigid backbone that can suppress segment rotation and promote high bond strength for larger phonon group velocity. Strong inter-chain interaction can also limit the segment rotation, as occur in polyketone, Kevlar™, Teflon™ and Nylon™. [39] Furthermore, thermal conductivity decreases with the increasing of the temperature, due to the higher molecules mobility, as observable in **Figure 7**.

Polymer	Short name	Thermal conductivity (W/mK)
High density polyethylene	HDPE	0.33-0.53
Low density polyethylene	LDPE	0.30-0.34
Ultrahigh molecular weight polyethylene	UHMWPE	0.41-0.55
Polypropylene	PP	0.11-0.17
Polystyrene	PS	0.10-0.15
Poly (ethylene terephthalate)	PET	0.15
Polytetrafluoroethylene	PTFE	0.27
Polyvinyl chloride	PVC	0.13-0.29
Poly (ethylene vinyl acetate)	EVA	0.34-0.35
Polycarbonate	PC	0.19-0.21
Urethane base TPE	TPU	0.19
Poly (acrylonitrile butadiene styrene)	ABS	0.15-0.33
Polyamide 6,6	PA66	0.24-0.33
Poly (methyl methacrylate)	PMMA	0.21
Epoxy resin		0.11-0.20

Table 2 Thermal conductivity of some polymers [35], [38]

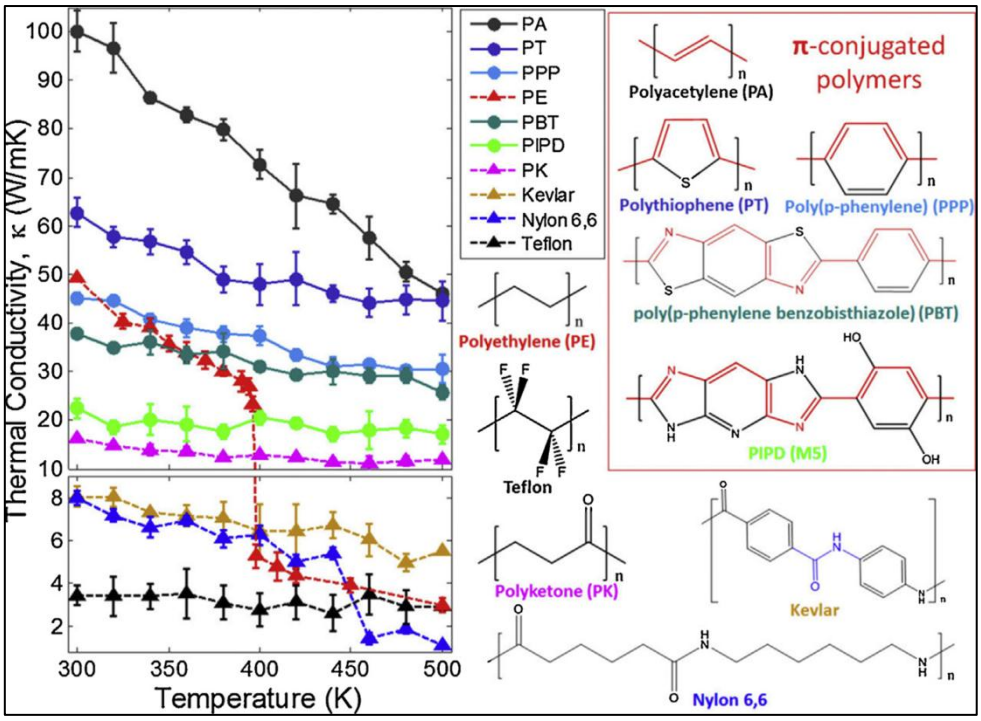

Figure 7 thermal conductivity and structure of π-conjugated polymers[39]

The presence of disordered structure promoted by the presence of lateral or functional groups as well as heavy atoms, reduces the thermal conductivity due to defect-phonon scattering process. An ordered structure can promote the formation of crystalline domain in the bulk polymer. Crystalline polymers show higher thermal conductivity with respect to the amorphous ones. In amorphous the heat flow follows the chain conformation which results in a conductive path that is essentially random, and in a reduction of the phonon mean free path because of scattering process. Crystalline domain can increase the intrinsic order which is responsible for high thermal conductivity. High density polyethylene (HDPE) presents a thermal conductivity value higher with respect to low density polyethylene (LDPE), due to the presence of higher amount of crystalline phase. Moreover, it has been also reported that the crystal form can affects the thermal conductivity. In fact, it was demonstrated that the increase of the lamellar thickness of ultrahigh molecular weight polyethylene (UHMWPE) from ~20 nm to the range of 100-150 nm results in an increase of 37% of the thermal conduction. [40] In contrast, due to the low chain stacking density and due to the presence of lateral methyl group (that involve incoherent phonon scattering) polypropylene is an exception. It is a crystalline polymers with low thermal conductivity value. [38]

As mentioned before, single oriented chain exhibits high thermal conductivity. In fact heat is transferred more easily along the chain than in transverse direction. This means that thermal conductivity can be significantly higher along chain directions with respect to the perpendicular ones. A mechanical stretching is able to orient not only a single chain, but also crystalline domains leading to an enhancement of ordered structures resulting in an enhancement of the thermal conductivity. Simple shear, or mechanical drawing as well as gel spinning and super-drawing [38] are nowadays available techniques able to orient semi-crystalline polymers such as polyethylene. The general observed trend suggests that the thermal conductivity along strain direction rapidly increases with increasing the strain or draw ratio (λ). Choy et al. [41] investigated both transverse and longitudinal thermal conductivity of HDPE at different λ, observing that at relatively low draw ratio (λ=25) the thermal conductivity along strain direction increases up to 14 W/mK at 300K. Moreover, superdrawing UHMWPE with highly oriented crystalline lamellae can exhibit a thermal conductivity value of more than 37 W/mK. Concerning amorphous polymers, such as Poly(methyl methacrylate) and polystyrene it was demonstrate that thermal conductivity of stretched polymers could be increased in the stretching direction. However, this increment was relatively small. This means that in draw crystalline polymers, the dominant phonon scattering mechanism is anharmonic phonon-phonon scattering and are not related to structural disorder. Despite some degree of chain orientation (in amorphous stretched polymers) the inter-chain scattering, related to the overall disorder is still dominant. In order to increase thermal conductivity of amorphous polymer, an engineered inter-chain interaction is required. This interaction could be done with the help of miscible polymers. There are several requirement for amorphous polymer blends to have high thermal conductivity: first of all strong intermolecular bonds are required in order to replace weak inter-chain interaction. Furthermore, the intermolecular connection must be as closely as possible to polymer backbone and an homogeneous bonds distributions at a concentration above percolation threshold is necessary to form a continuous network. [38] Similar to the thermoplastic materials, thermoset resin possess low thermal conductivity. This is due, also in this case, to the incoherent scattering process that occurs in disordered materials. Liquid crystalline thermosets, possessing rigid road-like “mesogen” groups can form ordered structure leading to a thermosetting materials with enhanced thermal conductivity. Typically non-mesogen thermosets, can only form isotropic amorphous structures, while the presence of ordered structure like liquid crystals leads to an increasing of the thermal conductivity of more than 5.5 times with respect to amorphous ones. Moreover,

the relationship between liquid crystalline domain and thermal conductivity is most affected by the size and by the content of anisotropic structures. Defining the ratio of anisotropic structure as the ratio between ordered and amorphous structure in the whole matrix, as a way to indicate the content of liquid crystalline domain, it was demonstrated that for a crystal domain larger than 400 nm and for a content ratio over 25%, an enhancement on the thermal conductivity could be achieved as reported in **Figure 8**.

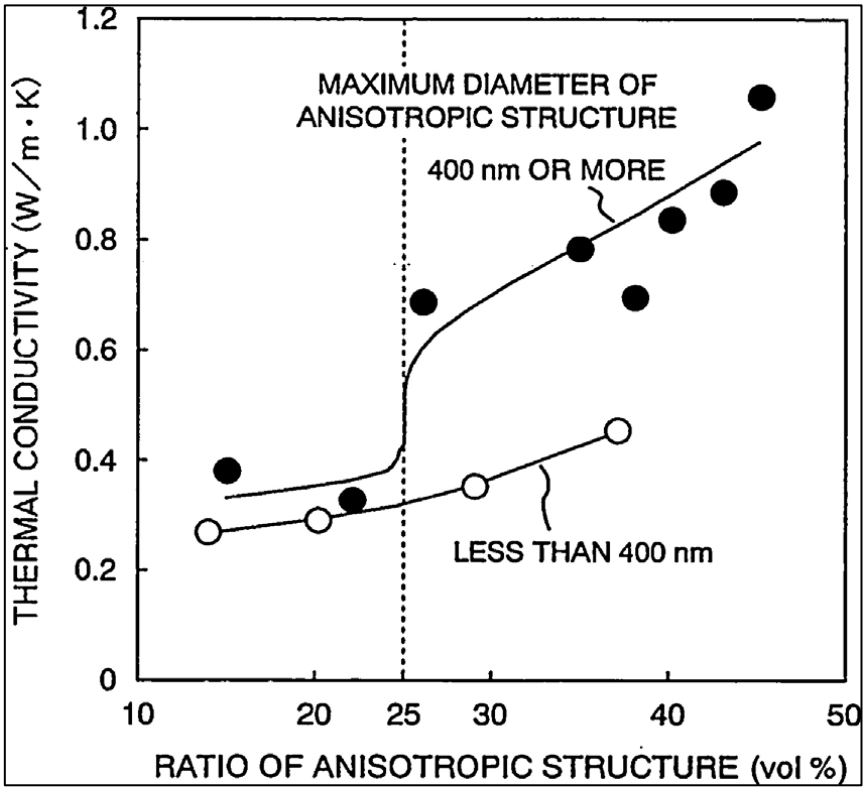

Figure 8 Relationship between ordered domain size and content with respect to thermal conductivity of DGEBA[38]

Curing conditions, as curing agent and temperature, is a key factor to the formation of liquid crystal domain. Finally, to achieve an effective enhancement of thermal conductivity of liquid crystalline thermoset polymers, different efforts have been made on the alignment of ordered structure by external electrical or magnetic field. As an examples, Harada and coworker, [42] cured diglycidyl ether of terephtalylidene -bis-(4-amino-3-methylphenol) (DGETAM) epoxy within 4,4-diaminodiphe- nylethane (DDE) curing agent under the presence of a magnetic field up to 10T at 170 °C. It was demonstrated that by applying an external magnetic field, the thermal conductivity increases from 0.43 up to 0.89 W/mK.

This is due to the direct alignment of the mesogenic group during curing process. The high thermal conductivity is due to the better phonon transmission along the ordered chain that minimizes phonon scattering. Moreover, it was also observed that DGETAM cured with DDE curing agent, shows a thermal conductivity value (0.43 W/mK) higher with respect to that of the ordinary epoxy resin system even for system cured under the nonmagnetic field, due to the curing agent.

1.3 Electrical conductivity in polymers

As for thermal conductivity, before starting to talk about electrical conductivity in polymers, we need to define some basic concept and equations.

Electrical conductivity is defined as the capability of a materials to conduct the electrical current. Mathematically it is represented by the Ohm's law, as the relationship between the electrical current *I* and the applied voltage *V* as:

$$V = RI \tag{6}$$

where *R* is the resistance of the material through which the current is passing. The electrical resistance *R*, depends from the intrinsic materials characteristics. The material property that determines the resistance is the electrical resistivity ρ:

$$\rho = \frac{A}{L}R \tag{7}$$

in which A is the cross-sectional area perpendicular to the current direction, while *L* is the distance between the two point at which the potential drop is measured as reported in **Figure 9**.

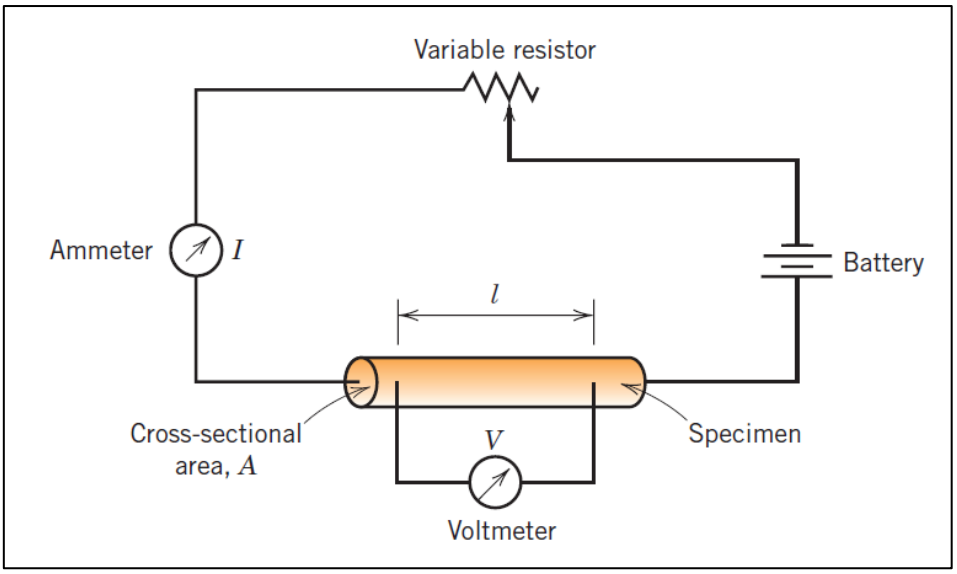

Figure 9 Schematic representation of the apparatus used to measure electrical resistivity.[3]

Combining the Ohm's law within equation 7, electrical resistivity becomes as:

$$\rho = \frac{VA}{IL} \tag{8}$$

Its unit in the metric system is ohm per meters (Ω*m) but it is also commonly used the subunits of μΩ*cm or Ω*cm. As mentioned before, the capability of a material to conduct the electrical current is defined as the electrical conductivity that is essentially the reciprocal of the electrical resistivity, defined as:

$$\sigma = \frac{1}{\rho} \tag{9}$$

Both electrical conductivity (S.I. S/cm or $\Omega^{-1}*m^{-1}$) and electrical resistivity are interchangeable, and usually are used both depending on the context.

Solid materials, show an immense range of electrical resistivity values. Starting from conductive materials ($10^{-8}\Omega*m$) until insulators ($10^{+16}\Omega*m$) there is a range of more than 24 order of magnitudes in between. Materials that present intermediate values are known as semiconductors. This discrepancy is related to the capability of a charge to pass through the entire materials. Conductivity is essentially promoted by electron or by ionic carriers. However, in ionic solids (as

an examples NaCl) the diffusive motion of ions is possible only at elevate temperatures. In fact it is possible to demonstrate that the ion mobility is inversely proportional to the temperature, therefore in spite of the ionic conductivity most of them are insulators. [3] Regarding the electrons contributions, in all conductors, semiconductors and in many insulating materials, the conductivity is strongly dependent on the number of available electrons that can participate to the conduction process. The number of available electrons is related to the electron arrangement states and to the occupied energy levels. As know from the quantum mechanics point of view, for each atom exist discrete energy levels that may be occupied by electrons into shell and subshell arrangement at increasing energy level. In according to the Pauli exclusion principle, each state is occupied by two electrons of opposite spin. Moreover, the electrons fill only the states having the lowest energies. In solid materials, the atoms are bonded together to form an ordered atomic arrangement. Initially, an atom, separated from another one is independent and its energy state is related to its electronic configuration. When N atoms, are so closely to interact with each other, the electrons are acted upon, or perturbed by the electrons and nuclei of adjacent atoms. This influence is such that each distinct atomic state may split into a series of closely spaced electron states to form the so called electron energy bands as illustrated in **Figure 10**.

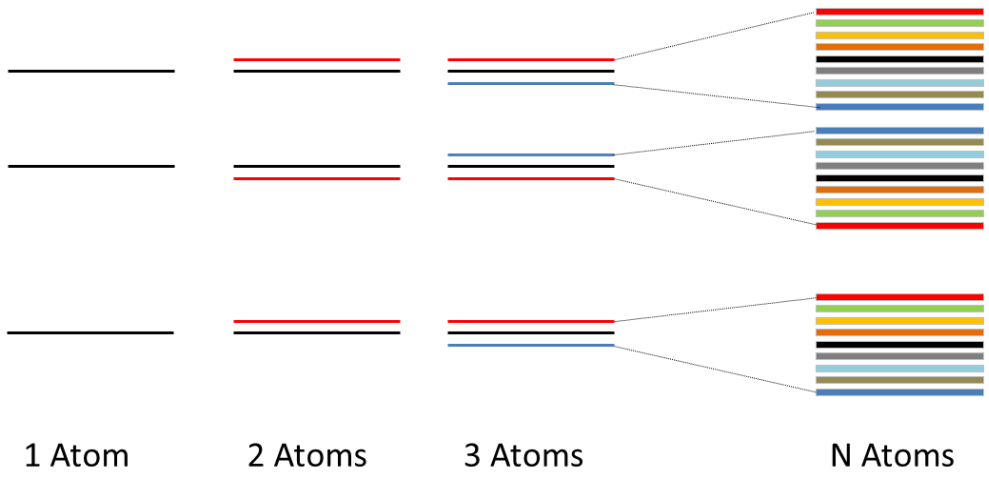

Figure 10 Energy bands formation. Starting from one single atom, the available energy states are represented by the each energy level. Passing from single isolated atom up to N atoms in solid materials, the perturbed atomic state split into a series of closely electron energy levels named as bands.

The extent of splitting depends on the interatomic distance and by the external electronic shells (number of available electron levels) since they are the first to be perturbed by the neighbors atoms. At the equilibrium distance, band formation does not happen for the electron subshells near the nucleus, meaning that the band formations is related only to the external electrons shells as reported in **Figure 11**. Between different energy bands a gap in energy could exist. The electrical properties of solids, depend on the band structure and on the energy gap between them. In fact, whether the materials are insulators or conductors or semiconductors depends from how full the band are, and by their separation or overlapping. Conductors, such as copper, iron and metals in general, have a partially filled outer band. Just above the last occupied levels there are many unfilled levels used by the electron (accelerated by an external field) to conduct their charge freely though the material. In contrast insulating materials are characterized by the presence of an energy gap between the filled valence band end the empty conduction band higher than 2 eV. Semiconductors, exhibit the same band structures, but in this case the energy gap is lower than 2 eV. [3]

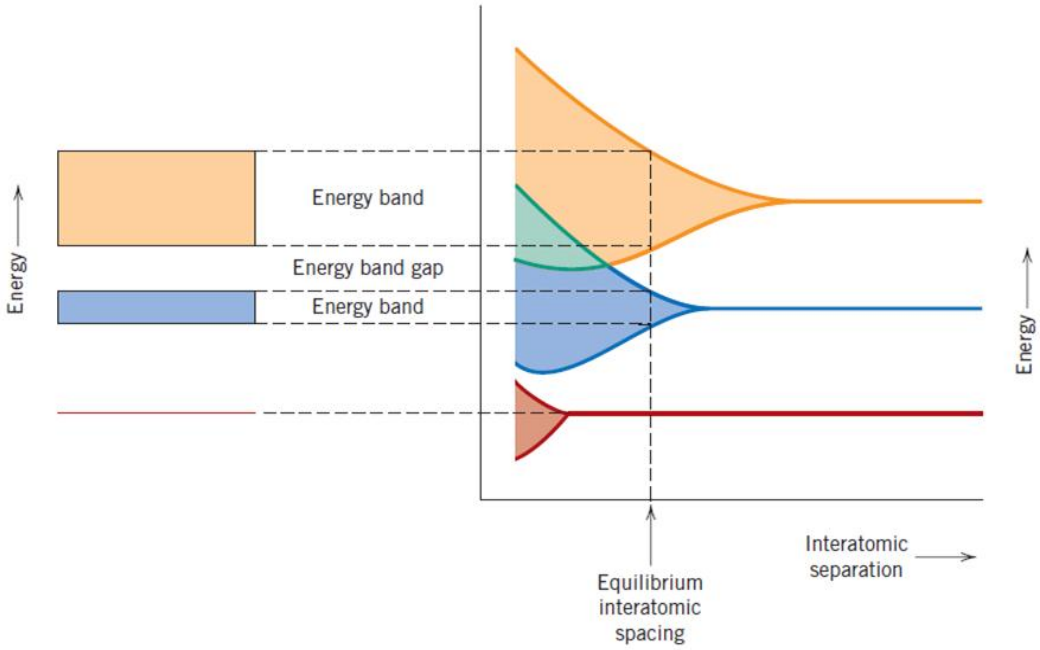

Figure 11 Band structure representation as function of the interatomic separation.[3]

In this scenario, polymers are classified as insulating materials. They present an electrical conductivity value lower than 10^{-9} $(\Omega*m)^{-1}$. Looking at the property chart of materials, also known as Ashby maps of material selections, in which thermal conductivity Vs electrical resistivity is reported (**Figure 12**) it is possible to observe that for metals this two properties are linked together because both depends mainly on free electrons. In contrast polymers are in the bottom right part of the chart located at high electrical resistivity and low thermal conductivity because of the unavailability of large number of free electron able to promote electrical (and also thermal) conduction. [5] Moreover, free electrons, moves through the materials under the force of an applied field with a current density that is proportional to it. The external field imposes an electron drift velocity $v_d=\mu_e E$, in which μ_e is named electron mobility, resulting in a current density that is effected by the external field, by the electron mobility and therefore by the number of available mobile electrons as well as by the electron charge as reported in the equation 10.

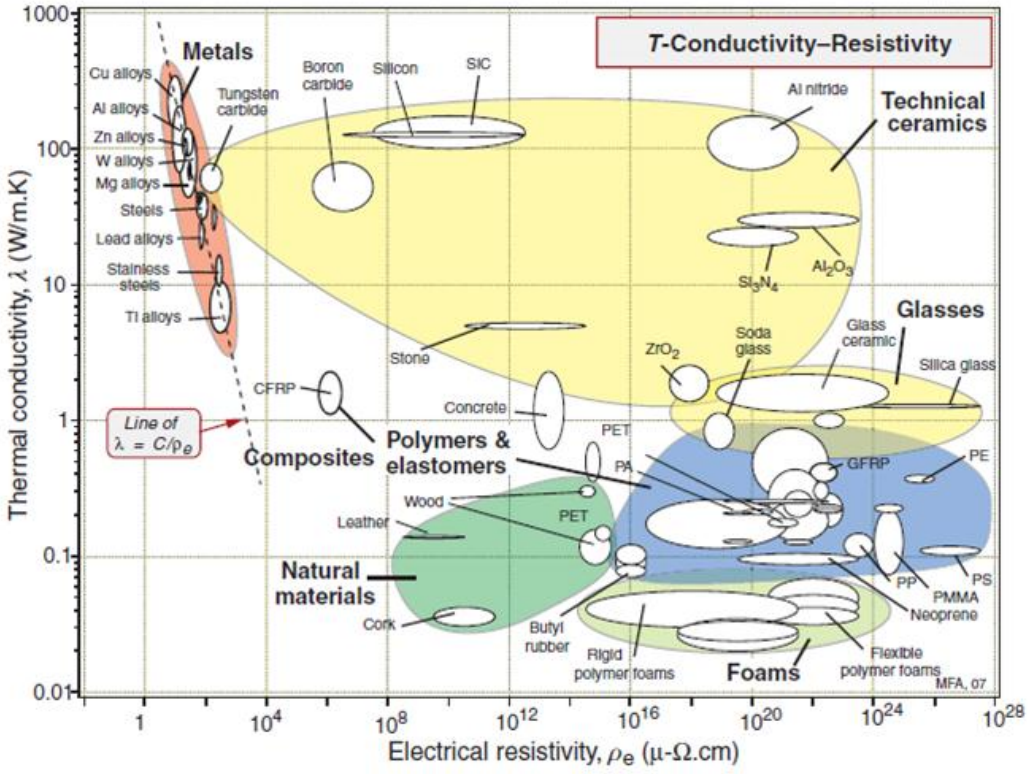

Figure 12 Ashby map of material selection: Thermal conductivity Vs Electrical resistivity.[5]

As can be seen, the current density "j" should increase with the increasing of the electrical field. However, the electrons collide with scattering centers bouncing off in a new direction, resulting in an electron mean free path that leads to a reduction in the electrons mobility.

$$j = \frac{i}{A} = ne\ \mu_e E \tag{10}$$

Scattering centers are represented by impurities, by lattice imperfections and by thermal vibration of atoms themselves. For this reason, coupled with an extremely low number of free carriers, the electrical resistivity of polymers is too high. The electron mobility could be promoted by conjugated π-electron consisting in a alternation of single and double bonds along the chain backbone or ring structure as schematically represented in **Figure 13**. [4]

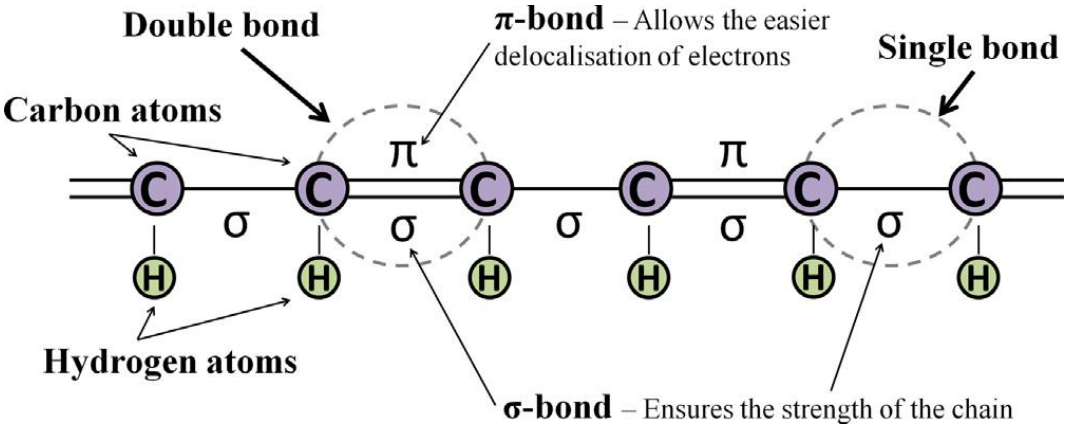

Figure 13Schematic representation of a conjugated backbone containing alternating single and double bonds.[43]

In this kind of conductive polymers, single and double bonds possess strong localized σ-bond while the double bonds possess less strongly localized π-bonds resulting in an overlapping of *p*-orbitals in the series of π-bonds allowing the electrons to be more easily delocalized and move freely along the chain. The resulting materials, possess an electrical conductivity value up to 10^3-10^5 S*cm^{-1}. However, since the first conductive conjugated polymers was produced in the late 1970s, today there are at least few conductive polymer systems. [43]

1.4 Polymeric composite materials with enhanced conductive properties

As reported until now, polymers possess poor conductive properties and it is obviously that there are different engineering approach to enhance both thermal and/or electrical conductivity. However, the most established way to enhance the intrinsic polymer properties is by incorporating conductive fillers into polymer matrices. Conductive polymers with a thermal conductivity from approximately 1 up to 30 W/mK can be used as heat sink in heat exchangers and heat management applications while electrical conductive polymers can be used in different fields according to their electrical conductivity values. In fact, polymer with electrical resistivity in the range between 10^8 to $10^3\Omega$*cm can be used in static dissipative applications while conductive polymer with electrical resistivity in the range of 10^2-$10^{-1}\Omega$*cm can be used for moderately electrically conducting applications. Polymer-based materials with electrical resistivity approximately $10^{-2}\Omega$*cm can be used in electromagnetic interference (EMI) and or radio frequency interference (RFI) shielding applications. [44]

1.4.1 Polymeric composite materials with enhanced thermal conductivity

Thermally conductive polymer composites offer new possibility to replace metal parts in different applications including power electronics, electric motor and generators, heat sink, heat exchangers, heat recovery etc. [35], [45].

There are many theoretical models developed to describe the thermal conductivity of heterophase polymer composites. The commonly adapted models, are those developed to describe the Young's modulus of two phase system. Modulus is not a transportation properties, but looking at its definitions is possible to observe that it is described by a force imposed over a cross sectional area divided by an increase in the relative dimension with respect to the original one, as reported in the following equation:

$$E = \sigma/\varepsilon = (F/A)/(\Delta x/x_0) \quad (11)$$

Comparing equation 11 with equation 1 it is possible to observe that a strong correlation between the two expressions exist. Since the prediction of the tensile modulus, in composites, is represented by a lower and an upper bound by means of rule of mixtures and Reuss equation, also thermal conductivity could be estimated starting from this approach. [32] The geometry and the orientation of the fillers are keys parameters that influence the thermal conductivity of composite materials. The possible scenario includes particulate (spherical or irregular) and flakes particles as well as short, long or continuous fiber oriented in an irregular or regular (laminated) structure.

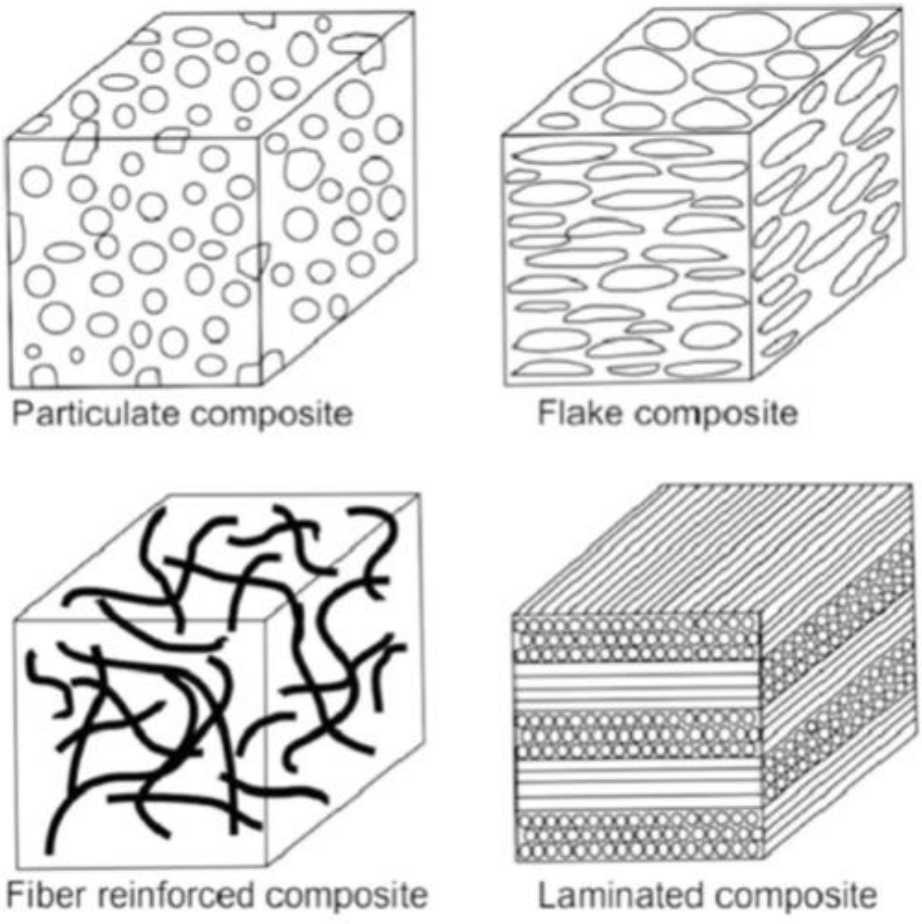

Figure 14 Composite materials with different forms of fillers [45]

Starting from the easiest possible scenario, in which spherical conductive fillers are added to polymeric materials, it is possible to predict the final thermal

conductivity by using two basic theoretical approaches. The first approach is used to predict the thermal conductivity of a percolation system as reported in **Figure 15**.

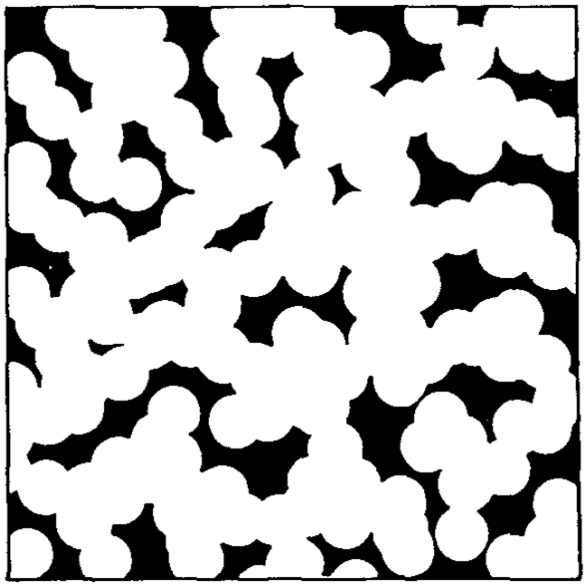

Figure 15 Basic model for predicting thermal conductivity of two phase system in which a fully interprenetrating spherical particles are dispersed into polymeric matrix.[32]

This model tends to maximize the effect of the dispersed phase. In fact in a percolation system, each component contribute to the thermal conductivity of the composite in an amount equal to the volume fraction of that component. Mathematically speaking it is represented by the simple rule of mixture as:

$$\frac{k_c}{k_m} = \Phi_m + \frac{k_f \Phi_f}{k_m} \qquad (12)$$

in which k_c, k_m and k_f are the thermal conductivity of the composite, of the filler and of the matrix respectively, while Φ_m and Φ_f are the matrix and the filler volume fractions.

The second approach for modelling the thermal conductivity consists in assuming that the composite material responds as a homogeneous system in which each particle is isolated with respect to the other ones, as schematically represented in **Figure 16**

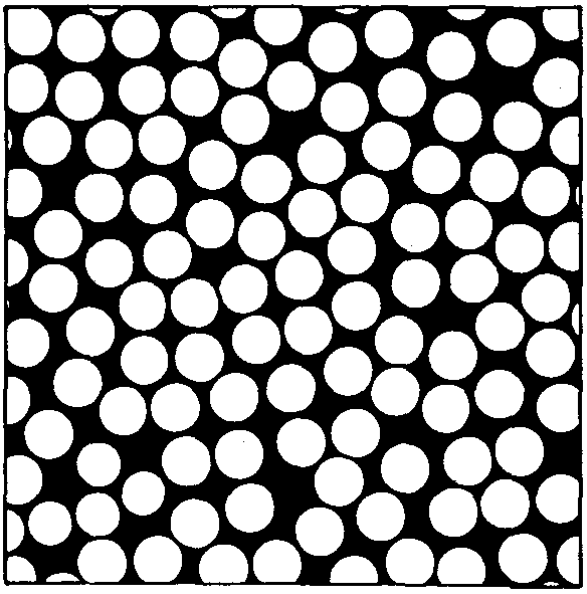

Figure 16 Basic model for predicting thermal conductivity of two phase system based on non-penetrating spherical particles dispersed into polymeric matrix. [32]

Such model assumes that there is no particles interaction and that each of them exhibits an isolated effect minimizing the effect of the fillers on the composite thermal conductivity, especially at low filler concentrations. This behavior is represented by equation 13. [32]

$$\frac{k_c}{k_m} = \frac{{}^{1}/_{k_m}}{({}^{\Phi_m}/_{k_m} + {}^{\Phi_f}/_{k_f})} \tag{13}$$

These two models are referred as the upper and the lower bound of thermal conductivity and are represented by the linear mixing rule, also known as the parallel model, and by the inverse mixing rule (series model) respectively. [38] Moreover, equation 12 and 13 could be rewritten in most commonly ways as equations 14 and 15 respectively. [35]

$$k_c = k_f \Phi_f + k_m \Phi_m \tag{14}$$

$$k_c = \frac{1}{(\Phi_m/k_m + \Phi_f/k_f)} \tag{15}$$

As observable the parallel model maximizes the contribution of the conductive phase assuming a continuous conductive network in which the contacts between each particles are perfect. The series models, assumes no contact between particles therefore it is confined to the region of matrix embedding the particles. **Figure 17** shows how the two models estimate the thermal conductivity of polymeric composite materials filled with spherical particles that possess a thermal conductivity 1000 times higher with respect to the matrix (k_f/k_m>1000). The upper bound (black line) predict an increasing of more than 10 times of the ratio between composite and matrix thermal conductivity at very low filler contents while the lower bound prediction (black dashed line) shows how the increasing of the thermal conductivity of the composites (with respect to the matrix) strongly depends on the amount of filler content. However, most of the experimental data (white dots), were found to fall in between the two models.

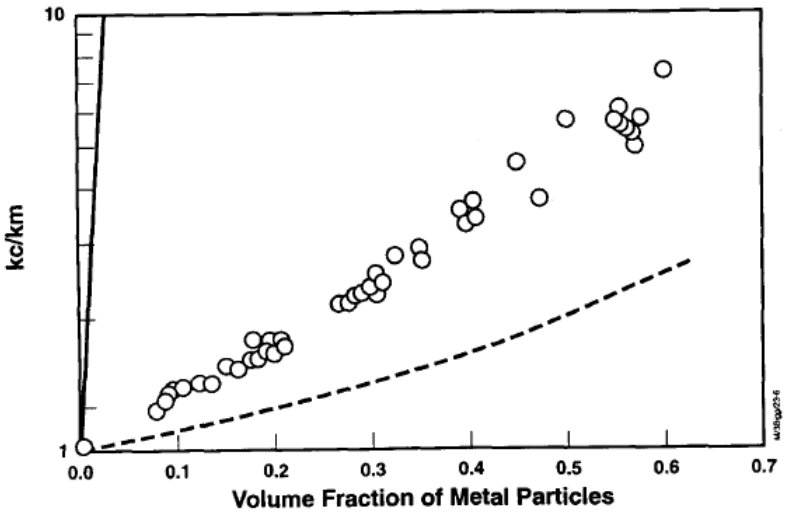

Figure 17 upper and lower bound predictions of a two phase system in wich the dispersed particles are spherical and the ratio between filler and matrix thermal conductivity is over 1000. [32]

The non-interactive lower bound model, provides a closer match to the data with respect to the rule of the mixtures. In fact, the upper bound model has some relevance only in the case of continuous fiber composites, in the direction parallel

to the fibers. In the other cases it tends to overestimate the predictions. [35] The main problem with the statistical approaches is that more information are required about the microstructure of the systems. In fact the lower bound approach results in a composite thermal conductivity that inherently includes the effect of the geometry of the filler particles giving to the development of a class of models based on the assumption of isolated filler particles. [32] The relative thermal conductivity of two phase system (particle-in-matrix) can be expressed as a series expansion of the localized average thermal conductivity determined by a localized heat transfer. This approach is defined as the second order low boundary models, including equation of Hashin and Shtrikman that describe the effect of randomly dispersed spherical particles on the thermal conductivity of two phase system. [32] Moreover Hamilton and Crosser, Hatta and Taya, Agary as well as Cheng and Vachon, discovered independently equations that provide better fitting by including experimental constant and geometrical parameters. These equations are weighted averages of the thermal conductivities and volume concentrations of the two components but in a more complex averaging scheme whit than the simple lower bound model. This equations lead to a better theoretical fitting with respect to the experimental data for composites based on isotropic particles, fiber and/or flakes, up to a filler content of about 30% in volume. Finally Nielsen introduced the maximum packing factors into the fitting equations, providing the best fit with respect to the rapid increase of the thermal conductivity above 30% of filler contents. [32], [35]

Filler concentrations and fillers thermal conductivity are the key factors that determine the thermal conductivity of heterogeneous randomly dispersed two phase polymer composites. Thermal conductivity of polymers is particularly important at low filler loading acting as thermal barrier and becoming rate-limiting in the thermal conductivity channel. To achieve high thermal conductivity significant amount of fillers is needed in order to form thermally conductive pathways. However, high filler contents not only can cause the final composite to be brittle, but also can limit its processability. Filler size is an important parameter to be taken into account. Composites with large fillers, have less filler/polymers interface lading to a lower amount of interfacial resistance and thus high thermal conductivity. However, for nanoscale materials, the filler properties could also change. To achieve high thermal conductivity an hybrid system, such as a mixture of fillers of different type, size and shape can help to achieve high oriented and isotropic pathways at low filler contents. Finally, filler surface treatments, can be used in order to provide better interaction between filler

and matrix leading to a betters filler dispersion and high thermal conductive composites. [38] Under ideal conditions, the thermal conductivity of polymeric composite material can be as high as 20 times that of the base polymer. [32]

1.4.2 Polymeric composite materials with enhanced electrical conductivity

Polymer composites containing electrical conductive fillers, are of great interest due to the potential applications in different sectors ranging from radar absorption up to sensors passing through electrical dissipative system and/or conductive applications. [9], [44], [46]

As reported in the previous sections, polymers are classified as insulating materials with a resistivity value higher than 10^9 Ω*cm. The sudden increase of the electrical conductivity of polymeric matrix filled with an electrical conductive filler at a critical filler concentration is a well-known phenomenon called percolation. This phenomenon is usually explained with the help of the percolation theory. [47] Percolation is a probabilistic process which exhibits a phase transition. Different percolation systems may contain clusters of different shapes and sizes. The statistical study of the clusters helps to identify the critical value of density to form infinite or long-range connectivity in randomly dispersed system. This critical value is known as percolation threshold. [48] Percolation is a general phenomenon that can be applied at every area of science as the simplest model for spatial disorder, and has application to a broad range of topics including mathematics, physics, hydrology, ecology as well as biology, chemistry and material science and engineering.

In most of the cases, the presence of a continuous network of filler particles does not change the basic mechanism of thermal transport in a composite system [32] but a continuous network is required to form an electrical conductive pathway able to promote the electrons transport leading to an enhancement of the electrical conductive properties of polymeric composite materials. This is due to a different mechanism in the electron propagation with respect to phonons. The electrical resistance in a composite system is the result of a large number of resistors combined in series and parallel. When an electrical field is applied to two media in contact with each other, charge polarization occurs at the interface due to the differences between the ratios of the electrical resistivity. [49] In order to have conduction in heterogeneous system, like polymeric composite materials filled with conductive particles, a conductive pathways is required. This is possible only

at a specific filler contents φ_c known as percolation threshold. The percolation threshold of an infinite system is well defined by a distinctive phase transitions at a specific value of filler content. In the case of electrical conductive composites materials, this phase transition is represented by the change from insulator to conductive behaviors. Mathematically speaking, percolation is represented by an exponential power law:

$$k_c = (\varphi - \varphi_c)^{\alpha} \tag{16}$$

Where k_c is the property under consideration, φ_c is the percolation threshold while α is the dimensionless critical exponent. The percolation threshold and the critical exponent may be determined with the help of different computational methods like series expansions, Monte Carlo simulation and other complex numerical methods. [46], [50] However, in most of the cases it is possible to estimate its value by curve fitting of experimental results. In **Figure 18**, the typical percolative S-shaped curve is reported.

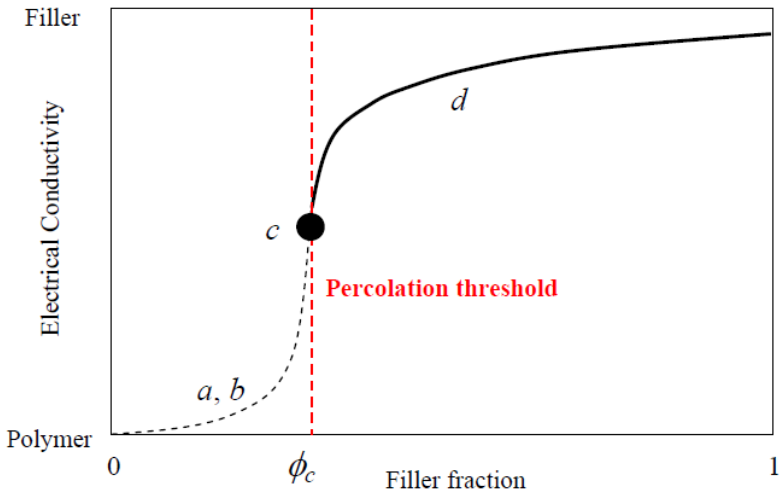

Figure 18 Typical S-Shaped curve related to the electrical conductivity of composite materials as a function of filler fraction.[51]

It is possible to divide the percolation curve in 4 different part, named as "a-b-c-d". By gradually adding a conductive filler (e.g. Carbon Short Fiber, CSFs) to insulating polymers, the electrical conductivity of the composite, increases with the filler contents. At low filler loading, the electrical conductivity of the composites is close to that of the polymer matrix. This is due to the absence of a filler network able to promote the charge transfer as schematically represented in

Figure 19(a). By comparing **Figure 18** and **Figure 19(b)**is possible to observe that at certain filler concentrations, marked as "b" in the percolation curve, the electrical conductivity of composites gradually increase due to the formation of some large cluster of conductive particles. Moreover, it should be noted that despite of the not completed formation of a continuous network, is possible to observe an increasing in the conductive properties due to the tunneling effect among neighboring conductive media. Further addition of filler, promote the formation of the "first" conductive path (represented by the red path) thought the entire composites as reported in **Figure 19(c)**. At this stage, percolation threshold, the electrical conductivity increases remarkably following the percolation power law. At filler concentration higher than φ_c the electrical conductivity of composites further increase gradually due to the creation of a lot of conductive paths, until leveling off at a constant value that is generally lower than that of the element of the conductive network as shown in the previous figures.[46], [50], [51]

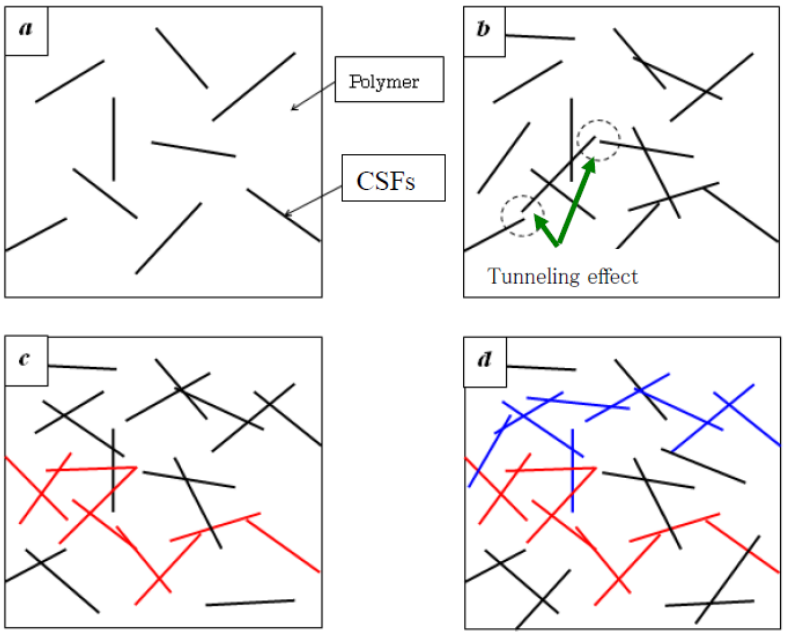

Figure 19 Percolation process in conductive composites[51]

As occurs in the case of thermal conductivity of heterogeneous insulator-conductive system, also in the case of electrical conductivity, the filler plays the most important role in the overall conduction. Intrinsic filler electrical conductivity as well as filler aspect ratio and filler affinity to the matrix, are the key parameters that must be taken into account. Moreover, the interfacial forces

between the conductive and the insulating materials plays a crucial role for the sudden increase of the conductivity at the critical concentration φ_c. Depending on the polymer matrix, on the filler characteristics as well as the manufacturing process adopted, percolation threshold could be ranging from less than 1.0% of filler content up to more than 10% in volume of conductive fillers. Many efforts have been made in order enhance the electrical conductive properties of polymer by using the minimum possible amount of fillers. In fact the use of the lowest possible filler contents not only provides a reduction on the cost of the final technological components, but also provides a lower cost in terms of manufacturing process (by the reduction of the viscosity of the medium, and therefore the reduction of the energy required), as well as density reduction that is a crucial point in the most technological application.

Chapter 2

Carbon based nano-fillers

14th November 1985 was a great day for the scientific community. On this day, Smalley and co-worker published in "Letters to Nature" their work entitled C_{60}: Buckminsterfullerene.[52] During their experiment "aimed at understanding the mechanism by which long chain carbon molecules are formed in interstellar space and circumstellar shells", a solid disk of graphite was vaporized by laser irradiation, producing a remarkably stable cluster consisting of 60 carbon atoms. Carbon atoms are fixed at each vertices of a truncated icosahedron based on 20 hexagonal faces linked together by 12 pentagonal faces leading to a spheroid and hollow structure. This structure (such as a soccerball) satisfies all the valences by two single bonds and one double bond. Its diameter is ~ 7Å providing an inner cavity which appear to be capable of holding a variety of atoms. Moreover it appears to be an aromatic structure in which both the inner and outer surfaces, are covered by a sea of π-electrons. This outstanding material is known as one of the allotropic phases of carbon. Carbon can exists as 3-D diamond face-centered cubic crystal in which each carbon atom has four nearest neighbors arranged in a tetrahedron. Unlike diamond, carbon atoms could be arranged in a hexagonal array. This structure is referred to the graphite structure. Graphite is the most stable carbon allotrope. It is based on a planar structure in which each atom is arranged in an honeycomb lattice and located at the vertices of an hexagon by strong covalent bond. Three of four potentially bonds are satisfied. The fourth free electron is able to migrate thought the plane. The interlayer distances is about 0.334 nm bonding together via weak van der Walls force. [53] Moreover, as diamond and graphite are well known carbon allotropes, the Smalley's work

opened up to a research field aimed to discovery other possible carbon forms. In light of this scenario, in 1991 Iijima [54] reported the preparation of helical microtubules based on graphitic carbon. This microtubules, actually known as carbon nanotubes (CNTs), are referred to be a 1-Dimension carbon allotrope. They could be represented by a single layer of graphite rolled up to form a tubular structure. This arrangement is possible due to the minimizing of the internal energy possessed by the single layer of graphite. In fact, from the theoretical point of views, 2D single layer of graphite did not exist without a 3D base. *AB initio* calculation showed that single layer of graphite, is thermodynamically unstable with respect to the other fullerenes structures, as carbon nanotubes are. [55] However, in 2004 Andre Geim and Konstantine Novoselov, by using a simple trick, were able to demonstrate the possibility to isolate a single layer of graphite. [56] Since its first isolation, this material received unbelievable attentions from the researcher communities, due to its outstanding mechanical, electrical, thermal and optical properties. From the IUPAC commission, it must be referred to it with term "graphene" to replace terms like "graphite layer" as the building block of graphitic materials.[57] In **Figure 20** the structures of carbon allotropes are reported.

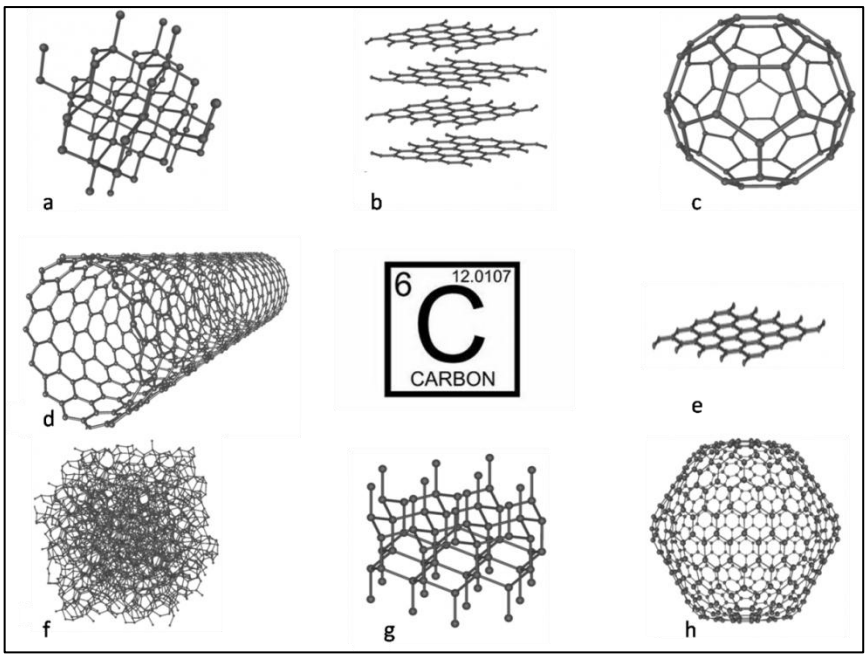

Figure 20Different Carbon allotropes. a) Diamond, b) Graphite, c) Fullerene, d) Carbon Nanotubes, e) Graphene, f) Amorphous Carbon, g) Lonsdaliete, h) C540.

As observable, carbon can exist not only in the above mentioned structures, but also in other forms such as amorphous carbon, lonsdaleite (known also as hexagonal diamond) and different Buckminsterfullerene-like cages based on different amount of carbon atoms such as C_{70}, C_{540} etc. Those materials possess different intrinsic characteristic that could be exploited in polymeric composites materials. However, due to the extremely high cost and/or low abundance from both natural and artificial point of views (diamond and hexagonal diamond cases) or due to the low aspect ratio of fullerene structures, those carbon materials are not good candidates as filler on polymeric composite materials. In contraposition, carbon nanotubes and graphene are nowadays the most promising fillers used to enhance the intrinsic polymer characteristics.

In the next sections, carbon nanotubes and graphene will be presented from a theoretical point of view in order to assess the actual scenario about the use of those fillers as conductive materials from both electrical and thermal point of views.

2.1 Carbon nanotubes

Since the first report of helical microtubules by Iijima in 1991, carbon nanotubes get an outstanding attention from the academic world due to their exceptional mechanical, thermal and electrical properties. It is possible to imagine CNTs as long, narrow fullerenes, based on graphitic carbon, structure capped at each end. In another way it is possible to visualize carbon nanotubes as a sheet of graphene rolled to form a tubular structure. The walls of CNTs, are entirely composed of sp^2 carbon-carbon bonds. This kind of bond, stronger than the sp^3 counterparts, provides extremely high mechanical properties such as Young's modulus up to 1.2 TPa and tensile strength of more than 50 GPa. [58] Moreover, the double bond is expected to provides electron and phonon transport. The properties of CNTs, are strongly affected by their atomic arrangement (in terms of how the graphitic sheet are rolled), by their diameters and length, and by their morphology.

Due to its fourth free electron, that is able to migrate thought the plane, graphite is considered to be a semi-metal. In contrast carbon nanotubes could be either metallic or semiconductor. The semiconductor or metallic behaviors depend from the atomic structure of nanotubes, in terms of chirality defined by chiral vector as:

$$\overrightarrow{C_h} = n\overrightarrow{a_1} + m\overrightarrow{a_2} \tag{17}$$

in which "n" and "m" are integer numbers that correspond to the number of steps along the zig-zag carbon bonds of the hexagonal lattice, while $\overrightarrow{a_1}$ and $\overrightarrow{a_2}$ are unit vectors. Moreover, CNTs properties depends also on the chiral angle that is formed between the chiral vectors and the $\mathbf{a_1}$ and $\mathbf{a_2}$ direction as reported in **Figure 21**.

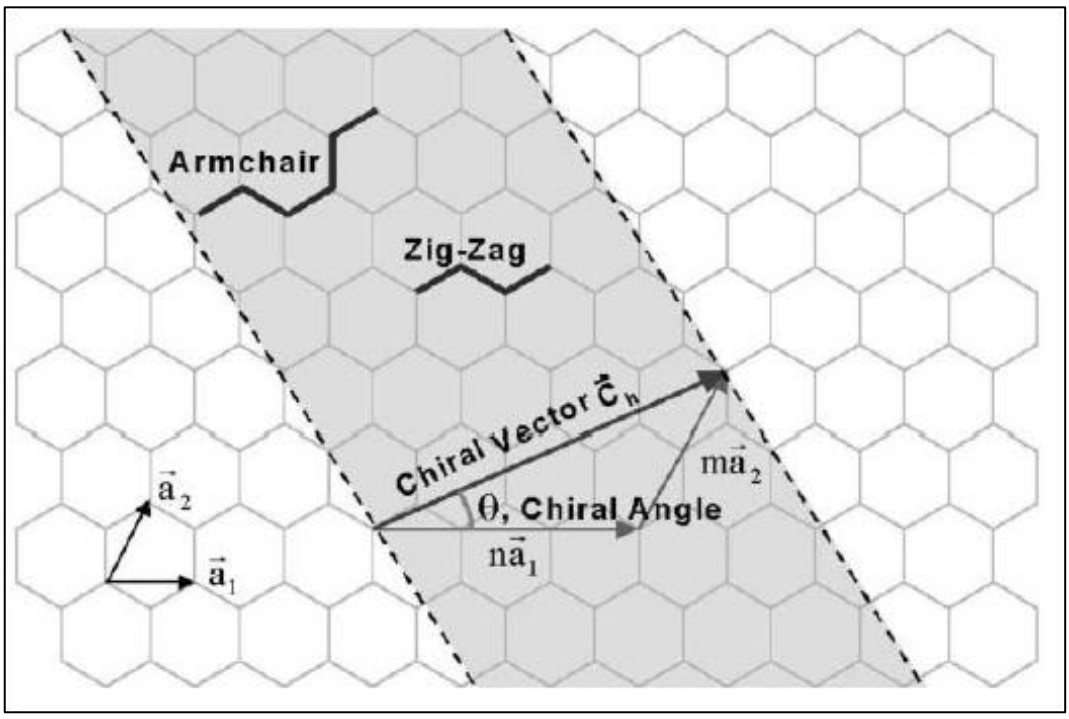

Figure 21 Schematic representation of chiral vector and angle.

The chirality has huge weight on the CNTs properties, in particular on the electronic ones. [59] In fact, the diameter and the helicity of CNTs are uniquely characterized by the chiral vector. It was predicted that (n,m) indices determine the metallic or semiconducting behaviors of CNTs. The tubes will be metallic when n/3 is an integer in ziz-zag (n,0) configuration. Otherwise they are classified as semiconductors. Moreover, chiral (n,m) configurations are possible with electronic properties similar to the zig-zag configuration when (2n+m)/3 is an integer number. In those cases the tubes are metallic while in the other cases are semiconducting. Finally, (n,n) cases are possible when the chiral vector rotates 30° relative to (n,0). This kind of tubes, named as armchair tubes are expected to be truly metallic. Armchair tubes has a band gap crossing at $\boldsymbol{k} = \pm 2/3$ of the first 1-D Brilluoin zone. [60] On the contrary it was demonstrated that the chirality has a relatively low influence on the mechanical properties. [61], [62]

Schematic representation of the formation of carbon nanotubes is reported in **Figure 22**.

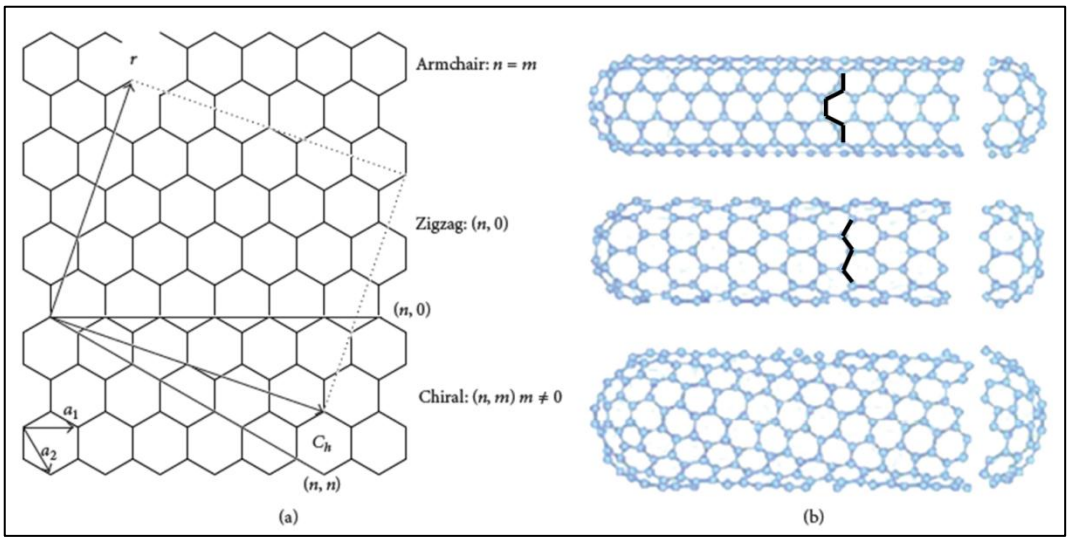

Figure 22 Schematic representation of the rolling up process of CNTs starting from the graphite sheet along lattice vectors which leads to armchair, zig-zag and chiral nanotubes (a) and (b). The three types of nanotubes are represented as long and narrow Fullerene capped at the end. Black line in armchair and zig-zag nanotubes represent how vectors $\mathbf{a_1}$ and $\mathbf{a_2}$ move on the graphitic lattice.

Carbon nanotubes are classified as single wall carbon nanotubes (SWCNTs) and multiwall carbon nanotubes (MWCNTs). The circumference of SWCNTs is usually composed by only 10 carbon atoms while the thickness is only one atom thick. The diameter is lower than 1 nm. MWCNTs are described as a multi stack of graphite sheets rolled up to form concentric cylinders. The diameters of MWCNTs is in the order of magnitude of ten nanometers. The concentric tubes are bonded together via van der Walls forces. The distance between each layer in the tubes is 0.34 nm as the interlayer graphite distances. However, in both the cases (single or multi wall) the length of the tube could be higher than tens of microns providing an aspect ratio (length-to-diameter ratio) higher than 1000. Therefore it is possible to considered both SWCNTs and MWCNTs as 1-dimensional structures. [63]

Schematic representation of how SWCNTs and MWCNTs are formed, is reported in **Figure 23**.

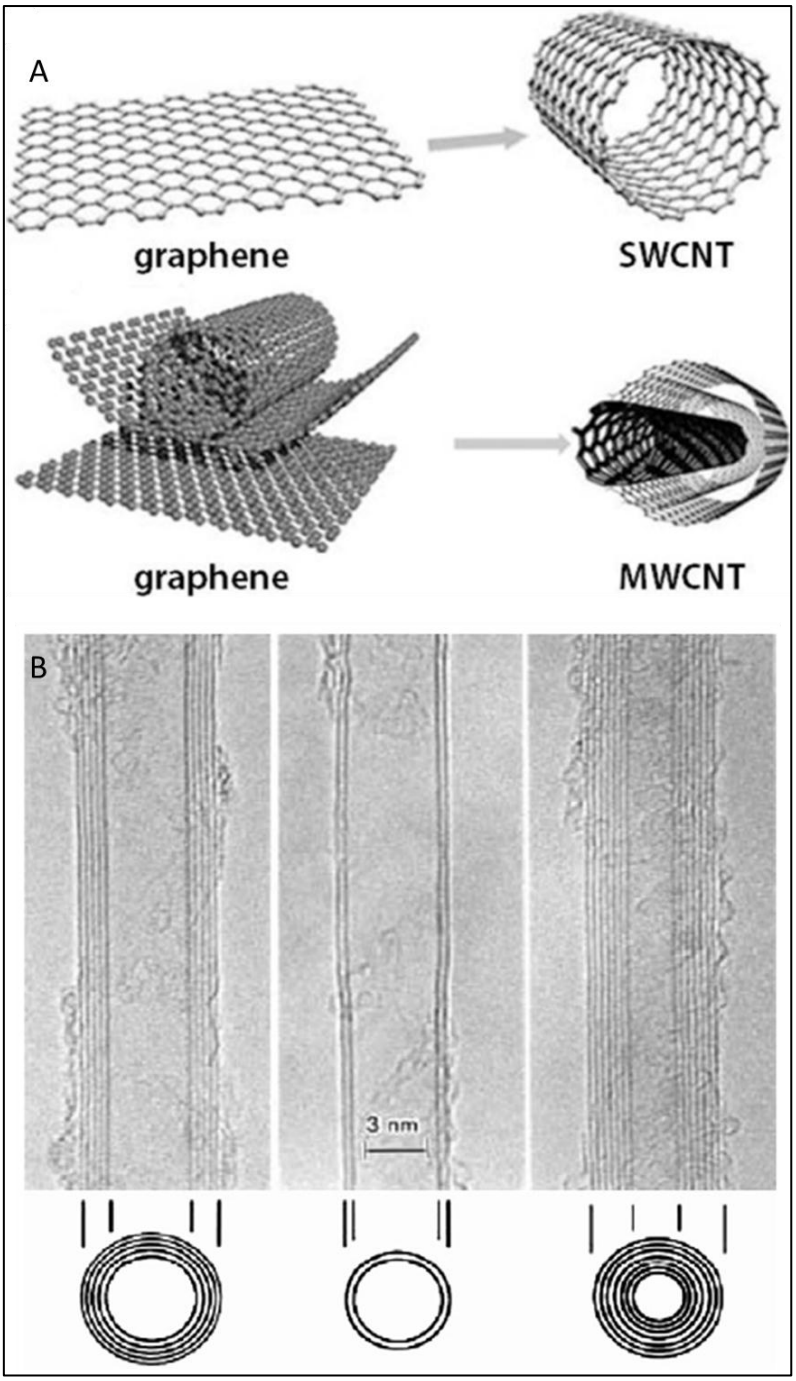

Figure 23 A) Schematic representation of SWCNTs and MWCNTs and how they are formed starting from a single or a multi graphene sheets and B) Transmission electron microscopy images of MWCNTs with different numbers of layer respectively 5, 2 and 7.

2.1.1 CNTs synthesis

Since carbon nanotubes were discovered, different techniques were developed to synthesize them. Main synthesis methods for multi and single wall carbon nanotubes include arc-discharge, laser ablations, gas-phase catalytic growth from carbon monoxide (CO) and several techniques based on chemical vapor depositions (CVD) from hydrocarbons. [54], [64]–[69]. The basic feature of these methods is the addition of energy to a carbon source in order to produce carbon fragments (such as group or single C atoms) that can recombine in order to generate CNTs, as occurred in the case of the fullerene synthesis.

Arc-discharge was used by Iijima in 1991 for the first preparation of CNTs. By creating an hot plasma discharge between two graphite electrodes, that are connected to the power supply (fixed at 20 Volts, providing a current of 100 Ampere in the presence of a inert He gas) nanotubes are generated from the condensation of hot gaseous carbon atoms generated by the evaporation of solid graphite. Arc-discharge provides the synthesis of MWCNTs. In order to obtain SWCNTs a metal catalyst, such as Co, Rh, Pt or Pb is required. [70], [71] Schematic representation of arc-discharge system is reported in **Figure 24**. The graphite rods are brought together under a helium atmosphere and a voltage is applied. The vaporized carbon materials pass from the anode to the cathode were re-condense forming a shell of fused materials and a softer fibrous core containing nanotubes. [59]

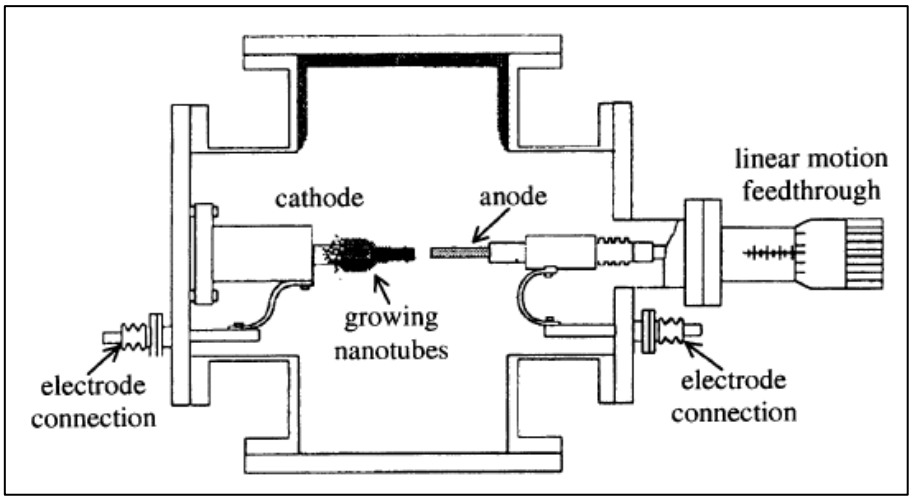

Figure 24 Arc-discharge system used to obtain CNTs.[71]

Laser ablation, the technique firstly used for the production of fullerene by Smalley and co-worker, [52] has been improved for the production of SWCNTs. An evaporation process was used in order to vaporize carbon atoms from a graphitic rod. The graphite source is doped with small amount of Co and/or Ni used as metallic catalysts to obtain SWCNTs. The starting material is vaporized by the laser source at very high temperature, approximately 1200°C under a constant pressure of 500 Torr in argon atmosphere. The carbon atoms finally condense on a water-cooled target generally based on copper. [72] However, both arc-discharge and laser ablation techniques require high amount of energy with respect to the amount of produced nanotubes. In fact it is reported that by using those techniques it is possible to synthesize no more than few grams of CNTs per day. [53], [63], [72] For application in polymer composites, large quantitative of CNTs are required. Moreover, during the above mentioned process, impurities, in form of catalyst particles or amorphous carbon as well as non-tubular fullerene are produced, which requires a further purification steps. For all of those reasons, the arc-discharge and laser ablations are not good candidates as massive CNTs synthesis techniques.

In light of this scenario, different techniques based on gas phase deposition has been developed. Chemical vapor deposition (CVD) involves the decomposition of gaseous carbon species, catalyzed by metallic nanoparticles that are used as nucleation sites for the CNTs growth. Different hydrocarbons are used as carbon species. First of all Kong and co-worker demonstrate the possibility to use methane as purchase gas. SWCNTs were obtained at relative low temperatures (1000°C) with the help of Fe_2O_3 supported on alumina used as catalyst. [73] Nikolaev et al. reported the gas phase growth of SWCNTs using carbon monoxide (CO) as carbon source operating at different temperatures and pressures in the range of 800-1200 °C and 1-10 atm respectively. The highest yield of SWCNNTs was observed by working at 1200°C and 10 atm. [66] Furthermore, at Rice university, Smalley's group refined the process to scale-up the process obtaining large quantities of SWCNTs. The so called HiPCO process (high pressure conversion of carbon monoxide) provides the synthesis of SWCNTs with remarkably purity, and it has been widely used for large-scale production. In fact CVD syntheses are considered continuous processes since carbon source is continually replaced by the flowing gas.[53], [72] Moreover, CVD techniques provide the synthesis of aligned carbon nanotubes with controlled length and diameters. **Figure 25** show the micrograph of multiwall carbon nanotubes obtained via plasma-enhanced chemical vapor deposition (PECVD). [74] As observable,

the plasma, originated by a DC source is able to generate well aligned multiwall carbon nanotubes with high control in tubes length and diameters with a growth direction that is parallel to the plasma. Plasma could be also generated by a microwaves source (MPECVD) as also reported by Bower et al. [75]

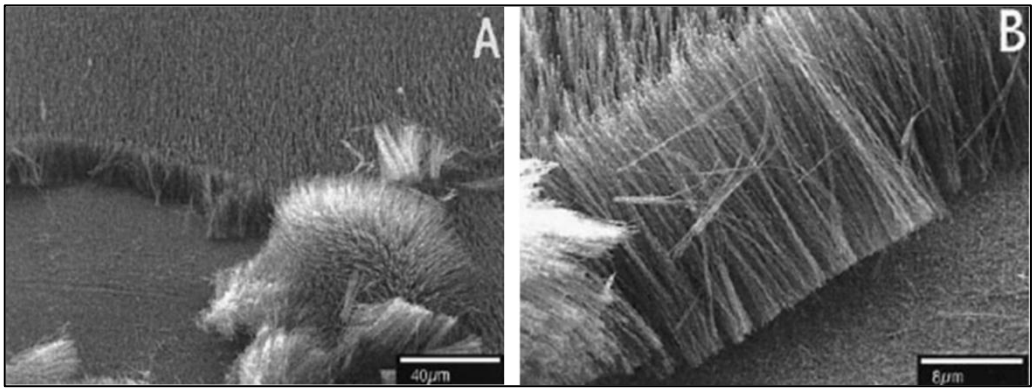

Figure 25 MWCNTs growth via PECVD[74]

Unlike plasma enhanced chemical vapor deposition, conventional CVD techniques could be used to obtain carbon nanotubes by using tubular furnace. The resulting material is characterized by the presence of tangled spaghetti-like nanotubes with diameters that range from 10 to 50 nm and with less control over length, diameter and structure, as observable in **Figure 26**. However, this technique provides an easy synthesis for large scale productions, particularly indicated as filler in polymeric composite materials field. [53]

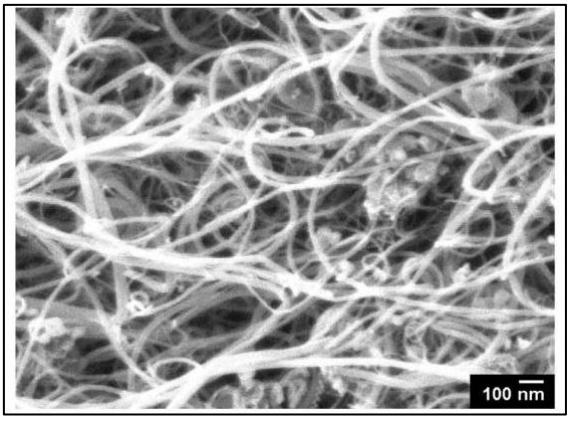

Figure 26 Micrograph of tangled spaghetti-like MWCNTs obtained via conventional CVD technique.

2.1.2 CNTs properties

In spite of its configurations as multi or single walls, as well as independently from synthesis routes, CNTs possess extraordinary physical and mechanical properties.

Since the first isolations, it was expected that the mechanical properties of CNTs could exceed that of all the other materials. In fact, Young's modulus is directly related to the cohesion of the solid, or in other words is strictly related to the chemical bonding of the constituent atoms. Covalent bond is well known as a strong bond that provides elastic modulus higher than 100 GPa, as occurs in graphite, diamond, SiC, BN etc. [76] Different computer simulations were used to estimate CNTs properties. First of all, Overnay at al. reported the structural stiffness of CNTs composed of 100, 200 and 400 atoms, in terms of low-frequency vibrational modes by using ab-initio models. The reported Young's modulus was 1500 GPa, similar to that of graphite. [53], [77], [78] Further, theoretical investigations, on both single and multiwall carbon nanotubes, were conducted by several research groups revealing that the theoretical elastic modulus of isolated CNTs is higher than 1TPa, associated to a tensile strength in the range of 50 to 200 GPa. [53], [61], [62], [72], [78]–[80]. Moreover, Vaccarini et al. [81] observed that the chirality and therefore the tube diameters, do not influence to much the mechanical properties of carbon nanotubes, as observable in **Figure 27**.

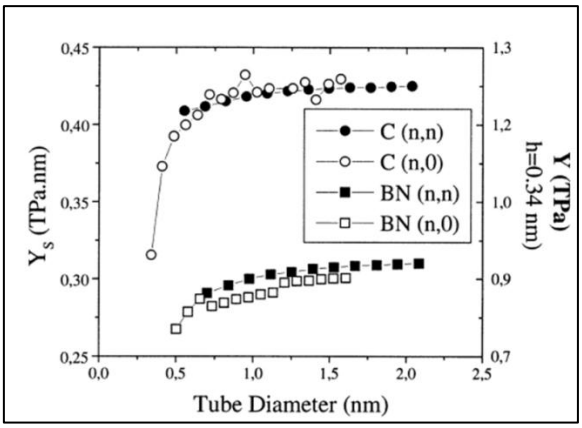

Figure 27 Young's modulus for zig-zag and armchair CNTs. The values are given in the unit of TPa per n (left axis) and converted to TPa (right part). Moreover, BN nanotubes are also reported in order to compare both chiral configurations and modulus values.[81]

The first direct evaluation of the mechanical properties of CNTs, was carried out by Wong and co-worker. [82] By using an atomic force microscopy (AFM) they were able to measure an average value of Young's modulus of 1.28 TPa for arc-discharge MWCNTs in good agreement with the theoretical values. Furthermore, Yu at al. have investigated the tensile behavior of multi and single wall nanotubes by attaching single tube to two AFM tips and loaded under tension as schematically reported in **Figure 28**.

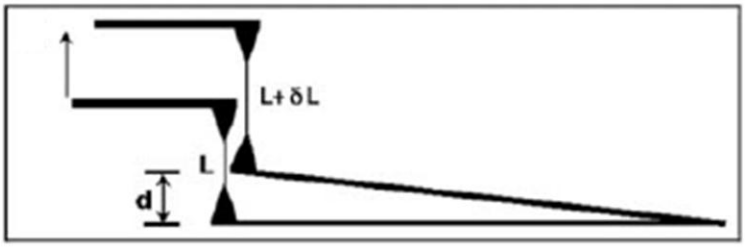

Figure 28 Schematic representation of the experimental set up

They derived an elastic modulus ranging from 270 to 950 GPa for MWCNTs while for SWCNTs it was observed an higher modulus up to 1470 GPa. Moreover the tensile strength was in the range of 11 to 63 and 13 to 52 GPa respectively. [83], [84]. However, different works have been reported on the mechanical properties of carbon nanotubes by using several direct and indirect techniques. [72],[76] The results indicate that in spite of the typology of CNTs as well as the synthesis route, that provides an higher and/or lower amount of defects in the tubes, the strength is one order of magnitude higher with respect to other carbon form and the modulus is higher than 1 TPa, resulting in a promising material for enhancing mechanical properties of many possible matrices.

CNTs, do not show only outstanding mechanical properties. Table3 reports the main physical properties of CNTs, also with respect to other carbon allotrope phases. As observable, their properties do not change to much in the case of SWCNTs with respect to MWCNTs. Electrical mobility, as well as electrical and thermal conductivity exceed those of carbon allotropes and they are coupled to the lowest specific gravity and the highest thermal stability, making them suitable for specific applications.

Property	Graphite	Diamond	Fullerene	SWCNTs	MWCNTs
Specific gravity (g/cm^3)	1.9-2.3	3.5	1.7	0.8	1.8
Electrical conductivity (S/cm)	4000^{p}, 3.3^{c}	10^{-2}-10^{-15}	10^{-5}	10^{2}-10^{6}	10^{3}-10^{5}
Electrical mobility (cm^2/Vs)	$2.0*10^{4}$	1800	0.5-6	$\sim10^{5}$	10^{4}-10^{5}
Thermal conductivity (W/mK)	298^{p}, 2.2^{c}	900-2320	0.4	6000	2000
Coefficient of thermal expansions (K^{-1})	$-1*10^{-6p}$ $2.9*10^{-5c}$	$\sim2*10^{-6}$	$6.2*10^{-5}$	Negligible	Negligible
Thermal stability in air (°C)	450-650	<600	~600	>600	>600

Table3 Physical properties of different carbon allotropes. p=in-plane; c=c-axis.[58]

As was explained in the previous section, CNTs could be ether metallic or semi-conductive, depending on the chiral vectors. Mintmire and co-worker [85] reported a theoretical calculation of the electronic structure of an infinite long fullerene tube (alias SWCNTs) by using a self-consistent method used in principle to treat long chain macromolecules. By using Gaussian-type orbitals, they were able to calculate the valence band of CNTs within a one-dimensional band structure in the first Brillouin zone as reported in **Figure 29**.

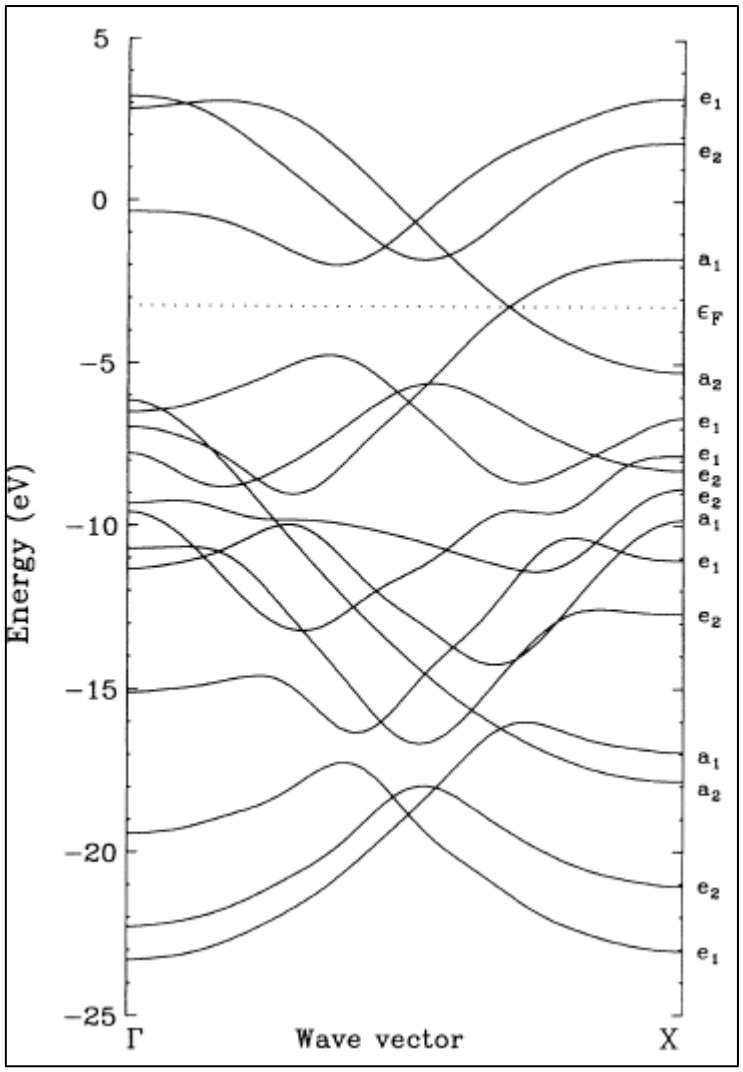

Figure 29 Local-density-functional valence band structure of Fullerene tubule (CNTs). Fermi level is represented by the dotted line.[85]

As observable, at 0.69 of the width of the half Brillouin zone from the origin, a bands crossing occurs (a_1-a_2) reveling a metal behavior. Fermi level (ε_f) coincides with this crossing. At the same time, Hamada et al. showed that the graphitic microtubules, known as CNTs, exhibit different electronic properties depending on the tubule structure. [86] By choosing different chiral vectors, they evaluated the band structure of the different tubes observing that the band gap is tunable by choosing the tubule structure. Their local density functions are reported in **Figure 30**. **Figure 30** (a) and (e) represent the possible tube configurations, obtainable by changing the chiral vectors while (b) and (f) represent the corresponding first

Brillouin zone of graphene sheet and the wave vectors allowed by the periodic boundary condition (n = 6) respectively.

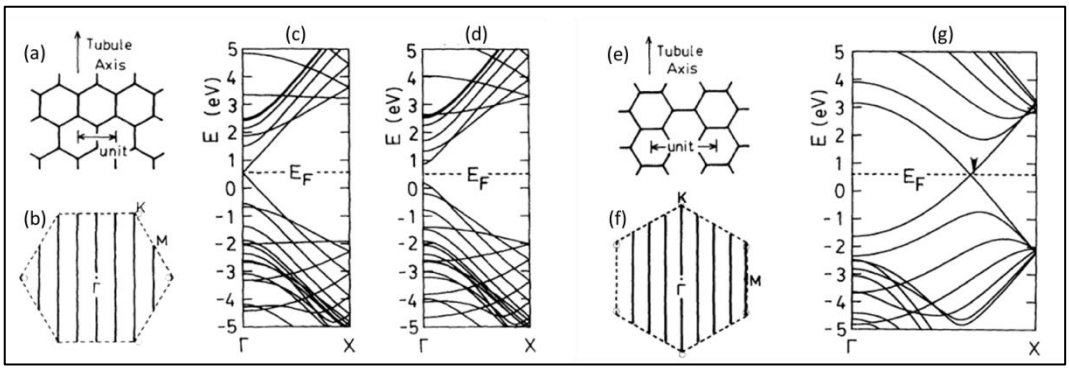

Figure 30 Band structures of CNTs in terms of chiral vectors as explained in the text.[86]

Different tube configuration leads to different band structures. Band structure marked as (c) and (d) in **Figure 30** are related to zig-zag configuration (related to a different tube diameters) while (g) is related to the armchairs nanotubes. [60] In the first two cases, the band structure exhibits an energy gap located at point **Γ**. A drastic change in the energy gap was observed by increasing the tube diameters passing from an energy gap of 8 meV to 0.697 eV by simply increasing of 1 unit the number of construction units on the tube circumference. Moreover, it was also observed a truly metallic behavior with a bands crossing at fermi level, in armchair configuration at **K** point (indicated in figure g as a black harrow), confirming Mintmire and co-worker prediction. [85], [86]. Practically, one third of the nanotubes are metallic, and two third would be moderate gap semiconductors. [53], [60], [72], [78], [86].

These predictions, generated considering interest in the direct evaluation of the electrical conductivity, as well as electrical resistivity of carbon nanotubes. However, initially measurements were very difficult due to the tube nanoscale dimension therefore only bulk conductivity has been measured revealing a electrical conductivity of ~100 S-cm. This value is underestimated since the bulk conductivity is obviously limited by the contact resistance. [87] Four-probe measurement of different isolated nanotubes were firstly reported by Ebbesen et al. [88] The designed experimental setup is reported in **Figure 31**. They observed that for metallic tubes, the current density is higher than 10^6 Acm^{-2}. Moreover, they were able to measure the electrical resistivity of eight different nanotubes with different radius. The obtained result indicates that carbon nanotubes possess

an electrical resistivity value in the range between 10^{-7} to $10^{-8}\Omega$m, further confirmed by several authors. [35], [58], [59], [63], [72], [78], [89]

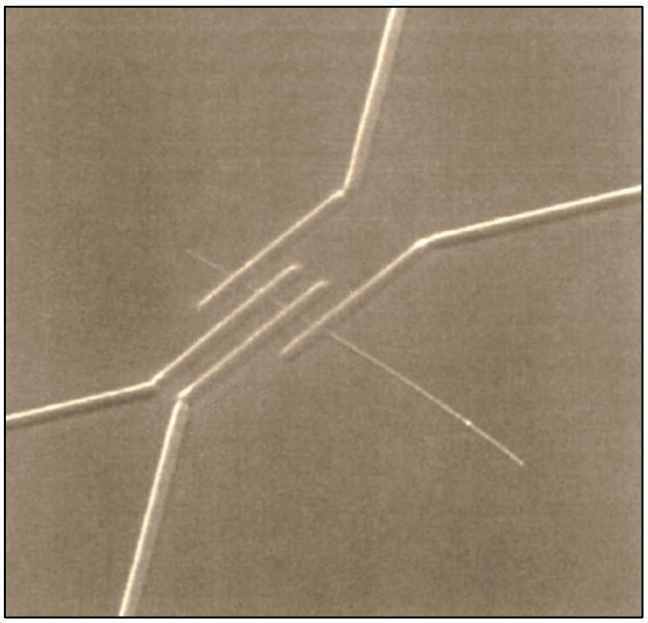

Figure 31 Experimental setup used to evaluate the electrical conductivity of isolated CNTs. A single nanotube is connected to four 80-nm wide tungsten wires.

Thermal conductivity is another important conductive property of carbon nanotubes. As for the electrical conductivity, the main challenge is to determine in an unequivocally way the thermal conductivity value of both SWCNTs and MWCNTs. As for the other non-metallic materials, thermal transport in carbon nanotubes is related to the phonon dispersion and therefore is strictly related to the number of available phonon active modes, phonon-phonon scattering, phonon mean free path as well as lattice defects. [35], [90]

Since the nanometric scale of CNTs is a limitation to the commonly analytic techniques, theoretical simulations were used to predict CNTs thermal transport. Berber and co-worker [91] reported a molecular dynamic simulation for the temperature dependence of thermal conductivity of isolated (10, 10) nanotube. In this work, they observed that CNTs thermal conductivity is proportional to the heat capacity and to the phonon mean free path. At low temperature, phonon mean free path is essentially constant meaning that thermal conductivity is strictly related to the specific heat. CNTs, show an unusually thermal conductivity value of 37000 W/mK at T= 100 K as reported in **Figure 32**. This value is very close to that of pure 99.9% ^{12}C crystal at T= 104 K (41000 W/mK). However at high

temperatures, thermal conductivity is more affected by the phonon mean free path. Due to the Umklapp process, the thermal conductivity decreases with the temperatures increasing as 1/T. At room temperature, CNTs thermal conductivity was evaluated as higher than 6000 W/mK, which is comparable with the hypothetical thermal conductivity of isolated single graphene sheet.

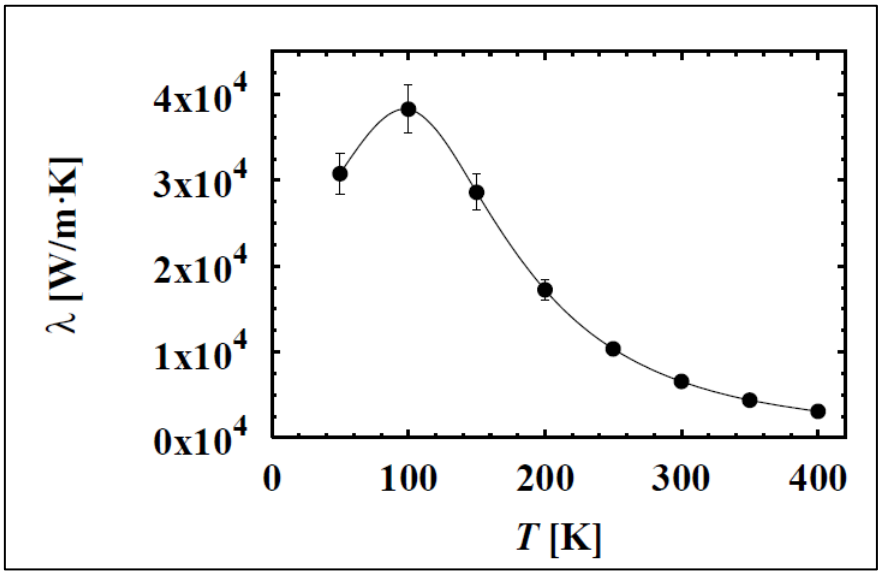

Figure 32Themperature dependence of the thermal conductivity of (10, 10) CNTs[92]

Hone et al. [93] reported the measurements of the thermal conductivity of high purity mats of tangled nanotube bundles, based on single wall carbon nanotubes, in the temperature range of 8 to 350 K. Because of the irregularity of nanotubes samples geometry and because of the assumptions adopted in this study, they observed a room temperature thermal conduction in the range of 1750-5800 W/mK. More important they observed that, despite the linear temperature dependence of the thermal conductivity below 30 K, thermal conductivity is always dominated by phonon conduction and not by electrons as occurs in metals. Few years later, by using an ad-hoc micro-suspended device, based silicon nitride/silicon oxide/silicon multi-layered system, Kim and co-worker were able to determine the thermal conductive properties of isolated MWCNTs. [94] Thermal conductance, measured in the temperature range of 8 to 370 K, increase by several orders of magnitude with the increasing of the temperate, reaching a maximum value of ~ $1.6*10^{-7}$ W/K at RT. The estimation of the thermal conductivity from the thermal conductance measurements, provides at room

temperature, a value of thermal conductivity that exceeds 3000 W/mK. Moreover, it was observed that thermal conductivity is temperature dependent as following:

- At low temperature, between 8 ÷ 50 K, thermal conductivity increases with the increasing in the temperatures following a power law with exponent 2.5
- At intermediate temperatures, 50 ÷ 150 K, the thermal conductivity increase following a quadratic law as T^2
- At high temperature, the temperature dependence deviates from the quadratic law, and has a peak at 320 K.

The temperatures dependence is observable in the lower inset of the thermal conductance graph reported in **Figure 33**

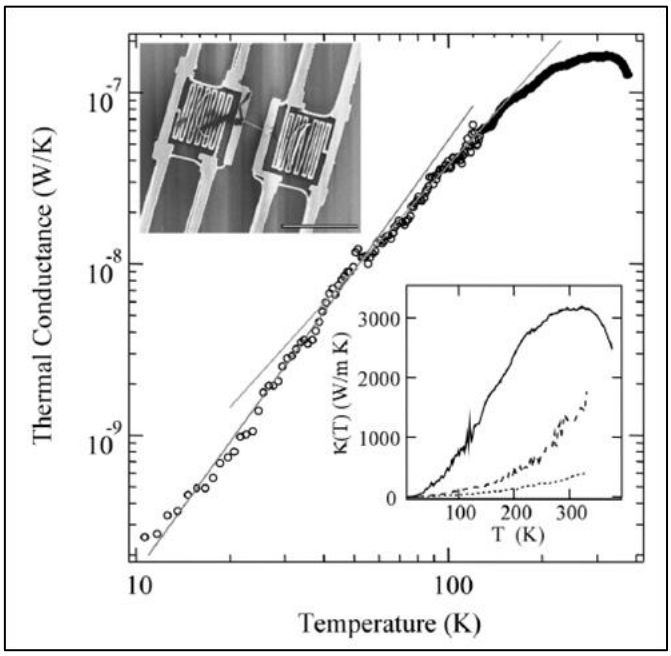

Figure 33 Thermal-conductance of individual MWCNTs as function of the temperatures. The solid lines represent the linear fits of the data reported. In the upper inset is reported the SEM image of the ad-hoc device used in the research, while in the lower inset thermal conductivity is reported. Solid line represents thermal conductivity behavior of isolated MWCNT while broken and dotted line represent the thermal conductivity of a small and large MWCNTs bundles.[95]

Furthermore, thermal conductance of isolated SWCNTs was measured by Yu and co-worker [96] by using a similar device used by Kim. [95] The obtained thermal conductivity is of the same order of magnitude of MWCNTs (at same

temperatures) determined by using the same experimental setup. However, it seems to be lower with a maximum thermal conductivity value of about 2000 W/mK at room temperature. This is due to the fact that the outer MWCNTs wall that make good thermal contact to the thermal bath gives an higher contribution to the thermal transport with respect to the inner tubes and the ratio between the axial to the radial thermal conductivity may influence the conversion of thermal conductance to thermal conductivity, leading to an overestimation of the MWCNTs thermal conductivity value. [95]

2.2 Graphene

Graphene is the 2-dimension carbon allotrope. Carbon atoms are arranged into a honeycomb lattice. As mentioned before, the International Union of Pure and Applied Chemistry recommended referring to the single layer of graphite with the terms “Graphene” as the building block ok graphitic materials. [57]

It could be:

- Wrapped into 0D fullerene
- Rolled up into 1D carbon nanotubes
- Stacked into 3D graphite

as schematically reported in **Figure 34**.

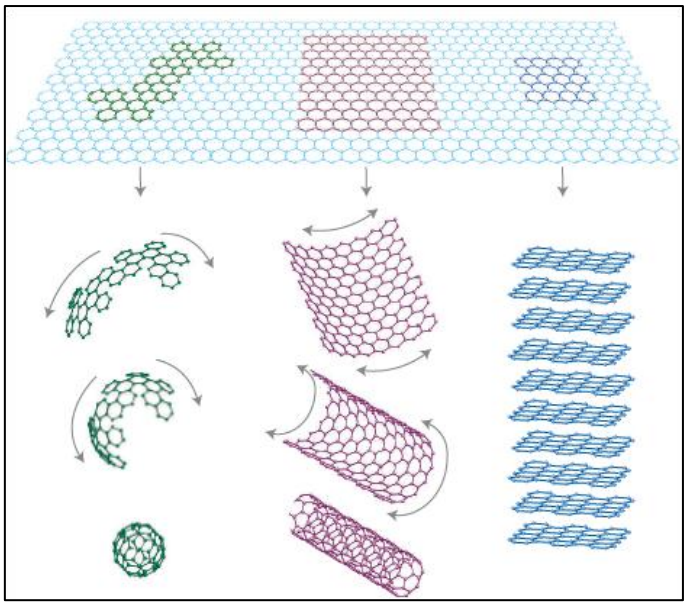

Figure 34 Graphene as the building block of all the other carbon allotropes.[97]

Since graphene is an integral part of larger 3D graphite, it was supposed that single layer could not exist without a graphitic 3D structure. In fact, as argued by several authors more than 80 years ago, 2D materials were thermodynamically unstable, therefore they could not exist. [97] However, in 2004 Novoselov, Geim and co-worker[98] reported the first isolation of an atomic thin film of graphite, well known as graphene. Starting from high oriented pyrolytic graphite (HOPG) and by using a simple peeling method, they were able to isolate and characterize the electronic properties of few and single graphene layers. The employed method is known as "scotch tape methods of making graphene" (see **Figure 35**).

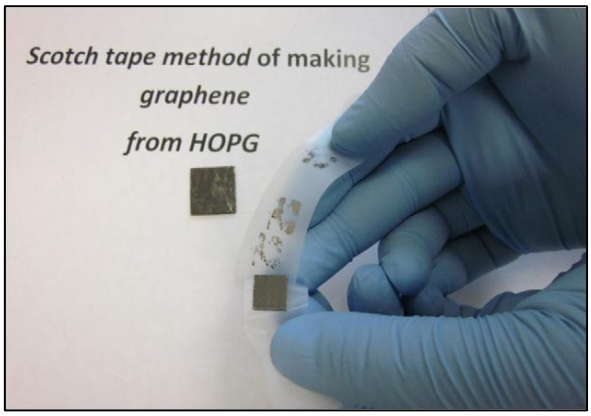

Figure 35 Scotch tape method used to isolate graphene from HOPG[57]

The honeycomb graphene lattice is characterized by the presence of two different interpenetrating triangular sub-lattices, as reported in **Figure 36**. The site of one sub-lattice (green atoms in the figure) is located at the center of the triangles defined by the first three neighbors' carbon atoms (depicted as orange spheres). The resulting unit cell is invariant under a rotation of 120° around any lattice point. Moreover the unit cell is characterized by the presence of two atoms, marker as A and B in the figure. The one *s* and the two in-plane *p* orbitals, provide a strong sp^2 carbon-carbon bond. Its length is 0.142 nm. In contraposition with graphite, the third *p* orbital provide an out of plane hybridized π and π^* bands. [99], [100]

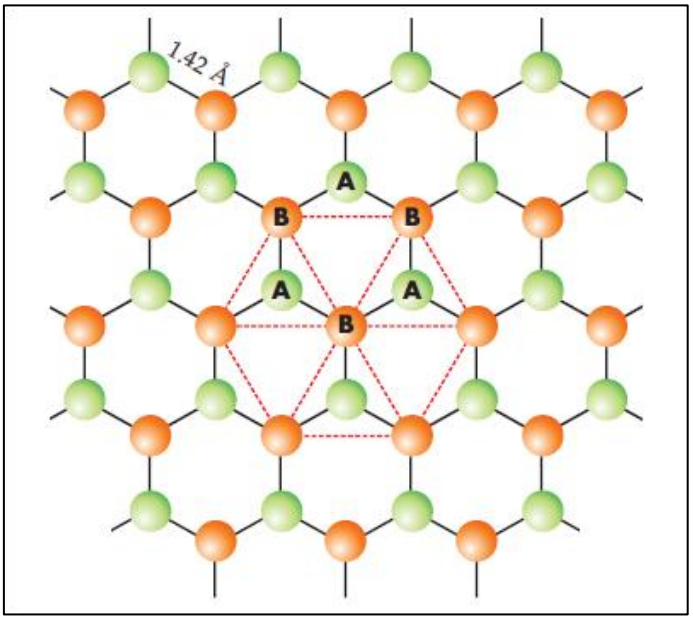

Figure 36 Graphene honeycomb lattice based on two interpenetrating triangular sub-lattice[99]

Since the first observation, it was immediately clear that the obtained material, was not completely based on single graphene layers. By using a combination of optical, electron-beam and atomic-force microscopy, different few-layer materials were observed by Geim and co-worker. [98] Obviously, per definition, only single layer (based on single atomic plane) is considered to be a 2-dimensional material, while one-hundred layers should be considered as 3-dimensional thin film. As happen in the nanotubes case, the term graphene is used in a generic manner in order to indicate many graphene based materials. As reported in literature we must to refer to graphene as the single-atom-thick sheet arranged in a honeycomb based-sp^2 lattice, that is not integral part of a carbon material but is freely

suspended or adhered on a foreign substrate. [101] With the increase of the layers number, it must to refer as bi or tri-layer graphene as free-standing films or flakes consisting of 2 or 3 well-defined and countable graphene layer. Multi-layer graphene is referred to 2-dimensional materials consisting of a small number of well-defined and countable stacked graphene layers. [101], [102] Moreover, it must be refer to graphite nanoplatelets to 2-D materials having a thickness lower than 100 nm. Graphene nanoplatelets are another important class of graphene like materials, based on 2-D structure, with micro-scale lateral dimension, composed of few graphene layers (thickness in << 100 nm). [101] However, it is possible to demonstrate (see graphene properties part) that the limit case between graphene and the approaching to bulky graphite is represented by the presence of 10 graphene layers. [97] Further classification must be done on the basis of the lateral size dimensions, on the basis of the oxygen content (i.e. graphene or graphite oxide) as well as on the mechanism used to fabricate them (exfoliated-graphite, intercalated-graphite, reduced-graphene oxide etc.).

2.2.1 Graphene and graphene like materials synthesis

Starting from the first graphene isolation, different techniques were developed to obtain graphene and graphene like materials. Essentially two different approaches have been used:

- Top down approach refers to those processes by which it is possible to obtain graphene and graphene related materials starting from graphite
- Bottom up approach refers to those processes by which graphene and graphene like materials are produced starting from carbon precursors.

Typical examples of top down approach are the mechanical as well as chemical exfoliation and the chemical synthesis while the most important bottom up syntheses are represented by the graphene epitaxial growth, chemical vapor deposition and other synthetic routes such as pyrolysis and unzipping carbon nanotubes. A schematic flow chart is reported in **Figure 37**.

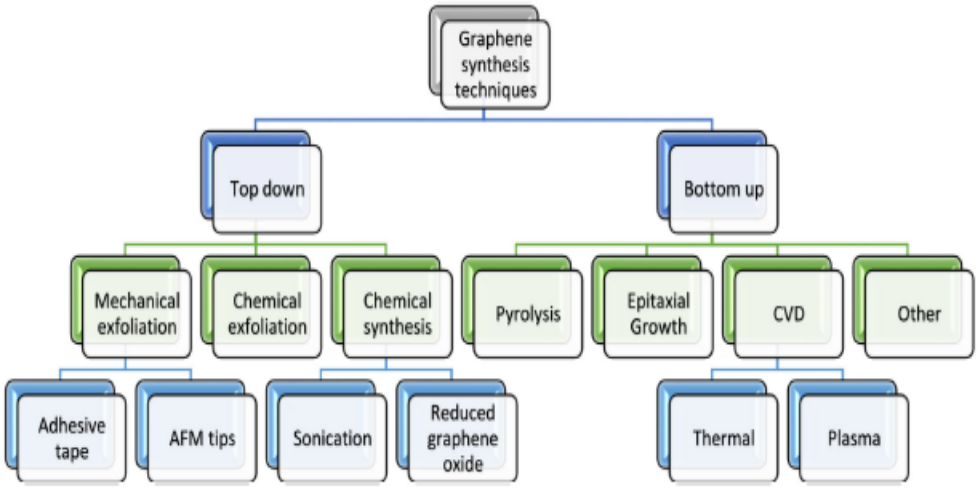

Figure 37 Flow chart of graphene synthesis[103]

The first recognized method to isolate graphene was made by top down approach. [98] The energy bond associate to the van der Walls forces established between two graphene planes in 3D graphitic structures were estimated to be equal to $2eV/nm^2$. An external force, provided by a longitudinal or transverse stress could be able to separate one mono-atomic layer from graphite. The required force is in the order of magnitudes of ~300 $nN/\mu m^2$. [103] Starting from HOPG, single crystal graphite as well as natural graphite, very different exfoliation methods could be used in order to obtain graphene sheets of different thickness. [57], [72], [104], [105] The obtained materials vary in terms of thickness and size where the size range from nano to micro scale. [103] Even though mechanical exfoliation provides well defined high quality single and few layer graphene, its yield is too low for commercial productions. Chemical exfoliation is one of the most commonly used methods to obtain graphene starting from graphite bulky materials. Chemical exfoliation is a two-step process. In the first step graphite is dispersed in a mineral acids mixture which initiates cleaving process. The acid molecules can penetrate within the graphene layers providing an increase in the graphene distances and reducing the van der Walls force. In the second step, the intercalated graphite is heated or sonicated to get single graphene layers. Further purifications are needed. Single layer of graphene oxide could be obtained by Hummer's methods involving strong oxidizing agents such as $KMnO_4$ and $NaNO_3$ in H_2SO_4/H_3PO_4 solutions. Under moderate ultrasonication, the oxide layers are exfoliated in water resulting in single or few layers graphene oxide (GO). The resulting material is characterized by the presence of different functional group such as hydroxyl, carboxyl and epoxy groups which are present on the edges or on

the basal planes of graphene sheet. Due to the presence of oxygen based groups, GO is strongly hydrophilic (respect to the hydrophobic graphene or graphite) resulting in a well dispersed material in water solution. However, due to the presence of extraneous species on the graphene sheets, physical properties are to worse with respect to single and or few layer graphene. Further GO reduction is required. To do this, thermal annealing (T > 1000°C) as well as chemical reduction has been proposed. [57], [104] Chemical reduction of GO is one of the most commonly procedures to prepare high quantitative of graphene. Park et al. [106] reported a simple method to reduce graphene oxide in water solution by using KOH. The addition of KOH to graphene oxide solution, provides the formation of slightly darker suspension caused by the reaction between potassium hydroxide and oxygen group anchored on the graphene sheets resulting in an extensive coated graphene with negative charges. The KOH treated graphene oxide was than mixed with a hydrazine solution (1:8 by weight). Hydrazine provides a good stability of the reduced graphene suspension in water solution up to 7 mg/ml. This methodology is recognized as a good procedures to obtain large quantitative of single layer graphene. Schematic representation of Park's methods is reported in **Figure 38**.

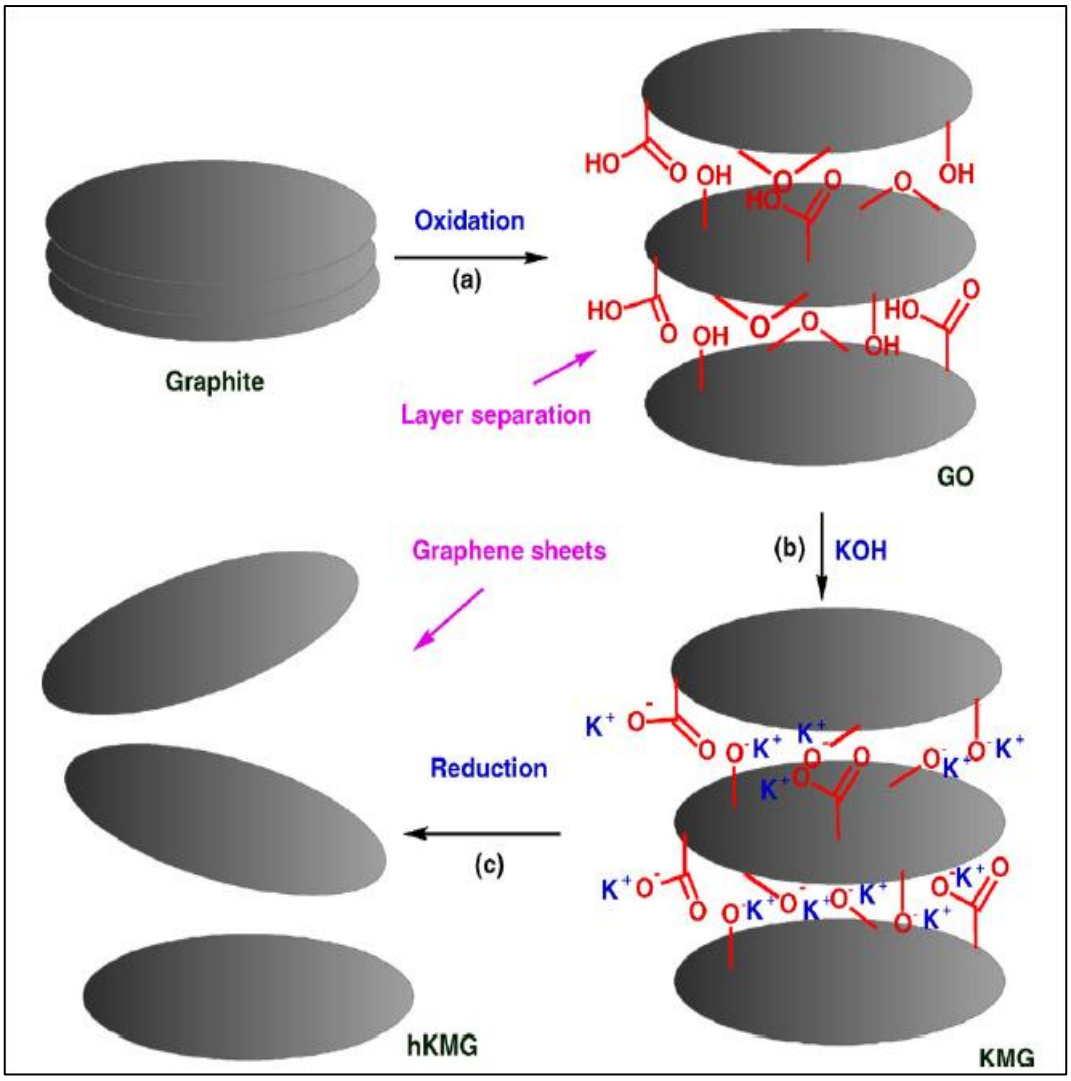

Figure 38 Park's method for obtaining a homogeneous aqueous solution of graphene sheets starting from graphite.[103]

Bottom up approaches represent a well-known class of techniques that provide good thickness control, large size and high quality single and few layer graphene.

Chemical vapor deposition is the most commonly used bottom-up approach. CVD provides large scale synthesis of single and few layers graphene, with low amount of defects. Differently from carbon nanotubes synthesis, in which metal nanoparticles are used as catalyst, in the production of graphene a metal foil is used to catalyze the process. [105] Due to the "dimensional effect" the size and the shape of the obtained sheets are strongly affected by the foil shape and dimension. [72] Somani et al. reported the first synthesis of graphene sheet by

using a thermal CVD by using camphor as carbon precursors and Ni foil as metal template in a moderate operating temperature range (750-800°C). Furthermore, different metal substrates and many strategies were adopted in order to have a better control on the layer numbers, and to minimize the graphene folding. Chae et al. [108] reported the synthesis of highly crystalline few-layer graphene. By optimizing the CVD parameters, instead of growth time, quenching rate, and carbon source, they were able to obtaining high crystalline large-area (up to 1 cm^2) few layer graphene. The substrate used as catalyst was a poly-Ni substrate while a mixture of C_2H_2/H_2 was used as carbon source. Li and co-worker reported the possibility to substitute the nickel catalyst with copper foil. [109] By using this new substrate, they were able to obtain film predominantly composed by single layer graphene with less than 5% of two or three layer flakes. Furthermore, Bhaviripudi developed a synthesis of graphene flakes by using atmospheric pressure and low pressure CVD (APCVD and LPCVD respectively) by several gas mixtures as carbon sources and copper foil as catalyst. Cu-LPCVD synthesis provides the formation of large area graphene sheet with thickness uniformity, confirming the previously study of Li and co-worker. Cu-APCVD provides graphene growth that varied from a monolayer to multilayer domain depending on the concentration of the gas source (methane). At a concentration of few ppm, the resulting material is characterized by the presence of large area single layer while increasing the methane concentration leads to the synthesis of multilayer graphene structures. [110] Plasma enhanced chemical vapor deposition was also reported as another route of graphene synthesis at a lower temperature (600-700 °C) with respect to traditional thermal CVD. The advantages of plasma deposition include short time deposition (lower than 5 minutes), and lower operation temperature. [57] However, to complete the CVD process, the deposited metals were etched in order to remove the graphene layers and transfer them on the new substrate, minimizing the complicated mechanical exfoliation process.[57], [72], [103], [104], [111]

Other bottoms up techniques, such as epitaxial growth of graphene on single crystal of silicon carbide and/or pyrolysis of graphene, were reported in literatures. However, as the unzipping CNTs methods, those approaches are not good candidates to obtain single or few layer graphene with high purity levels at industrial levels.

2.2.2 Graphene properties

Before starting to talk about graphene properties, a special mention must be done on the relation between 3D, 2D and 1D materials, as graphite, graphene and CNTs. Graphene could be treated as a single sheet of graphite or as an unrolled carbon nanotubes. The rapid progress on graphene synthesis and property characterizations has certainly benefited from the mature research on the related 3D or 1D structures. Therefore, in few years many important graphene properties were investigated, including extremely high charge (electrons and holes) mobility (200,000 cm^2/Vs), thermal conductivity (5000 W/mK), and the high strength (130 GPa), coupled with the high theoretical specific surface area (2600 m^2/g), and half integer quantum Hall effect even at ambient temperature. Moreover, it is transparent to the visible light. [57] However, as for the CNTs case, the most important exploited properties in the polymeric composite materials field are the mechanical, thermal and electrical properties. [112]

In general, mechanical properties of a crystalline solid are controlled by the characteristics of its pristine crystal lattice and structural defects like dislocations and grain boundaries. [113] Since graphene is based on sp^2 covalent bond, it was predicted that its mechanical properties could exceed those of all the others materials. Starting from theoretical studies above mentioned on the prediction of carbon nanotubes mechanical properties, several researchers have determined the intrinsic mechanical properties of single, and few layer graphene by using several techniques. First of all Lee et al. [114] reported the measurement of the elastic properties and the intrinsic strength of single graphene layer by using atomic force microscope nano-indentation techniques. A monolayer was deposited on Silicon substrate. This substrate is characterized by the presence of circular holes, providing an empty space under the graphene layer. By using a diamond based AFM tip, they were able to characterize the elastic modulus and the intrinsic strength of single layer graphene. Schematic representation of the experimental set-up is reported in **Figure 39**. The obtained values (E=1.0 TPa, σ= 130 GPa) are in good agreement with theoretical computer simulation. [113], [115]

Further investigations (by using the same technique) performed on bi-layers and tri-layers graphene revealed that the elastic modulus and intrinsic strength are almost constant. In fact it was observed that the Young's modulus of single, bi and tri-layer graphene are all identical, within the experimental error, and are equal to the modulus of bulky graphite. [116] However, mechanical properties are strongly affected by the presence of defects. Typical defects in graphene are: (i)

vacancies, (ii) dislocations, (iii) Stone-Wales defects and (iv) grain boundaries (GBs) composed of dislocations. [117]–[120] Dislocations can serve as carriers of plastic flows, while GBs are responsible of graphene strength decrease. [113]

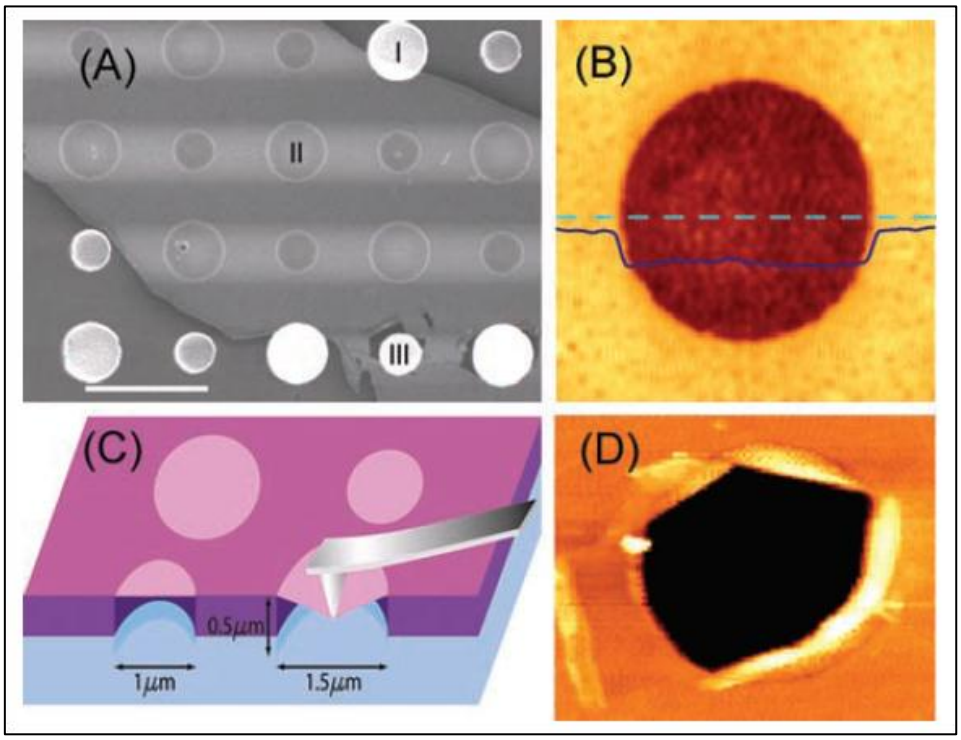

Figure 39 Schematic set up used to measure graphene mechanical properties. (A) Graphene layer deposited on Si substrate. (B) AFM non in contact measurement of graphene deposited on silicon hole substrate, (C) schematic representation of experimental set up, (D) performed graphene layer (AFM images) [114]

In addition to mechanical properties, graphene shows interesting physical transporting behaviors as reported in **Table 4**

Property	Graphite	Graphene	SWCNTs
Electrical conductivity (S/cm)	4000^{p}, 3.3^{c}	10^{4}	10^{2}-10^{6}
Electrical mobility (cm^2/Vs)	$2.0*10^{4}$	$2.0*10^{6}$	~10^{5}
Thermal conductivity (W/mK)	298^{p}, 2.2^{c}	~5000	6000
Coefficient of thermal expansions (K^{-1})	$-1*10^{-6p}$ $2.9*10^{-5c}$	Negative	Negligible
Thermal stability in air (°C)	450-650	>600	>600

Table 4 Main physical graphene, graphite and SWCNTs properties.

As mentioned in the introduction part, graphene lattice could be represented as two interpenetrating triangular sub-lattice. The single *s* and the two in plane *p* orbitals provide strong covalent bonds while the third out of plane *p* orbital hybridize to form π (valence) and π^* (conduction) bands. It is possible to demonstrate that in the Block band descriptions, the orbital energies depend on the momentum of the charges in the first Brillouin zone. In it, the valence and the conduction bands are decoupled from the σ-σ* bands providing that π and π* are closer to the Fermi level forming a conical valleys that touch at **K** and **K'**[99] as reported in **Figure 40**.

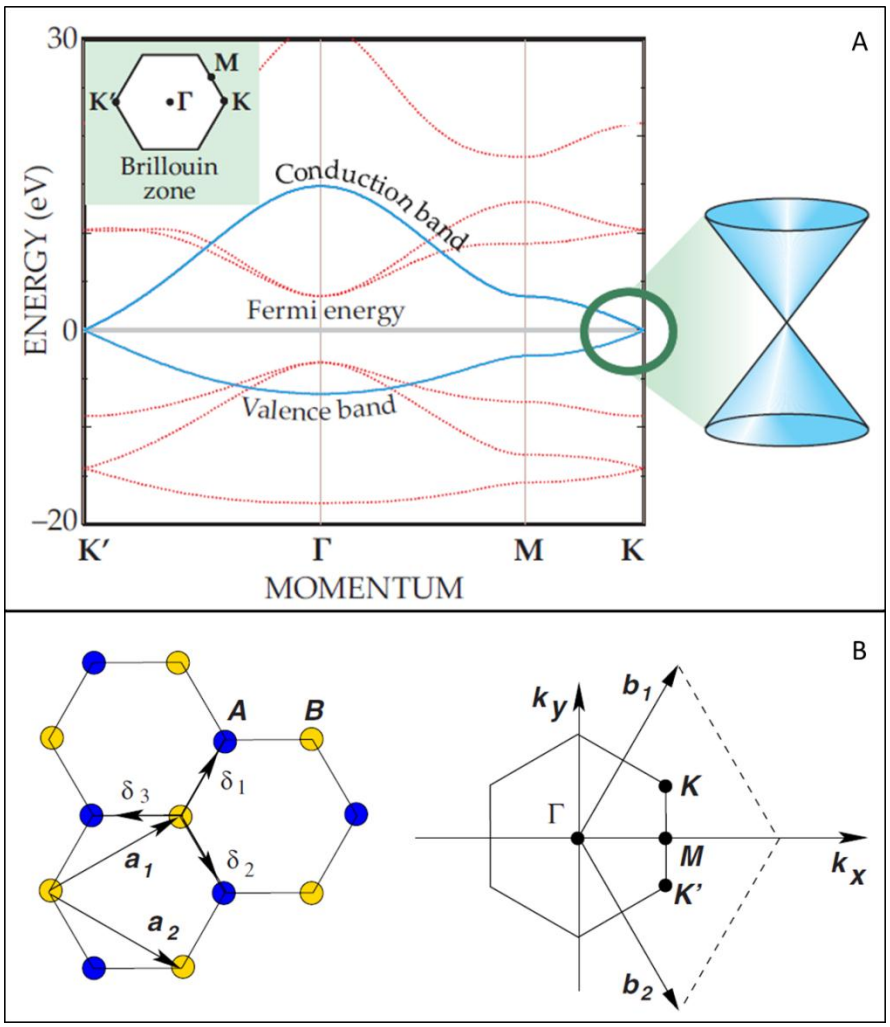

Figure 40 (A)Band structures of graphene, (B) Representation of the honeycomb lattice of graphene as two interpenetrating sub-lattices (left) and its relative Brillouin zone. [99][121]

As observable, graphene is a zero gap semiconductor in which valence and conduction bands (that are linear function of the momentum) meet at the most symmetric point **K** and **K'** in the first Builloun zone (reported in **Figure 40** b). The electron speed is independent from the momentum and it is a constant (10^6 m/s) likely the phonon speed *c* is. From the quantum mechanics point of views, electrons in graphene, are represented as mass-less particles (also vanishing their intrinsic small mass) described as Dirac fermions able to cross between valence and conductive bands at the **K** boundaries. [97], [99] This particular band structure, provided by the honeycomb lattice symmetry, confers particular electronic properties to graphene such as ambipolar field effect. This effect is

related to polar inversion of the charge carriers as function of the applied external voltage. In positive gate bias Fermi level rise above **K** and **K'** points promoting electron population into conduction band, while when the applied voltage is negative the Fermi level drop below, promoting holes transport in the valence band. [57] Charge carriers, electrons as well as holes, can be tuned continuously in concentration $n_e=n_h > 10^{13}$ cm^{-2} associated to a mobility carriers that exceed 15000 cm^2/Vs even at ambient conditions. However, charge mobility is weakly affected by the temperatures, meaning that it is limited by impurities scattering. [97] Electrical conductivity estimated up to 10^4 S/cm (see table 4) is provided by those exceptional relativistic conductive behaviors. However this band structure and therefore this behavior is related to single layer graphene that for several applications in polymeric composites materials (such as industrial polymers master-batch preparation) is not a well suitable candidate. On the contrary, graphene nanoplatelets could be more indicated to overcome this drawback. As mentioned before, with the term graphite nanoplatelets it is possible to indicate a class of graphene like materials, based on 2D, structure with thickness lower than 100 nm. If the thickness is much less than 100 nm (i.e. 10 nm) the graphene like material is referred as graphene nanoplatelets. Remembering that, interlayer distance between stacking graphitic layer is 0.34 nm, graphite nanoplatelets could be represented as a thin film composed by ~300 graphene layers. However, several authors considered 100 graphene layers as a thin film of 3D materials opening questions on how many layers are needed before the structure is regarded as 3D. It was shown that the electronic structures, rapidly evolve with the layer numbers approaching the 3D limit at 10 layers. [97] In fact, Partoens and Peeters [122] reported a theoretical study in which they examined the band structures near **K** point for bi, tri and few layers graphene. The obtained band structures are reported in **Figure 41** for single layer (a), bi-layer (b) and bulky graphite (c) respectively. As mentioned until now, single layer graphene show a band crossing at **K** point as zero-gap conductors. The upper insert in **Figure 41** (a) also show the linear dependence between energy and momentum near the symmetric point. While single layer is characterized by the presence of one energy level, bi-layer graphene is characterized by two different energy levels, providing a parabolic energy-momentum relationship. There is a clear small band overlap between valence and conduction bands of only 1.6 meV provided by the interaction between two sub-lattice "B-atoms". The system based on two graphene layers, is a semimetal but with an extremely small band overlap. This overlap is also present in bulky graphite. However, graphite show three distinct energy band E_1, E_2, E_3 as observable in figure. Energy band E_3, is twofold degenerate leading to a band

overlap of ~41 meV which is 25 times larger than the overlap of bi-layer graphene. By considering how the band structure near **K** point evolves to graphite structure, researchers were able to estimate the band overlap (difference between the last and the first building E_3 level) of finite layer system. The horizontal line in **Figure 41** (d) is related to the limit of bulky graphite. Is possible to observe that for more than 11 layers the difference between few layer graphene and graphite is smaller than 10 % demonstrating that the approaching 3D electronic structures of graphite occurs at 10 graphene layers.

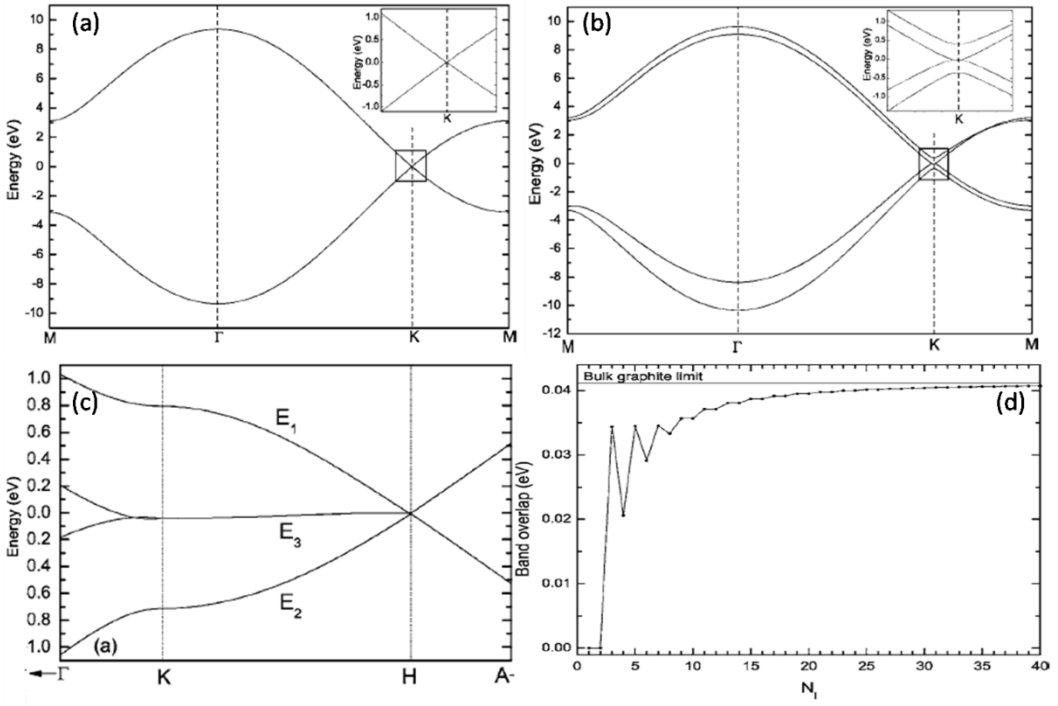

Figure 41 Calculated band structure of (a) single graphene layer, (b) bi-layer graphene and (c) graphite. The upper insert in (a) and (b) are a focus near K point respectively. (d) is the energy band overlap value estimated. Horizontal line at 41meV is related to the graphite bulky limits.

As reported in table 4, graphene thermal conductivity is another important intrinsic characteristic that could be exploited to increase the thermal conductivity of polymers.

Starting from the end of the last century, thermal conductivity of graphite and related materials (i.e. amorphous and pyrolytic carbon) has been studied due to its

fundamental importance in nuclear industry. **Figure 42** shows the thermal conductivity values of bulk carbon allotropes as function of temperature.

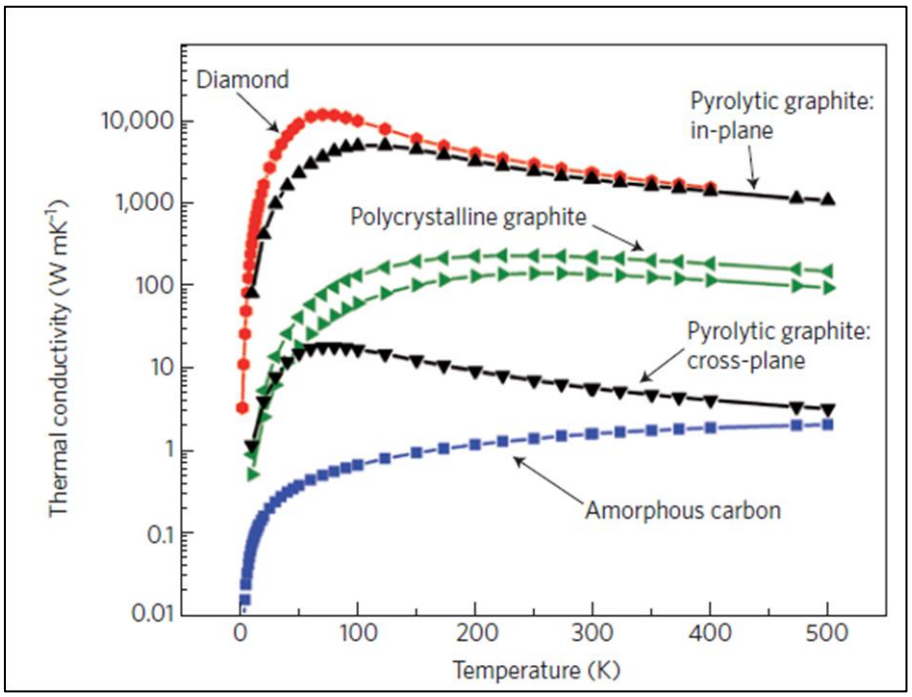

Figure 42 Thermal conductivity of bulk carbon allotropes as function of the temperatures. [33]

In all bulk carbon allotropes, thermal conduction is dominated by the acoustic phonons. As observable, in amorphous carbon, thermal conductivity varies from ~0.01 W/mK up to ~2 W/mK and it increases monotonically with temperature as expected for disordered materials. Diamond shows the highest value of thermal conductivity. At room temperature it is estimated higher than 2000 W/mK. Pyrolytic graphite and polycrystalline graphite are refer as high purity oriented pyrolytic graphite and high-purity pitch-bonded graphite respectively. As observable from the figure pyrolytic graphite has an in-plane thermal conductivity that is more than two orders of magnitude higher with respect to its cross-plane conductivity. Despite of one order of magnitude in difference between pyrolytic and polycrystalline graphite, the difference between cross and in plane thermal conduction, in polycrystalline graphite, is less pronounced. Both the materials are polycrystalline. However, pyrolytic graphite is based on highly oriented crystallites providing higher thermal conductivity while polycrystalline graphite is based on different large not-in-plane oriented crystallites leading to a higher amount of incoherent scattering process but resulting in a lower discrepancy

between cross and in-plane thermal conductivity. This means that, the thermal conductivity of graphitic planes is strongly affected by grain size and by their orientation and, of course, by their quality and purity. [33]

Ferrari and co-worker [123] observed the evolution of the Raman spectra from single to multi-layer graphene demonstrating the possibility to estimate the layer numbers from the Raman shift. It was demonstrated from several authors [124], [125] that the temperature variation of Raman spectra of carbon based materials, such as CNTs, is related to a downshift of the mode frequencies with the temperature increasing. Starting from these results, different efforts have been made on the use of Raman spectroscopy as a tool to evaluate the thermal conductivity of graphene and graphene like materials. First of all, Calizo et al. [126] reported for the first time the temperature dependence (in the range between -190° to 100° C) of the Raman spectra of graphene and multi-layers graphene observing a linear dependence between G peak position with the increasing temperature for both single and bi-layer graphene as reported in **Figure 43**.

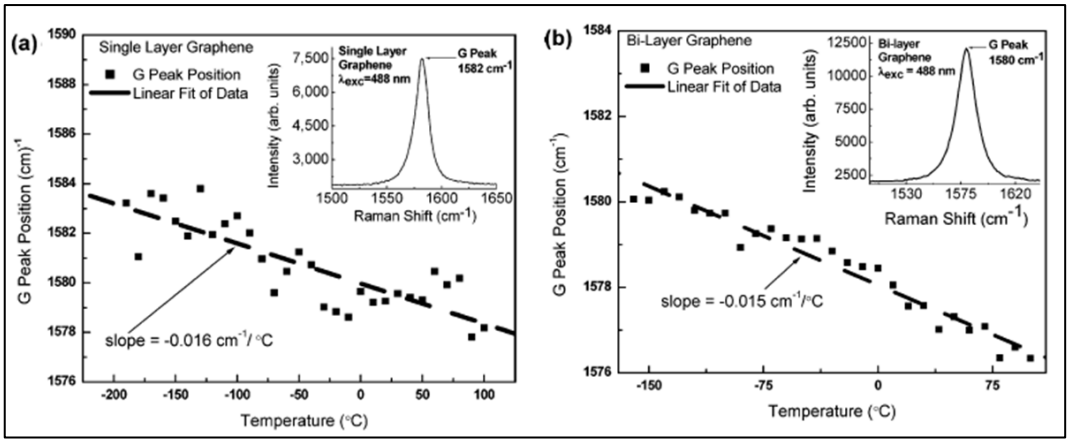

Figure 43 Raman G frequency for (a) single and (b) bi layer graphene as function of temperature.

The relationship between mode frequency and the temperature is represented by $\omega = \omega_0 + \chi T$ where the temperature coefficient χ (curve slope) determines the frequency shift (ω) of the G peak mode (ω_0) when the sample temperature is increased by 1 K.

Starting from this observation, Balandin and co-worker reported the thermal conductivity analysis of suspended single graphene layer by using optothermal Raman technique. In fact the frequency dependence of G peak Vs temperature

allows us to convert Raman spectra into "optical thermometers". [33] Experimental setup is reported in **Figure 44** in which single graphene layer is suspended on a Si/SiO_2 hollow substrate clamped to a heat sink. The temperature increase (ΔT) is related to the heating power (ΔP) provided by the laser source. Locally, ΔT is determined by $\Delta T=\Delta\omega/\chi$. It is possible to demonstrate that the thermal conductivity could be evaluated by knowing the peak shift provided by the power source variation multiplied by temperature coefficient and by several geometric factors.

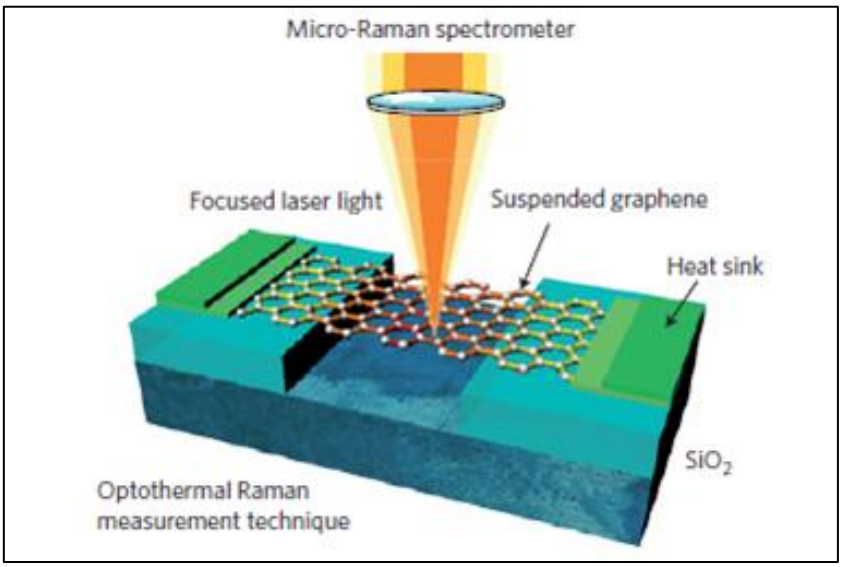

Figure 44 Experimental setup used to determine the thermal conductivity of single layer graphene by Balandin and co-worker.

By using optothermal Raman spectroscopy, Balandin and co-worker were able to estimate a thermal conductivity of single layer graphene as high as 5000 W/mK. [127] Moreover they also confirmed that the thermal conductivity in graphene is carried out by phonon dispersion and that the electrons contribution is negligible. Furthermore, Ghosh and co-worker reported the optotermal Raman analysis for different few layer graphene (from n=2 up to n=10 were n indicates the number of layers). Room-temperature thermal conductivity is reported in **Figure 45**. As observable, starting from the maximum thermal conductivity, previously reported from Balandin for single graphene layers, [127] a decreasing in the thermal conductivity was observed related to the increasing of the layers number reaching the bulky graphite limits at n=4. This is due to an increasing of the available phonon dispersion modes resulting in a transverse component different to zero (as occurs to single layer).

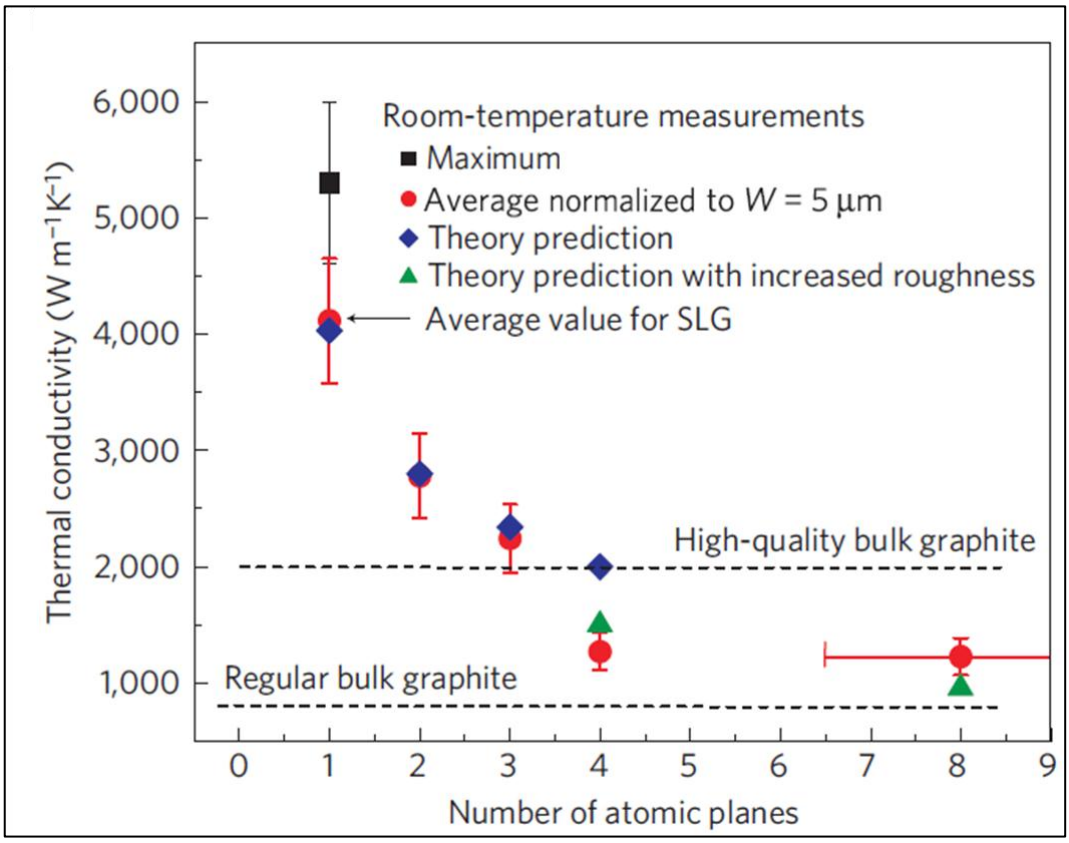

Figure 45 Few-layer graphene thermal conductivity as function of the number of layer.

Chapter 3

Materials and methods

In this chapter, the lists of the starting materials and the methods used to fabricate and to characterize the nanocomposites are reported.

In this thesis work, several polymers were used as matrices and different carbon based nanomaterials were used as fillers. The polymer-filler coupling was chosen according to the final purpose.

This chapters is divided in three main sections according to the three main chapters dealing with result and discussion.

3.1 GNPs based polymeric composite materials with enhanced thermal conductivity

To investigate the effect of the graphene nanoplatelets on the thermal conductivity behavior of polymeric composite materials, different polymers (both thermoplastic and thermoset) were used as matrices while three different graphene nanoplatelets and a natural graphite were used as filler.

The polymer matrices, used as starting materials were:

- Polypropylene, PP HP500N purchased from Basell
- Acrylonitrile Butadiene Styrene, ABS Cycolab by Sabic
- Thermoplastic polyurethane, TPU Desmopan from Bayer

- Bisphenol-a-epichlorhydrin epoxy resin coupled with Triethylenetetramine used as curing agent, Struers EpoFix purchased from Struers.

The carbon based materials used as fillers were:

- Graphene nanoplatelets GAbcr, purchased from ABCR Gute Chemie, with a thickness of 6 to 8 nm x 5 µm wide
- Graphene nanoplatelets GAbcr_25, purchased from ABCR Gute Chemie, with a thickness of 6 to 8 nm x 25 µm wide
- Graphene nanoplatelets Grade 4, G4 produced by Cheaptube Inc. whit a plane dimension of 1 to 2 µm and thickness lower than 4 nm when exposed to high shear or sonication.
- Natural graphite flakes, purchased from Alfa Aesar with median size of 7 to 10 µm, metal basis with a purity level of 99%.

In **Table 5** the specific properties of the various fillers are reported.

Filler	Short name	Thickness (nm)	Wide (µm)
GNPs Abcr	GAbcr	6-8	5
GNPs Abcr	GAbcr_25	6-8	25
GNPs Grade4	G4	< 4	1-2
Graphite	Graph	>10	7-10

Table 5 Main filler properties.

All the purchased materials were used without further modification and purification.

Fillers characterization was performed by exploiting several techniques:

- **Field Emission Scanning Electron microscopy:** Fe-SEM from Zeiss Merlin to investigate fillers morphology at different magnification
- **X-Ray Diffraction:** XRD measurements were performed using a Siemens D500 diffractometer (Cu-Kα radiation) in the range between 10 to 80 2θ degree with a $\Delta 2\theta$ step of 0.02° for a step time of 2 seconds

- **Raman spectroscopy:** the spectra were collected by means of a Renishaw Ramascope MicroRaman, 514.5 nm excitation in the range between 500 to 3500 cm^{-1}
- **Thermogravimetric analysis:** TGA was performed in inert atmosphere (Ar) with a Mettler-Toledo TGS/SDTA851e instrument in the temperature range between 25 to 700 °C with a heating rate of 10°C/min.
- **Filler density:** it was measured using an automatic density analyzer Ultrapyc 1200e from Quantachrome industries. *He* was used as gas probe at 18 psi.

To process thermoplastic composites, the melt-blending technique followed by the injection molding process was used. First of all, the required amount of polymers and fillers were mixed together in an internal mixer Brabender operating at 190 °C for PP and TPU or at 240 °C for ABS. Since the loading process was conducted at 30 rpm, the mixing process was conducted at 60 rpm for 3 minutes. The obtained composites, were re-granulated by means of a RSP 15 open-type rotor granulator made by Piovan. The obtained pellets were finally process with a Babyplast injection moulding machine, operating on molten materials temperature of 190 °C for PP and TPU and 240 °C for ABS. The injection time was of 7 seconds at 75 bar and 6 second at 55 bar for a total time cycles of 20 seconds in order to obtain the final dog-bone specimens (ISO 527 standard, specimens 5A). The processing parameters were selected in according to the supplier datasheet.

Thermoplastic based composites were characterized by means of:

- **Optical microscope:** Leica DMI 5000 M. A surface, parallel to the injection molded flow was observed at 200 X after polishing process by means of 1 μm diamond paste.
- **Field Emission Scanning Electron microscope:** Fe-SEM from Zeiss Merlin. Cryofracture surface was observed. To avoid charging, a few nanometers layer of chromium was deposited on the sample.
- **X-Ray Diffraction:** XRD measurements were performed using a Siemens D500 diffractometer (Cu-Kα radiation) in the range between 24 to 29 2θ degree with a $\Delta 2\theta$ step of 0.02° for a step time of 2 seconds
- **Tensile test: it** was carried out at room temperature on dog-bone samples by using a Sintech 10D testing machine. An experimental procedure according to ISO 527 standard was adopted. Young's modulus, yield

strength and elongation at break measurements were determined by using an extensometer with a gauge length of 50 mm at a crosshead speed of 10 mm/min.

- **Thermogravimetric analysis:** TGA was performed in inert atmosphere (Ar) with a Mettler-Toledo TGS/SDTA851e instrument in the temperature range between 25 to 700 °C with a heating rate of 10°C/min. DTG curves, were calculated fromTGA thermograms. TGA was also used to evaluate the degradation process of the polymeric composites, using an isothermal treatment carried out for 90 minutes at the starting degradation temperatures.
- **Differential scanning calorimetry:** DSC were performed with a Netzsch DSC 204 F1 Phoenix System in the temperature range from -50 to 250 °C for PP and PP-based nanocomposites, and for TPU and TPU-based nanocomposite, and from 30 to 350 °C for ABS and ABS-based nanocomposites, with a heating/cooling rate of 10°C/min under nitrogen flow (50 mL/min). For each experiment the sample was heated from starting to final temperature and then cooled for two times. The first heating/cooling cycle was performed in order to eliminate the thermal history of the samples. The thermal transitions of the materials studied were measured on the second heating/cooling cycle.
- **Thermal conductivity:** it was investigated at room temperature using the Hot Disk Thermal Constants Analyser equipment (Hot disk TPS 2500). Each sample was measured five times, and the obtained data were processed as function of the sample density in order to obtain the specific thermal conductivity.

To process thermoset materials several dispersion processes were adopted. First of all, the stoichiometric amounts of the epoxy oligomer and the curing agent were mixed together. The filler was added in order to create a mixture which was then processed accordingly to the following different dispersion techniques.

- **Hand mixing**. The mixture was manually mixed for 2 minutes with the help of a glass rod.
- **Ultrasound sonication bath.** After a first “hand mixing” process, the mixture was processed by means of an ultrasonic bath for 15 min by using a Soltec sonica ultrasonic cleaner 2400MH S3.
- **Sonication probe.** The filler and epoxy resin were mixed together with the help of a glass rod. After the homogenization step, probe sonication was

conducted using a Sonics vibra cell VCX750. A ½ inch sonication tip at 30% amplitude for 15 minutes, corresponding to roughly 50 W, was used. During this sonication process, the temperature increase can cause the oligomer and curing agent mixture to start the cross-linking process. Therefore to avoid this undesired process, the curing agent was added at the end of the sonication process.

- **Three rolls mill.** The mixture was processed by means of a three roll mill equipment Exact 80E. Three rolls mill (TRM) is a calendaring machine based on three different rolls able to rotate in the opposite direction. Three rolls mill is able to achieve a good nano-fillers disaggregation and dispersion due to the combined effect of the high shearing forces and the continuous matrix mixing. Schematic representation of TRM is reported in **Figure 46**. The mixture was loaded between the first and the second roll (Feed roll) and it was collected at the end of the last roll (Apron roll). It is possible to work in two different modes: Gap mode and Contact mode. In the Gap mode it is possible to set the rolls distances at a fixed values, while in the contact mode, the roll al forced to be in contact. The roll speed velocity is another parameter. The roll speed velocity is linked by a 1:3:9 ratio and according to the mass balance a ratio as 3:1 has to be set between gap 1 and gap 2. By varying these parameters, different shear stresses occur in the suspension and therefore the severity of the dispersion process can be tuned. In this work, several set of parameters were chosen in order to better understand the effect of the processing parameters on the filler dispersion. The different three rolls mill cycles, will be presented in the chapter 4.

Despite the adopted technique, the resulting materials were cast into a cylindrical mould to let cross-linking occurs at room temperature for 12 hours.

To characterize thermoset-based nanocomposites, the following techniques were adopted:

- **Thermal conductivity:** it was investigated at room temperature using the Hot Disk Thermal Constants Analyser equipment (Hot disk TPS 2500).
- **Optical microscope:** Leica DMI 5000 M. A surface was observed at 200X, after polishing process by means of 1 μm diamond paste.

- **Field Emission Scanning Electron microscope:** Fe-SEM from Zeiss Merlin. Cryofracture surface was observed. To avoid charging, a few nanometers thick layer of chromium was deposited on sample.
- **Electrical conductivity.** It was measured by using an Agilent 34420A NanoVolt/Micro-Ohm Meter equipment. Resistance was measured at room temperature (23 °C) using a four-point setup, by placing the clips on the polished surfaces without any conductive paste.

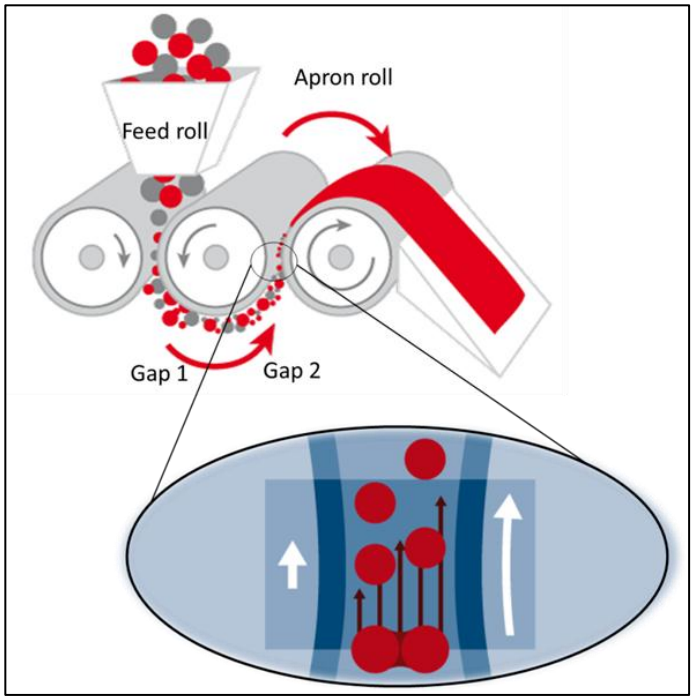

Figure 46 Schematic representation of the three roll mill equipment.

3.2 Laser printed conductive tracks on MWCNTs-based polymers surface

An industrial polycarbonate/acrylonitrile-butadiene-styrene PC/ABS blend filled with 2.25 wt. % of multiwall carbon nanotubes (MWCNTs) was used as starting material.

The matrix was purchased from Covestro with the commercial name "BAYBLEND T65XF" and filled with MWCNTs NC7000 by Nanocyl. The specific characteristics of the MWCNTs NC7000 are reported in **Table 6**.

Properties	Value	Unit	Method of measurement
Average diameter	9.5	10^{-9} m	TEM
Average length	1.5	μm	TEM
Carbon purity	90	%	TGA
Transition metal oxide	< 1	%	ICP-MS
Surface Area	250-300	m^2/g	BET
Volume rescstivity	10^{-4}	Ωcm	Resistivity on powder

Table 6 Characteristics of NC7000. Data obtained from the producer datasheet.

Starting from the commercial masterbatch, three different formulation (at 0.5, 0.75 and 1.0 wt. % of MWCNTs) were prepared by means of the addition of unfilled matrix. The dilution process was carried out by means of a twin screw extruder Thermo Haake Eurolab 16 (16/25). The obtained materials were than processed by means of injection molding process in order to obtain a 140x90x3 mm plates by using a Sandretto MICRO 65 machine for thermoplastics. Moreover, dog-bone ASTM D638 type V specimens were obtained using a Babyplast 6/10P. Basic injection parameters were selected according to supplier datasheet. To avoid thermal degradation, the temperatures of the main three zones were fixed at 250-255-260 °C.

To obtain electrical conductive path on the surface of the filled polymer, a CO_2 laser Towermark XL from Lasit, emitting in the infrared range at λ=10600 nm

was used. As will be better discussed in the Chapter 5, it is possible to modify five different parameters:

- Power
- Frequency
- Defocus
- Writing speed
- Number of repetition

Laser process was conducted under nitrogen flow. To analyze the effect of the different parameters on the laser treatment response, a design of experiment (DOE) approach was adopted. Therefore, all of the parameters and their combinations were modified in according to the DOE. For each combination of laser setup parameters, 4 different tracks were produced with a length of 10 cm at a distance of 1 cm. The surface was gently clean with a jet of compressed air in order to eliminate carbonaceous species not well adherent to the surface. The DOE analysis was conducted with the help of the software Minitab for statistical calculation.

Nanocomposites characterization was carried out by investigating the following properties and using the following characterization techniques:

- **Electrical resistance:** the measurement was carried out by means of two-point probe digital multimeter Keithley 2700 with a full scale of 120 MΩ. The measured data were normalized on the tracks length obtaining the values of the surface electrical resistance per length unit. To grant a better contact between steel probe and the conductive tracks, a very low amount of silver-based conductive paint was deposited at the beginning and the end of the tracks.
- **Field Emission Scanning Electron microscope:** Fe-SEM from Zeiss Merlin was used in order to evaluate the laser tracks morphologies. To avoid charging, a few nanometers layer of chromium was deposited on the sample.
- **Surface tracks topography:** it was evaluated by means of profilometer confocal microscope Leica DCM8.
- **Thermogravimetric analysis,:** TGA was performed in inert atmosphere (Ar) with a Mettler-Toledo TGS/SDTA851e instrument in the temperature range between 25 and 700 °C with a heating rate of 10°C/min. DTG curves were calculated on TGA thermograms.

- **Differential scanning calorimetry:** DSC were performed with a Netzsch DSC 204 F1 Phoenix System in the temperature range from 30 to 300 °C with a heating/cooling rate of 10°C/min under nitrogen flow (50 mL/min). For each experiment the sample was heated from starting to final temperature and then cooled for two times. The first heating/cooling cycle was performed in order to eliminate the thermal history of the samples. The thermal transitions of the materials studied were measured on the second heating/cooling cycle.
- **Tensile test:** it was carried out on the dog-bone specimens by using a dynamometer Instron 5544 equipped with 2 kN load cell.

3.3 Hybrid carbon-based material for electrical and thermal conductivity

To obtain hybrid carbon-based materials with enhanced electrical and thermal conductivity the following process was adopted.

An industrial high density polyethylene (HDPE) filled with 6 wt. % of MWCNTs was used. One must refer to this material as starting masterbatch. Unfilled HDPE, commercial name Lupolen 4261 AG, was purchased from Basell. The MWCNTs used as filler are the well-known NC7000 from Nanocyl, already used and presented in **Table 6**.

Moreover, starting from the unfilled HDPE, two secondary masterbatches were homemade prepared by means of the well-known internal mixing process by using an internal mixer Brabender operating at 200 °C. The neat HDPE was filled with 12 wt. % of graphene nanoplatelets GAbcr_25 or with 12 wt. % of natural flakes graphite. This two fillers were chosen according to the chapter 4 outcomes. Their specific properties are reported in **Table 5**.

To obtain hybrid materials, the starting masterbatch containing MWCNTs was mixed with the homemade prepared masterbatches in a fixed proportion of 2/3 and 1/2 by means of twin screw extruder Leistritz ZSE 18 HP. The resulting materials were than processed by means of injection molding with the help of the Babyplast injection molding machine. First of all dog-bone specimens (ISO 527 standard, specimens 5A) were obtained. Moreover, flexural bar specimen (80x10x4 mm) were also processed according to ISO 178.

Finally to achieve good electrical conductivity the laser treatment was carried out on the dog bone specimens according to the chapter 5 outcomes.

To characterize the hybrid materials, as well as the industrial masterbatch and of course the unfilled neat matrix, different techniques were adopted.

- **Thermogravimetric analysis:** TGA was performed in inert atmosphere (Ar) with a Mettler-Toledo TGS/SDTA851e instrument in the temperature range between 25 to 700 °C with a heating rate of 10°C/min. DTG curves were calculated from TGA thermograms.
- **Differential scanning calorimetry:** DSC measurements were performed with a Netzsch DSC 204 F1 Phoenix System in the temperature range from 25 to 200 °C with a heating/cooling rate of 10°C/min under nitrogen flow (50 mL/min). For each experiment the sample was heated from starting to final temperature and then cooled for two times. The first heating/cooling cycle was performed in order to eliminate the thermal history of the samples. The thermal transitions of the materials studied were investigated on the second heating/cooling cycle.
- **Tensile test:** it was carried out at room temperature on dog-bone samples by using a Sintech 10D testing machine. The experimental procedure was defined according to ISO 527 standard. Young's modulus, yield strength and elongation at break measurements were determined by using an extensometer with a gauge length of 50 mm at a crosshead speed of 10 mm/min.
- **Flexural test,** were carried out at room temperature on flexural bar specimens Zwick Roell Zwick-Line z050 testing machine. The experimental procedure was defined according to ISO 178 standard.
- **Thermal conductivity:** it was investigated at room temperature using the Hot Disk Thermal Constants Analyser equipment (Hot disk TPS 2500). Each sample was measured five times.
- **Electrical resistance:** the measurement was carried out by means of two-point probe by using an Agilent 34420A NanoVolt/Micro-Ohm Meter equipment. The measured data were normalized on the tracks length obtaining the values of the surface electrical resistance per length unit. To have a better contact between steel probe and the conductive tracks, a very low amount of silver-based conductive paint was deposited at the beginning and the end of the tracks.

Chapter 4

GNPs based polymeric composites materials with enhanced thermal conductivity

"Part of the work described in this chapter has been previously published in J. Appl. Polym. Sci. 2017, 134, 44814"

4.1 Preface to chapter 4

As reported in the first part of the manuscript, due to several features such as lightweight, easy processing for integrated parts or complex geometry, electrical tunability behaviors as well as chemical stability, polymers with enhanced thermal conductivity has been attracted the attention from both academic and industrial researchers. Electronic thermal sink for LED devices, electronic packaging, automotive electronic control units, are some of the most important fields that can take advantage from those materials. Moreover, several efforts have been devoted to implement the use of thermally conductive polymers in solar and batteries industries. [38] Furthermore, liquid-to-liquid, liquid-to-gas and gas-to-gas heat exchangers were developed to exploit polymers corrosion resistance. [128]

To achieve high thermal conductivity high filler loading is needed (up to 40 wt.%). High filler content results in a poor composite processability associated to an increasing in the relative composites density. How to reduce filler loading and keep the same thermal conductivity is a significant challenge. [38]

Tekce and co-worker reported the filler shape dependence of conductive polyamide-based copper composite. By properly choose different shape of copper based powders, as spheres, plates and short fibers, they were able to demonstrate a strong dependence between filler morphologies and composites thermal conductivity. High thermal conductivity associated to a low amount of filler was achieved by using short fiber based copper powders.[129] Furthermore, Kemaloglu et al. [130] reported the effect on the thermal conductivity enhancement of different micro and nano-size boron nitrite (BN) filling silicon rubber. The authors claimed that the highest thermal conductivity was achieved by using a filler with high aspect ratio. This is due to the ability to form a conductive path through the matrix able to promote thermal conduction at low filler content. Moreover, an increase of about 10 times of the neat matrix thermal conductivity was observed at 50 wt.% filler loading.

As reported in the introduction part, carbon based nanomaterials present the highest aspect ratio associated to the highest thermal conductivity and the lowest relative density. This open up to the possibility to obtain high thermal conductive polymer composites by using low amount of filler solving several drawbacks as poor processability and density increase.

Since CNTs were widely used as thermally conductive medium, several parameters have been recognized to play an active role on the overall thermally conduction including preparation techniques, CNTs dispersion and distribution as well as CNTs alignment. Obviously an active role is played by the coupling of CNTs typologies and matrices in terms of polymer-filler interface. Most of those factors are often interrelated. However, several interesting and exhaustive reviews were published till now with the aim to analyze each of them. [35], [38], [53], [58], [72], [131]–[134] In contraposition graphene layer and graphene nanoplatelets are still young materials. Therefore the study of graphene and graphene nanoplatelets as thermally conductive fillers for polymer nanocomposites is an attractive field of research.

Khan et al. [135] investigated the effect of different micro and nano-sized carbon fillers, such as carbon fiber (CF), multiwall carbon nanotubes (MWCNTs) and graphene nanoplatelets (GNPs) on the thermal properties of polyphenylene sulfide (PPS) based composites. By using a simple melt compounding method followed by compression molding process, authors were able to obtain PPS-based composites filled with different concentrations (up to 30 wt.%) of the three carbon based materials. Despite the amount of fillers, the higher thermal conductivity was always achieved by using graphene nanoplatelets with respect to MWCNTs and CF, thus demonstrating the potential application of GNPs as thermally conductive fillers. The highest thermal conductivity was 1.9 W/mK at 30 wt% GNPs content. However, for all the three types of fillers, thermal conductivity does not change significantly after a certain filler concentration. The same trend was also reported by King et al. [136] In this work, researchers compared the electrical and thermal conductivity of polycarbonate (PC) filled GNPs with respect to CNTs and carbon-black (CB). Despite the lower electrical percolation threshold observed for CNTs and CB with respect to GNPs (~1, ~2 and 4 vol.% for CNTs, CB and GNPs respectively), the higher thermal conductivity was always observed for GNPs filled PC, reaching a maximum value of thermal conduction of 0.49 W/mK at 15 wt.% loading (approximately 9.6 vol.% of GNPs). Kalaitzidou and co-worker reported a new compounding methods to obtain GNPs based PP. [137] A significant CTE (coefficient of thermal expansion) reduction of ~20-25% was observed in both transverse and longitudinal directions at 3 vol.% of GNPs. The maximum observed thermal conductivity was six times higher with respect to neat PP at 25 vol. %. Due to the high in-plane thermal conductivity of graphitic layers, it was expected an higher increase of the composites thermal conductivity. However, the analytical method used to its evaluation is strictly affected by fillers orientation within polymer matrix. [138] In addition to thermoplastic matrices, several efforts has been devoted to thermoset (like epoxy) based composites. This is due to the possibility to use different, and relatively low cost, dispersion methods. [57], [137] Chandrasekaran et al. [139] reported the temperature dependence (between 30 to 100° C) of the thermal conductivity of GNPs-epoxy based nanocomposites obtained by using calendaring dispersion method. A linear dependence between temperature and thermal conductivity was observed. Maximum thermal conductivity (~0.22 W/mK) was achieved at 2 wt.% of filler loading at 100 °C. At low filler content (0.3-0.5 wt.%) the authors observed a sharp increase of the electrical conductivity due to formation of a percolative network able to promote electrical transport through epoxy matrix. This discrepancy in the electrical/thermal behavior could be explained by considering

that in the electrical conductivity case, the clusters formed by the conductive fillers alone contribute to the overall conductivity while thermal conduction is related to the acoustic phonons and therefore matrix-to-filler interface leads to the lack of the thermal "percolation curve". The same trend was further confirmed by Moghadam and co-worker [140]. They observed an increasing of about 80% of the room temperature thermal conductivity at 2 wt. % of GNPs-based epoxy resin (with respect to neat matrix), while a drastic decrease on the electrical resistivity (from 10^{15} to $10^{6}\Omega$*m) was achieved already at 1.5 wt. % of filler loading.

To achieve good interaction between filler and matrix, several chemical modified GNPs were coupled with epoxy resin. By using "3-amin-opropoxyltrietoxy silane" (γ-APS) Ganguli et al. [141] were able to graft silane group on the surface of exfoliated graphite. Chemically modified fillers were dispersed into epoxy resin and the thermal conductivity was evaluated as function of filler content. Improved thermal conductivity was observed for chemically functionalized exfoliated graphite with respect to unmodified systems. Moreover, non-covalent functionalized graphene/epoxy nanocomposites were reported by Teng and co-worker. By using a chemical oxidation route (Hummers method) followed by thermal reduction, authors were able to obtain graphene sheet starting from natural graphite. A non-covalent functionalization by using pyrene-end poly(glycidil methacrylate) (Py-PGMA) was performed and the functionalized graphene sheet were dispersed in epoxy resin. Thermal conductivity of epoxy-based composites with Py-PGMA-graphene sheet increased about 16.4% compared with that of pristine system at 1 parts per hundred rubber (phr) loading.[142] Furthermore, to overcame thermal resistance issues, Conrado [143] reported the synthesis of self-standing 3D aerogel structure based on thermally reduced graphene oxide. Due to the highly filler orientations a thermal conductivity improvement of more than 25% was achieved at very low filler concentration (0.27 wt.%).

It is obvious that several efforts have been made on this topic. However, most of the authors often used different fillers purchased from several industries (with different grade and/or obtained with unknown processes) while other researchers used "home-made" graphene obtained from different precursors. Moreover, starting from the easiest PP up to PPS (passing through several industrial epoxy resin) different matrices were studied. In addition to melt blending, which is a consolidated technique to process thermoplastic polymers, some difficult, expensive and potentially environmental harmful reactions were reported to

disperse graphene-like materials within both thermoplastics and thermoset matrices. Furthermore, very different fillers concentrations were dispersed within matrices thus achieving very different increase in the conductive properties. It is also important to observe that at each combination of the above mentioned strategies, different thermal behaviors were reported. For all of these reasons it is very difficult to compare the available data. Due to the fact that the researchers used commercially or self-made materials, with different grade, purities and morphologies, obtained by particular synthesis routes, not fully characterized (in most of the cases), and dispersed in different matrices by means of different dispersion methods, at this stage the key points concerning the effectiveness of GNPs for increasing the thermal conductivity of polymeric materials are not completely clear. In other words the following question is still open: "which is the real role played by GNPs in polymeric composite materials with enhanced thermal conductivity and which is the main property of the fillers that allows to obtain the final result?"

In order to try to answer to this question, the present work aims to focus the attention on the effect of different GNPs on the thermal conductivity behavior of polymeric composite materials. Three different thermoplastic materials were filled with two commercially available GNPs and with a commercially available natural graphite used as a reference. Thermoplastic matrices were filled by using the same amount of fillers (5 wt.%) and by using the same dispersion technique. Furthermore, in order to analyze the effect of the different amount of fillers, and in order to understand the relationship between thermal conductivity and dispersion degree, a commercially available epoxy resin was used as a matrix and several dispersion methods were compared. Before starting to talk about composites materials processing and properties, a full fillers characterization will be presented.

4.2 Fillers Characterization

Two different kind of commercially available GNPs were used as filler: GNPs Abcr, produced by Abcr with a thickness of 6-8 nm x 5 μm wide and GNPs Grade 4, produced by Cheaptubes with a plane dimension of 1-2 μm and thickness lower than 4 nm when exposed to high shear or sonication. Natural graphite flakes produced by Alfa Aesar with a median size of 7-10 μm (purity 99%, metal basis)

were also used as reference. **Table 7** reports the specific properties of the different fillers employed.

Filler	Short name	Thickness (nm)[A]	Wide (µm)[A]	Aspect ratio[B]	Density (g/cm^3)[C]
GNPs Abcr	GAbcr	6-8	5	~700	1.5
GNPs Grade4	G4	< 4	1-2	>350	2.1
Graphite	Graph	>10	7-10	~160	2.2

Table 7 Properties of the different fillers. A) data from supplier data sheet. B) Geometrical aspect ratio, obtained using both supplier data in comparison with FESEM observation. C) data obtained using a Helium pycnometer.

To characterize GNPs and graphite powder, different available technique were used. First of all filler morphology was investigated by means of FESEM analysis. **Figure 47** show the morphology of employed fillers at different magnification (500 and 50 kX).

Magnification 500 X **Magnification 50000 X**

GNPs Abcr

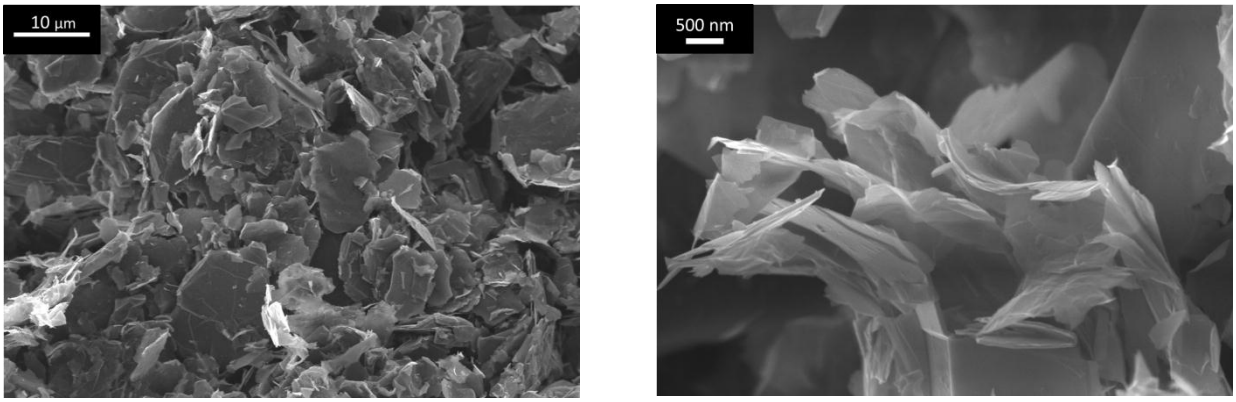

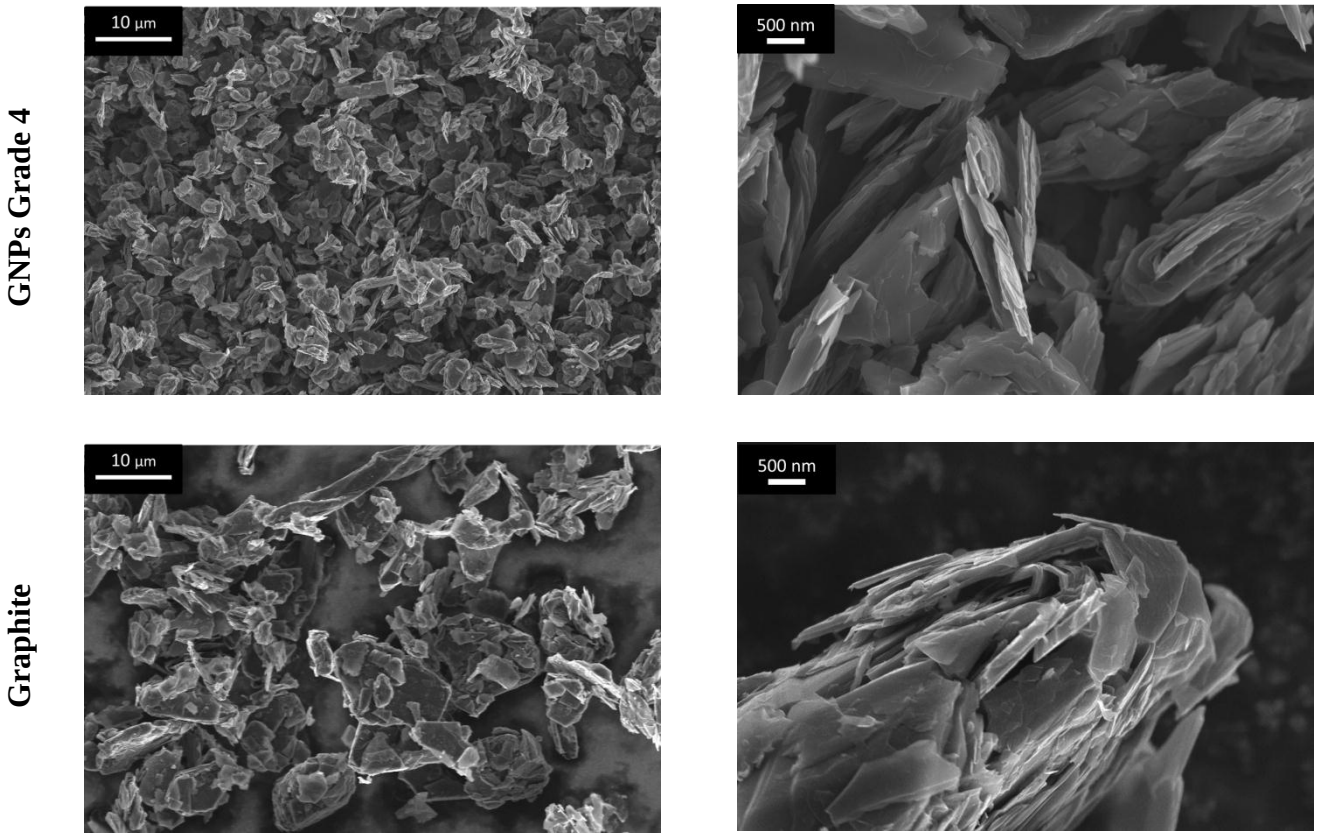

Figure 47 FESEM micrographs of employed fillers at different magnifications. Scale bar 10 µm and 500 nm on low and high magnification pictures respectively.

Both GAbcr and G4 are characterized by the presence of agglomerated multi-layer graphene sheets. This is probably due to the graphene restacking provided by van der Walls forces occurring at the end of the synthesis route. [57], [105], [112] At low magnification is possible to observe that the filler dimensions are always in good agreement with supplier datasheets. While most of the GAbcr flakes are in good agreement with the supplier datasheet, GAbcr micrograph also show the presence of several bigger and smaller flakes resulting in an average value of 5 µm wide. On the other hand G4 is characterized by a narrow size distribution near 2 µm. At 50 kX G4 shows a most regular structure with respect to GAbcr, that reveals an indented morphology instead. This is probably due to the different (unknown) synthesis route adopted by the suppliers. The micrograph of the graphite, used as reference, also shows the presence of bigger and more compact agglomerates with respect to the GNPs ones. From the FESEM images, it was also possible to observe a thickness of natural graphite multilayers (reported on the supplier data-sheet as higher than 10 nm) in the range of 50 nm. On the

basis of both supplier and FESEM outcomes it was possible to calculate the geometrical aspect ratio, reported in **Table 7**.

As reported in introduction parts, carbon materials can exist in different allotropic forms. To each of them corresponds a different X-ray diffraction pattern. To analyze the crystalline phase of the involved fillers, XRD analysis was conducted in the range between 10 and 80 2ϑ. XRD normalized patterns of GAbcr, G4 and Graphite are reported in **Figure 48**. No significant differences were observed for the different carbonaceous fillers. All of the XRD spectra show the characteristic diffraction peaks (002) and (004) of graphite-2H located at 26.4° 2 ϑ (d=3.37 Å) and 54.7° 2 ϑ (d=1.68 Å) respectively. The peaks located in the range from 42° to 45° 2 ϑ are related to (100), (101) reflexes of hexagonal graphite and (101) reflex of rhombohedral graphite. Finally, no evidence of amorphous phase was found, and no difference, for all the involved fillers, were observed in term of intensity ratios of diffraction peaks, that are in good agreement with the literature. GNPs materials show off the same graphitic structures of natural graphite. This is due to the presence of no isolated single layer graphene while the materials are characterized by an ABABAB stacking of graphene layers typical of hexagonal (2H) graphite. A small amount of rhombohedral graphite exists in natural graphite due to a stacking defect producing the ABCABC stacking sequence. [141] The same rhombohedral structure was observed in both GAbcr and G4 probably due to the precursors used for the synthesis. In fact, despite the unknown process adopted from both ABCR and Cheaptubes industries, by combining FESEM and XRD analyses with the literature data, it is possible to infer that the adopted precursor for both GAbcr and G4 synthesis was a natural graphite.

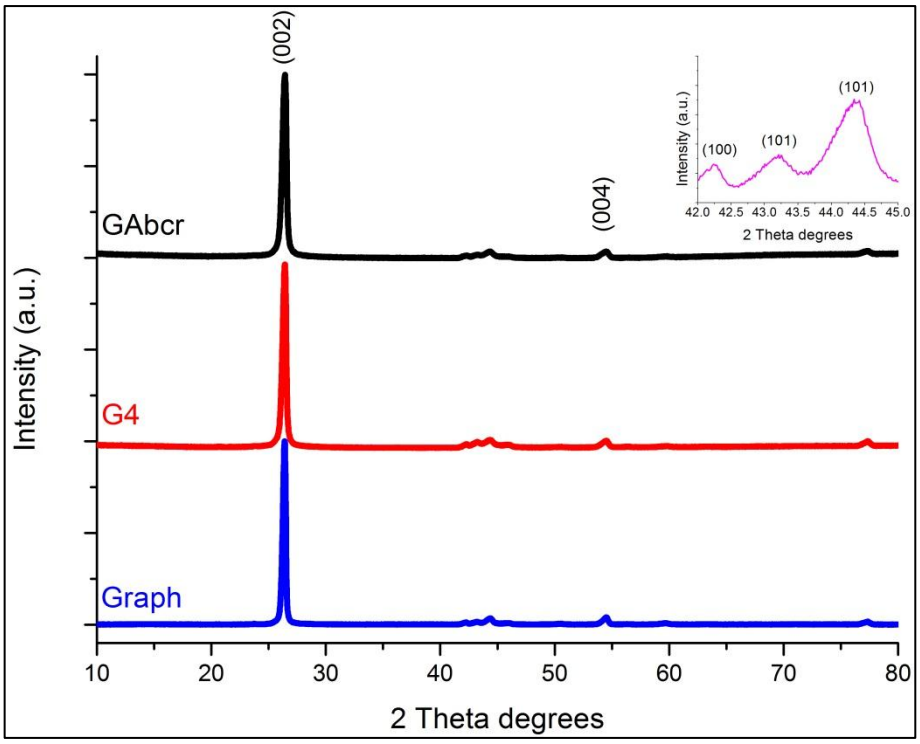

Figure 48 Normalized XRD patterns of GAbcr, G4 and graphite powders. In upper insert, a focus of the diffraction peaks in the range of 2 theta between 42 and 45 degrees is reported.

Until now, no particular differences were observed between the involved fillers. Of course from FESEM analysis it was possible to observe a difference in the fillers dimensions, that are in good agreement with respect to the supplier datasheet, while all of them are based on a graphitic structure. The same structure was observed by means of Raman spectroscopy.

It was demonstrated the possibility to estimate the number of graphene layers by the evolution of the Raman spectra. [123] Even though this feature is only relevant for isolated and/or suspended systems, Raman spectroscopy is an important tool for the characterization of carbonaceous materials. The Raman spectra of graphene nanoplatelets GAbcr and G4 collected in the range between 500 to 3500 cm^{-1}, are reported in **Figure 49** in comparison with the Raman spectra of the employed natural graphite.

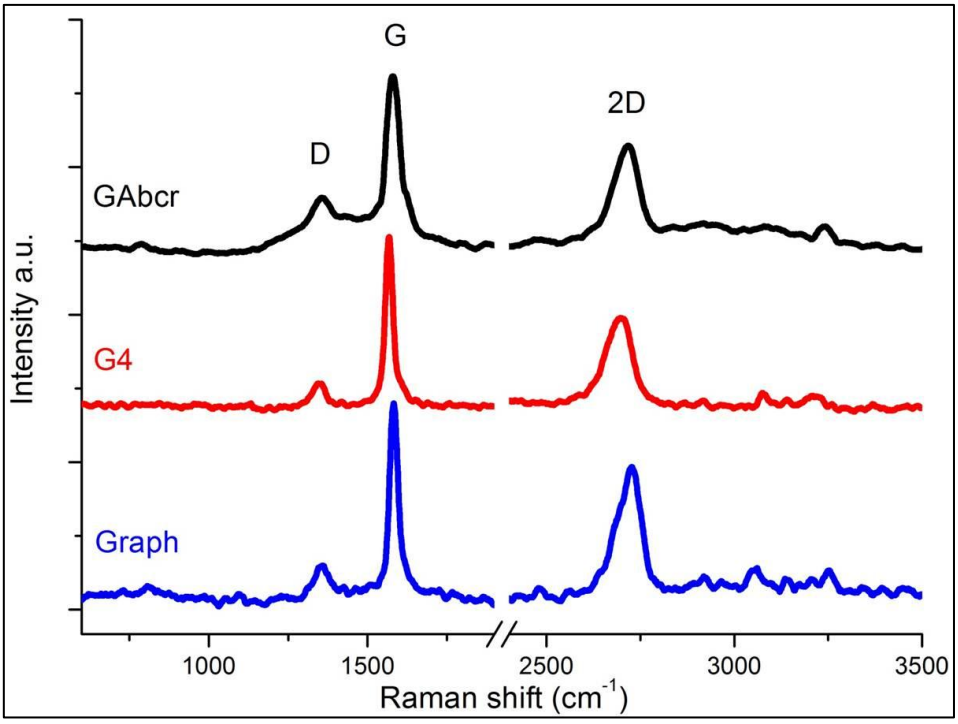

Figure 49 Raman spectra of GNPs, GAbcr, G4 and Graphite powders.

All the collected Raman spectra are characterized by the presence of the typical D, G and 2D Raman peaks characteristic of graphitic materials. The most intense signals are the G peak, placed at ~1580 cm^{-1}, and the 2D band located in the range between 2500 and 2800 cm^{-1} (historically also named G'). The G band, which is associated with the doubly degenerated phonon mode at the center of the Brillouin zone, is the only band that is associated to the normal first order Raman scattering process in graphene and related graphitic materials. On the other hand, the 2D band is related to the second order process of zone-boundary phonons. Moreover, D peak located at ~1350 cm^{-1} (one half of 2D peak) is related to the presence of edges in GNPs or graphite lattice. [100], [123] Raman spectroscopy also provides an easy structural and quality characterization of the nanofillers under investigations through the comparison of the intensity ratios between G and 2D peak (IG/I2D) and between D and G peaks (ID/IG). In fact, since G band is related to the first order phonons scattering, it arises due to the in plane vibration of sp^2 carbon atoms. In other word, it is related to the amount of graphitic structures in graphite, graphene and related GNPs. Moreover, it was reported that the 2D peak intensity is strongly affected by the number of graphene layers. [57], [123] Mathematically speaking it is obviously that an high value of IG/I2D ratio is

provided by a highly graphitic structure based on few graphene layers while, at the same time, this highly graphitic structure is probably associated to a low amount of defects providing a low value of ID/IG ratio. However, for this evaluations we considered not the maximum peak intensity but the area of the Gaussian curve that fits the peak, obtained by using a Matlab Gaussian fit. Raman peak ratios for the involved fillers, are reported in **Figure 50**. The higher IG/I2D ratio combined with the lower value of ID/IG of the GNPs G4, indicates that this nanofillers show a higher level of purity and lower defects with respect to the GAbcr and the graphite. On the other hand, graphite also shows lower amount of defects with respect to the GAbcr but this can be probably due to the higher plane dimensions that minimizes the effect of boundary defects.

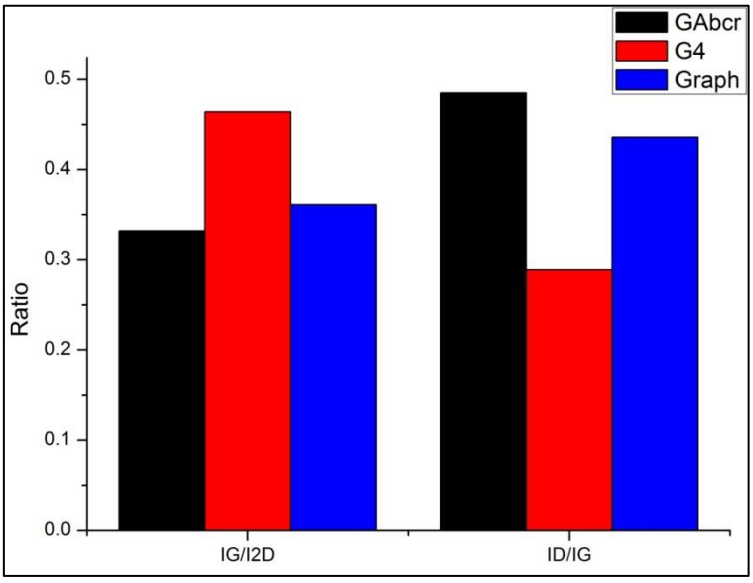

Figure 50 The IG/I2D and ID/IG peaks area ratios calculated from Raman spectra of GAbcr, G4 and graphite.

Finally, thermogravimetric analysis was performed in inert atmosphere (Ar) on each carbon-based material from 25 to 700 °C with the aim of investigating their thermal stability. The analyses were performed after sample treatment for 24 h in an oven at 80°C, performed in order to eliminate the moisture adsorbed on the surface of the powders. The TGA thermograms are reported in **Figure 51**.

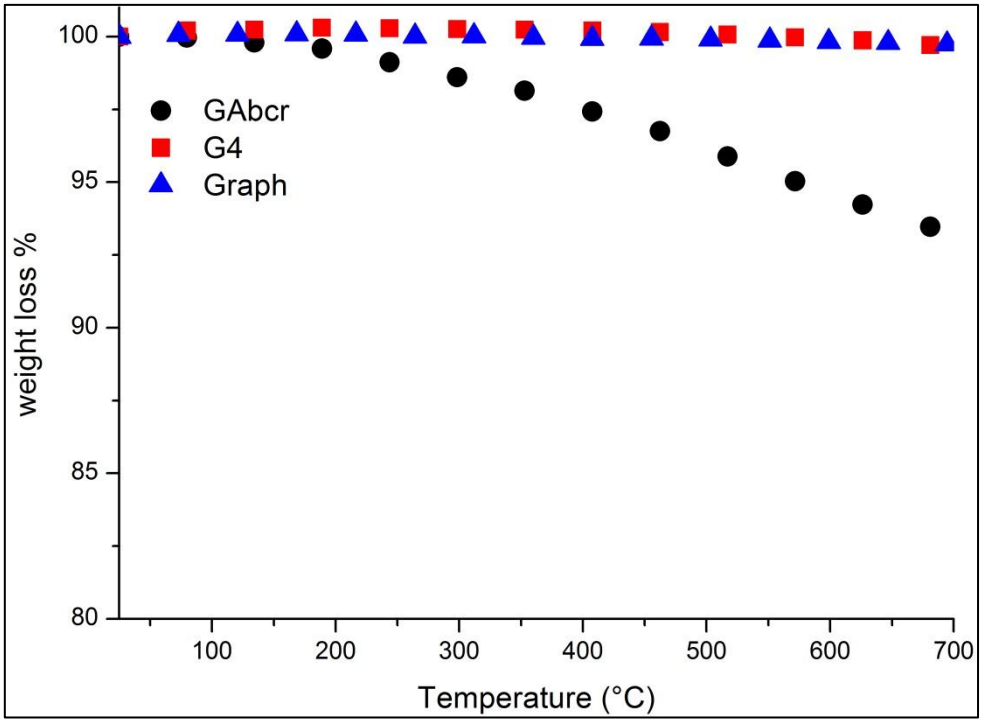

Figure 51 Thermogravimetric curves of GNPs G4, GAbcr and Graphite powders.

As it is possible to see, GAbcr shows lower thermal stability with respect to graphite and G4. The weight loss percentage, at 700° C, is 6.7% for GAbcr and only 0.3% for both G4 and graphite powders. This trend was nearly expected from the EDS outcomes given that this semi-quantitative analysis performed on each untreated sample revealed different ratios between carbon, oxygen and metallic impurities: 96:3:1 wt.% for G4, 98:2:0 wt.% for graphite, and 95:4:1 wt.% for GAbcr. The higher content of oxygen within this last filler is likely responsible for the formation of enhanced amounts of gaseous products during the TGA run.

At the end of the fillers characterization process, it was possible to attribute better intrinsic properties to graphene nanoplatelets G4 with respect to the other counterparts. It is important to observe that the intrinsic graphene or, more in general the intrinsic graphitic materials properties are strongly affected by the defect presence and by its graphitic structure. Despite the lower plane dimension, G4 shows the lower ID/IG Raman peak ratio providing the highest graphitization levels associated to the lowest amount of defect. This was also confirmed by thermogravimetric analysis that reveals a good thermal stability up to 700°C. The same thermal stability behavior was observed in the natural graphite. However,

due to the highest thickness and due to the presence of the highest amount of agglomerated structures, the employed graphite is characterized by the lowest aspect ratio. Finally, it was observed that GNPs GAbcr possess the lowest thermal stability associated to the highest amount of defect. Moreover an indented structure was observed by means of FESEM analysis.

4.3 Effect of GNPs on the thermal conductivity and mechanical behavior of thermoplastic polymer nanocomposites

In order to analyze the effect of GNPs on the thermal conductivity enhancement of polymeric composites materials, first of all three different thermoplastic polymers were filled with 5 wt.% of the employed carbon based materials.

The polymer matrices used as starting materials were:

- Polypropylene (PP)
- Acrylonitrile butadiene styrene (ABS)
- Thermoplastic polyurethane (TPU)

These matrices were chosen in order to cover a wide range of thermoplastic materials. In fact PP is recognized as the most important polyolefin while ABS is a well know copolymers. Finally, TPU was chosen as an elastomeric polymer. Moreover, these three thermoplastic matrices were selected because of their wide range of application fields, due to their relatively low cost, high processability, good final mechanical properties and lower environmental impact with respect to all the other composites based on thermosets.[144]

The polymeric nanocomposites materials were prepared by means of the well-known melt blending technique, using an internal mixer Brabender, operating at 190 °C for PP and TPU, or at 240 °C for ABS, at a screw speed of 30 rpm. The fillers, GNPs and graphite, were added at 5 wt.% to the molten polymer and the screw speed was increased to 60 rpm for 3 minutes. The obtained nanocomposite materials were re-granulated by means of a RSP 15 open-type rotor granulator produced by Piovan. Afterwards they were re-melted and processed with a Babyplast injection moulding machine, with a melting temperature of 190 °C for PP and TPU or 240 °C for ABS,

injection time of 7 s at 75 bar and 6 s at 55 bar and a total time cycle of 20 s, in order to obtain the final dog-bone specimens. The processing parameters were selected according to the suggestions of the material supplier datasheets. Schematic process chart flow is reported in Figure **52**.

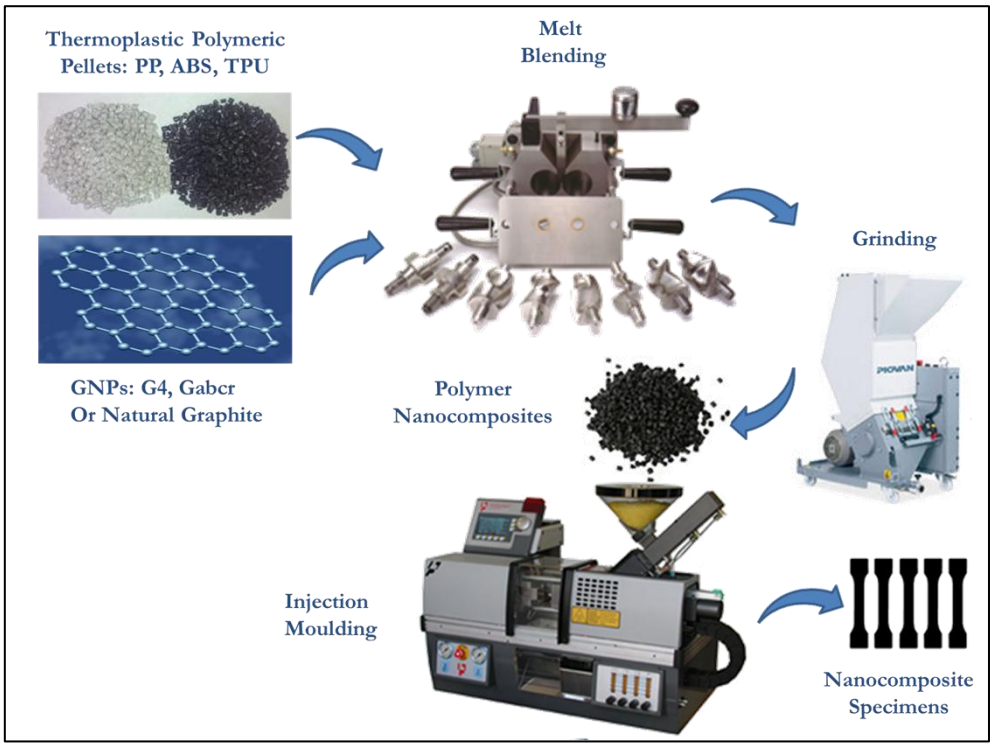

Figure 52 Schematic nanocomposites chart flow production

The prepared nanocomposites were named in according to "MWG" nomenclature, where M is the polymer matrix, W is the filler weight percent (5 wt. %) and G is the involved filler. Nine sets of samples were obtained and labelled as:

- PP5GAbcr, PP5G4, PP5Graph.
- ABS5GAbcr, ABS5G4, ABS5Graph.
- TPU5GAbcr, TPU5G4, TPU5Graph.

Moreover, unfilled matrices were labelled as PP, ABS and TPU.

The dispersion of GNPs and graphite within the thermoplastic polymer matrices was investigated by means of optical microscopy. A surface

parallel to the direction of the injection moulding flow was polished by means of 1 µm diamond paste and the polished surface was observed at high magnification (200X). As it is possible to observe in **Figure 53** a rather homogeneous dispersion degree of fillers, appearing as bright spots, [145] was achieved in all the prepared samples, although some aggregates of filler particles could be detected. By using optical microscope it is also possible to observe that the plane dimension of the employed fillers are different as was put in evidence by FESEM analysis. In fact, GAbcr based nanocomposites, are characterized by bigger bright spots with respect to G4 counterparts. No particular differences were detected by comparing the dispersion degree of the same nanofillers within different matrices.

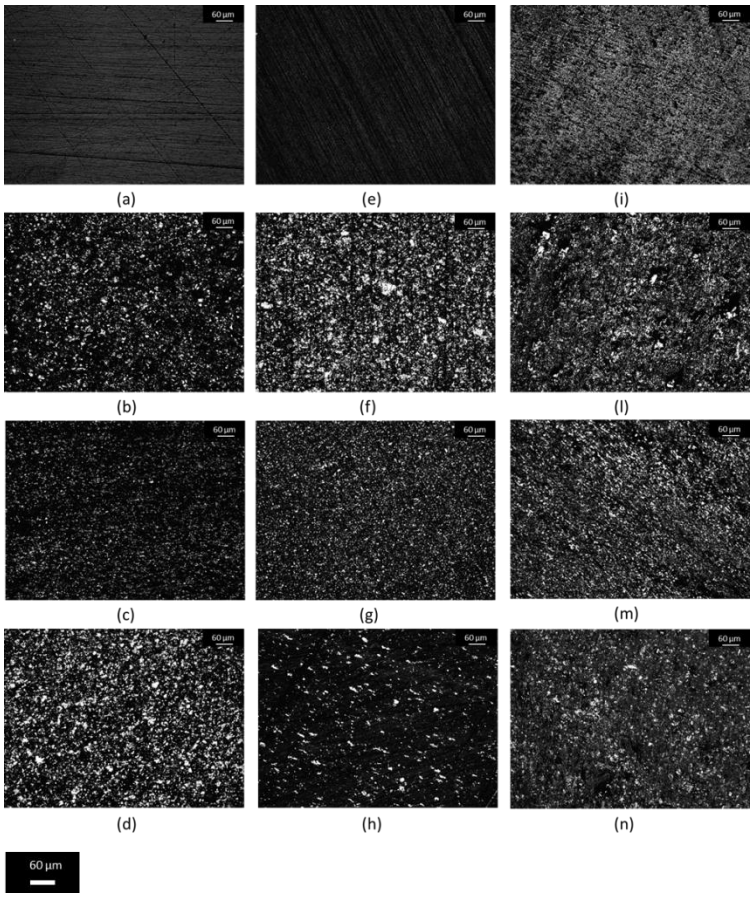

Figure 53 Optical microscope images (200X, scale bar 60 µm) of PP, PP5GAbcr, PP5G4, PP5Graph (a, b, c, d respectively), ABS, ABS5GAbcr, ABS5G4, ABS5Graph (e, f, g, h, respectively) and TPU, TPU5GAbcr, TPU5G4, TPU5Graph (i, l, m, n, respectively).

Nanocomposites cryofracture surface was observed at high (50kX) with the help of FESEM equipment after chromium metallization process. Cryofracture surface of all prepared nanocomposite is reported in

Figure 54. First of all a significant degree of interaction between matrices and fillers was achieved without using any compatibilizer. Graphite based composites show bigger agglomerate of particles with respect to GAbcr and G4 nanocomposites. However, filler dimension seems to be in good agreement with the starting powder dimension, revealing that during the melt compounding process no plane breakage occurs due to the sheer stress applied. Finally, no single layer sheets were detected. This was also further confirmed by XRD analysis.

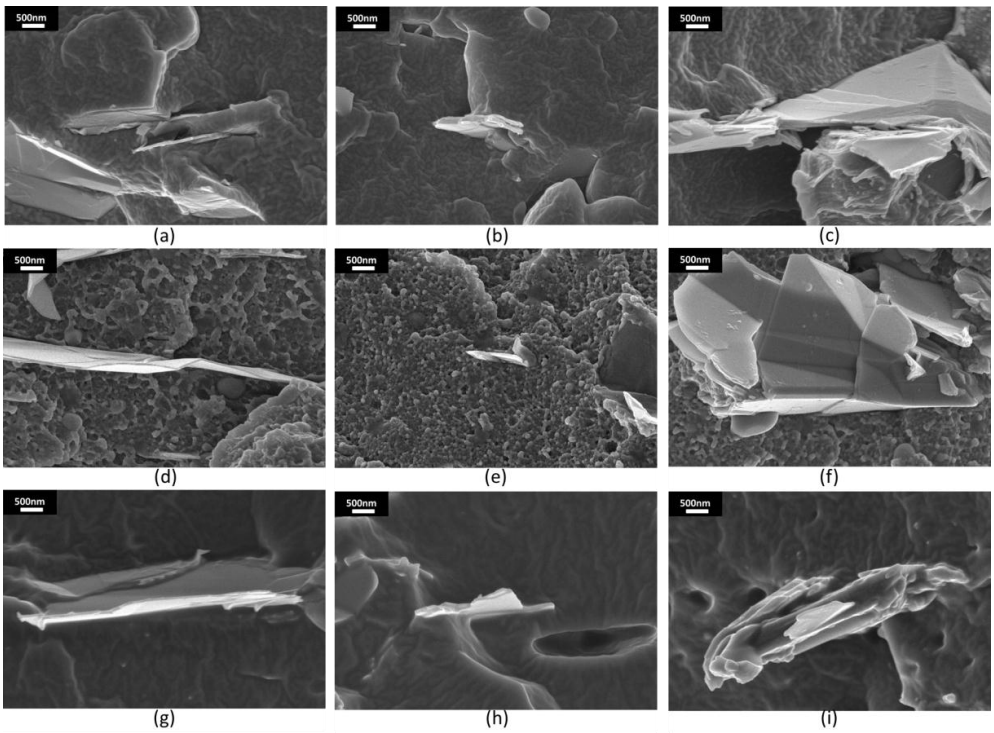

Figure 54 FESEM micrographs (50 KX, scale bar 500 nm) of cryofracture surface of PP5GAbcr, PP5G4, PP5Graph (a, b, c respectively), ABS5GAbcr, ABS5G4, ABS5Graph (d, e, f, respectively) and TPU5GAbcr, TPU5G4, TPU5Graph (g, h, i, respectively).

XRD is an effective method to evaluate the interlayer changes of nano-layered filler in the nanocomposites materials. [146] Therefore, XRD analysis was used to investigate the possible changes in the degree of intercalation of the GNPs and the graphite flakes after the compounding process. Figure 55 reports parts of the XRD patterns of the different nanocomposites filled with GAbcr (a), G4 (b) and graphite (c) focused on (002) diffraction peak. Only the first diffraction peak is reported her due to the much low intensity of the (004) diffraction peak. The black line indicates the position of the powder diffraction peak centered at 26.4° 2 theta degrees.

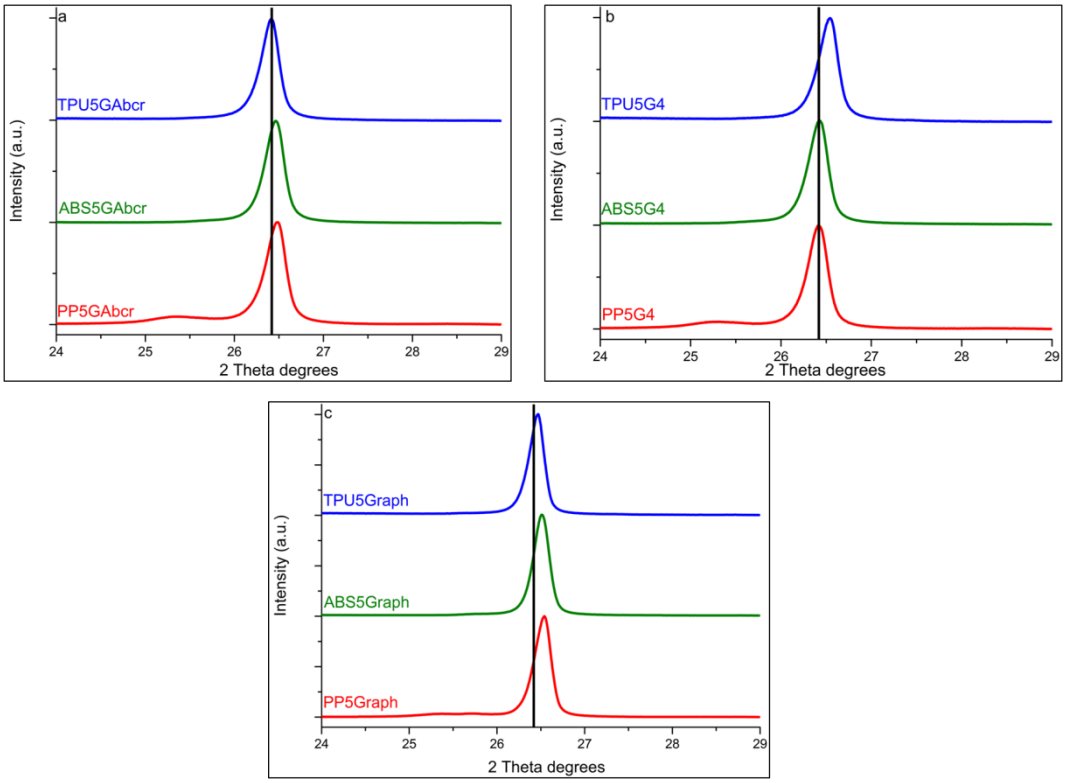

Figure 55 XRD patterns of composites materials containing GAbcr (a), G4 (b) and graphite (c) focused on (002) diffraction peak

It is evident that, for all the prepared samples, there is not a shift toward lower theta angles which could possible arise from polymer chain intercalation within graphene layers. On the contrary it is possible to observe a slightly shift of the peak at higher values of 2 theta degrees, with a maximum 2 theta value of 26.54° for PP5Graph. This shift is probably due to residual mechanical stresses caused by the compounding process.

At the end of this first part of composites characterization it is obvious that all the fillers are present as unmodified particles within the polymer matrices and not as exfoliated single graphene layers. Furthermore, this was also confirmed by the mechanical properties.

Tensile test was performed on the dog bone specimens in order to investigate the effect of the employed filler on the mechanical properties of polymeric composites materials. In fact, one of the most important differences between the involved matrices and their composites deal with the mechanical properties. The neat ABS matrix is a rigid copolymer with an elastic modulus of more than 2,5 GPa and an elongation at break of 4%. On the contrary, PP is an elastic polymer with much lower modulus and deformation at break of more than 500%. A similar behavior is show by the elastomeric TPU which shows the lowest elastic modulus. The mechanical properties (Young's Modulus, tensile strength and deformation at break) of GNPs-based and Graphite-based polymer nanocomposites are reported in **Table 8**. The obtained results for PP-based composites clearly show that the presence of the carbon-based fillers induces an increases on the matrix elastic modulus. This is probably due to the reinforcing effect played by the fillers within the polymeric matrix. PP-based nanocomposites shows a Young's modulus increase of more than 380% when filled with GAbcr, and over 330% for the samples containing graphite. Lower increment was observed by using G4. Moreover, PP based composites show a slight decrease of the tensile strength associated to a great reduction of the elongation at break. This is probably due to the hindering effect induced on the motion of polymeric chains by the presence of particles and agglomerates of GNPs or graphite. Different trends occur for the ABS-based nanocomposites. ABS5GAbcr and ABS5G4 shows higher elastic modulus values with respect to the sample filled with graphite. Tensile strength is only slightly affected by the presence of fillers as well as the deformation at break. Finally TPU-based materials, sometimes show an increase of the Young's modulus (up to 100% when filled with GAbcr), even though it remains very low. In addiction TPU5Graph shows a clear increase in tensile strength, contrary what happened for all the other nanocomposites. These improvements very likely are due to the very poor mechanical properties of unreinforced TPU. Summarizing, in every case, GAbcr addition leads to a higher improvement in the stiffness respect to G4. The lower stiffness increase for G4-based nanocomposites, with respect to GAbcr, can be attributed to the lower aspect ratio. The presence of the different nanofillers induces a noticeable decrease of the elongation at break for PP and

TPU, but they display only smaller effect for ABS-matrix composites since the ABS matrix itself undergoes only little deformation at break. However this kind of trends are typical for polymeric composites filled either with nano or micro particles, confirming that the dispersed carbon based materials are present as inclusions and not as single layer materials.

Samples	E'(Gpa)	σ (MPa)	Def. %
PP	0.53 ± 0.05	40.0 ± 5.0	>500
PP5GAbcr	2.56 ± 0.21	33.4 ± 0.2	7.5±0.6
PP5G4	1.98 ± 0.02	32.6 ± 1.9	9.3 ± 4.0
PP5Graph	2.31 ± 0.14	36.4 ± 1.2	10.6 ± 1.6
ABS	2.85 ± 0.18	48.1 ± 0.2	4.7 ± 0.3
ABS5GAbcr	3.86 ± 0.21	45.5 ± 0.2	4.0 ± 0.6
ABS5G4	3.43 ± 0.74	44.6 ± 0.2	4.4 ± 0.6
ABS5Graph	3.12 ± 0.25	47.6 ± 1.3	3.8 ± 1.2
TPU	0.010 ± 0.001	14.3 ± 1.0	> 500
TPU5GAbcr	0.020 ± 0.001	13.8 ± 0.6	175 ± 16
TPU5G4	0.010 ± 0.001	13.8 ± 0.5	450 ± 100
TPU5Graph	0.010 ± 0.001	17.1 ± 0.5	200 ± 100

Table 8 Mechanical properties of GNPs-based and graphite-based nanocomposites

Thermogravimetric analysis (TGA) was performed from 25 to 700°C in inert atmosphere (Ar) in order to study the thermal stability of the polymer nanocomposites containing GNPs. TGA was also used in order to check the amount of nanofillers dispersed within the polymeric matrix. The weight of the residue, experimentally detected, were in good agreement with the theoretical content of GNPs or graphite introduced within the thermoplastic polymer systems during the melt blending. As summarized in **Table 9** and shown in Figure 56 (a) for the PP-based nanocomposites, the addition of GAbcr and G4 leads to an increase of more than 20°C of the temperature of at which 5% of weight loss is observed (T_5). The increase of the temperatures at which there is 50% of weight loss (T_{50}) was found to be 14°C for PP5GAbcr and 11°C for PP5G4 respectively. However, the best improvement of the thermal stability was obtained by adding 5 wt. % of graphite flakes to the PP matrix, with an increment of 31°C for T_5 and 18°C for T_{50}. Conclusively a larger effect on thermal stability was observed for graphite flakes, followed by GAbcr and G4 which suggests that the stabilization depends on the particle size. Similar results were also reported in literature when comparing the effect of double wall carbon nanotubes (DWNT) and multiwall carbon nanotubes (MWNT). [147] It can be inferred that thermal stabilization is more pronounced when the dimension of the nanofillers is higher, because the protection action can be attributed to a barrier effect implying a hindered transport of degradation product from the condensed to gas phase. In addition impurities do not seem to play an important role in the thermal nanocomposites decomposition. [148] On the other hand for both ABS-based and TPU-based nanocomposites, no significant changes were observed in the degradation temperatures for all the three different fillers (GAbcr, G4 and graphite), as evidenced in **Table 9** and Figure 56 (b) and (c). DTG curves (reported in the inset graph) reveal that only for the PP-based nanocomposites a significant increase of the temperature for the maximum rate of degradation occurred. In the case of TPU-based nanocomposites, a two-step degradation process was found, not related to the presence of GNPs. [149] Moreover, Figure 56 (d) reports for all the prepared materials the TGA isothermal analyses, performed at the temperatures at which the 5% of the weight loss was observed for the neat matrices (390°C, 366°C and 332°C for PP, ABS and TPU respectively). It is clear that the presence of GNPs or graphite increased the amount of the residue after 90 minutes only in PP-based composites. In fact, while the neat PP matrix was completely degraded the other materials had up to 40% of residual char. The GAbcr shows the best result probably owing to a better dispersion within the polymer matrix. Regarding the samples based on ABS and

TPU, the TGA isothermal analyses showed no difference in the degradation behavior when filled with GNPs or graphite. After 90 minutes of isothermal treatment the same amounts of residue were detected (near 25 wt. % for ABS-based materials and 40 wt. % for TPU and TPU-based composites). The better stability improvement of PP-based composites is probably due to a better adhesion and compatibility between filler and polyolefin respect to co-polymer and elastomer.

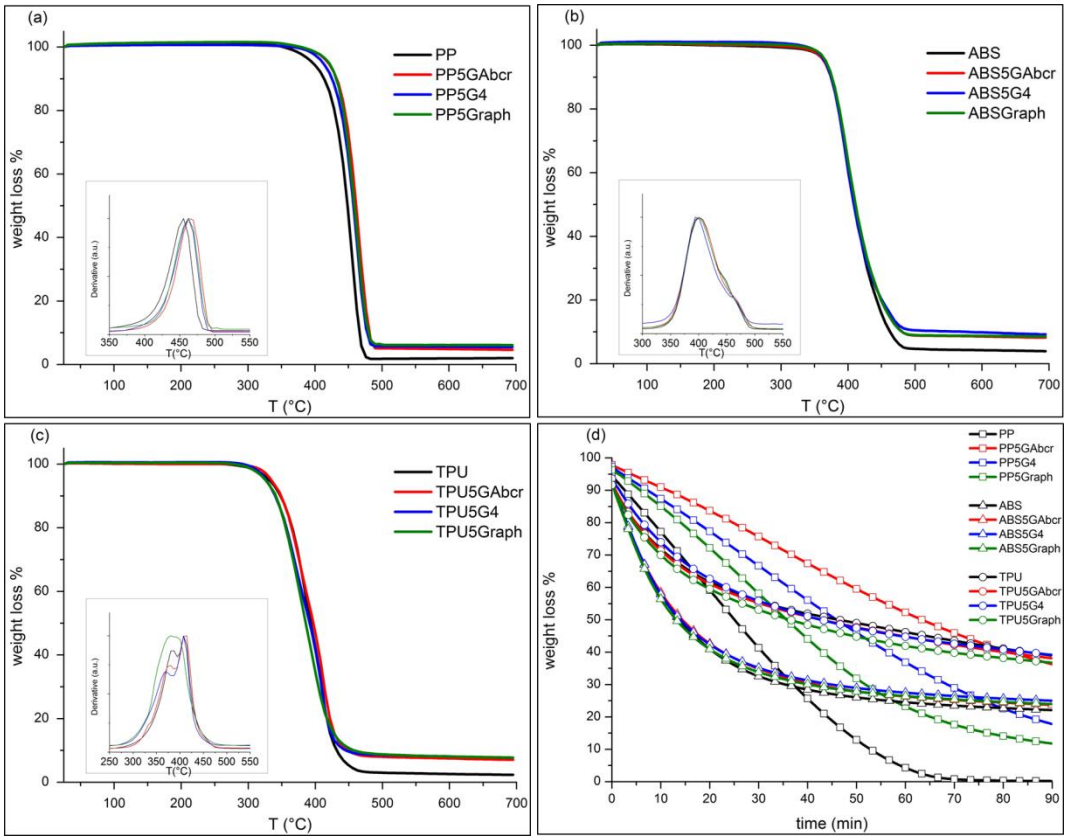

Figure 56 Thermogravimetric analyses of PP-based (a), ABS-based (b), TPU-based (c) materials in Ar atmosphere. (d) TGA isotherm performed at T_5

Finally DSC analyses were carried out to complete the thermal properties characterization. PP is a semi-crystalline polymer, while ABS and TPU are characterized by the presence of amorphous phase only. As can be seen in **Table 9**, PP melting temperature in not influenced by the presence of the carbon based fillers. Moreover, the same behavior was detected concerning glass transition

temperature. These outcomes corroborated the choice of the operating temperatures used for the melt blending process.

Samples	T_5 (°C)[a]	T_{50} (°C)[a]	T_{max} (°C)[b]	T_g (°C)[c]	T_m (°C) [c]
PP	390	444	436	-20	180
PP5GAbcr	414	459	460	-20	180
PP5G4	417	455	461	-20	180
PP5Graph	421	462	462	-20	180
ABS	366	407	400	115	-
ABS5GAbcr	366	414	402	115	-
ABS5G4	366	414	401	115	-
ABS5Graph	366	414	402	115	-
TPU	332	394	374/414	-25	-
TPU5GAbcr	332	394	373/413	-25	-
TPU5G4	332	394	373/414	-25	-
TPU5Graph	326	387	373	-25	-

Table 9 TGA and DSC outcomes for GNPs and Graphite based nanocomposites; a: Temperature at which there is 5 and 50 wt.% of weight loss by TGA; b: Temperature of the maximum peak of degradation by DTG, c: T_g and T_m values determined by DSC in nitrogen.

Focusing the attention on the main aim of this work, specific thermal conductivity of all the unfilled and carbon filled polymers are shown in **Figure 57**. Thermal conductivity analyses were performed as a function of the different fillers within the different thermoplastic polymeric matrices. The data reported in figure are the average values of five measurements, and the standard deviation (less than 0.6% in every case) is put in evidence.

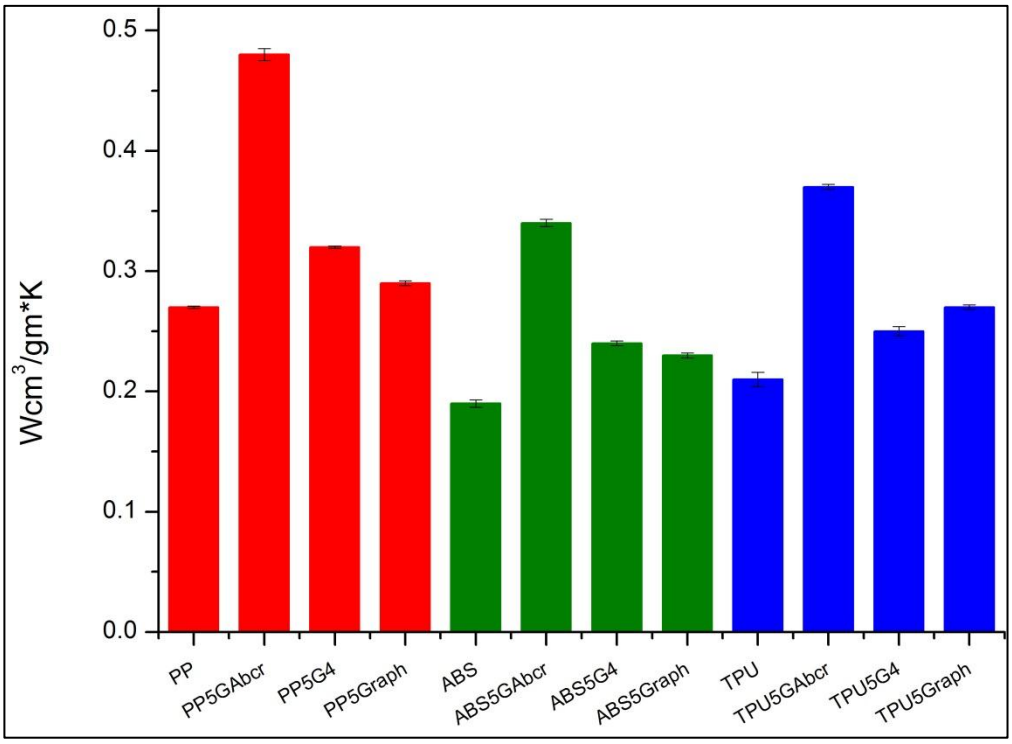

Figure 57 Specific thermal conductivity of the neat thermoplastic polymers and of polymer-based nanocomposites containing 5 wt.% of GAbcr, G4 and graphite.

As expected the addition of 5 wt.% of the carbon based fillers always led to an increase of the thermal conductivity of neat polymeric matrices. In every case, the maximum increments were obtained by using GAbcr which caused an increase of thermal conductivity greater than 76% with respect to the pure matrices. G4 addition allowed to achieve better properties with respect to graphite in PP and ABS, but lower performance in TPU composites, as also reported in **Table 10**. However, the G4 based materials always exhibited comparable conductivity values with respect to graphite-based nanocomposite. It is also interesting to observe that the thermal conductivity enhancement of GAbcr-based nanocomposite is still the same despite the hosting matrix.

These results seemed in contrast with the outcomes expected on the basis of the filler characterization. In fact, better properties were assigned by Raman spectroscopy, TGA and FESEM/EDS (due to the high purity and number of layer) at graphene nanoplatelets G4 with respect to GAbcr and, of course, graphite.

All the specimens were prepared using the same weight ratio between the fillers and the polymeric materials. In fact this is the simplest way to design composites materials. However, it was further observed (by means of helium pycnometers) significant differences between the densities of the fillers. These differences can be appreciated also by comparing the volume of 1 gram of the different fillers (**Figure 58**). Therefore the different volume fraction of the filler with respect to the matrix has to be taken into account. [136] In fact, nanocomposites containing GAbcr, had a higher volume fraction of the filler with respect to the same matrix filled with G4 or graphite, as reported in **Table 10**. The different volume fractions could affect the thermal conductivity of the final nanocomposites.

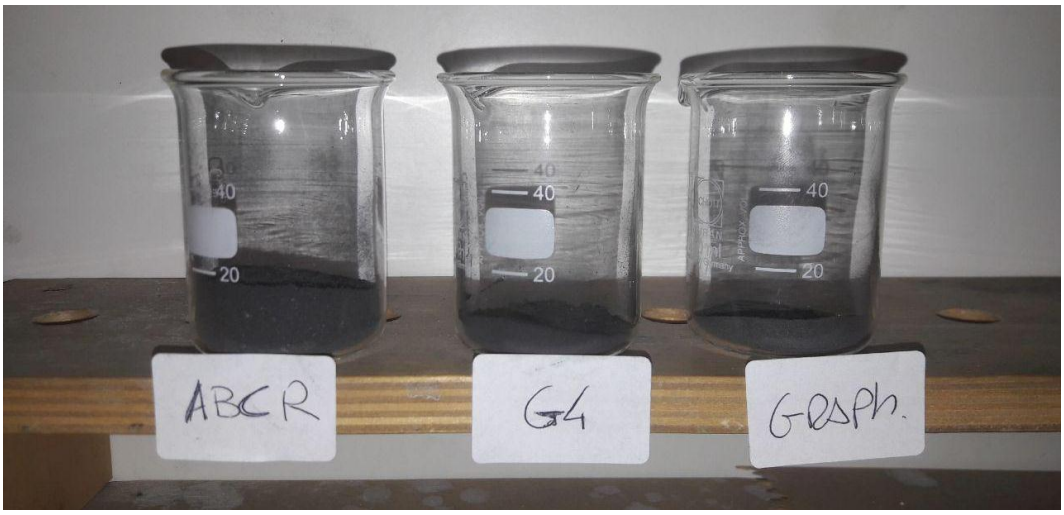

Figure 58 pictures of 1 grams of the employed fillers.

However, also after normalizing the results to the highest value of filler volume fraction no changes in trend were observed. The highest thermal conductivity enhancement was always achieved by using GAbcr with respect to G4 and graphite. Moreover G4 still showed higher conductivity enhancement with respect to graphite in PP-composite while graphite showed better performance in TPU-

based materials with respect to G4 counterpart. Finally comparable increment was observed for both G4 and graphite filled ABS materials as reported in **Figure 57** and in **Table 10**.

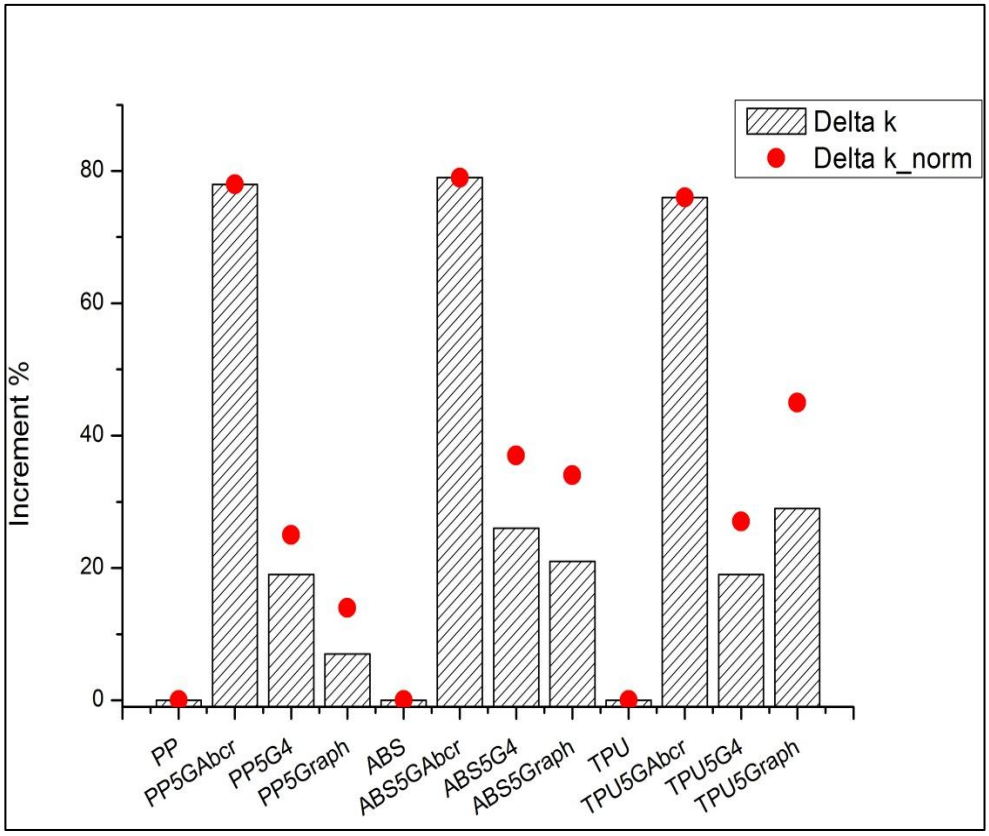

Figure 59 Thermal conductivity enhancement expressed as increment % of each nanocomposite with respect to the neat matrix (delta k) and theoretical increment normalized with respect to the highest volume fraction of filler (delta k_norm)

Theoretically specking, this result can be explained by the low boundary model as reported in equations 15. In fact, such a model assumes that there is no particles interaction and that each of them exhibits an isolated effect minimizing the effect of the fillers on the composite thermal conductivity, especially at low filler concentrations. [32]

$$k_c = \frac{1}{(\Phi_m / k_m + \Phi_f / k_f)} \qquad (15)$$

Additional improvement of the thermal conductivity of the nanocomposites by using filler with higher thermal conductivity could be negligible when the ratio between the filler thermal conductivity and the matrix thermal conductivity is over 100.[135] In fact, by looking at equation 15, it is clear that the ϕ_f/k_f goes drastically to zero resulting in a composites thermal conductivity that is strongly affected by the matrix conductivity. This means that, for low amounts of filler, the thermal conductivity, purity, and concentration of the filler are not the key parameters which enhance the thermal conductivity of the final composite materials. On the contrary, the key role is played by the aspect ratio, plane dimension and the dispersion degree of the GNPs.

As reported by Balandin, [33] in GNPs the thermal transport is limited by intrinsic properties, or by extrinsic effect, such as phonon-boundary or defect scattering. This means that for higher plane dimension, phonon-boundary scattering process is limited with respect to GNPs with lower plane dimensions. Since mean free path in GNPs, is 775 nm, [150] the coherence scattering process occurs more times in GNPs with higher plane dimensions. In fact, Nika et al. reported a simple method for calculating thermal conductivity of GNPs from a theoretical approach, demonstrating that, for small flakes, thermal conductivity has a stronger dependence on lateral size. This becomes less important for flakes with a dimension higher than 10 μm. [151] Probably in G4-based nano-composites, thermal conductivity is limited by the presence of a higher amount of interfaces and their thermal resistance, while in GAbcr-based materials it is more limited by defect presence. Concerning graphite-polymers composites, the higher plane dimensions does not lead to a higher increase in conductive properties, due to the lower aspect ratio, which results in the largest interface between filler and matrix because of the greater thickness. In addition, it seems more difficult to disperse fillers with lower dimension, as occurs for G4. Nika's approach seems consistent with the present results, thus demonstrating that lateral size is the crucial point in the choice of GNPs for increasing the thermal conductivity of polymeric matrices. In fact, in spite of the higher amount of defects present in GAbcr, the higher lateral plane size plays a crucial role in improving thermal conductivity, thus allowing to obtain better results.

Samples	k ± SD[a]	Δk (%)[b]	Wt.%[c]	Vol.%[c]	Δk_norm[d]
PP	0.27 ± 0.1%	-	0	0	-
PP5GAbcr	0.48 ± 0.5%	78	5	3.0	78
PP5G4	0.32 ± 0.1%	19	5	2.3	25
PP5Graph	0.29 ± 0.1%	7	5	2.1	14
ABS	0.19 ± 0.2%	-	0	0	-
ABS5GAbcr	0.34 ± 0.3%	79	5	3.5	79
ABS5G4	0.24 ± 0.2%	26	5	2.6	37
ABS5Graph	0.23 ± 0.1%	21	5	2.4	34
TPU	0.21 ± 0.6%	-	0	0	-
TPU5GAbcr	0.37 ± 0.2%	76	5	3.8	76
TPU5G4	0.25 ± 0.4%	19	5	2.8	27
TPU5Graph	0.27 ± 0.2%	29	5	2.6	45

Table 10 Specific thermal conductivity (a) ;(b) Thermal conductivity enhanment (c) filler content both in wt. and vol. % (d) thermal condcutivity enhancement normalized with respect to the higest filler vol.%.

Finally, thermal conductivity was measured for different percentages of graphene GAbcr in PP matrix in order to analyse the effect of the filler concentration. In **Figure 60** specific thermal conductivity of PP-GAbcr at different filler contents (1, 2.5, 5 and 10 wt.%) is reported. As it can be seen, the increase of filler concentration leads to an increase on the thermal conductivity of final nanocomposites. A maximum value of specific thermal conductivity up to 0.66 $Wcm^3/gm*K$ was obtained by using 10 wt.% of GAbcr, that corresponds to an increase of more than 140 % with respect to the unfilled matrix. In addition the same value of conductivity of PP5G4 containing 5% wt. of filler was achieved using only 2.5 wt.% of GAbcr, which highlights the crucial role played by the filler morphology in the enhancement of thermal conduction of polymeric composites.

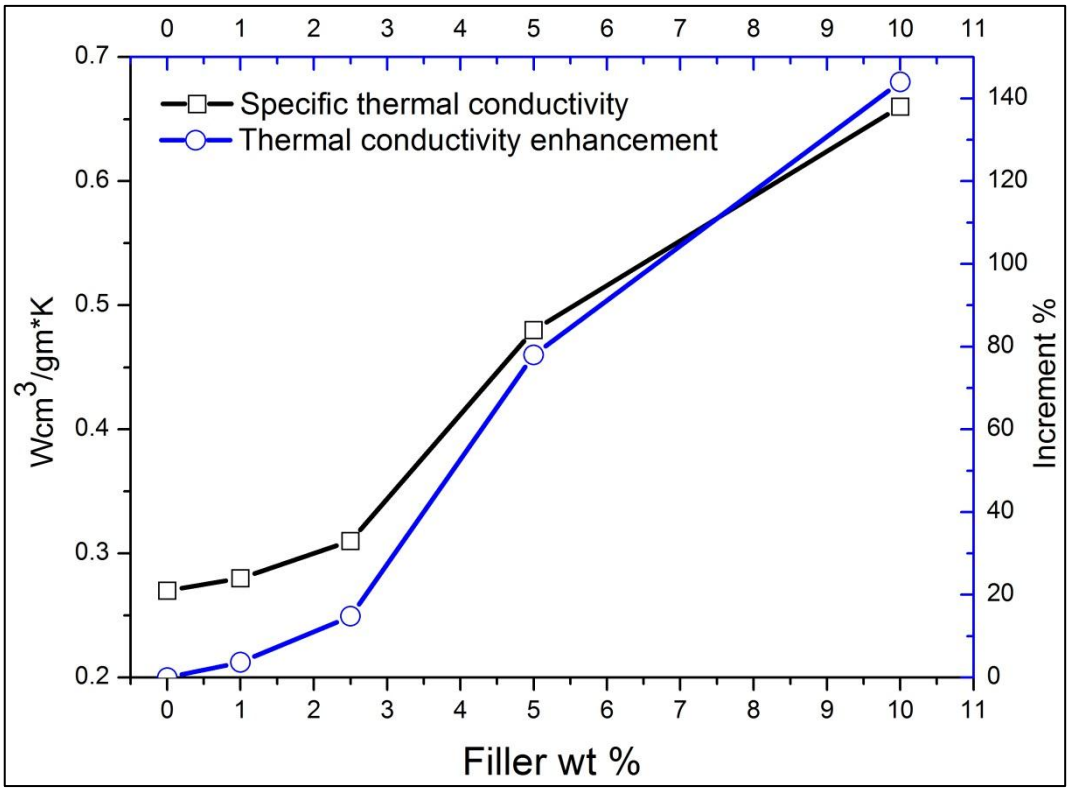

Figure 60 Specific thermal conductivity of PP-based GAbcr nanocomposites at different filler concentration (black square) and thermal conductivity enhancement with respect to the neat matrix (blu circle)

4.4 Effect of the dispersion degree on the thermal conductivity of GNPs-based nanocomposites

As reported in the previous section, polymers with enhanced thermal conductivity can be obtained by filling several matrices with thermally conductive fillers. The GNPs are the most promising fillers able to improve polymers properties.

By filling three different thermoplastic matrices with different GNPs purchased from different industries with different grade and purity, it was possible to demonstrate that, in spite of the filler purities, the main filler characteristic responsible for the improvement of thermal conductivity is the lateral flake dimensions. However, this trend was observed by filling polymeric matrices with the same amount of fillers by means of the same dispersion technique.

To understand the effect of the dispersion technique adopted, here we report a study in which a commercial epoxy resin was filled with the previously characterized carbon based fillers, and by exploiting several dispersion methods. Moreover, the effect of different amount of content will be further analyzed.

Epoxy resin based on bisphenol-a-epichlorhydrin is a slow-curing liquid resin, which possesses a viscosity value suitable for processing composites by using several dispersion techniques, and suitable for providing a wide processing window before the cross-link occurrence. In fact, the curing process occurs in 24 hour at room temperature after the addiction to the resin of the required amount of curing agent (triethylenetetramine), which progressively leads to the formation of cross-linked solid materials. For this reason, this epoxy resin was chosen as starting matrix.

The materials were prepared by mixing the stoichiometric amount of the epoxy oligomer and the curing agent. The filler was added in order to create a mixture which was then processed according to the different dispersion techniques. Four dispersion techniques were compared.

First of all hand mixing technique was conducted with the help of a glass rod. Ultrasound bath and sonication probe were also used as dispersion methods. In both these cases the process was conducted for 15 minutes. The specific processing parameters for these most commonly used technique are reported in **Table 11**.

Sample	Epoxy	Amine	Filler wt.%	Preparation methods
Pure resin	25	3	0	Manual mixing
TQ	25	3	2	Manual mixing
Bath	25	3	2	15 minute ultrasound bath
Probe	25	3	2	15 minute sonication probe at 30 % of the max. power

Table 11 Preparation methods adopted to create composites by means of the most commonly used techniques. Epoxy-to-Amine wt. % ratio is also reported.

Finally three rolls mill equipment was used as dispersion method. According to the literature, Three Rolls Mill (TRM) is able to achieve a good nano-fillers disaggregation and dispersion due to the combined effect of the high shearing forces with the continuous matrix mixing [139], [140], [152] As reported in materials and methods part, it is possible to work in two different modes: gap mode and contact mode. In the gap mode it is possible to modulate the distance between the different rolls in order to obtain the best filler dispersion in the polymeric matrix. In contact mode, the different rolls are in contact one to each other providing the highest shear stress to the system. Different three rolls mill cycles were tested in order to analyze also the effect of the different parameters. The adopted three rolls mill cycles are reported in **Table 12**.

Sample	Epoxy	Amine	Filler wt.%	Three rolls mill Cycles				
				Cycle	Gap 1	Gap 2	Contact	rpm
1	25	3	2	3	45	15	no	600
				3	15	5	no	600
2	25	3	2	3	45	15	no	600
				3	15	5	no	600
				3	0	0	yes	300
A	25	3	2	9	45	15	no	600
B	25	3	2	9	45	15	no	600
				9	15	5	no	600
C	25	3	2	9	45	15	no	600
				9	15	5	no	600
				3	0	0	yes	300
D	25	3	2	9	45	15	no	600
				9	15	5	no	600
				3	0	0	yes	300
				3	0	0	yes	300

Table 12 Three rolls mill cycles adopted in this study. Gap1 and Gap 2 are expressed as μm.

As observable from the table two different group of cycles were adopted. First of all cycles labelled as Cycle 1 and Cycle 2 were investigate. Cycle 1 represents the less severe conditions. The resin passes through the rolls for six times according to the gap modes. Gap distance was maintained constant for three times at 45 and 15 µm (between the first and second roll, and between the second and the third respectively) and then reduced to 15 and 5 µm and the mixture was processed for more three times. Cycle 2 was developed on the basis of Cycle 1. However, in this case the resin passes though the rolls three more times in contact mode. Beside them, four additional cycles (labelled with letters A, B, C and D) were investigated. Starting from the Cycle A, all the others were designed on the basis of the previous ones by increasing the number of passages through the rolls and stress the applied to the mixture. The rolls speed has been kept constant at 600 rpm in the gap mode and 300 rpm when the rolls are in contact (which are the instrumental limits).

Independently from the dispersion technique adopted, first of all graphene nanoplatelets (GAbcr and G4) or graphite were added to epoxy matrices at 2 wt. % filler content. Once the compounding was completed the resulting materials were cast into a cylindrical mould to let cross-linking occur at room temperature. Schematic representation of the materials production process is reported in Figure 61.

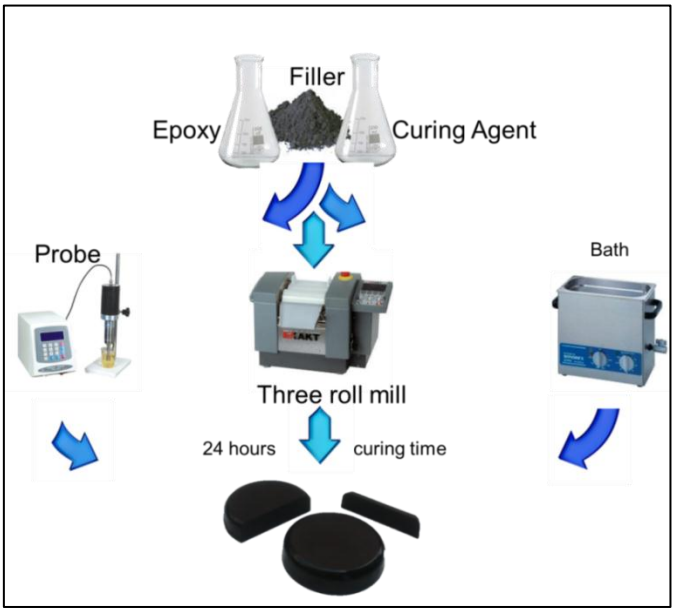

Figure 61 Schematic representation of the materials production processes

Thermal conductivity analyses were performed on all the composites obtained by using the different fillers and the different dispersion techniques. Thermal conductivity of 2 wt.% filled epoxy resin is reported in **Figure 62**.

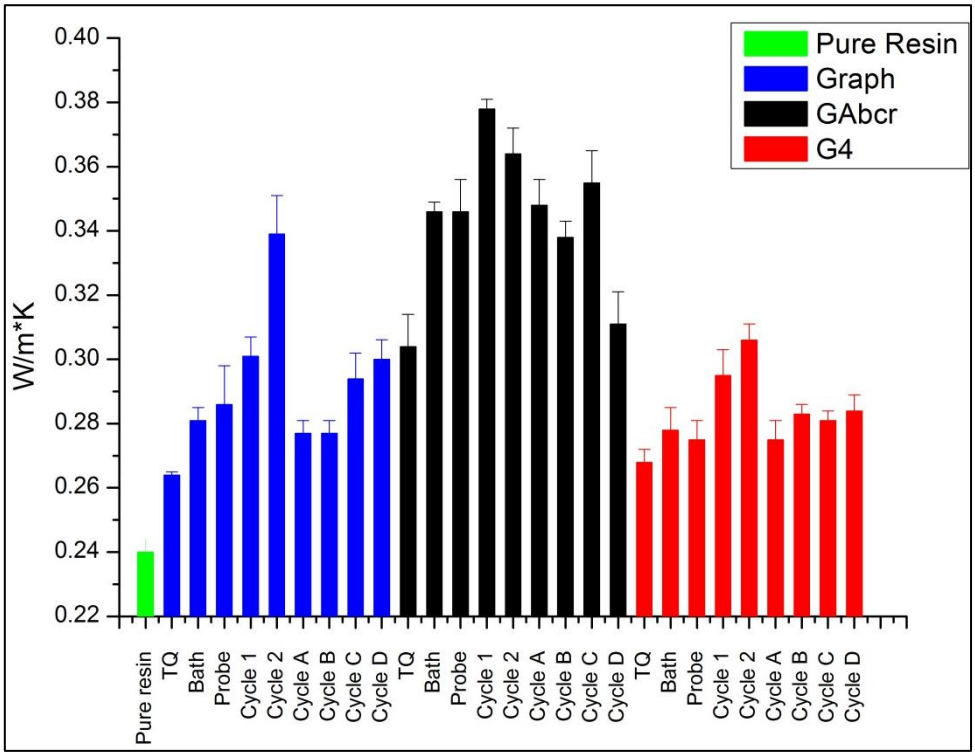

Figure 62 Thermal conductivity of all the prepared epoxy based composites at 2 wt.%

As shown in **Figure 62**, the addiction of 2 wt. % of carbon-based fillers, always increases the thermal conductivity of the neat matrix. However, at different dispersion techniques correspond different increment of the thermal conductivity of the epoxy resin. To have a better comparison between the experimental results, the thermal conductivity enhancement (%) is reported in **Figure 63**.

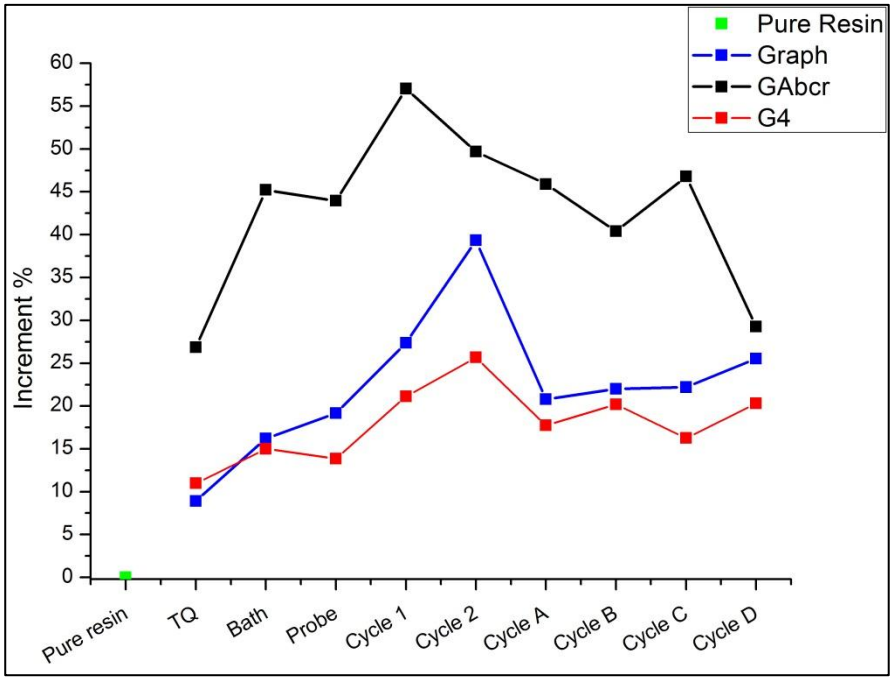

Figure 63 Thermal conductivity increment % of epoxy based composites (with 2 wt.% of filler).

As can be seen, in spite of the dispersion technique adopted, the best thermal conductivity enhancement was always achieved by using graphene GAbcr, highlighting again the importance of the lateral filler dimensions. Lower enhancement were observed by using natural graphite followed by graphene G4.

Regarding the different dispersion routes it is possible to observe that the lowest increment was always achieved by using the hand mixing technique (TQ method). In fact the amount of shear stress transmitted to the system is the lowest, leading to a poor dispersion and distribution of the filler inside the matrix. By increasing the amount of energy transferred to the different systems, an increase of the thermal conductivity enhancement was observed. In fact samples obtained by means of ultrasound bath showed an higher gain in the thermal conductivity than the hand mixed ones. This is of course due to a better filler dispersion with respect to the previous case. However, a comparable thermal conductivity enhancement (within their standard deviations) was observed by using sonication probe. It was reported for the carbon nanotubes case that, by using sonication probe, CNTs can be easily and seriously damaged. [58] In extreme cases the graphene layers of the CNTs are completely destroyed, also leading to the formation of amorphous

carbon nanofiber. This effect could be also observed for graphene-like fillers. In spite of the higher amount of energy applied to the systems that can provide a better filler dispersion, sonication probe probably leads to a partial reduction of the flake dimension and then to the formation of higher amount of interfaces inside the materials. Whit reference to the materials processed by three rolls mill, it is possible to observe better thermal conductivity with respect to the composite obtained by using other techniques, in particular for samples produced according to Cycle 1 and Cycle 2. Lower improvement was always achieved by using three rolls mill Cycles A, B, C, D. Since the different TRM cycles were based on two different approaches, the outcomes must be considered separately.

First of all, concerning the less severe Cycle 1 and Cycle 2 no particular differences were observed in G4-based materials. In fact, the same thermal conductivity was observed within their statistical errors. Different trend was observed for materials containing graphite, since an higher value of thermal conductivity was achieved with respect to the G4 materials by using Cycle 1, and a further improvement of conductivity was observed when using the more severe Cycle 2. In this case, the high shear stress provided by the contact mode, probably leads to a partial exfoliation process and then a reduction of the filler-matrix interface because of the increasing filler aspect ratio. GAbcr-based composite processed by Cycle 1 exhibits the highest thermal conductivity value with an enhancement of more than 57 % at 2 wt. % of filler content. However, in this case, no further enhancement was observed by working with the rolls in contact. This is probably due to the breakage of the lateral plane dimension. It seems that three roll mill is able to partially exfoliate thick graphite, while once the dimension is in the nanometric scale this does not happen any longer, as in the GAbcr and G4 cases.

Moving to the most severe TRM cycles, labelled as A, B, C, and D, no advantages were observed, but a drastic decrease in the thermal conductivity for GAbcr and graphite based materials. Also in this cases, this behavior could be attributed to a reduction of the plane dimension. Since the polymer mixtures were processed for a longer time (Cycle A) with respect to the previous cases, the initial graphite exfoliation (or the partial breakage of the graphene planes), leads to an increasing of the numbers of the nanoparticles resulting in an increasing of the medium viscosity. At this viscosity enhancement, an increasing of the shear stress is associated. Therefore the higher energy given to the systems leads to a continuous filler disaggregation resulting in a lower plane dimension. However a different

conductivity trend was observed concerning samples containing G4: the conductivity only slightly changes when increasing the number of cycles, in both gap or contact mode. Its seems to be very hard to reduce the filler lateral dimension in the case of G4 materials, due to the low starting value.

All of these hypothesis seem to be confirmed by looking to the samples morphology. As occurred in the case of thermoplastic nanocomposites, the polymer surface was polished by means of 1 μm diamond paste and observed at high magnification (200X).

Figure 64 reports the optical images of the composites obtained by means of hand mixing (TQ), ultrasound bath (bath), sonication probe (probe) and three roll mill Cycle 1 and Cycle 2 for the different fillers.

In the case of hand mixing it is possible to observe the presence of big agglomerates of particles and a poor particle distribution, in particular regarding GAbcr. A better distribution of the graphite particles, was observed. However also in this case the presence of big aggregates was detected. In the case of Grade 4 TQ composite, it is evident how the dimension of filler aggregate are smaller in comparison to the other filler types, but this feature is also related to the lower filler plane dimensions. This behavior was expected, due to the extremely low shear stresses generated by the hand mixing, even though the dispersion could be affected by external factors such as the operators force. Better results, in terms of dispersion and distribution, can be obtained by using a sonication bath. However, also in this cases the presence of aggregates is detectable, in particular for the fillers with the high plane dimensions (GAbcr and graphite). Sonication probe provides an higher amount of energy to the system during the dispersion process. A better filler distribution and dispersion was observed. Regarding GAbcr, the disappearance of the big aggregates is evident, however this could be also related to a decrease in the filler dimension due to the high amount of energy delivered to the system. This phenomenon is also evident in graphite-based composites. Finally a homogeneous distribution of small particles was observed when using Grade 4 filler.

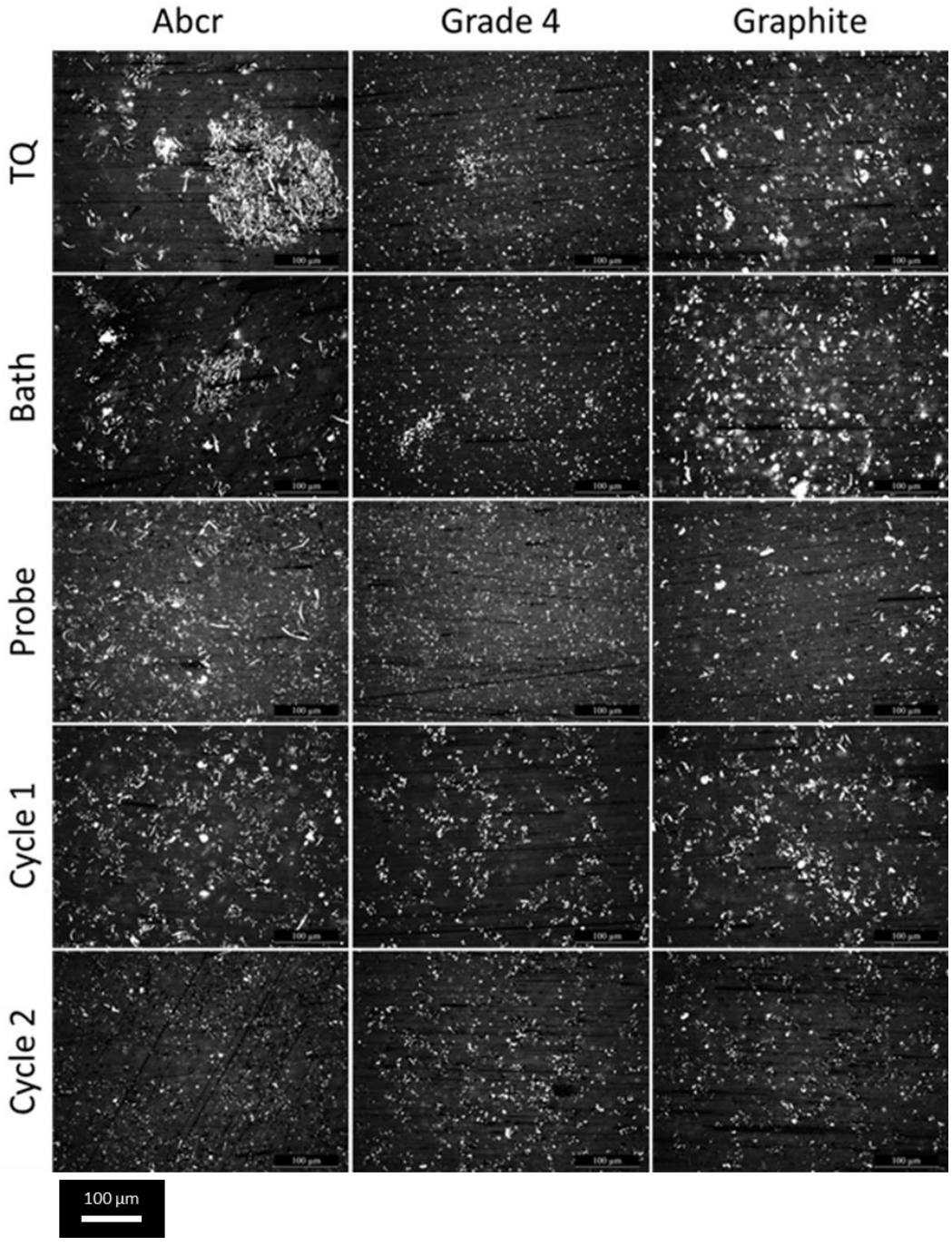

Figure 64 Optical images of TQ, bath, probe and Cycle 1 and Cycle 2 composites at 2 wt.% of the employed fillers. (200X)

Regarding three rolls mill dispersion methods, it is possible to observe that in the case of Cycle 1 a good dispersion and distribution of GAbcr was achieved. In fact a similar distribution of the filler, with respect to composite obtained by sonication probe, was observed. The presence of the fillers aggregates has been drastically decreased and a homogeneous distribution of the flakes is observed. Moreover, the its seems that the lateral size filler dimensions remains rather large. The most severe Cycle 2 gives very different results: flakes lateral dimension is drastically decreased. A similar behavior can be observed also in the case of graphite nanocomposites. An improvement in the distribution and dispersion degree was further observed in G4 nanocomposites moving from Cycle 1 to cycle 2. However no particular differences in filler dimensions was detected. This could be attributed to the fact that is harder to break fillers with very low lateral dimension.

This behaviors were also confirmed by FESEM analysis.

Figure 65 shows the cryo-fracture surfaces of GAbcr-based composites processed according to Cycle 1 and Cycle 2. At low magnification is possible to observe a less homogeneous fracture surface after Cycle 1 (fig. a) with respect to Cycle 2 (fig. c). This could be related to then disaggregation of flakes and the redistribution of the resulting particles occurring during the more severe Cycle 2. Nonetheless, at high magnification thinner flakes were detected also in the case of Cycle 2. However, also a reduction on the later size dimensions could be observed.

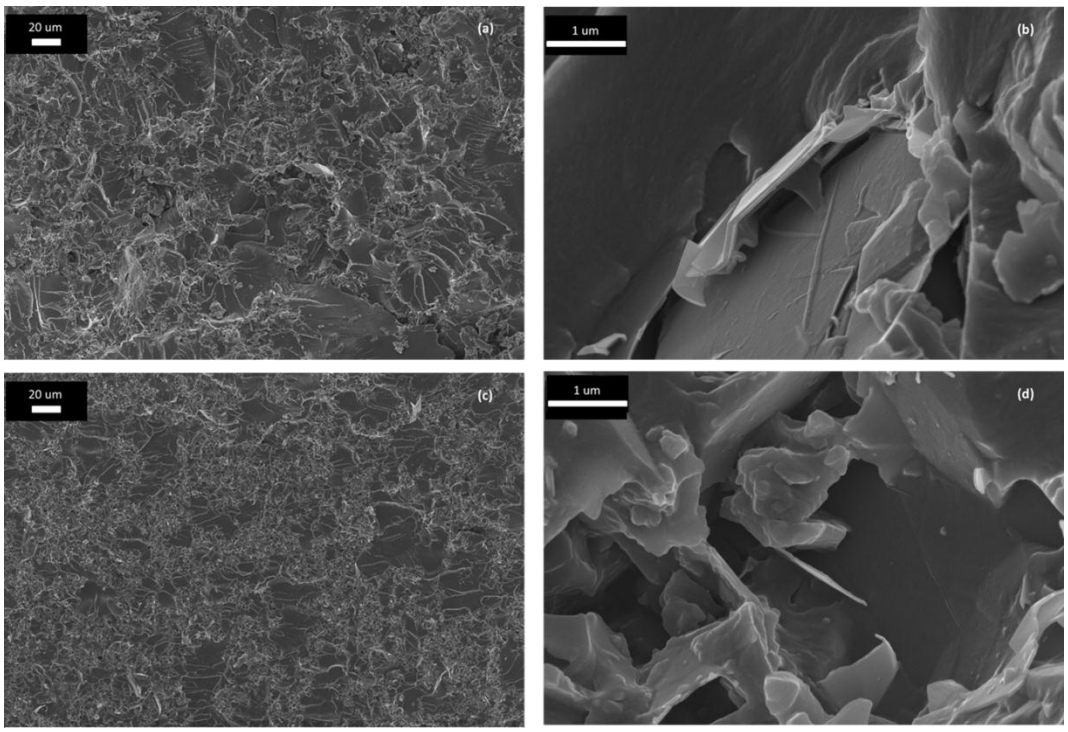

Figure 65 Cryo-fracture surface of GAbcr-based composites after Cycle 1 (a and b) and Cycle2 (c and d) at low (1kX, scale bar 20 µm) and high (50 kX., scale bar 1 µm) magnification.

FESEM images at both low and high magnification of G4-based composites processed by Cycle 1 and Cycle 2 are reported in **Figure 66** As observable at low magnification, G4 particles seems to be better dispersed after Cycle 2. This means that the filler distribution was improved with the help of TRM contact mode. At high magnification a reduction of the flakes thickness was detected moving from the less severe Cycle 1 to the harsher Cycle 2. However, since the lateral dimension of the flakes is already small, the decreasing of the lateral dimension is less evident.

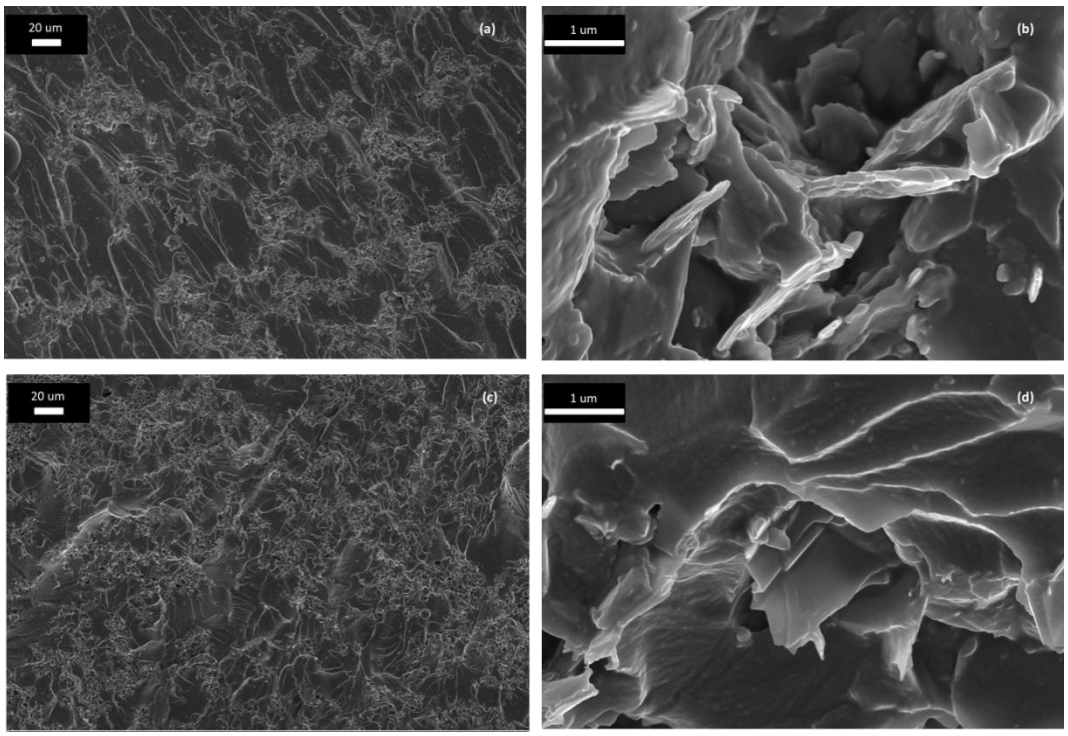

Figure 66 Cryo-fracture surface of G4-based composites after Cycle 1 (a and b) and Cycle2 (c and d) at low (1kX, scale bar 20 μm) and high (50 kX., scale bar 1 μm) magnification.

Regarding graphite-based three rolls mill materials, at low magnification **Figure 67** (a and c) puts in evidence some differences in the fracture surface after Cycle 1 and 2. As previously observed in the GAbcr case, a less homogenous fracture surface was detected after Cycle 1 sample with respect to Cycle 2. This is related, also in this case, to a reduction on the flakes dimension. At high magnification, both thin and thick aggregates can be seen. However, in the case of Cycle 2 nanocomposites the bigger aggregates observed after Cycle 1 disappear. This is probably due to an better filler dispersion coupled with a partially exfoliation of graphite. The partial exfoliation of the graphitic plane could have a positive effect since this would result in an increase of the aspect ratio.

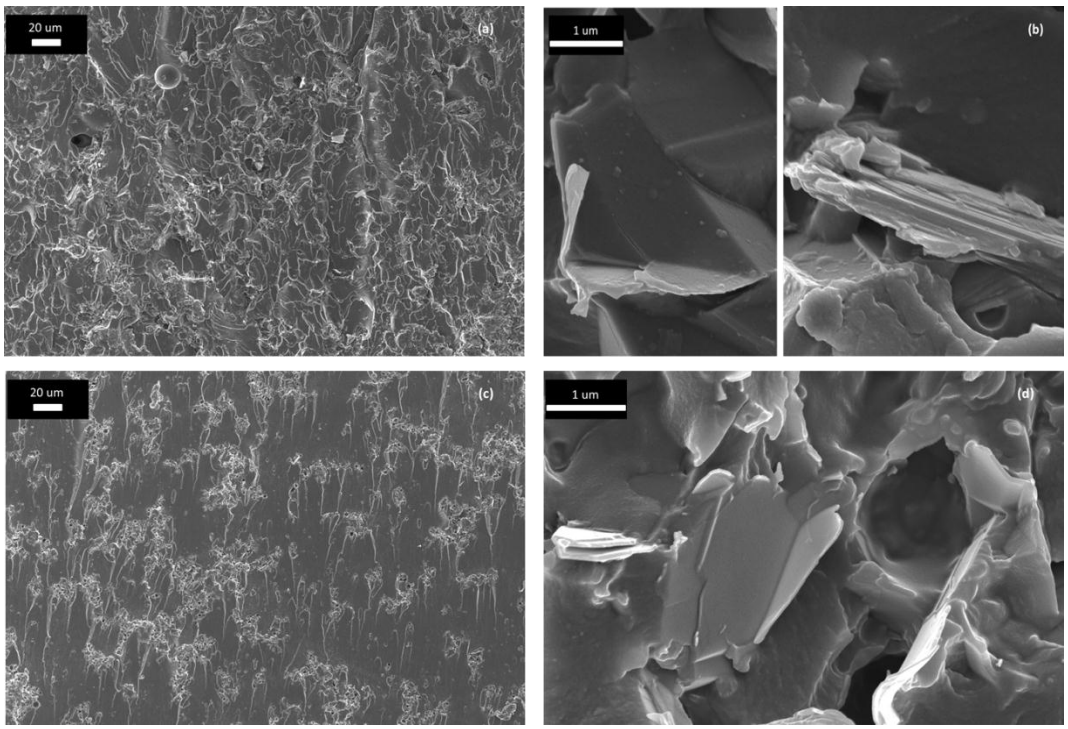

Figure 67 Cryo-fracture surface of Graphite Cycle 1 (a and b) and Cycle2 (c and d) materials at low (1kX, scale bar 20 μm) and high (50 kX., scale bar 1 μm) magnification.

Figure 68 shows the optical images of the polished surfaces of the three rolls mill samples obtained with the most severe cycles, labelled with the letters A,B, C and D. For all the analyzed materials a progressive improvement of dispersion and particle distribution occurs moving from Cycle A to Cycle D. On the other hand, contemporaneously, a progressive reduction of both lateral dimension and aspect ratio was observed for GAbcr and graphite containing composites. Moreover, starting from Cycle C, its seems that no more aggregates exist, and therefore the filler dimensions become comparable with those of Grade 4 platelets. However, as mentioned before, also in these cases, its seems very hard to further reduce the filler lateral dimension when it becomes very low.

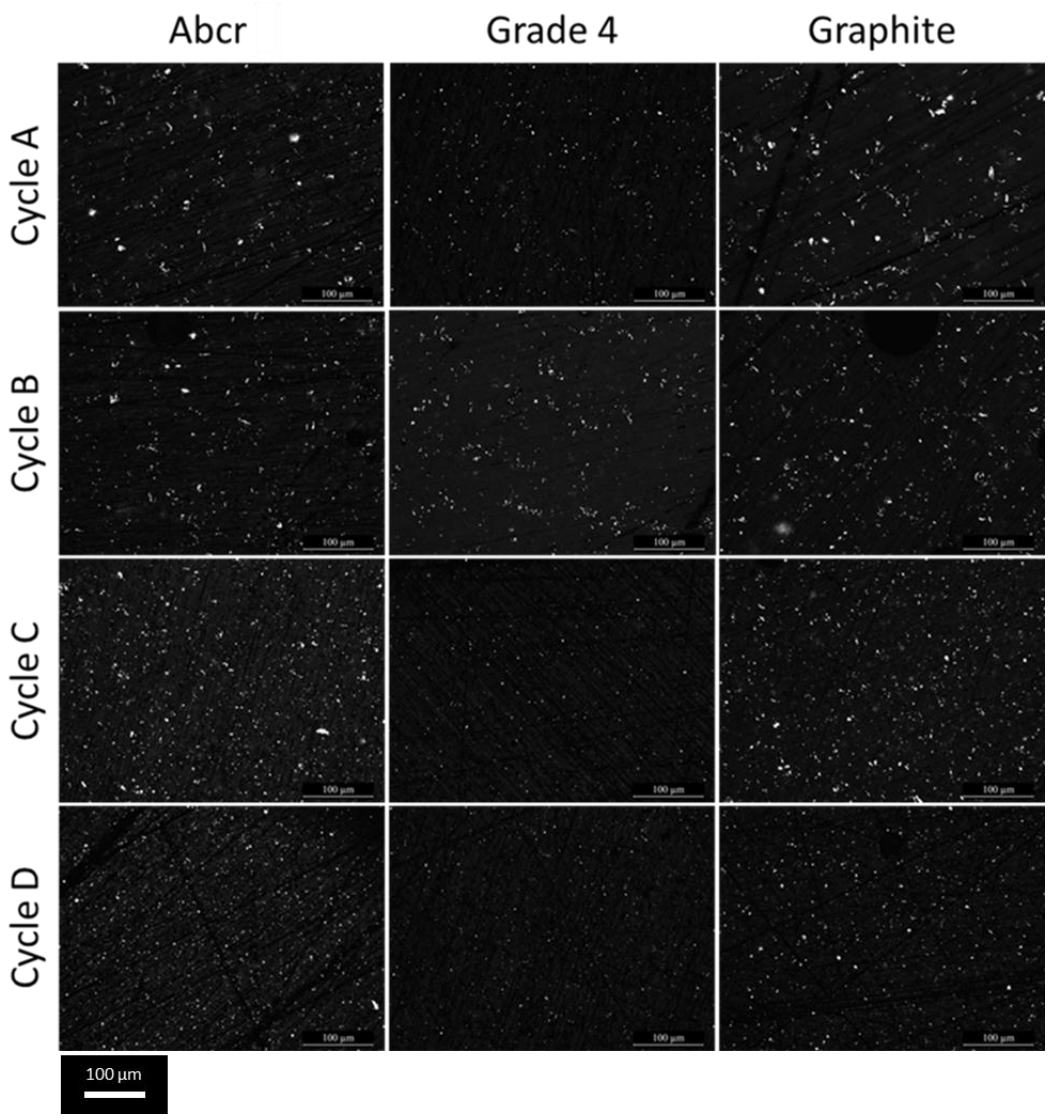

Figure 68 Optical images, after three rolls mill cycles A, B, C and D, of composites at 2 wt.% of the employed fillers. (200X, scale bar 100 µm)

In light of this scenario, the effect of the use of different amount of fillers was also analyzed. Since the best results were achieved by using Cycle 1 and Cycle 2, with respect to TQ, ultrasonic bath and probe, and since the adoption of more severe TRM cycles (A, B, C and D) did not give any advantage, further investigation were focused on the most promising TRM cycles only. Thermal conductivity of composites processed according to Cycle 1 and Cycle 2, at different wt. % of filler is reported in **Figure 69**.

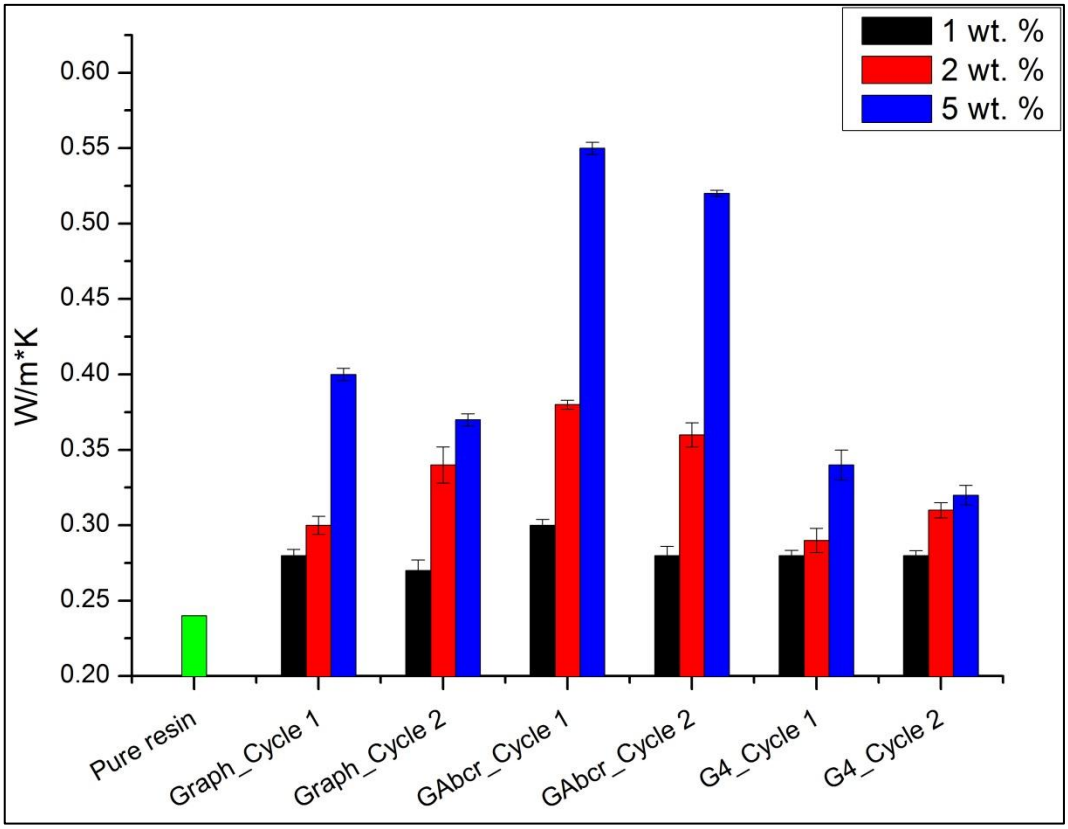

Figure 69 Thermal conductivity of composites processed according to Cycle 1 and Cycle 2 and using different wt. % of fillers

As expected, the enhancement of the thermal conductivity is proportional to the filler loadings. Sample with 1 wt. % of carbon based fillers show a similar and small improvement in thermal conductivity. The reason of the low increment is obviously due to the low amount of conductive fillers that are not enough to promote the thermal transport. An higher increase of the conductive properties were achieved by filling the epoxy resin with 5 wt.% of the carbon-based fillers. When using a filler content of 5 wt.%, a reduction of the thermal conductivity was achieved passing from Cycle 1 to Cycle 2 which is probably due to the particles breakage. However, whatever was the amount of fillers and the dispersion technique adopted, the maximum increment of conductivity was always achieved by using GAbcr.

Figure 70 the increment (%) of the thermal conductivity is reported as function of the filler content (wt.%) in the case of Cycle 1 based materials. A quite linear dependence between thermal conductivity increment and

filler weight percent was observed. The maximum thermal conductivity increase was observed by filling the epoxy resin with 5 wt. % of GAbcr reaching an increment on the conductive properties of more than 130%. However, it is important to note that it is possible to achieve the same thermal conductivity enhancement by using very different amounts of fillers: a low amount of filler characterized by an higher lateral dimension (1-2 wt.% of GAbcr) grants the same thermal conductivity of much more higher contents of G4.

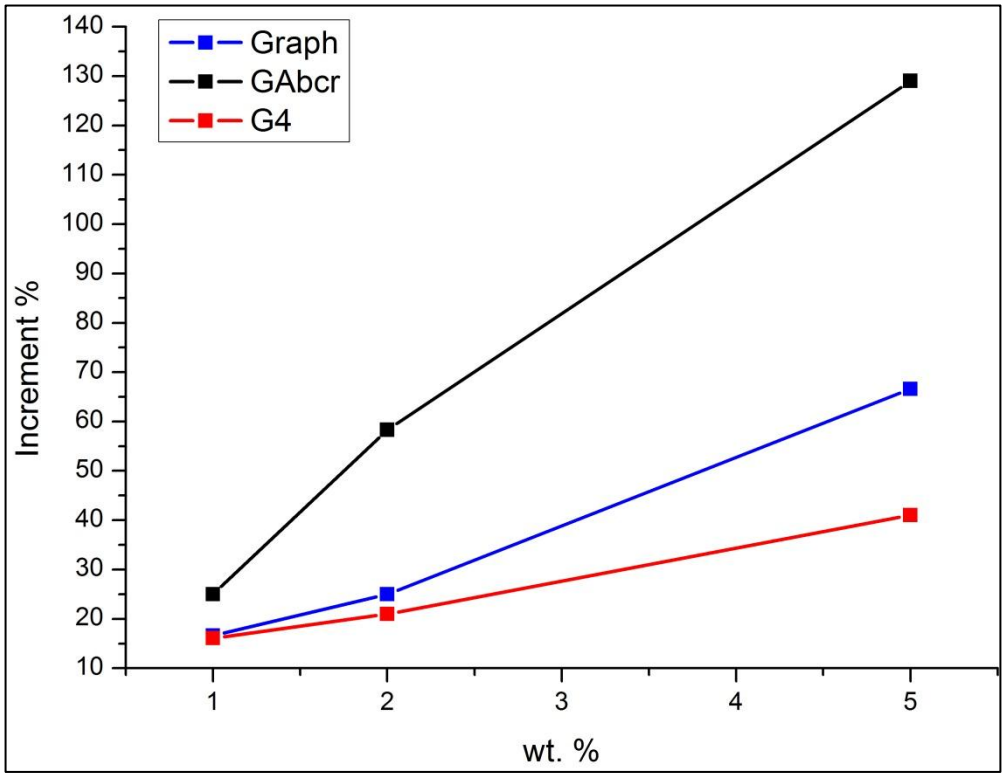

Figure 70 Thermal conductivity increment as function of filler loading, regarding composites produced by using Cycle 1.

Finally, as the involved carbon-based nanofillers are electrically conductors, the electrical conductivity of all the prepared materials was checked. The electrical conductivity of the material should increase very much, if continuous pathways between the filler were present all across the material. In turn, the formation of such kind of pathway is expected to depend from the dispersion technique adopted for the production of the composite. The electrical conductivity of the materials

was measured using the four point technique and the results are reported in **Figure 71**.

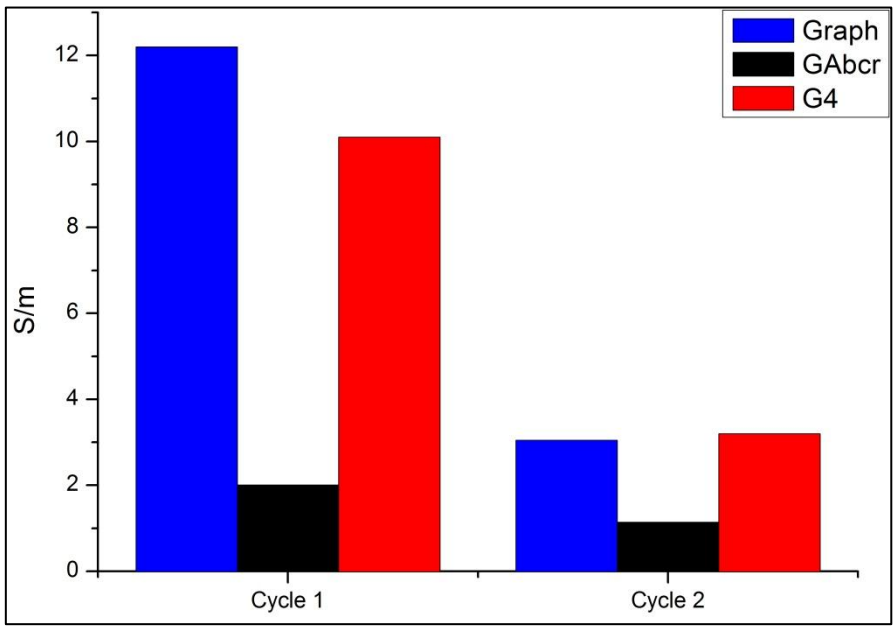

Figure 71 Electrical conductivity of epoxy based composites containing 5 wt. % of filler.

Only in the case of samples containing 5 wt.% of fillers a change in the electrical behavior was observed with respect to the neat matrix. In fact, when using 1 and 2 wt.% of filler contents it was not possible to obtain a percolation threshold inside the material. As mentioned in the introduction part, the percolation threshold depends on different factors such as filler dispersion and distribution, filler dimension, shape and therefore aspect ratio. Focusing on the dimension of the fillers, Moghadam et al. [140] demonstrated how the obtainment of the theoretical percolation threshold for graphene and graphite based polymer composites is a function of the size of the filler, as reported in **Figure 72**. The results reported above are in good agreement with respect to the Moghadam's prediction. The involved carbon-based fillers show a broad distribution of the lateral size of the flakes, with the average dimensions below 10 μm. Moreover, during the roll mill dispersion a decrease of the lateral flake dimension occurs leading to a percolation threshold higher than 2 wt. %.

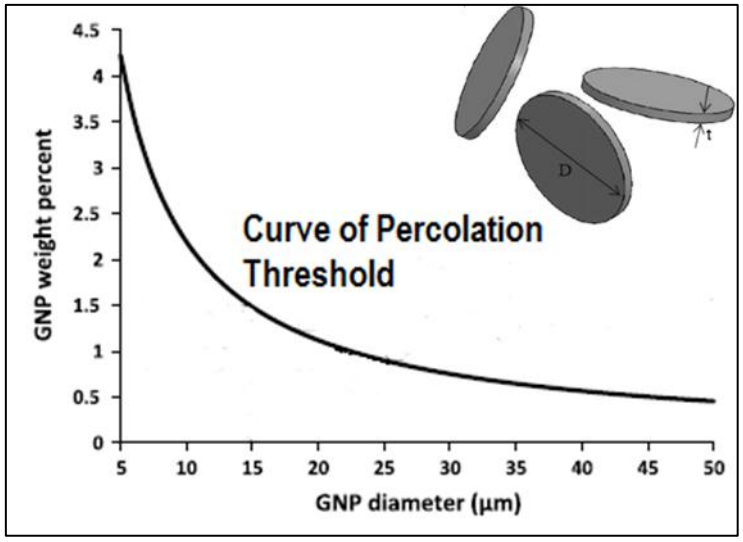

Figure 72 Graphene (GNP) weight percent that has to be used to obtain the percolation threshold as a function of the diameter (d) of the graphene flakes [140]

A decrease in the electrical conductivity was observed in Cycle 2-based materials with respect to Cycle 1, despite of the fillers used. Very likely the use of more severe Cycle 2 leads to the decrease of the lateral flake dimension and the increase of the number of interfaces. Therefore, an higher percentage of filler is required to reach the percolation threshold when processing the composites according to Cycle 2. In fact, the best results were always achieved by using Cycle 1. As evident in the **Figure 71** an higher enhancement of electrical conductivity was obtained by using graphite and G4 as conductive fillers. The opposite rank for the capability of improving conductivity was observed in the case of thermal conductivity. This discrepancy is related to the low purities of GAbcr which was put in evidence by TGA, Raman and EDS analysis. Probably GAbcr itself possesses a lower intrinsic electrical conductivity in comparison to the other fillers. However, this difference in the electrical conductivity seems negligible if compared to the electrical conductivity of the pure epoxy resins, which is around ten orders of magnitude lower in comparison to that measured for composite materials.

Conclusively, by filling a commercial epoxy resins with the employed carbon based materials, and using several dispersion routes, it was possible to confirm what was previously observed in the case of thermoplastic nanocomposites. The main filler property suitable for enhancing the thermal conductivity of polymeric

composites is the lateral dimension of graphene platelets. In addition, by comparing the different dispersion techniques it was possible to confirm the promising effect of the three rolls mill equipment which grants a linear dependence between thermal conductivity increment and filler contents.

Starting from these conclusions, in order to try to push up the thermal conductivity of epoxy resin a new carbon-based nanomaterial (GAbcr_25) was tested as conductive filler. This material, with the same grade of GAbcr previously tested, but showing lateral dimension in the range of 25 µm, was still purchased from Abcr company.

FESEM analysis showed that the average dimension of the flakes is greater than that stated by the producer. Even if some small flakes are still detectable, the average lateral diameter seems effectively to be larger, with the presence of some very big flakes which reach a lateral dimension higher than 50 µm (**Figure 73**.)

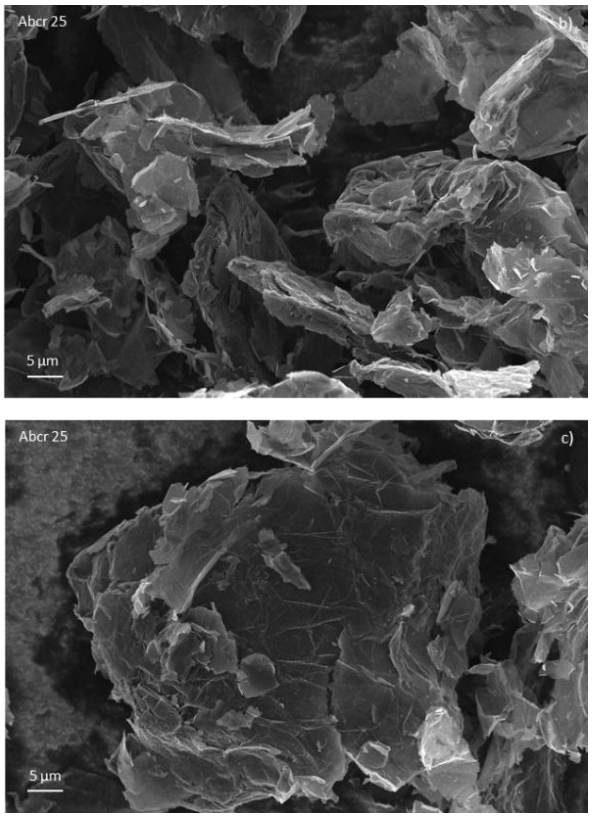

Figure 73 FESEM images of GAbcr_25 (scale bar 5 µm).

The composites were processed by TRM according to Cycle 1 condition at 5 and 10 wt. % loading. The thermal conductivity achieved by using GAbcr_25 is compared in **Figure 74** with those of similar composites, processed in the same manner by using the fillers prviously investigated.

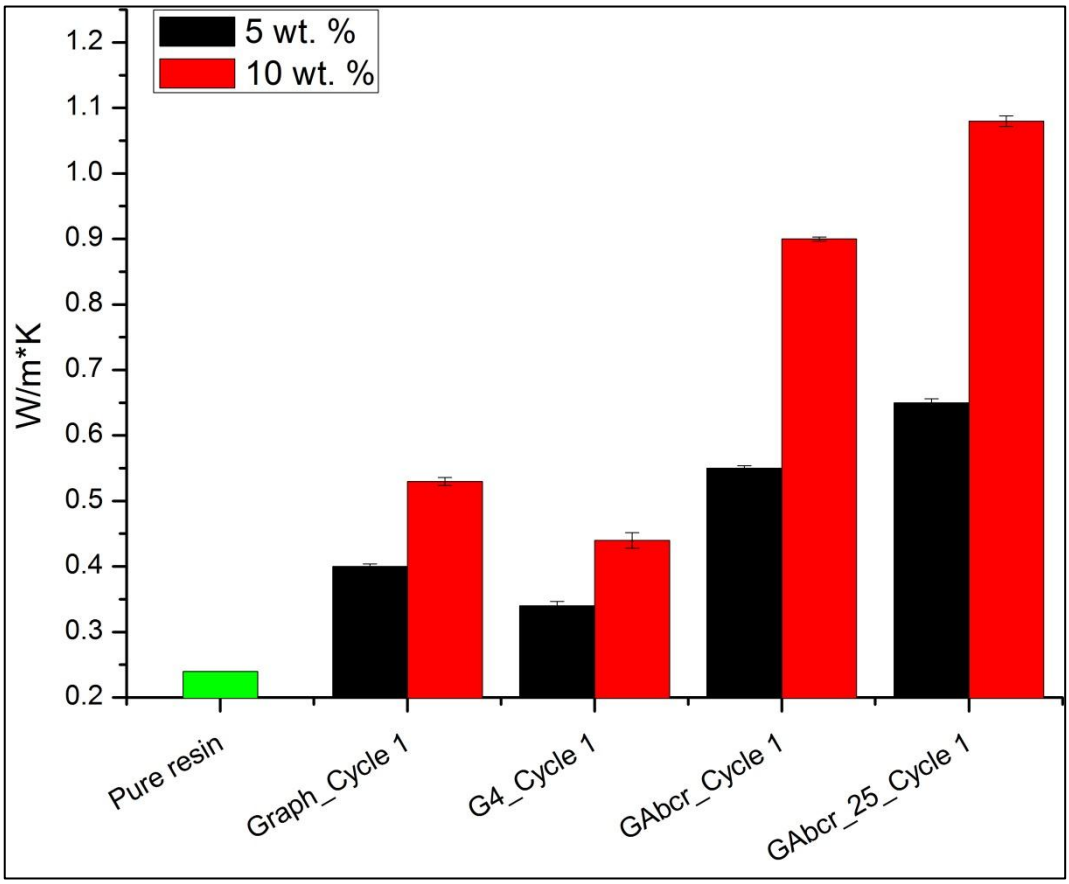

Figure 74 Thermal conductivity of epoxy composites processed according to Cycle 1 and using 5 and 10 wt.% of filler

By increasing the filler content from 5 wt. % to 10 wt. % a significant increase of thermal conductivity was observed when using graphite, G4 and GAbcr, as expected from the previous outcomes. More important conductivity increases were observed when using GAbcr_25, which highlight one more time the important role played by the lateral filler dimension. The maximum thermal conductivity was achieved by filling the epoxy resin with 10 wt. % of GAbcr_25; this composite reached a thermal

conductivity value of 1.08 W/mK that is more than 6 time higher with respect to the neat matrix.

4.5 Chapter conclusion

In this work, different commercially available graphene like materials were characterized and used as carbon-based nanofillers to enhance the thermal conductivity of several polymers.

First of all, three thermoplastic polymers (polyolefin, copolymer and elastomer) were filled with the same amount of the carbon based materials by means of the same dispersion technique. The previous outcomes reveals that the thermal conductivity is more affected by the lateral size of the involved filler, and only slightly affected by the presence of impurities and defects. However, from the literature point of views is clear that the dispersion technique and the filler loading plays an important role on the final conductivity enhancement. Therefore, an epoxy resin was chosen as thermoset matrix and processed by means of four different dispersion techniques at different filler content. Also in those cases, it was observed that the main filler properties that provide an higher increasing in the conductive properties is the lateral filler dimension. In fact, in spite of the dispersion technique and in spite of the amount of defects and impurities the highest enhancement was always achieved by using the graphene nanoplatelets with the highest plane dimension.

Chapter 5

Laser printed conductive tracks on MWCNTs based polymers surface

"Part of the work described in this chapter has been previously published in Polym. Eng. Sci. doi:10.1002/pen.24717"

5.1 Preface to chapter 5

Multifunctional material can be defined as "those materials presenting specific desirable electronic, magnetic, optical, thermal, or other properties to satisfy previously unattainable performance metrics. These properties are combined with each other, or with specific mechanical properties including stiffness, ductility, and strength." [153]

According to this definition, it is obvious that polymeric composites materials can be classified as multifunctional materials. In fact, they can find applications as structural or functional materials. In structural composites the mechanical properties of fillers are exploited, while functional polymer-based composites generally take advantage from the intrinsic electrical and thermal conductivity of the fillers. One of the most promising class of fillers able to cover both structural and functional purposes is represented by carbon-based materials, like carbon fibers, graphite, graphene nanoplatelets (GNPs) and carbon nanotubes (CNTs). In particular, GNPs and CNTs show superior mechanical properties associated with the highest values of electrical and thermal conductivity. However, since the first

study on CNTs published in 1991 by Iijima et al. [54] and since the first paper on CNTs-polymer nanocomposites published in 1994 by Ajayan et al.,[154] this field has been intensively investigated. Nowadays CNTs are the most established and promising fillers able to enhance the intrinsic properties of polymeric matrices. From the technological point of view, considerable efforts have been focused on the fabrication of electrical conductive polymers. CNTs can be used to achieve this goal due to their high electrical conductivity, and their ability to create a percolation network granting electron transport inside an insulating materials. As reported in the introduction part, the minimum amount of filler able to promote percolation is called percolation threshold. At this concentration, a sharp increase in the electrical conductivity occurs according to the percolation theory.

Several interesting reviews concerning the effect of the addition of CNTs to polymeric matrices have been published. [53], [58], [132]–[134], [155] The experimental outcomes reveal a strong dependence of the composite performance on the intrinsic characteristics of both matrix and CNTs used. Types of matrices (thermoplastic or thermoset), filler purity, chemical functionalization as well as dispersion methods play an important role in the conductive properties of composites. Different combination of the above mentioned factors correspond to different values of percolation threshold. Once the percolation pathway is achieved the whole material becomes an isotropic conductor. On the other hand, for many industrial applications, conductivity along selected directions and/or an electrical anisotropy is required. To achieve this goal many efforts have been made to align CNTs [131] However also in those cases, only one electrical signal can pass through the entire composite. In order to obtain conductive tracks on polymer-based materials, a variety of techniques have been developed. Stencil lithography, [156] metal base [157] or carbon based conductive inkjet [158] are nowadays consolidated techniques to obtain printed circuit on the polymers surface. The possibility of replacing metal wires for electrical conductivity is an important goal from the industrial point of view, which can be exploited in several sectors like flexible electronics and the automotive field. As reported in literature, moulded interconnected devices (MID) are electronic components in which metallic conductive tracks are applied to injection molded polymeric parts. The conductive paths can be created either by subtractive or additive procedures, that is by means of metal removal from a fully metallized surface or by a selective surface metal deposition respectively. However, this consolidated techniques requires 4-5 different process steps to generate the conductive tracks. [159]–[161] A patent also reports that electrical conductivity can be obtained locally by

melting the surface of a polymer containing CNTs. [162], [163] After the melting caused by the contact with a heating body, IR irradiation or the laser beam effect the CNTs migrate towards the molten zone until their concentration overtakes the percolation threshold, and this part of the composites becomes electrically conductive after cooling. In the last few years, some papers [164]–[166], based on a patent [167], demonstrated the possibility of functionalizing the CNTs-polymer composite surface by using laser printing. In this case the laser beam acts on the surface of the composite inducing the formation of conductive tracks embedded in an insulating polymer. A pyrolysis process occurs, leading to a localized and directional formation of a percolation pathway. Laser treatment of the surface of CNT-polymer composites is a very promising, simple, flexible, environmental friendly and cheap method suitable for obtaining conductive metal free tracks

Cesano et al. [164] published a study in which laser treatment was performed on composites containing multiwall carbon nanotubes (MWCNTs) in high density polyethylene (HDPE) matrix, obtaining a stimulated percolation at 3 wt.% loading content of MWCNTs. Moreover in this case, the researchers focused their attention on the structure of conductive tracks. Leibscher and co-workers [165] analysed the effect of laser printing on the electrical conductivity of MWCNTs based polypropylene/polycarbonate (PP/PC) blend with different PP/PC ratios. They observed that it is possible to reduce the resistivity of the induced conductive tracks by increasing the PC content, due to a better filler dispersion. Moreover, both Leibscher and Colucci et al. [166] observed that, depending on the laser parameter setup, different values of electrical resistance can be achieved. In fact, laser treatment can be tuned on the basis of five different parameters:

(i) power, P (expressed as % of the maximum power available);
(ii) frequency, F (kHz);
(iii) writing speed, V (mm/s);
(iv) number of repetitions, N;
(v) defocusing, D.

However, due to the high number of possible combinations of these parameters, the comprehension of the effect of each of them on the process effectiveness must be improved.

In order to better understand the key parameters that govern this process, we carried out a systematic study of laser-polymer interaction by using a Design Of Experiments (DOE) approach. DOE consists in the simultaneous study of several

variables that can affect a process. This useful method is based on the principle that it is possible to achieve a complete understanding of process parameters by combining several factors in only one study, thus greatly reducing the total amount of experiments. [168] By using an appropriate design of experiment, it is possible to discriminate between the strongest and weakest variables that affect the final material properties or the efficiency of an industrial process. When attention is focused on the strongest ones, all the other parameters become irrelevant, and then it is possible to set up the process in the cheapest possible way.

This chapter aims to investigate the influence of the different parameters adopted in the laser treatment on the electrical resistivity of laser printed conductive tracks, obtained on the surface of polycarbonate/acrylonitrile-butadiene-styrene blend (PC/ABS) filled with multiwall carbon nanotubes (MWCNTs). Due to its excellent physical and mechanical properties, PC/ABS is an important matrix used in automotive sector for different applications. [169], [170] Three PC/ABS-MWCNTs nanocomposites with different composition (0.5; 0.75; 1.0 wt.% of MWCNTs) were processed and submitted to laser treatment according to the DOE approach. Once the best parameter setups were detected, additional restrictions on the final outcomes were applied for obtaining multifunctional and multidirectional electrical materials. In fact, for the practical exploitation of the laser writing method several requirements must be fulfilled: low surface electrical resistance per length unit inside the tracks (e.g. below 10 kΩ/cm), absence of electrical signal between not in contact adjacent tracks (inter-tracks resistance Rinter) and absence of sample deformation after laser treatment. Microstructure, mechanical and thermal behaviour were also studied in order to have a complete characterization of the nanocomposites after laser functionalization.

5.2 Materials and laser functionalization

Starting from a commercial master-batch of PC/ABS filled with 2.75 wt. % of commercially available MWCNTs, several PC/ABS nanocomposites were obtained by diluting the starting materials. However, three different composition, at 0.5, 0.75 and 1.0 wt.% (labeled as 0.5CNT, 0.75CNT and 1.0CNT) were studied because nanocomposites filled with higher amount of MWCNTs, shown the presence of percolative network, while the aim of this work is to obtain electrical conductivity along selected tracks obtained by laser printing technology.

Laser treatments were carried out by using a CO_2 laser Towermark XL from Lasit, emitting in the infrared range (λ = 10600 nm) as was reported in previous papers. [164]–[166] Five different parameters were considered and modified in order to tune the interaction with polymer. The maximum available power was 100 W operating in a frequency range between 0.1 to 30 kHz. The distance between sample and focus lens is called defocusing and it is expressed in mm; a higher defocusing value results in a wider surface treated. Writing speed (mm/s) and number of repetitions were the other two laser parameters that were tuned. In order to cause pyrolysis only and avoid polymer combustion, laser printing was carried out under N_2 atmosphere. The typical experimental setup is reported in **Figure 75**. Two trials were performed on a single polymer plate. For each trial, 4 ablated tracks, with a length of 10 cm and a distance between the tracks of 1 cm were processed. After laser treatment, the surface was gently cleaned with a jet of compressed air in order to eliminate carbonaceous volatile species. Silver conductive paint was deposited at the beginning and end of the tracks in order to stabilize the signal and to reduce signal noise during the electrical resistance measurements.

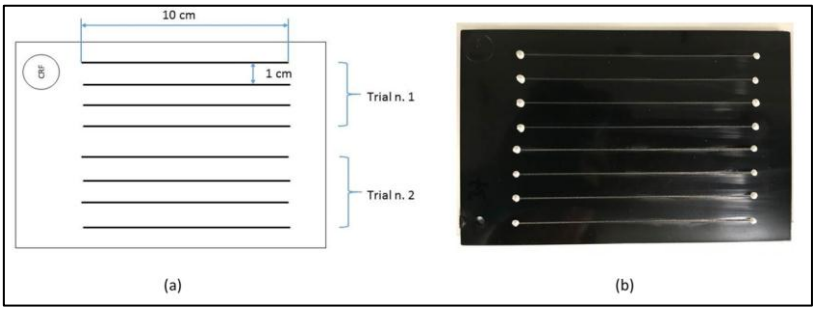

Figure 75 Typical experimental setup: (a) CAD program of each experiment, (b) picture of the treated materials.

Design of Experiment (DOE) approach was adopted in order to study the laser-polymer interaction. The effect of all the laser parameters mentioned above was investigated. Since the number of factors was higher than 4, a two level fractional factorial design approach was adopted with a design resolution V. Several trials were performed adopting different sets of parameters. According to the DOE method each trial differed from the other ones because two parameters out of five were differently set. Therefore the total amount of trials was 16 for each kind of nanocomposite. [171] The low level and high level adopted for each parameter are reported in **Table 13**. From the basis of the literatures outcomes, the maximum number or repetitions was fixed at 20. [166] Instrumental limits were adopted for

writing speed. Defocusing, frequency and maximum power were selected in order to have well defined tracks and no sample deformation. [164], [166]

Parameters	Low limit (-1)	High limit (+1)
Writing speed (V) [mm s^{-1}]	100	600
Frequency (F) [kHz]	5	30
Power (P) [%]	5	50
Number or repetition (N)	1	20
Defocusing (D) [mm]	0	50

Table 13 Low and high limits of the parameters adopted in the DOE

Supplementary restrictions were applied to the design. Randomized controlled trials were adopted. This means that the sequence of trials performed according to the different set of parameters was chosen in a random manner, in order to remove all sources of not controllable extraneous variation. By properly randomising the experiment it is possible to obtain an averaging out effect of noise factors that may affect the process. In fact randomisation can ensure that all levels of a factor have an equal chance of being affected by noise factors. Replications of the experiment were applied to the most promising trial, allowing the operator to have e more accurate appraisal of the experimental error. Replication can decrease the experimental error and thereby increase precision. No blocking process (a method of eliminating the effect of extraneous variation due to noise factors) was applied due to the unique master-batch and operator. [171] After this consideration the matrix design was finally developed based on the possible combination of low (-1) and high (+1) levels as it is possible to observe in **Table 14**. The inputs are represented by the five laser parameters, while the output is surface electrical resistance of the laser printed tracks.

Trial	*v (mm/s)*	*F (kHz)*	*P (%)*	*N*	*D (mm)*
1	-1	-1	-1	-1	1
2	1	-1	-1	-1	-1
3	-1	1	-1	-1	-1
4	1	1	-1	-1	1
5	-1	-1	1	-1	-1
6	1	-1	1	-1	1
7	-1	1	1	-1	1
8	1	1	1	-1	-1
9	-1	-1	-1	1	-1
10	1	-1	-1	1	1
11	-1	1	-1	1	1
12	1	1	-1	1	-1
13	-1	-1	1	1	1
14	1	-1	1	1	-1
15	-1	1	1	1	-1
16	1	1	1	1	1

Table 14 Matrix of design based on the different possible combination of Low (-1) and High (+1) level

The obtained data were analysed by using Minitab software for statistical calculations. This software quantifies the "effect" of single parameters or parameter combinations. In some cases the electrical resistance values exceeded the range (over range) of the multimeter (120 MΩ), and therefore it was not possible to measure the real value of electrical resistance. Statistical analysis (resulting in Pareto plot and Main effect plot, see Results and Discussion) was first of all performed fixing the electrical resistance over range value equal to 120 MΩ and then repeated by adopting 130 MΩ for the over range measurements. By comparing the obtained results in these two cases (adoption of 120 MΩ or 130 MΩ) it was possible to see that no difference in the statistical analysis outcomes occurred. This means that very high values of resistance bring to the same trend and conclusions of statistical analysis, independently from the numerical value of resistance used for calculation. At the end we established to use a conventional value of 130 MΩ for the over range values of resistance. Schematic chart flow is reported in **Figure 76**. Laser setup parameters were tuned in according to the matrix of design. A statistical approach was used to analyze the effect of each parameter. Finally a full characterization of the final materials was carried out.

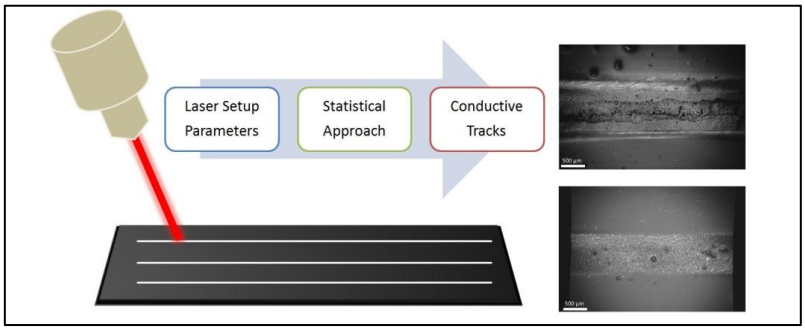

Figure 76 Experimental chart flow

5.3 Effect of laser parameters setup on the electrical behavior of conductive tracks.

According to the Design of Experiment approach, the first step in the study of laser-polymer interaction for obtaining conductive tracks is the creation of the experimental layout by substituting the low and high level in the matrix design with the adopted values. [168] Experimental layout is reported in **Table 15**. Trial 0 is referred to the untreated materials.

Trial	*v (mm/s)*	*F (kHz)*	*P (%)*	*N*	*D (mm)*
0	/	/	/	/	/
1	100	5	5	1	50
2	600	5	5	1	0
3	100	30	5	1	0
4	600	30	5	1	50
5	100	5	50	1	0
6	600	5	50	1	50
7	100	30	50	1	50
8	600	30	50	1	0
9	100	5	5	20	0
10	600	5	5	20	50
11	100	30	5	20	50
12	600	30	5	20	0
13	100	5	50	20	50
14	600	5	50	20	0
15	100	30	50	20	0
16	600	30	50	20	50

Table 15 Design matrix, obtained by all the possible combination of Low (-1) and High (+1) levels. Trial 0 is related to the untreated materials

Mean values of electrical resistance per length unit of all the analysed samples and trials are schematically reported **Figure 77** and **Table 16**. For each sample composition and trial, two different columns are shown in the table. On the left column, the mean value of electrical surface resistance per length unit is reported. Resistance values over the multimeter full scale, were reported as OR (over range), and in DOE calculations they were put equal to 130 MΩ. On the right column the inter-track electrical resistance (R_{inter}) was reported. Also in that case, no interaction is labelled as OR, while the presence of an electrical signal between two not adjacent tracks is labelled as Y (yes). No numerical evaluation of R_{inter} is here reported because, for the final technological application, electrical interaction must be completely avoided, independently from its intensity. However, for the polymer-laser interaction study (DOE approach) only track electrical resistance has been considered and not their interaction. The importance of R_{inter} will be discussed later. Several trials were performed on the unfilled matrix according to the matrix design; in every case no-change in the electrical behaviour occurred after laser writing. The electrical resistance (not reported here) of both untreated and laser treated matrix was very high and over the range of values that we could measure.

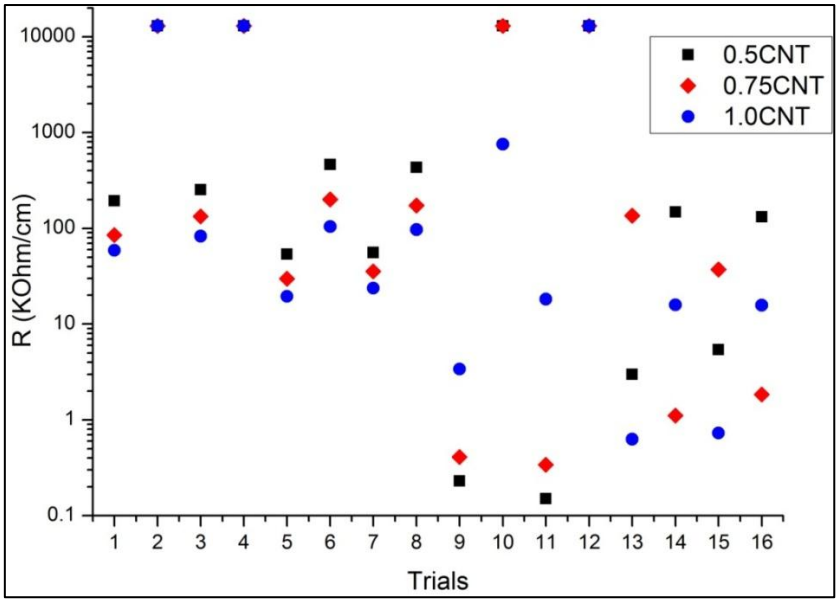

Figure 77 Electrical resistance per length unit of all the different trails and MWCNTs concentrations (Log. Scale).

Trial	0.5CNT		0.75CNT		1.0CNT	
	R ***(kΩ/cm)***	***R_{inter}*** ***(OR, Y)***	***R*** ***(kΩ/cm)***	***R_{inter}*** ***(OR, Y)***	***R*** ***(kΩ/cm)***	***R_{inter}*** ***(OR, Y)***
0	OR	/	OR	/	OR	/
1	193.67	OR	85.19	OR	58.80	OR
2	OR	OR	OR	OR	OR	OR
3	252.70	OR	133.60	OR	82.89	OR
4	OR	OR	OR	OR	OR	OR
5	53.60	Y	29.78	Y	19.52	Y
6	464.46	OR	200.48	OR	104.49	OR
7	55.90	Y	35.62	Y	23.79	Y
8	433.37	OR	173.28	OR	96.92	OR
9	0.23	OR	0.41	OR	3.39	OR
10	OR	OR	OR	OR	756.70***	OR
11	0.15	OR	0.34**	OR	18.24	OR
12	OR	OR	OR	OR	OR	OR
13	3.00	Y	135.84	Y	0.63	Y
14	147.95	Y	1.11	Y	15.94	Y
15	5.41	Y	37.16	Y	0.73	Y
16	131.83*	Y	1.84	Y	15.76	Y
STD	Max.Std (%)* 53		Max.Std (%)**146		Max. Std (%)***109	

Table 16 Electrical resistance per length unit of all the performed trials for every nanocomposite compositions as reported in the text. The standard deviation is reported only for the samples that showed its maximum value (marked samples).

As expected, laser-polymers interaction is a very complex process. Different trials give rise to different electrical behaviours. The same trial performed on composites with different CNT content provided different resistance per length unit values. In most cases, the increase of the amount of filler led to a decrease of electrical resistance. This is well in agreement with percolation theory. [155], [172] However, for some trials, the opposite happened. Furthermore, materials containing the same amount of fillers, but laser treated under different conditions, clearly showed a strong dependence on the laser setup. For this reason, a statistic approach was required in order to analyse the effect of each laser parameter and the result of their possible combinations.

In this section only data coming from the statistical analysis performed for 0.75CNT nanocomposites will be presented and discussed, as a representative case.

To show the relative importance of the effect of parameters and their combinations, a useful tool is the Pareto plot of factor effect. Moreover the Pareto plot reports a statistical significance level for which any effect, greater than a reference threshold, is potentially important. [168], [171]

The Pareto plot related to 0.75CNT samples is reported in **Figure 78**. As it is immediately clear, each parameters has a different weight on laser-polymer interaction for the laser printing process of conductive tracks. Writing speed and laser power are the most important parameters that govern the process. In addition, their interaction plays an important role. Statistical significance level, represented by red dashed line, was calculated as 21.86, as observable in figure. This means that frequency and defocusing clearly do not provide a significant variation on the electrical behaviour of laser printed tracks. Their combination and the number of repetitions have very little influence on it. Finally, all the other input combinations are irrelevant.

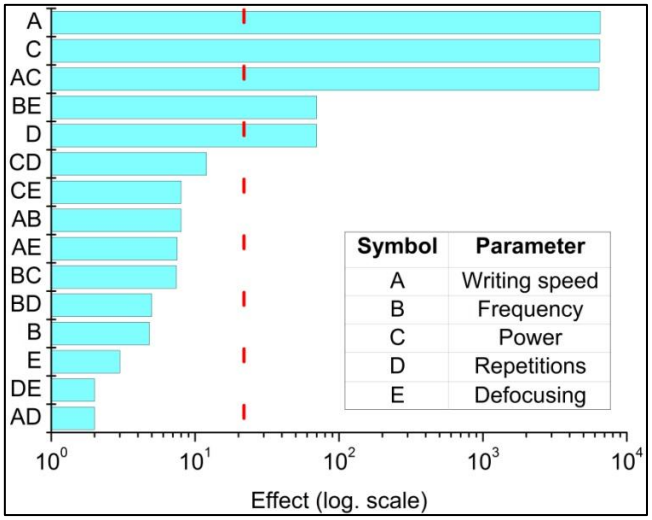

Figure 78 Pareto plot related to 0.75CNT sample expressed in logarithmic scale. Red dashed line is the statistical significance level, calculated as 21.86.

The real effect and importance of parameter changes is highlighted with the help of the main effect plot (**Figure 79**).The sign of the slope of straight curves related to each parameter indicates the effect of the parameter increase on the track electrical resistance, while the amplitude of the resistance change represents the weight of the parameter on the final output. [171] For instance, high power value corresponds to low electrical resistance, while at high writing speed corresponds to high resistance. Obviously, the opposite occurs for low power and low writing speed. Moreover, the main effect plot demonstrates that the system is not influenced by laser frequency and defocusing input parameters (constant effect). Finally, a very weak effect is observed for number of repetitions, as highlighted in the Pareto plot.

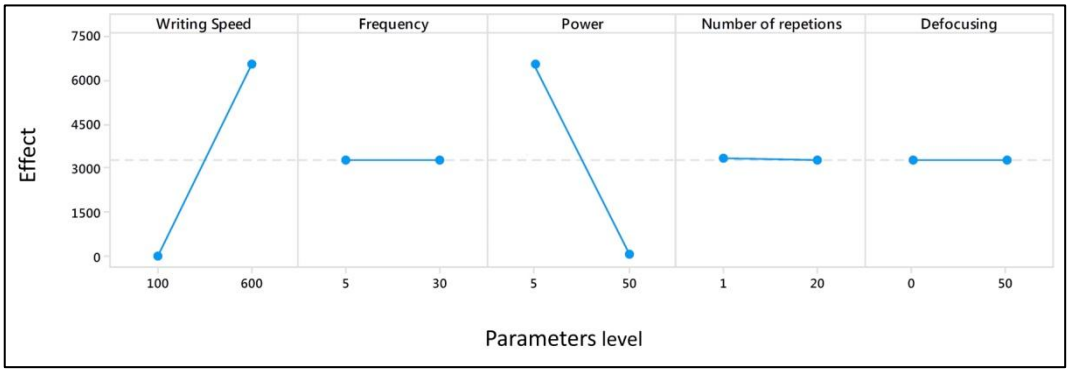

Figure 79 Main effect plot of parameters levels for sample 0.75CNT.

The outcomes put in evidence by the main effect plot could be explained by considering the presence of an insulating polymer coating, also called "skin effect". According to the literature the filler concentration is higher in the inner materials with respect to the surface due to the migration of MWCNTs during the injection moulding process. [155] Laser ablations promote a stimulated percolation by the combined effect of laser power and laser writing speed. In fact, the laser treatment is able to partially remove the surface materials through the breakage of the macromolecules, [173], [174] which results in a localized increase of MWCNTs content on the polymer surface.

Laser-polymer interaction is governed by the power delivered to the system and by the time required to promote macromolecules breakage. In fact, by looking at the matrix design and trial results (**Table 15** and **Table 16**), no conductive tracks were obtained by fixing the highest writing speed associated to the lower power value, despite of number of repetitions (over range value in trials 2,4,10 and 12). The highest measurable values of electrical resistance were obtained by coupling maximum power and maximum writing speed values (trials 6 and 8). Better results were obtained when the treatment performed according to this setup was repeated for several times (trials 14 and 16). Interesting results were observed for sample treated at low speed and high power (trials 5, 7, 13 and 15). However, the best results were obtained for samples treated by adopting the following laser parameters: v=100mm/s, P=5% and N=20 (trials 9 and 11). This means that, laser treatments performed at both low writing speed and low power performed for a long time (high number of repetitions) were less invasive and granted to MWCNTs the possibility and the time to migrate from the inner materials to the polymer surface, resulting in conductive tracks embedded in the polymer, that show an electrical resistance per length unit lower than 1 kΩ/cm.

The results above reported only show the effect of the different laser parameters on the electrical resistance, as DOE requires. However, the final goal is to obtain multifunctional and multidirectional conductive tracks embedded in an insulating polymers. In fact, as explained in introduction section, inter-tracks signal and samples deformations must be avoided. For each material and trial the right column in **Table 16** shows that inter-tracks electrical signal was frequently observed for samples obtained by applying 50% of the maximum available power, in particular when adopting low writing speed. In addition the inter-track conductivity seems scarcely affected by the number of repetitions. This means that applying high power for long time (low writing speed or high number of repetitions), macromolecules breakage occurs not only at polymer surface within

a wider zone but also deep inside, thus creating percolation pathways between the tracks. Furthermore, also a macroscopic sample deformation was observed for trials 13-14-15 and 16. For all of that reasons, those samples are not good candidates for the final applications.

By using a design of experiment approach, it was demonstrated that the main roles are played by the writing speed, the applied power source and their interactions. However, in some cases, high power leads to sample deformation and inter-track electrical signal as well (trials 13-16 performed on samples containing 0.5, 0.75 and 1.0%wt of CNTs). The best results (good track conductivity and no deformation) were obtained after trials 9 and 11, carried out with the minimum values of writing speed (100 mm/s) and power (5%). Moreover it can be inferred that some further advantages could be achieved by setting the power at an intermediate level. In addition it is obvious that it would be convenient to adopt a CNT percentage as little as possible. In light of this scenario, additional experiments were performed on sample containing 0.5CNT by reducing the power source, replicating trials in which that sample deformations and R_{inter} were observed. Table 17 reports the new setup parameters for additional trials, associated to the relevant electrical resistance per length unit values. Under these treatment conditions no sample deformation was observed.

By comparing for 0.5CNT samples the results coming from the first and the second set of trials (Table 16 and Table 17 respectively) further considerations can be made about the combined effect of power and writing speed. Samples treated at 600 mm/s writing speed show that the resistance decreases with the power increase from 10% to 50% (trial 18 Vs 14, trial 20 Vs 16). The opposite happens if the trials are performed with lower writing speed (100mm/s) since the resistance increases with the power increase from 10% to 50% (trial 17 Vs 13 and trial 19 Vs 15), thus demonstrating the strong dependence of the resistance from the coupling of power and writing speed. Moreover, by increasing the energy delivered to the surface, that is by increasing the power and decreasing the writing speed, the wideness and the thickness of the tracks becomes so high that there is dissipation of the signal between adjacent tracks. Finally, it is also possible to observe that, using a power in the range between 5% and 10%, the power increase always results in the conductivity increase for both writing speed of 100mm/s and 600mm/s (trial 9 and 11 Vs 17 and 19, and 10 and 12 Vs 18 and 20 respectively). In this range of power there is never dissipation of the signal between adjacent tracks whatever is the writing speed.

Trial	V (mm/s)	F (kHz)	P (%)	N	D (mm)	0.5CNT	
						R (kΩ/cm)	*Rinter (OR,Y)*
17	100	5	10	20	50	0.025	OR
18	600	5	10	20	0	414.12*	OR
19	100	30	10	20	0	0.021	OR
20	600	30	10	20	50	420.03	OR
						Max.Std (%)* 7.8	

Table 17 New trials setup parameters, adopted for samples obtained by decreasing the maximum power at 10% of maximum power, and resulting surface electrical resistance. Inter-track resistance is also reported as explained in table 3.

The best result was obtained for trial 19, which results in an electrical resistance per length unit value of 0.021 ± 0.001 kΩ/cm. The comparison of this result with the available literature [164]–[166] shows that, with the help of the design of experiment approach, it was possible to obtain the lowest value of electrical resistance per unit length at the lowest filler contents. The result of trial 19 confirms that laser printing is very promising for processing conductive tracks, therefore further characterization was focused on this sample.

5.4 Materials characterizations

To analyse the effect of laser parameters on morphological features, surface topography and FESEM analysis were performed on sample 0.5 CNT, trials 19 and 6. As already outlines, trials 19 and 6 showed the lowest and the highest electrical resistance per length unit respectively. **Figure 80** (a) and (b) show the surface topography of the trial 19 and 6 respectively. The sample treated by fixing low writing speed and low power for 20 times (trail 19, **Figure 80** (a)) presents a conductive track 200 µm depth for ~1 mm wide, while the sample treated at high speed and high power (trial **Figure 80** (b)) reveals a lower laser penetration leading to a 50 µm track depth.

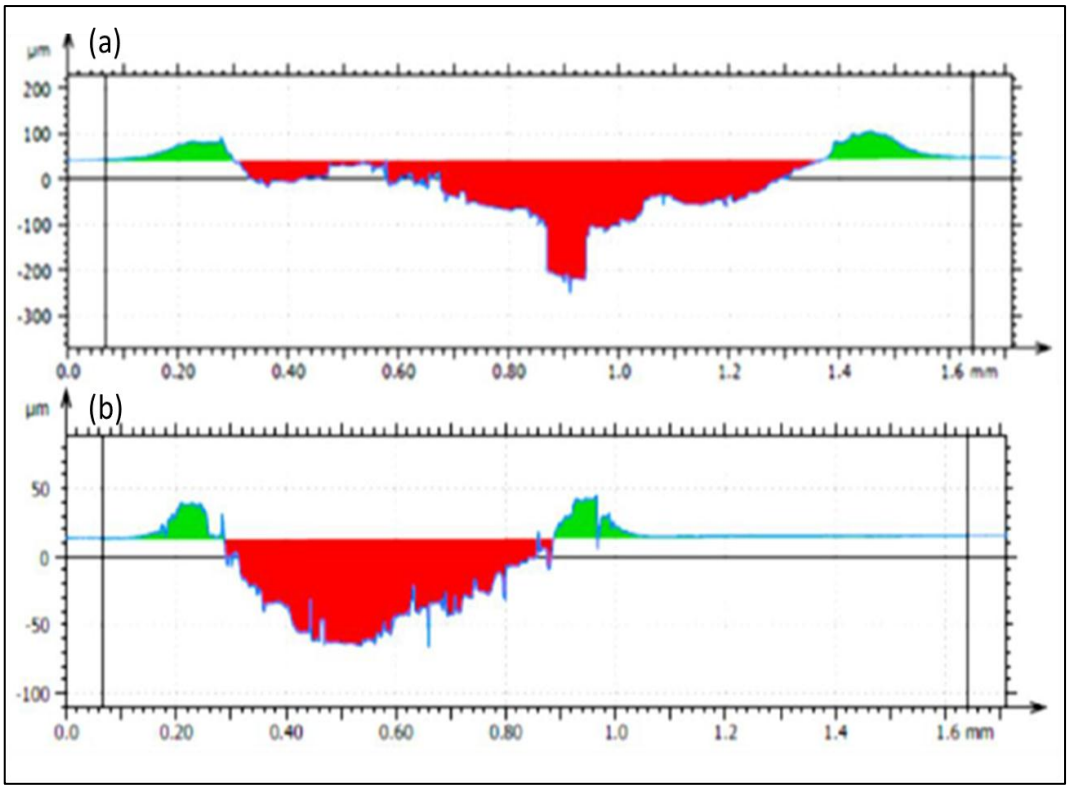

Figure 80 Surface topography of the conductive tracks obtained by adopting trials 19 (a) and trials 6 (b).

FESEM analysis, performed at 100X and 1000X, shows a strong dependence of the track morphology from the laser setup parameters, as depicted in Figure **81**. In fact, in sample resulting from trial 19 (**Figure 81** a and b) ablation process occurs deeply inside the material, revealing a percolation pathway that is not localized at the polymeric skin, as occurs for trial 6 (Figure **81** c and d) instead. Electrical conductivity is clearly dependent on the polymer skin effect. Sample treated for short time, in spite of laser power, does not show extensive polymer chain breakage and this results in the higher electrical resistance. As also reported observable from the surface topography in Figure **80**.

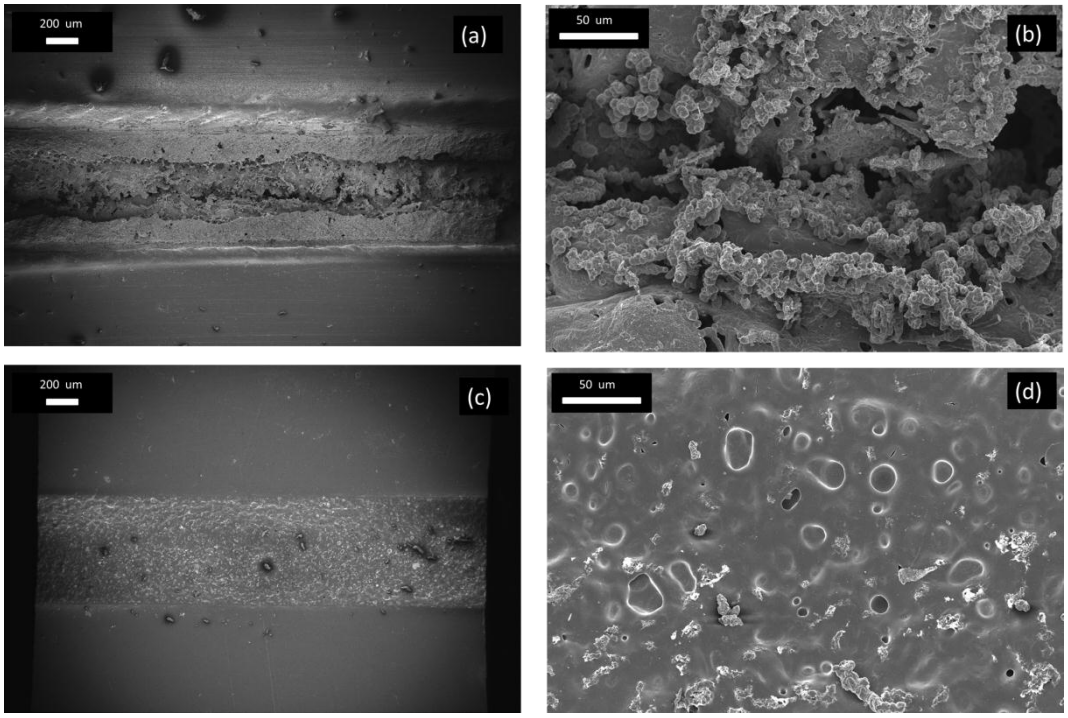

Figure 81 FESEM images of laser track at different magnification (100X and 1KX, scale bar 200 µm and 50 µm respectively): (a) and (b) trial 19; (c) and (d) trial 6.

Tensile tests were carried out with the aim of assessing the effect of the presence of fillers and laser printed conductive tracks on the mechanical behaviour of the functionalized materials. Stress-strain curves related to unfilled matrix and 0.5CNT composite, before and after laser treatment (Trial 19), are reported in **Figure 82**. The presence of MWCNTs induces a slight increase of tensile modulus and of tensile strength. This can be attributed to the reinforcing effect played by MWCNTs within the polymeric matrix. On the other hand, a reduction of the deformation at break was observed due to the reduced mobility of polymers chains caused by carbon based nanoparticles. This is more pronounced in laser treated samples. In fact as shown in figure, after laser treatment the maximum elongation is lower with respect to filled and unfilled PC/ABS. Conductive track probably acts as starting point for crack nucleation. At the same time, the reinforcing effect played by MWCNTs is more pronounced with respect to the untreated materials. This could be explained by the increased concentration of MWCNTs along the tracks entailing a local increase of stiffness and strength.

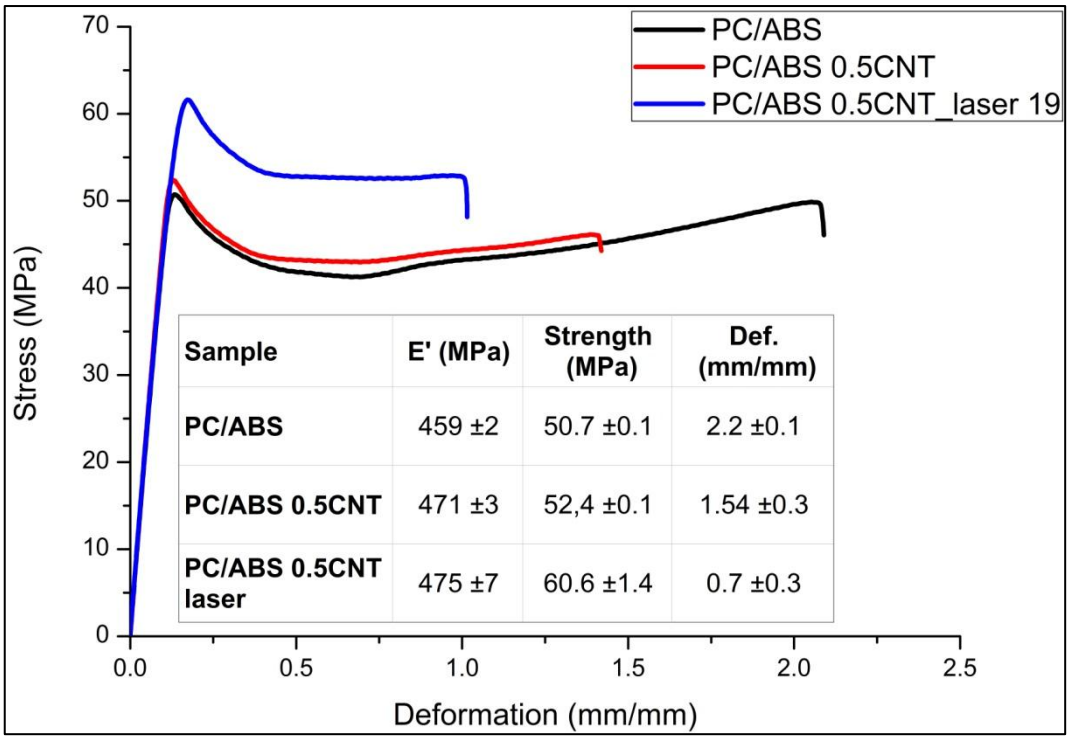

Figure 82 Tensile test curves related to unfilled PC/ABS, untreated 0.5CNTs based PC/ABS and laser treated (trial 19) samples.

Finally thermal analyses were performed in order to complete the characterization of the most promising composite material.

Thermo-gravimetrical analysis (TGA) was performed in argon atmosphere, from 25 to 700 °C, in order to evaluate the thermal stability of PC/ABS filled with 0.5 wt.% of MWCNTs. As reported in **Figure 83** (a) and (b) the addition of MWCNTs leads to a little increase of the temperatures at which 5% and 50 % of weight loss (T5 and T50 respectively) is observed. Neat blend presents a not well defined multi-steps decomposition process. In composite materials, the first degradation peak tends to disappear while the intensity of the second one increases. Moreover, the slightly increase in composite T5 and T50 very likely is due to the high thermal conductivity of CNTs implying better heat dispersion and the barrier effect resulting in a hindered transport of degradation product. [148]

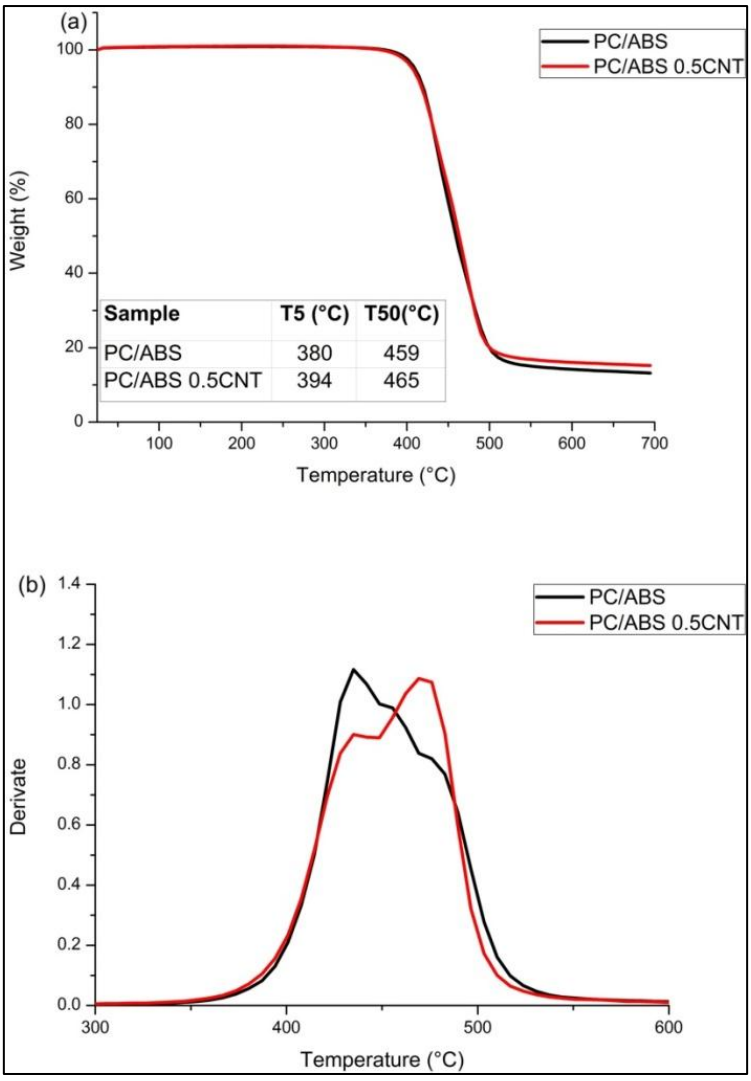

Figure 83 (a) Thermogravimetric curves related to the unfilled and 0.5CNTs sample. (b) DTG curves

Differential scanning calorimetric analyses were performed in the range between 30 to 300 °C in order to detect possible phase transitions. As reported in **Figure 84** PC/ABS blend and its MWCNTs-based nanocomposites, present a completely amorphous structure, at despite of the MWCNTs presence. No melting/crystallization peaks were observed. However, ABS and PC glass transition occurs at 108 and 140 °C respectively.

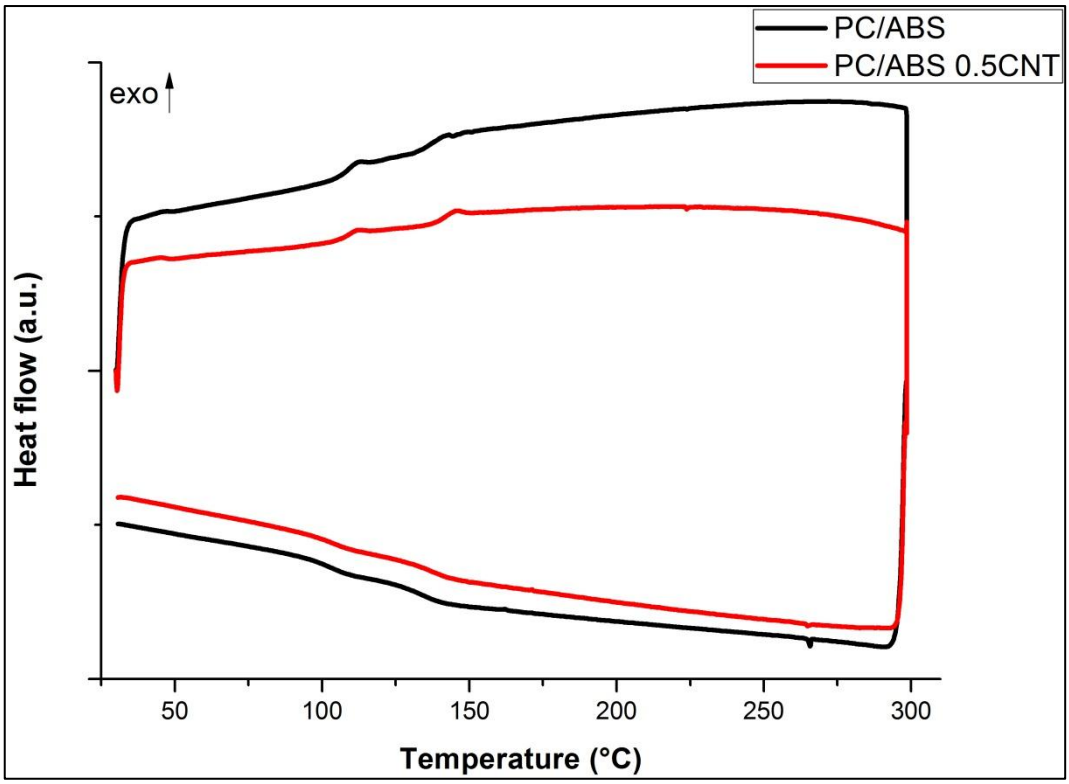

Figure 84 DSC curves related to unfilled and 0.5 filled PC/ABS

5.5 Chapter conclusions

In this work three different MWCNTs based PC/ABS nanocomposites were laser treated with the aim of obtaining metal free conductive tracks. A systematic approach (Design of Experiment) was used in order to analyse the effect of the laser parameters setup on the electrical resistance of the obtained conductive tracks. By analysing the outcomes from a statistical point of view, it was possible to observe that the main laser characteristics that affected the conductivity were the writing speed, the applied power source and their combinations. Defocusing and frequency did not participate in an active way to determine the final properties. A small effect was played by the number of repetitions. In addition DOE approach showed that the laser processing performed by applying the lowest writing speed combined with lowest power source for several times, resulted in the lower electrical resistance value. This is due to a better interaction between laser and nanocomposites giving an electrical resistance per length unit value below 1 kΩ/cm. Starting from these first outcomes, it was possible to further modulate laser parameters obtaining no interactive conductive tracks embedded in

polymer insulators with electrical resistance per unit length value of 21 Ω/cm in composite filled with 0.5 wt.% of MWCNTs. This result shows that composite 0.5CNT is a promising material for the creation of metal free multifunctional and multidirectional printed circuit board.

Conductive tracks morphology was analysed by means of FE-SEM and surface topography analysis revealing a strong dependence between laser setup, tracks morphology and electrical behaviours, as expected.

Tensile tests showed only slight difference between mechanical properties of neat and filled matrix. However, maximum tensile strain value was observed for laser treated materials at despite of a reduction of the elongation at break.

Finally no important differences in thermal behaviour were detected between filled and unfilled polymers.

Chapter 6

Hybrid carbon-based material for electrical and thermal conductivity

6.1 Preface to chapter 6

As reported until now, carbon based nanofillers have been widely investigated to enhance the conductive properties of polymeric composites materials. Since GNPs are recognized to be a new and quite young materials, CNTs are nowadays the most established filler used to enhance both electrical and thermal conductivity.

In Chapter 4, the suitability of GNPs as thermal conductive fillers has been analyzed. Starting from the filler characterization, several polymers were used as matrices. Moreover, different dispersion methods were adopted. By following this scheme, it was possible to claim that the main filler property that we must to be considered to enhance the thermal conductivity of the polymer is the lateral flake dimension. However it was also observed that in several cases, graphite could be used as an alternative to GNPs. At the same time, in most of the cases, no electrical conductivity was observed. Electrical conduction is also an important target for most common polymeric composites, as reported in the previous chapters. No electrical percolation threshold was observed in GNPs-based thermoplastic composite, while by using three roll mill equipment, a changing in the electrical behavior was observed in the epoxy resin filled with 5 wt. % of both the GNPs and graphite. In addition, in Chapter 5 a new methodology for obtaining electrical conductivity in carbon nanotubes based materials was developed. By

using this emerging technology, a localized percolation threshold was observed at 0.5 wt. % of fillers that, for sure, implies no changes in the thermal conductivity. However, polymer systems that possess both thermal and electrical conductivity are widely used in the electronics, automotive, and aerospace industries to dissipate heat and prevent the build-up of static charge. [175]

To enhance both electrical and thermal conductivity, an hybrid system could be used. An hybrid systems is a materials in which "two or more reinforcing and filling materials are placed in a single matrix". This approach leads to a new material that can exhibit new properties that are not necessarily found in the individual components. The main purpose of using hybrid fillers in carbon nanocomposite is to obtain materials with enhanced conductivities without deterioration of mechanical properties or possibly with an ulterior improvement. Moreover, it is possible to design and prepare low-cost and environmental friendly polymer composites. In fact, by using mixed conductive fillers it is possible to partially replace a more expensive and or less environmental friendly filler without worsening the pristine properties. For instance, a significant amount of CNTs, could be replaced by alternative conductive nanoparticles. [176]

In light of this scenario, here we report a study in which the electrical and the thermal conductivity of carbon based hybrid materials were investigated. Moreover, mechanical properties as tensile and flexural strength were studied. The main purpose is to assess the possibility of partially replacing the high amount of MWCNTs used to enhance the conductive and mechanical properties of a commercially available high density polyethylene (HDPE). In fact, high density polyethylene is one of the most commonly used polymers in packaging and functional applications. However, it presents poor mechanical properties coupled with insulating behaviors. [40]

Starting from a commercially available HDPE filled with 6 wt. % of MWCNTs, two hybrid system based on the addition of GNPs or graphite were studied. Starting from our first considerations, GNPs GAbcr_25 platelets 25 µm wide and natural flakes graphite were used as very low cost alternatives to the most expensive fillers. HDPE filled with 12 wt. % of GNPs or graphite was homemade prepared by means of an internal mixer, as reported in the previous cases. After nanocomposites preparations, the hybrid systems were prepared by means of twin screw extruder, used for mixing 2/3 of MWCNTs masterbatch and 1/3 of homemade GNPs or graphite based HDPE. The resulting materials are therefore characterized by the presence of 4 wt. % of MWCNTs (2 wt. % less with respect

to the initial masterbatch) plus 4 wt. % of GNPs or graphite for a total amount of carbon based filler equal to 8 wt. %. This increased amount of fillers was chosen on the basis of preliminary tests. In fact, as reported in chapter 4, no electrical conductivity was observed in all the thermoplastic materials filled with graphite or graphene at 5 wt. %.

In **Figure 85** the flow chart depicting the fabrication process is reported.

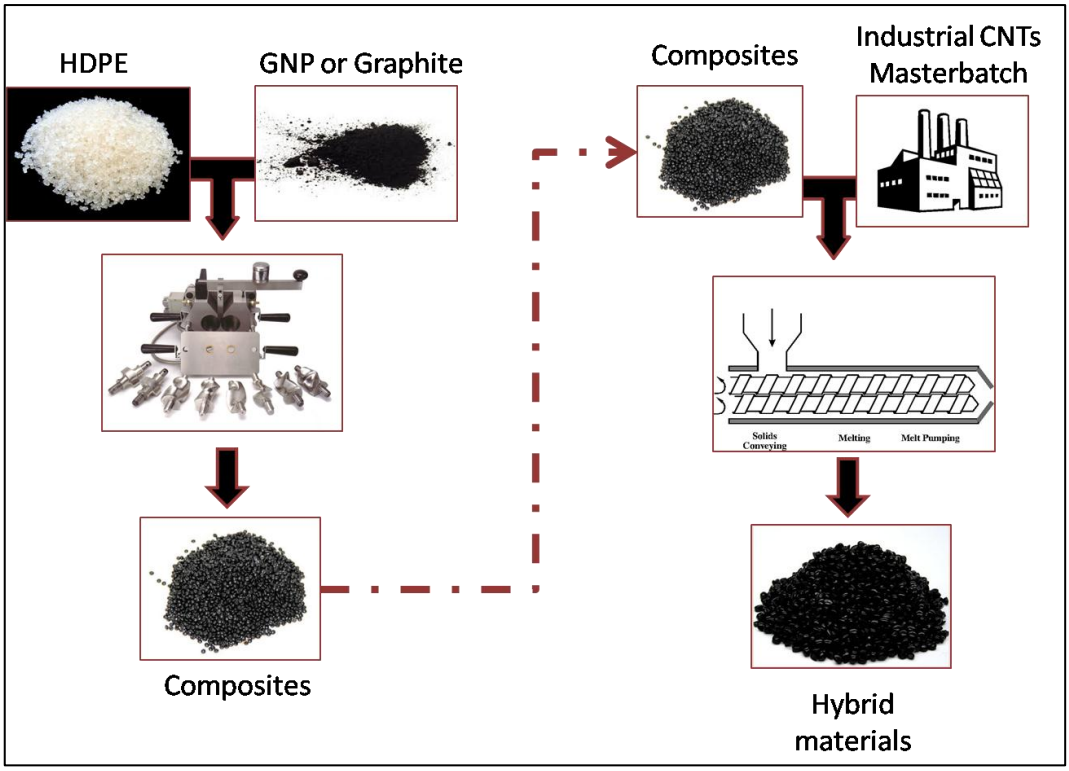

Figure 85 Schematic flow chart for hybrid materials preparation

In the following, first of all the results related to the behavior of the industrial masterbatch will be analyzed in terms of mechanical, thermal and conductivity properties. Finally hybrid materials will be analyzed. The experimental outcomes for the different composites (industrial masterbatch and hybrid composites) will be compared in order to verify the possibility to partially replace carbon nanotubes with cheaper carbon fillers such as graphite.

The samples were labelled according to the following nomenclature:

- “HDPE” is the unfilled matrix

- "Master" is the industrial masterbatch based on HDPE filled with 6 wt.% of MWCNTs
- "Master_Graphene" is the homemade prepared hybrid system based on 4 wt.% of MWCNTs and 4 wt.% of GNPs GAbcr_25
- "Master_Graphite" is the homemade prepared hybrid system based on 4 wt.% of MWCNTs and 4 wt.% of natural flakes graphite.

6.2 Masterbatch characterization

In order to evaluate the possibility to partially replace MWCNTs with cheaper carbon based materials, first of all, a complete characterization of the starting materials is required.

Thermogravimetric analyses, conducted in both inert (Ar) and oxidizing (Air) atmospheres in the temperature range between 25 to 700 °C are reported in **Figure 86**. In the insert table T_5, T_{50} and T_{max} are showed.

As reported in figure 86 (A), degradation of the commercial masterbatch starts at 351 °C in oxidizing atmosphere. Moreover as observable from the blue curve the masterbatch is characterized by a multi-step degradation process. This behavior is not related to the presence of the MWCNTs. In fact, also for the neat HDPE, a multi-step degradation process was observed as reported in the figure 86 (B), in which DTG curve of masterbatch was compared with the DTG curve of neat HDPE. However, the presence of MWCNTs lead to a shift of the degradation at higher temperatures. Maximum degradation temperature occurs at 481 °C. Finally, no residue was observed at 700°C. Regarding thermogravimetric analysis performed in inert atmosphere, it is possible to observe that the degradation starts at 446 °C. Also in this case, neat matrix is characterized by a multi-step degradation process as observable from the DTG curve reported in figure 86 (C). However, the presence of the MWCNTs, modifies the degradation behavior due to the barrier effect played by the nanofillers implying a hindered transport of degradation process from the condensed to the gas phase, as occurred in the previous cases. Maximum degradation temperature occurred ad 478 °C and a residue value of 5.9 wt. % was detected at 700 °C due to the presence of MWCNTs. This value is in good agreement with the expected MWCNTs content of 6 wt. %.

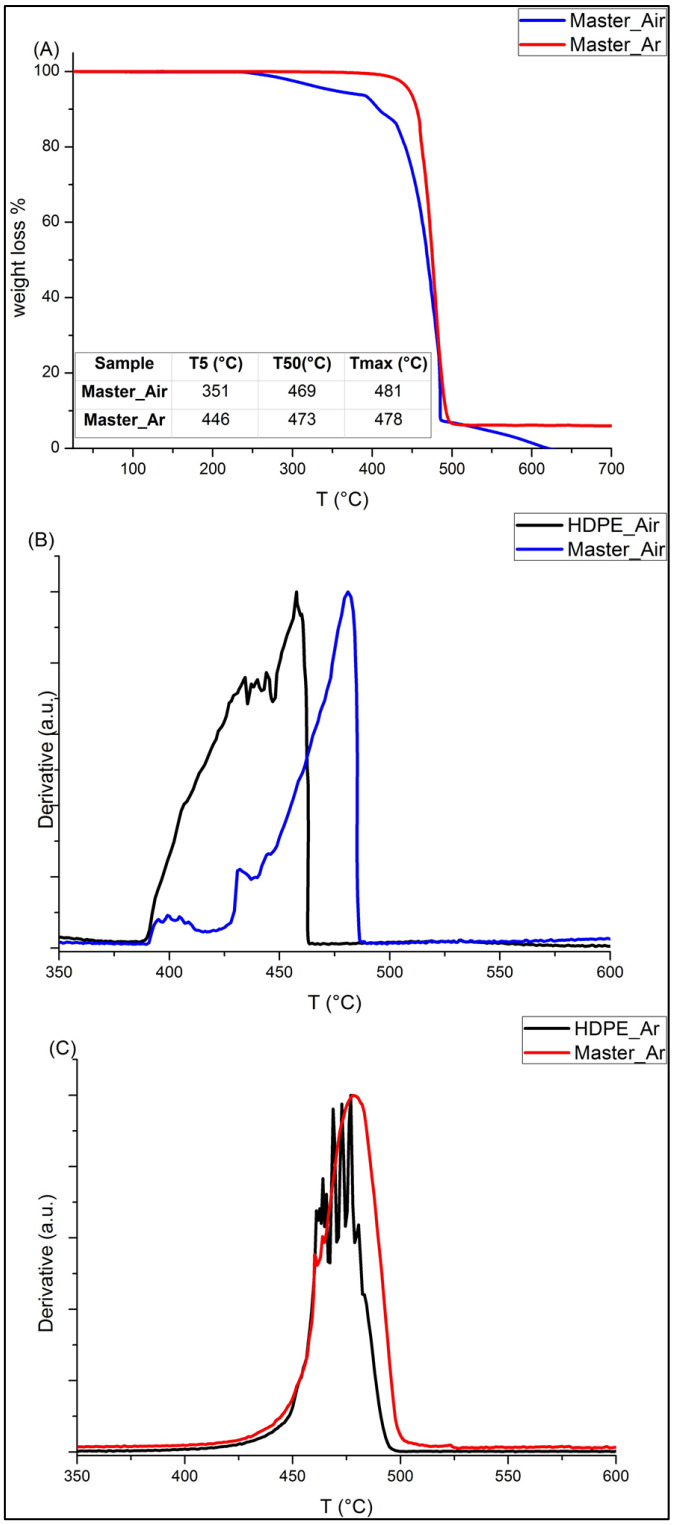

Figure 86 (A) TGA analysis performed in Air and Ar of MWCNTs based masterbatch. (B) DTG curves of masterbatch and neat HDPE in Air and (C) in Ar.

Polyethylene is recognized to be a semi-crystalline polymer. As reported in the introduction part, an ordered structures could provide better properties in terms of thermal and electrical conductivities, and mechanical behavior as well. DSC curve related to the masterbatch as well as to the unfilled HDPE are reported in **Figure 87** (in the temperature range from 25 to 200°C).

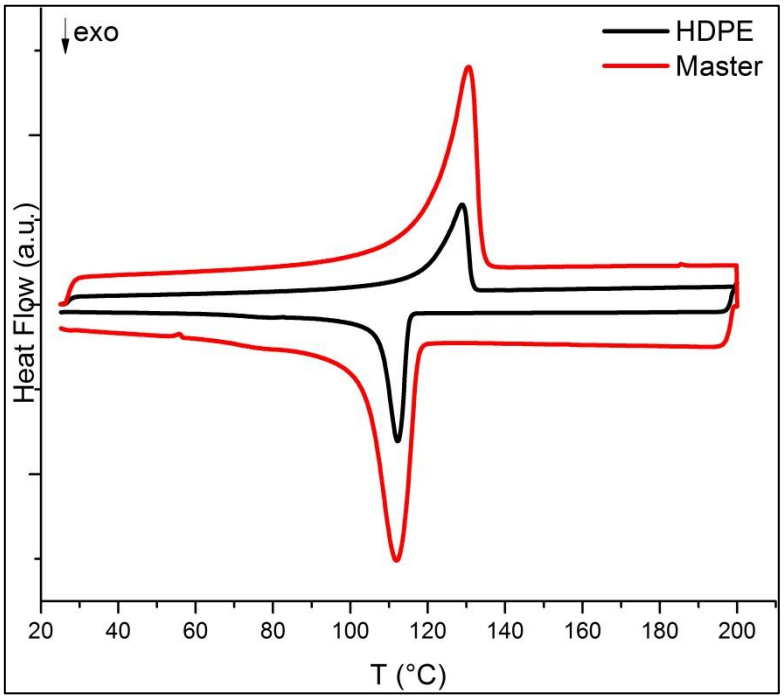

Figure 87 DSC curve of Master and neat HDPE

No differences were observed regarding the melting and the crystallization temperatures of the filled and unfilled HDPE. From the upper part of the DSC curve, it is possible to note that both the materials start to loss their solid form at around 85 °C. As the temperature increases, the rate of heat flow also rises until it reaches the peak point at 130 °C. In the second part of the DSC curve, related to the cooling process, an exothermic peak was observed due to the crystallization process, that occurred for both the materials at 112 °C. Crystallinity level (χ_c)was evaluated from the following equations: [171]

$$\chi_c = \left(\frac{\Delta H_{exp}}{\Delta H}\frac{1}{W_f}\right) * 100 \qquad (17)$$

where ΔH_{exp} is the experimental heat of fusion per gram, determined from DSC curve, while ΔH is the heat of crystallization of fully crystalline HDPE (293 J/g) reported in literature and W_f is the weigh fraction of matrix in the composites. [177] T_m, T_c and crystallinity grade of HDPE and the masterbatch are compared in **Table 18**.

Sample	T_m (°C)	T_c (°C)	χ_c (%)
HDPE	130	112	58.1
Master	130	112	51.0

Table 18 T_m, T_c and crystallinity degree of HDPE and Master

The introduction of 6 wt. % of MWCNTs to the neat matrix leads to a decrease of the crystallinity degree probably due to the steric hindrance providing a low crystalline material.

Since a multifunctional material is characterized by specific conductive properties coupled with good mechanical behaviors, MWCNTs based HDPE was analyzed in terms of tensile and flexural properties. The outcomes are reported in **Table 19**.

	Tensile			Flexural		
Sample	E_t' (GPa)	σ_t (MPa)	Def.$_t$(%)	E_f' (GPa)	σ_f (MPa)	Def.$_f$ (%)
HDPE	0.9*	24*	-	0.92 ±0.03	25 ± 1	7.8 ± 0.1
Master	1.52 ±0.07	38 ± 1	16 ± 0.6	1.06 ±0.01	31 ± 1	7.9 ± 0.2

Table 19 Mechanical properties of neat matrix and of MWCNTs based masterbatch. Markered values were taken from the datasheet.

On the left part of the table the tensile test outcomes are reported. As observable, the industrial masterbatch possesses a Young's modulus of 1.5 GPa associated to a tensile strength of 38 MPa and a deformation at break of 16 %. Moreover, on the right part of the table, flexural modulus, maximum flexural strength and deformation at maximum strength are reported. In this case the flexural modulus

is about 1 GPa, while flexural strength is about 31 MPa, associated to a deformation at maximum strength of about 7.9 %.

Going deeply into the detail of the conductive properties of the starting materials, in **Figure 88** thermal conductivity of the industrial masterbatch in comparison with neat matrix is reported.

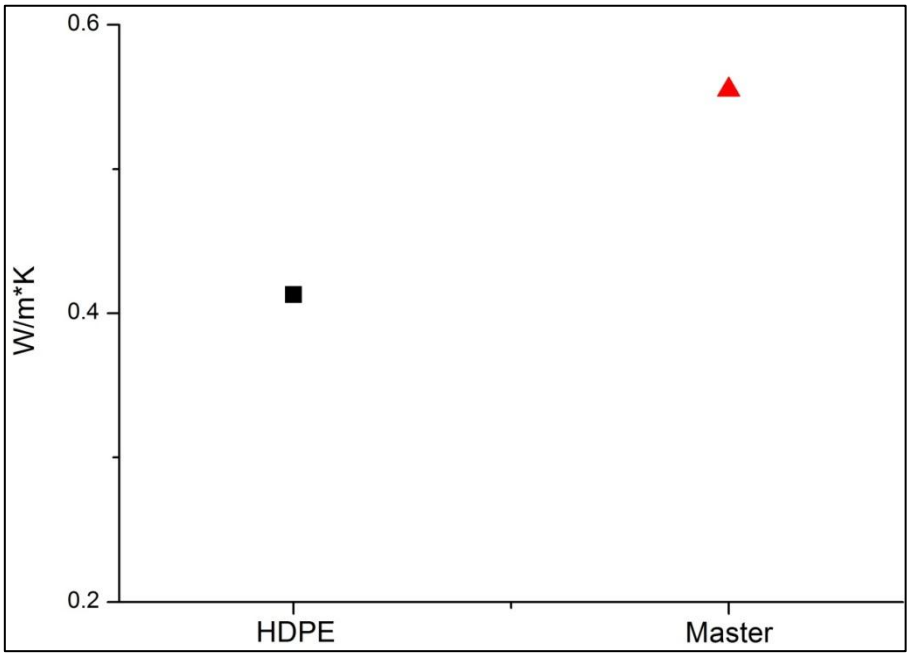

Figure 88 Thermal conductivity of Master and neat HDPE.

Since HDPE is a semi-crystalline polymer, neat matrix show the highest value of thermal conductivity observed with respect to all the other matrices analyzed in this thesis revealing that HDPE is a good candidate to be used as thermally conductive system. However, the observed thermal conductivity value (0.41 W/m*K) is in good agreement with the value reported in literature. [35] The addition of 6 wt. % of MWCNTs leads to the enhancement of the thermal conductivity, that reaches a value of 0.55 W/m*K, 34 % higher with respect to the neat matrix.

Also electrical conductivity was analyzed. Four point electrical conductivity measurement were performed on the filled and unfilled materials. Obviously, no electrical conductivity was observed for the neat HDPE. Moreover, also in the case of the MWCNTs base masterbatch, no electrical conductivity was detected. The obtained materials possess a resistance value over 120 MΩ. This is probably

due to the so called polymer skin effect. In fact, as previously reported, MWCNTs concentration tends to be higher in the inner part of materials due to the filler migration during the injection molded process. On the other hand this drawback can be overtaken by means of laser printing technology, that allows to promote a localized increase of the filler concentrations and that to overcame the percolation threshold. In this way the resulting material is characterized by an electrical resistivity value of 1.2 ± 0.6 kΩ/cm.

At this stage of the characterization it is important to understand if, after partially replacement of MWCNTs with low cost alternative nanofillers, the mechanical properties, as well as the electrical and thermal conductivity can be conserved and/or partially enhanced. Moreover, it is also important to note that not only these properties must be conserved but also the thermal behaviors must be guarantee.

In the next sections, the outcomes coming from the hybrid system characterization will be compared to the starting materials in order to provide a low cost alternative to the analyzed system.

6.3 Hybrid systems characterization

Following the same characterization steps adopted for the masterbatch, in **Figure 89** thermogravimetric analysis in oxidizing (A) and inert (B) atmospheres of both master_graphene and master_graphite hybrid materials are reported. The numerical outcomes (in terms of T_5, T_{50} and T_{max}) are collected in **Table 20** and compared with the masterbatch values. As observable, also in this case, the thermogravimetric curves recorded under oxidizing atmosphere, are characterized by a multi-step degradation process. Initial degradation occurs at 401 and 422 °C for graphene and graphite based hybrid materials respectively. By comparing the obtained outcomes with respect to the result coming from the industrial masterbatch, it is possible to observe an enhancement of the starting degradation temperatures higher than 50 °C for both the hybrid materials. An higher enhancement of T_5 was observed in the case of master_graphite nanocomposites. A lower temperatures enhancement with respect to the masterbatch was observed in the case of both T_{50} and T_{max}. However, the highest enhancement was always observed in the case of the graphite-based hybrid composites. Concerning thermogravimetric analysis performed in inert atmosphere, no particular differences were observed in terms of degradation temperature, while by looking at the DTG curves of hybrid materials, only one well defined degradation peak

was detected. The presence of graphite or graphene nanoplatelets leads to a better thermal stability than that observed in the case of the masterbatch containing MWCNTs only (see **Figure 86** for a comparison).

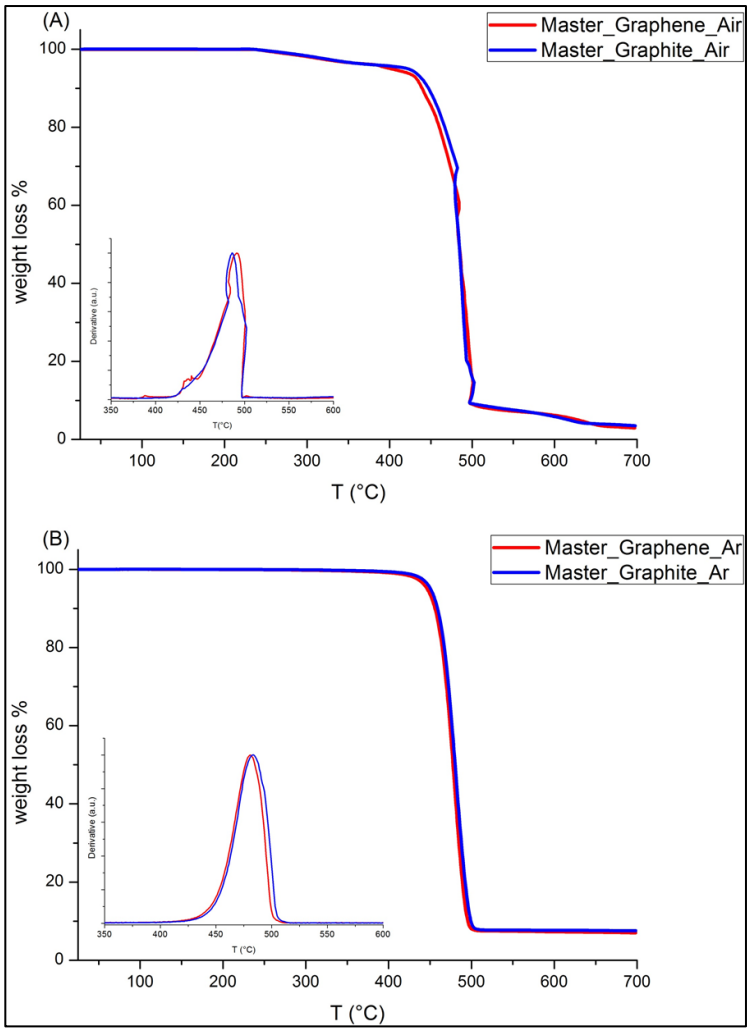

Figure 89 TGA analysis of the hybrid systems in both oxidizing (A) and inert (B) atmosphere

	AIR			ARGON		
Sample	**T_5 (°C)**	**T_{50} (°C)**	**T_{max}(°C)**	**T_5 (°C)**	**T_{50} (°C)**	**T_{max}(°C)**
Master_Graphene	401	484	491	446	477	481
Master_Graphite	422	484	486	450	480	483
Master	351	469	481	446	473	478

Table 20 Degradation temperatures of the starting masterbatch and hybrid composites, in both inert and oxidizing atmospheres.

Differential scanning calorimetric analyses, related to graphene and graphite based hybrid materials are reported in **Figure 90**.

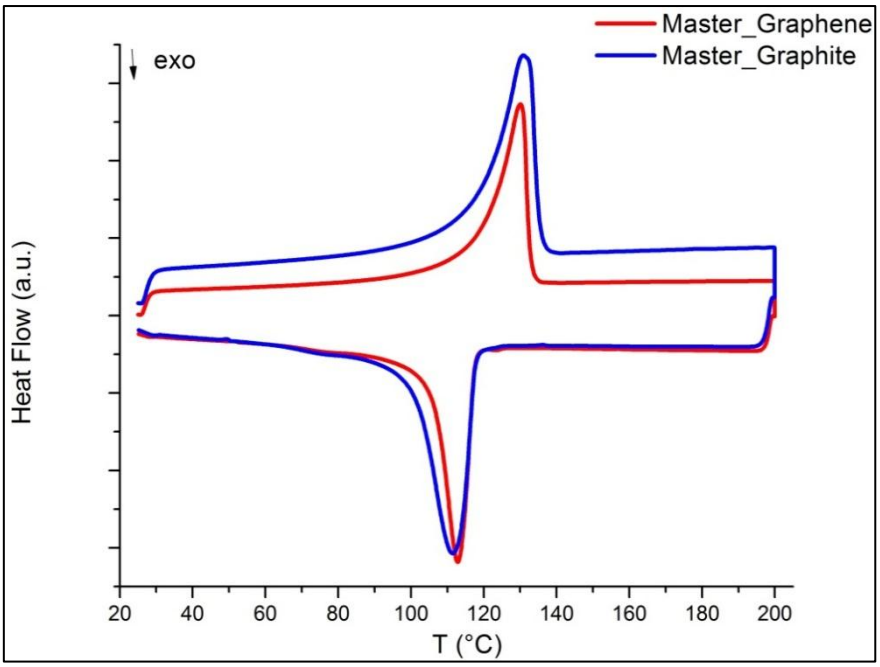

Figure 90 DSC curves reletad to the graphene and graphite based hybrid materials.

Also in the case of these composites DS curve puts in evidence the presence of a partially crystalline matrix. A slight shift at higher T_m and a slight shift at lower temperatures of T_c was observed in the case of graphite-based hybrid system with respect to the graphene-based material. However, by comparing the melting and crystallization temperatures of both the hybrid systems with respect to the MWCNTs based masterbatch, no significant differences were detected. Both T_m and T_c are in good agreement with respect to the starting materials as reported in **Table 21**.

Sample	T_m (°C)	T_c (°C)	χ_c (%)
Master_Graphene	129	113	53.1
Master_Graphite	131	111	53.0
Master	130	112	51.0

Table 21 T_m, T_c and crystallinity degree of the hybrid systems and of masterbatch

As observable, hybrid systems are characterized by a slightly higher level of crystallinity with respect to the starting masterbatch. GNPs and graphite probably favor the nucleation of crystals inside matrix. This enhancement in the crystallinity degree could be exploited in terms of thermal conductivity.

In order to provide the possibility to partially replace some amount of MWCNTs with an alternative and low cost carbon based nanofillers, not only thermal stability should be considered but also mechanical and conductive properties must be guaranteed.

Tensile properties of both the hybrid materials are compared with those of the starting masterbatch in **Figure 91**. As previously reported, the starting masterbatch possess an elastic modulus of 1.5 GPa, associated to a tensile strengh of 38 MPa. By replacing 2 wt. % of MWCNTs, with 4 wt. % of GNPs or natural graphite flakes, a slight enhancement of both Young's modulus and of the tensile strenght was observed, as reported in the **Figure 91** (A) and (B). Moreover, only in the case of the composite containing graphene a slight increase of deformation at break was observed. On the other hand all of the materials showed a comparable elongation at break when consdering the relevant standard deviations (C). The highest improvement of the tensile properties were obtained in the case of graphite-based hybrid material, that for instance shows an increase of the Young's modulus of more than 24 % with respect to the 17 % of the graphene-based materials. The same behavior was observed for the tensile strenght.

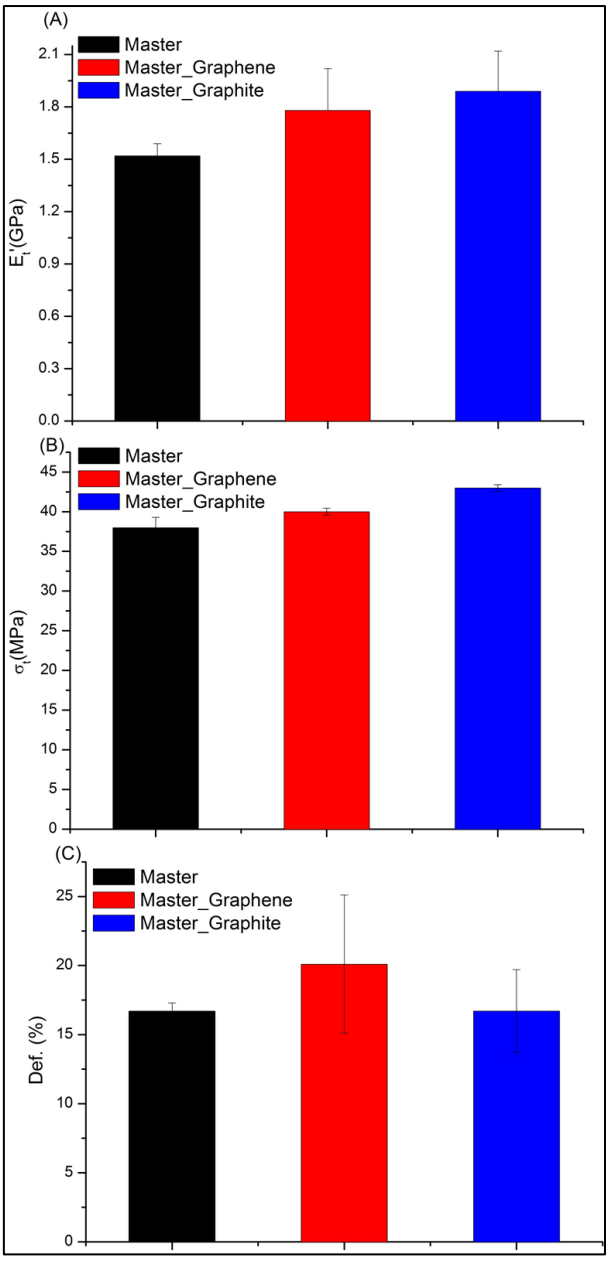

Figure 91 Tensile properties of hybrid materials and of the starting masterbatch

Flexural properties were also tested and the obtained outcomes are reported in **Figure 92**. The partial MWCNTs substitution with other carbon-based fillers, leads to an enhancement of the mechanical properties. However, in this case, the highest increment of the flexural modulus was observed for the graphene-based

hybrid materials with respect to the graphite counterparts (22 and 15 % respectively). This is probably due to the higher plane dimension of the graphene nanoplatelets GAbcr_25. In fact, as previously reported, during the injection molding process, the GNPs tends to align within the molded flux. Therefore, when a force is applied to the perpendicular direction, the wider GNPs planes provide a better response with respect to the graphite. However, no differences were observed regarding deformation at maximum strength.

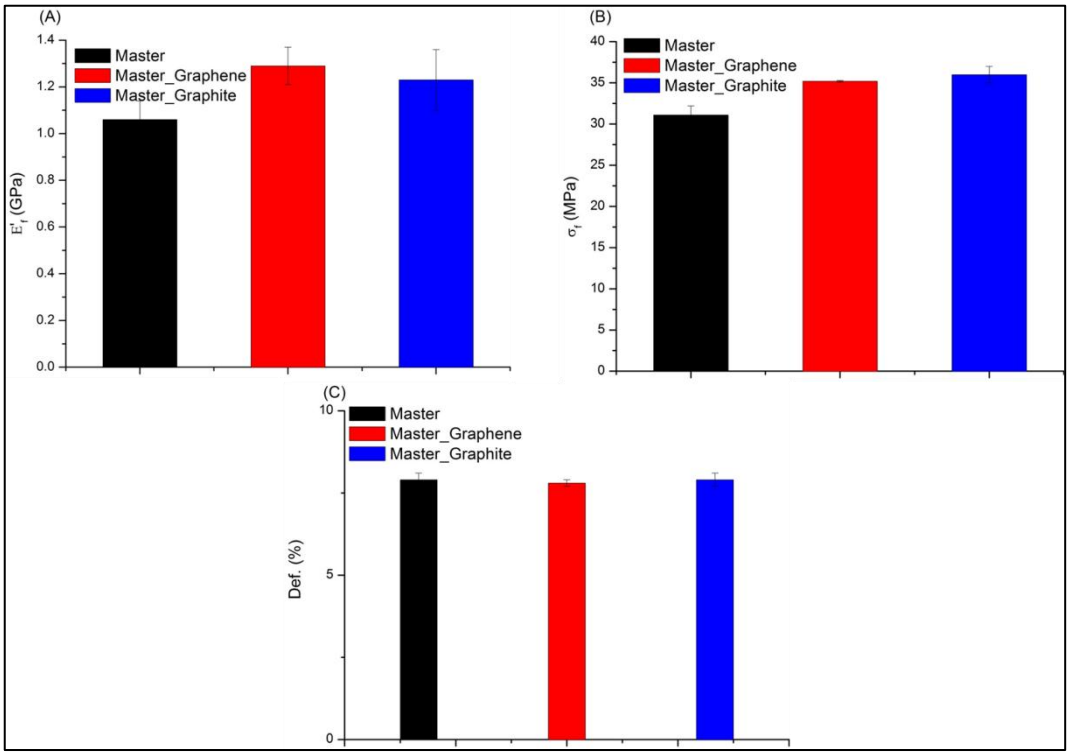

Figure 92 Flexural properties of hybrid materials and of the starting masterbatch

In **Table 22** and **Figure 93** thermal conductivity of hybrid system is reported in comparison with the previously analyzed industrial masterbatch.

Sample	W/m*K ± SD	Δk (%)
Master	0.555 ± 0.01	-
Master_Graphene	0.675 ± 0.05	21.6
Master_Graphite	0.580 ± 0.002	4.5

Table 22 Thermal conductivity and thermal conductivity enhancement whit respect to masterbatch of hybrid systems

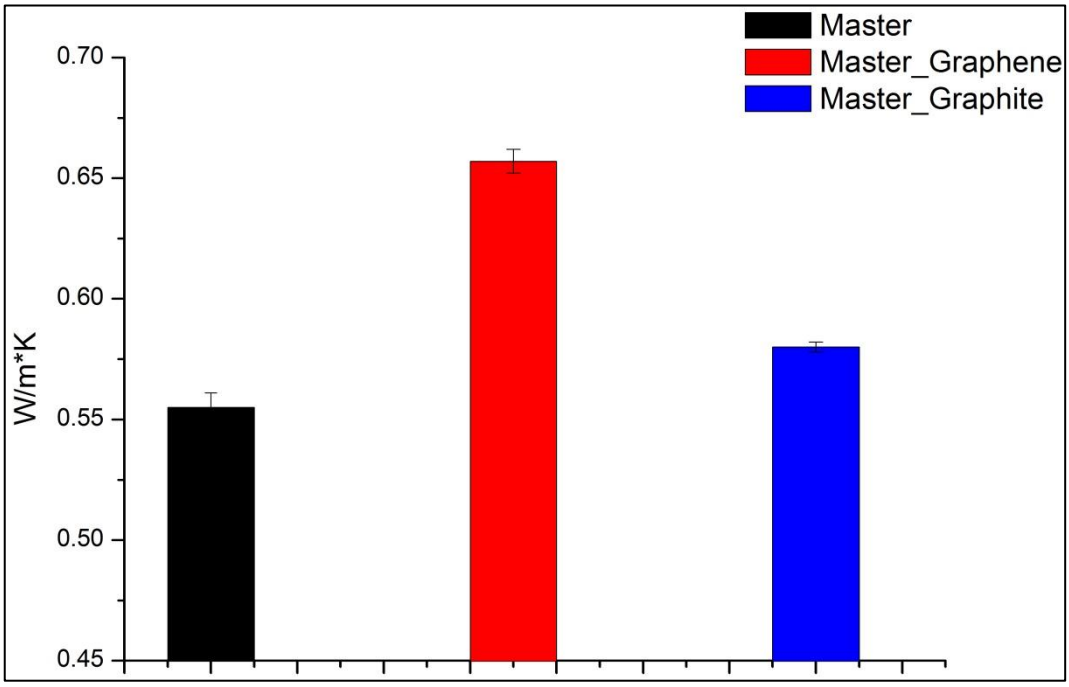

Figure 93 Thermal conductivity of hybrid materials and starting masterbatch

As evident, the partial MWCNTs replacing, coupled with the addiction of the other carbon allotropes forms, leads to an increasing of more than 21 % and of more than 4 % of the thermal conductivity of the graphene-based and graphite-based hybrid materials respectively. For sure, this enhancement is associated to the highest amount of filler contents, however by comparing the hybrid systems it is possible to observe that the highest thermal conductivity was achieved by using graphene nanoplatelets. This is in good agreement with the theoretical prediction. In fact, as observed in the previous cases, due to the lower aspect ratio, which results in the largest interface between matrix and filler because of the higher

thickness, the presence of the graphite flakes provides a lower enhancement of the thermal conductivity with respect to the GNPs-based counterpart. Moreover, the high plane dimension of the GAbcr_25 tends to maximize the thermal conductivity.

Finally electrical conductivity was tested. As for the industrial masterbatch, no electrical conduction was detected on the as-fabricated hybrid systems. However, by using the laser writing treatment, it was possible to locally enhance the electrical conductive properties of the hybrid composites. Electrical resistivity per unit of length values after laser functionalization are reported in **Table 23** and compared with the starting materials.

Sample	R (kΩ/cm)	SD
Master	1.7	± 0.5
Master_Graphene	7.0	± 0.7
Master_Graphite	46.0	± 0.9

Table 23 Electrical surface resistivity per unit of length of hybrid systems in comparison with the starting material

Graphene-based hybrid nanocomposite shows an electrical resistivity per unit of length value three time higher with respect to the starting material. However, the same material, filled with the mixture of MWCNTs and natural graphite flakes, shows a R value that is one order of magnitude higher with respect to the industrial masterbatch. In fact, despite the higher amount of electrical conductive fillers within the polymeric matrix, the lower electrical resistivity per unit of length value was observed in the case of the industrial masterbatch filled with 6 wt.% of MWCNTs. It is clear that a no constructive synergic effect is provided by the combination of the hybrid systems in terms of electrical conductivity. This is probably due to:

- Low intrinsic electrical conductivity value in the case of graphite based materials
- Low aspect ratio of the GNPs with respect to the MWCNTs providing an higher filler-matrix interface.

However, by comparing the starting electrical resistivity of the unfilled matrix (neat HDPE R > 120 MΩ/cm) with respect to the final outcomes, it is possible to

assert that the electrical resistivity per unit of length value of both the hybrid nanocomposites is well improved.

6.4 Chapter conclusion

At the end of this materials characterization it is possible to conclude that the obtained hybrid carbon based nanocomposites are characterized by a comparable conductive properties with respect to the starting MWCNTs-based material. In fact a low reduction in the electrical conductivity was observed for both graphene and graphite based hybrids, but an enhancement in the thermal conductivity was achieved by replacing 2 wt.% of MWCNTs with 4 wt.% of graphene nanoplatelets. Moreover the final hybrid materials are characterized by comparable mechanical properties and thermal stability comparable with the masterbatch. These outcomes demonstrate as it is possible to reduce the amount of the most expensive and environmental unfriendly MWCNTs with low cost and ecofriendly carbon based fillers as GNPs and graphite, without worsening the starting properties.

Chapter 7

Conclusion

In this thesis work, different polymeric composite materials with enhanced conductive properties were developed. Due to their outstanding electrical and thermal conductivity, carbon-based micro- and nano-materials such as carbon nanotubes, graphene nanoplatelets and graphite were chosen as conductive fillers.

Initially (chapter 4) the suitability of graphene nanoplatelets as thermal conductive fillers was investigated. Starting from an accurate fillers characterization, two commercially available graphene nanoplatelets and natural graphite flakes were used as conductive materials. Three thermoplastic polymers were filled with 5 wt. % of the employed carbon-based nanomaterials by means of melt blending technique. Furthermore, in order to analyse the effect of the different dispersion methods and the effect of the different filler loading on the thermal conductivity enhancement, epoxy resin composites were processed by means of four different dispersion techniques at different filler contents. The different matrices were chosen in order to cover a wide range of polymeric materials and with the aim of identifying a guideline in the use of the GNPs as thermal conductive filler. The obtained outcomes reveals a strong correlation between the lateral flake dimensions and the thermal conductivity enhancement. In fact, in spite of the amount of defects and impurities, the highest enhancement was always achieved by using the graphene nanoplatelets that are characterized by the highest plane dimensions. This is due to the lower amount of polymer-filler interfaces resulting in a better phonon propagation. The maximum thermal conductivity was obtained

by filling the epoxy resin by means of three rolls mill equipment, thus reaching a thermal conductivity 6 times higher with respect to the unfilled matrix.

Moving to polymeric composite materials with enhanced electrical conductivity, in chapter 5, a novel approach to obtain electrical conductive tracks on the surface of a PC/ABS matrix filled with multiwall carbon nanotubes is reported. A systematic investigation of the parameters that affect the laser printing process was performed. By analysing the outcomes from a statistical point of view, it was possible to assess that the main laser parameters affecting the conductivity were the applied power source and the laser writing speed. By optimizing these two laser parameters and their combinations it was possible to obtain electrical conductive tracks embedded in polymer insulators with electrical resistance per unit length of 21 Ω/cm. This achievement represent the highest electrical conductivity per unit length at the lowest filler content reported in literature. This result was achieved by laser treating a composite material filled with 0.5 wt.% of MWCNTs. Furthermore, mechanical properties and thermal stability were evaluated highlighting the possibility of using this kind of composites as a multifunctional material.

Finally, in chapter 6, investigation on MWCNTs-GNPs and MWCNTs-Graphite hybrid systems are reported. Starting from an industrial MWCNTs-based HDPE masterbatch, hybrid composites were produced by adding GNPs GAbcr_25 and natural graphite flakes. By comparing the masterbatch behaviour in terms of electrical and thermal conductivity with the hybrid systems, it was assessed that it is possible to partially replace MWCNTs with a low cost carbon-based fillers, without worsening conductive and mechanical properties.

References

[1] M. A. Vadivelu, C. R. Kumar, and G. M. Joshi, "Polymer composites for thermal management : a review," *Compos. Interfaces*, vol. 23, no. 9, pp. 847–872, 2016.

[2] F. A. Bovey and F. H. Winslow, *Macromolecules. An introduction to polymer science*. .

[3] W. D. Callister, *Materials science and engineering : an introduction*, 7th ed. John Wiley & Sons, Inc.

[4] J. R. Fried, *Polymer science & Technology*, 2nd ed. PTR.

[5] M. Ashby, H. Shercliff, and D. Cebon, *Materials Engineering, Science, Processing and Design*, 1st ed. Elsevier, 2007.

[6] K. S. Munir, Y. Li, D. Liang, M. Qian, W. Xu, and C. Wen, "Effect of dispersion method on the deterioration , interfacial interactions and re-agglomeration of carbon nanotubes in titanium metal matrix composites," *JMADE*, vol. 88, pp. 138–148, 2015.

[7] S. S. Samal and S. Bal, "Carbon Nanotube Reinforced Ceramic Matrix Composites- A Review," vol. 7, no. 4, pp. 355–370, 2008.

[8] G. Xingmei, Y. Yongzhen, Z. Xuexia, and L. Xuguang, "Carbon spheres surface modification and dispersion in polymer matrix," *Appl. Surf. Sci.*, vol. 261, pp. 159–165, 2012.

[9] R. F. Gibson, "A review of recent research on mechanics of multifunctional composite materials and structures," *Compos. Struct.*, vol. 92, no. 12, pp. 2793–2810, 2010.

[10] M. H. G. Wichmann, J. Sumfleth, and F. H. Gojny, "Glass-fibre-reinforced composites with enhanced mechanical and electrical properties – Benefits and limitations of a nanoparticle modified matrix," vol. 73, pp. 2346–2359, 2006.

[11] S. Azeem and M. Zain-ul-abdein, "International Journal of Engineering Science Investigation of thermal conductivity enhancement in bakelite – graphite particulate filled polymeric composite," *Int. J. Eng. Sci.*, vol. 52,

pp. 30–40, 2012.

[12] J. Zhang, G. Li, and Q. Wu, “RSC Advances retardants and nanoclay on fl ame performance of,” pp. 24895–24902, 2017.

[13] S. Singaravelu, D. C. Mayo, H. M. Park, K. E. Schriver, and R. F. Haglund, “Anti-reflective polymer-nanocomposite coatings fabricated by RIR-MAPLE,” vol. 8607, pp. 1–6, 2013.

[14] Y. Chen *et al.*, “Li + ‑ Conductive Polymer-Embedded Nano-Si Particles as Anode Material for Advanced Li-ion Batteries,” pp. 3508–3512, 2014.

[15] D. F. Mohshim, H. Mukhtar, and Z. Man, “Composite blending of ionic liquid – poly (ether sulfone) polymeric membranes : Green materials with potential for carbon dioxide / methane separation,” vol. 43999, pp. 1–8, 2016.

[16] S. Haider, A. Kausar, and B. Muhammad, “Overview on Polystyrene / Nanoclay Composite : Physical Properties and Application,” *Polym. Plast. Technol. Eng.*, vol. 56, no. 9, pp. 917–931, 2017.

[17] S. Ramakrishna, J. Mayer, E. Wintermantel, and K. W. Leong, “Biomedical applications of polymer-composite materials : a review,” vol. 61, 2001.

[18] L. Bokobza, “Multiwall carbon nanotube-filled natural rubber : Electrical and mechanical properties,” vol. 6, no. 3, pp. 213–223, 2012.

[19] D. Bloor, K. Donnelly, P. J. Hands, P. Laughlin, and D. Lussey, “A metal–polymer composite with unusual properties,” vol. 38, pp. 2851–2860, 2005.

[20] K. Mallick, M. J. Witcomb, and M. S. Scurrell, “In situ synthesis of copper nanoparticles and poly (o -toluidine): A metal – polymer composite material,” vol. 42, pp. 670–675, 2006.

[21] K. Zdiri, A. Elamri, and M. Hamdaoui, “Advances in Thermal and Mechanical Behaviors of PP / Clay Nanocomposites,” *Polym. Plast. Technol. Eng.*, vol. 56, no. 8, pp. 824–840, 2017.

[22] V. P. Singh, K. K. Vimal, S. Sharma, G. S. Kapur, and V. Choudhary, “Polyethylene / sepiolite clay nanocomposites : Effect of clay content , compatibilizer polarity , and molar mass on viscoelastic and dynamic mechanical properties,” vol. 134, p. 45197, 2017.

[23] R. Sengupta, A. Bandyopadhyay, S. Sabharwal, T. K. Chaki, and Anil K.

Bhowmicka, “Polyamide-6 , 6 / in situ silica hybrid nanocomposites by sol – gel technique : synthesis , characterization and properties,” vol. 46, pp. 3343–3354, 2005.

[24] A. Agrawal and A. Satapathy, “Experimental investigation of micro-sized aluminium oxide reinforced epoxy composites for microelectronic applications,” vol. 5, pp. 517–526, 2014.

[25] Y. Xu, D. D. L. Chung, and C. Mroz, “Thermally conducting aluminum nitride polymer-matrix composites,” vol. 32, 2001.

[26] Q. Nadeem, M. Rizwan, R. Gill, M. Rafique, and M. Shahid, “Fabrication of alumina based electrically conductive polymer composites,” vol. 133, p. 42939, 2016.

[27] E. C. Botelho, M. C. Rezende, and B. Lauke, “Mechanical behavior of carbon fiber reinforced polyamide composites,” vol. 63, pp. 1843–1855, 2003.

[28] J. P. Donoso *et al.*, “Electric and magnetic properties of polymer electrolyte / carbon black composites,” vol. 115, pp. 149–160, 1998.

[29] G. Chen, D. Wu, W. Weng, and W. Yan, “Preparation of Polymer / Graphite Conducting Nanocomposite by Intercalation Polymerization,” no. December 2000, pp. 2506–2513, 2001.

[30] V. D. Punetha *et al.*, “Functionalization of carbon nanomaterials for advanced polymer nanocomposites : A comparison study between CNT and graphene,” *Prog. Polym. Sci.*, vol. 67, pp. 1–47, 2017.

[31] W. Cai, Y. Huang, D. Wang, C. Liu, and Y. Zhang, “Piezoresistive Behavior of Graphene Nanoplatelets / Carbon Black / Silicone Rubber Nanocomposite,” pp. 1–6, 2013.

[32] D. M. Bigg, “Thermal conductivity of heterophase polymer compositions.” Advanced in polymer science. vol 119, 1995.

[33] A. A. Balandin, “Thermal properties of graphene and nanostructured carbon materials,” *Nat. Mater.*, vol. 10, no. 8, pp. 569–581, 2011.

[34] J. Callaway, “Model for lattice thermal conductivity at low temperatures,” *Phisical Rev.*, vol. 113, no. 4, pp. 1046–1051, 1959.

[35] Z. Han and A. Fina, “Thermal conductivity of carbon nanotubes and their polymer nanocomposites : A review,” *Prog. Polym. Sci.*, vol. 36, no. 7, pp.

914–944, 2011.

[36] A. Henry and G. Chen, “High Thermal Conductivity of Single Polyethylene Chains Using Molecular Dynamics Simulations,” vol. 235502, no. December, pp. 1–4, 2008.

[37] T. Luo *et al.*, “Molecular dynamics simulation of thermal energy transport in polydimethylsiloxane Molecular dynamics simulation of thermal energy transport in polydimethylsiloxane (PDMS),” vol. 74321, no. 2011, 2017.

[38] H. Chen *et al.*, “Thermal conductivity of polymer-based composites : Fundamentals and applications,” *Prog. Polym. Sci.*, vol. 59, pp. 41–85, 2016.

[39] T. Zhang, X. Wu, and T. Luo, “Polymer nanofibers with outstanding thermal conductivity and thermal stability : fundamental linkage between molecular characteristics and macroscopic thermal properties,” *ournal Phys. Chem. C*, vol. 118, pp. 21148–21159, 2014.

[40] J. Yu, B. Sundqvist, B. Tonpheng, and O. Andersson, “Thermal conductivity of highly crystallized polyethylene,” *Polymer (Guildf).*, vol. 55, no. 1, pp. 195–200, 2014.

[41] C. L. Choy, W. H. Luk, and F. C. Chen, “Thermal conductivity of highly oriented polyethylene,” vol. 19, no. September 1977, pp. 155–162, 1978.

[42] M. Harada *et al.*, “Thermal-Conductivity Properties of Liquid-Crystalline Epoxy Resin Cured under a Magnetic Field,” *J. Polym. Sci. Part B Polym. Phys.*, vol. 41, pp. 1739–1743, 2003.

[43] R. Balint, N. J. Cassidy, and S. H. Cartmell, “Conductive polymers : Towards a smart biomaterial for tissue engineering,” *Acta Biomater.*, vol. 10, no. 6, pp. 2341–2353, 2014.

[44] J. a. King, K. W. Tucker, B. D. Vogt, E. H. Weber, and C. Quan, “Electrically and thermally conductive nylon 6,6,” *Polym. Compos.*, vol. 20, no. 5, pp. 643–654, 1999.

[45] X. Chen, Y. Su, D. Reay, and S. Riffat, “Recent research developments in polymer heat exchangers – A review,” *Renew. Sustain. Energy Rev.*, vol. 60, pp. 1367–1386, 2016.

[46] Y. Pan, G. J. Weng, S. A. Meguid, W. S. Bao, Z. Zhu, and A. M. S. Hamouda, “Percolation threshold and electrical conductivity of a two-phase composite containing randomly oriented ellipsoidal inclusions,” *J. Appl.*

Phys., vol. 110, pp. 123715–123719, 2011.

[47] B. Wessling, "Electrical conductivity in heterogeneous polymer systems . V (1): Further experimental evidence for a phase transition at the critical volume concentration.," *Polym. Eng. Sci.*, vol. 31, no. 10, pp. 1200–1206, 1991.

[48] G. Grimmett, *Percolation*, Second edi. Berlin: Springer, 1991.

[49] E. Tuncer, V. Serdyuk, and M. Gubanski, "Dielectric Mixtures: Electrical Properties and Modeling," *IEEE Trans. Dielectr. Electical Insul.*, vol. 9, no. 5, 2002.

[50] J. Aneli, G. Zaikov, and O. Mukbaniani, "Physical principles of the conductivity of electrical conducting polymer composites (review)," *Chem. Chem. Technol.*, vol. 5, no. 1, pp. 75–87, 2011.

[51] N. Hu, H. Fukunaga, S. Atobe, Y. Liu, and J. Li, "Piezoresistive Strain Sensors Made from Carbon Nanotubes," *Sensors*, vol. 11, pp. 10691–10723, 2011.

[52] H. W. Kroto, J. R. Heath, S. C. O'Brien, R. F. Curl, and R. . Smalley, "C60: Buckminsterfullerene," *Nature*, vol. 318, pp. 162–163, 1985.

[53] E. T. Thostenson, Z. Ren, and T. Chou, "Advances in the science and technology of carbon nanotubes and their composites : a review," vol. 61, pp. 1899–1912, 2001.

[54] S. Iijima, "Helical microtubules of graphitic carbon," *Lett. to Nat.*, vol. 354, pp. 56–58, 1991.

[55] O. A. Shenderova, V. V. Zhirnov, and D. W. Brenner, "Carbon Nanostructures," *Crit. Rev. Solid State Mater. Sci.*, vol. 27, no. 3–4, pp. 227–356, 2002.

[56] K. S. Novoselov *et al.*, "Electric field effect in atomically thin carbon films," *Science (80-.).*, vol. 306, no. 5696, pp. 666–669, 2004.

[57] V. Singh, D. Joung, L. Zhai, S. Das, S. I. Khondaker, and S. Seal, "Graphene based materials: Past, present and future," *Prog. Mater. Sci.*, vol. 56, no. 8, pp. 1178–1271, 2011.

[58] P. C. Ma, N. A. Siddiqui, G. Marom, and J. K. Kim, "Dispersion and functionalization of carbon nanotubes for polymer-based nanocomposites: A review," *Compos. Part A Appl. Sci. Manuf.*, vol. 41, no. 10, pp. 1345–

1367, 2010.

[59] E. T. Thostenson, Z. Ren, and T. Chou, “Advances in the science and technology of carbon nanotubes and their composites : a review,” *Compos. Sci. Technol.*, vol. 61, pp. 1899–1912, 2001.

[60] T. W. Odom, J.-L. Huang, P. Kim, and C. M. Lieber, “Atomic structure and electronic properties of single-walled carbon nanotubes,” *Nature*, vol. 391, no. 6662, pp. 62–64, 1998.

[61] B. I. Yakobson, C. J. Brabec, and J. Bernholc, “Nanomechanics of carbon tubes: Instabilities beyond linear response,” *Phys. Rev. Lett.*, vol. 76, no. 14, pp. 2511–2514, 1996.

[62] B. I. Yakobson, G. Samsonidze, and G. G. Samsonidze, “Atomistic theory of mechanical relaxation in fullerene nanotubes,” *Carbon N. Y.*, vol. 38, no. 11, pp. 1675–1680, 2000.

[63] N. Saifuddin, A. Z. Raziah, and A. R. Junizah, “Carbon nanotubes: A review on structure and their interaction with proteins,” *J. Chem.*, vol. 2013, pp. 1–18, 2013.

[64] C. Journet, W. K. Maser, P. Bernier, and a Loiseau, “Large-scale production of single-walled carbon nanotubes by the electric-arc technique,” *Nature*, vol. 388, no. August, pp. 20–22, 1997.

[65] A. G. Rinzler *et al.*, “Large-scale purification of single-wall carbon nanotubes: process, product, and characterization,” *Appl. Phys. A Mater. Sci. Process.*, vol. 67, no. 1, pp. 29–37, 1998.

[66] P. Nikolaev *et al.*, “Gas-phase catalytic growth of single-walled carbon nanotubes from carbon monoxide,” *Chem. Phys. Lett.*, vol. 313, no. 1–2, pp. 91–97, 1999.

[67] Z. F. Ren *et al.*, “Growth of a single freestanding multiwall carbon nanotube on each nanonickel dot,” *Appl. Phys. Lett.*, vol. 75, no. 8, pp. 1086–1088, 1999.

[68] Z. P. Huang, J. W. Xu, Z. F. Ren, J. H. Wang, M. P. Siegal, and P. N. Provencio, “Growth of highly oriented carbon nanotubes by plasma-enhanced hot filament chemical vapor deposition,” *Appl. Phys. Lett.*, vol. 73, no. 26, pp. 3845–3847, 1998.

[69] Z. F. Ren, “Synthesis of Large Arrays of Well-Aligned Carbon Nanotubes on Glass,” *Science (80-.).*, vol. 282, no. 5391, pp. 1105–1107, 1998.

[70] D. S. Bethune *et al.*, "Cobalt-catalysed growth of carbon nanotubes with single-atomic-layer walls," *Nature*, vol. 363, no. 6430, pp. 605–607, 1993.

[71] Y. Saito, K. Nishikubo, K. Kawabata, and T. Matsumoto, "Carbon nanocapsules and single-layered nanotubes produced with platinum-group metals (Ru, Rh, Pd, Os, Ir, Pt) by arc discharge," *J. Appl. Phys.*, vol. 80, no. 5, p. 3062, 1996.

[72] G. Mittal, V. Dhand, K. Y. Rhee, S.-J. Park, and W. R. Lee, "A review on carbon nanotubes and graphene as fillers in reinforced polymer nanocomposites," *J. Ind. Eng. Chem.*, vol. 21, pp. 11–25, 2015.

[73] J. Kong, A. M. Cassell, and H. Dai, "Chemical vapor deposition of methane for single-walled carbon nanotubes," *Chem. Phys. Lett.*, vol. 292, no. 4–6, pp. 567–574, 1998.

[74] Z. F. Ren, "Synthesis of Large Arrays of Well-Aligned Carbon Nanotubes on Glass," *Science (80-.).*, vol. 282, no. 5391, pp. 1105–1107, 1998.

[75] C. Bower, W. Zhu, S. Jin, and O. Zhou, "Plasma-induced alignment of carbon nanotubes," *Appl. Phys. Lett.*, vol. 77, no. 6, pp. 830–832, 2000.

[76] J.-P. Salvetat, J.-M. Bonard, and N. H. Thomson, "Mechanical properties of carbon nanotubes," *Appl. Phys. A*, vol. 69, no. 3, pp. 255–260, 1999.

[77] G. Overney, W. Zhong, and D. Tomanek, "Structural Rigidity and Low-Frequency Vibrational-Modes of Long Carbon Tubules," *Zeitschrift Fur Phys. D-Atoms Mol. Clust.*, vol. 27, no. 1, pp. 93–96, 1993.

[78] J. N. Coleman, U. Khan, W. J. Blau, and Y. K. Gun'ko, "Small but strong: A review of the mechanical properties of carbon nanotube-polymer composites," *Carbon N. Y.*, vol. 44, no. 9, pp. 1624–1652, 2006.

[79] R. S. Ruoff and D. C. Lorents, "Mechanical and thermal properties of carbon nanotubes," *Carbon N. Y.*, vol. 33, no. 7, pp. 925–930, 1995.

[80] S. Govindjee and J. L. Sackman, "On the use of continuum mechanics to estimate the properties of nanotubes," *Solid State Commun.*, vol. 110, no. 4, pp. 227–230, 1999.

[81] L. Vaccarini, C. Goze, L. Henrard, E. Hernández, P. Bernier, and A. Rubio, "Mechanical and electronic properties of carbon and boron-nitride nanotubes," *Carbon N. Y.*, vol. 38, no. 11, pp. 1681–1690, 2000.

[82] E. W. Wong, "Nanobeam Mechanics: Elasticity, Strength, and Toughness

of Nanorods and Nanotubes," *Science (80-.).*, vol. 277, no. 5334, pp. 1971–1975, 1997.

[83] M. Yu, "Strength and Breaking Mechanism of Multiwalled Carbon Nanotubes Under Tensile Load," *Science (80-.).*, vol. 287, no. 5453, pp. 637–640, 2000.

[84] M.-F. Yu, B. S. Files, S. Arepalli, and R. S. Ruoff, "Tensile Loading of Ropes of Single Wall Carbon Nanotubes and their Mechanical Properties," *Phys. Rev. Lett.*, vol. 84, no. 24, pp. 5552–5555, 2000.

[85] J. W. Mintmire, B. I. Dunlap, and C. T. White, "Are fullerene tubules metallic?," *Phys. Rev. Lett.*, vol. 68, no. 5, pp. 631–634, 1992.

[86] N. Hamada, S. I. Sawada, and A. Oshiyama, "New one-dimensional conductors: Graphitic microtubules," *Phys. Rev. Lett.*, vol. 68, no. 10, pp. 1579–1581, 1992.

[87] T. W. Ebbesen, "Carbon Nanotubes," *Annu. Rev. Mater. Sci.*, vol. 24, no. 1, pp. 235–64, 1994.

[88] T. T. Ebbesen, T. W., Lezec H. J., Hiura H., Bennett J. W., Ghaemi H. F, "Electrical conductivity of individual carbon nanotubes," *Nature*, vol. 382. pp. 54–56, 1996.

[89] P. R. Bandaru, "Electrical Properties and Applications of Carbon Nanotube Structures," *J. Nanosci. Nanotechnol.*, vol. 7, no. 4, pp. 1239–1267, 2007.

[90] J. Maultzsch, S. Reich, C. Thomsen, E. Dobardžić, I. Milošević, and M. Damnjanović, "Phonon dispersion of carbon nanotubes," *Solid State Commun.*, vol. 121, no. 9–10, pp. 471–474, 2002.

[91] S. Berber, Y.-K. Kwon, and D. Tomanek, "Unusually high thermal conductivity of carbon nanotubes," *Phys. Rev. Lett.*, vol. 84, no. 20, pp. 4613–4616, 2000.

[92] S. Berber, Y.-K. Kwon, and D. Tomanek, "Unusually high thermal conductivity of carbon nanotubes," *Phys. Rev. Lett.*, vol. 84, no. 20, pp. 4613–4616, 2000.

[93] J. Hone, M. Whitney, C. Piskoti, and A. Zettl, "Thermal conductivity of single-walled carbon nanotubes," *Phys. Rev. B*, vol. 59, no. 4, pp. R2514–R2516, 1999.

[94] P. Kim, L. Shi, A. Majumdar, and P. L. McEuen, "Thermal transport

measurements of individual multiwalled nanotubes," pp. 19–22, 2001.

[95] P. Kim, L. Shi, A. Majumdar, and P. L. McEuen, "Thermal transport measurements of individual multiwalled nanotubes," pp. 19–22, 2001.

[96] C. Yu, L. Shi, Z. Yao, D. Li, and A. Majumdar, "Thermal conductance and thermopower of an individual single-wall carbon nanotube," *Nano Lett.*, vol. 5, no. 9, pp. 1842–1846, 2005.

[97] A. K. Geim and K. S. Novoselov, "The rise of graphene," *Nat. Mater.*, vol. 6, no. 3, pp. 183–191, 2007.

[98] K. S. Novoselov *et al.*, "Electric Field Effect in Atomically Thin Carbon Films," vol. 306, no. October, pp. 666–670, 2004.

[99] A. K. Geim, A. H. Macdonald, A. K. Geim, and A. H. Macdonald, "Graphene : Exploring carbon flatland," vol. 60, no. 8, 2007.

[100] L. M. Malard, M. A. Pimenta, G. Dresselhaus, and M. S. Dresselhaus, "Raman spectroscopy in graphene," *Phys. Rep.*, vol. 473, no. 5–6, pp. 51–87, 2009.

[101] A. Bianco *et al.*, "All in the graphene family - A recommended nomenclature for two-dimensional carbon materials," *Carbon N. Y.*, vol. 65, pp. 1–6, 2013.

[102] P. Wick *et al.*, "Classification framework for graphene-based materials," *Angew. Chemie - Int. Ed.*, vol. 53, no. 30, pp. 7714–7718, 2014.

[103] M. S. A. Bhuyan, M. N. Uddin, M. M. Islam, F. A. Bipasha, and S. S. Hossain, "Synthesis of graphene," *Int. Nano Lett.*, vol. 6, no. 2, pp. 65–83, 2016.

[104] Z. U. Khan, A. Kausar, H. Ullah, A. Badshah, and W. U. Khan, "A review of graphene oxide, graphene buckypaper, and polymer/graphene composites: Properties and fabrication techniques," *J. Plast. Film Sheeting*, vol. 32, no. 4, pp. 336–379, 2016.

[105] Y. Yang *et al.*, "Graphene-based materials with tailored nanostructures for energy conversion and storage," *Mater. Sci. Eng. R Reports*, vol. 102, pp. 1–72, 2016.

[106] S. Park *et al.*, "Aqueous Suspension and Characterization of Chemically Modified Graphene Sheets," *Chem. Mater.*, vol. 20, no. 21, pp. 6592–6594, 2008.

[107] W.-W. Liu, S.-P. Chai, A. R. Mohamed, and U. Hashim, "Synthesis and characterization of graphene and carbon nanotubes: A review on the past and recent developments," *J. Ind. Eng. Chem.*, vol. 20, no. 4, pp. 1171–1185, 2014.

[108] S. J. Chae *et al.*, "Synthesis of large-area graphene layers on poly-nickel substrate by chemical vapor deposition: Wrinkle formation," *Adv. Mater.*, vol. 21, no. 22, pp. 2328–2333, 2009.

[109] X. Li *et al.*, "Large-Area Synthesis of High-Quality and Uniform Graphene Films on Copper Foils," *Science (80-.).*, vol. 324, no. 5932, pp. 1312–1314, 2009.

[110] S. Bhaviripudi, X. Jia, M. S. Dresselhaus, and J. Kong, "Role of kinetic factors in chemical vapor deposition synthesis of uniform large area graphene using copper catalyst," *Nano Lett.*, vol. 10, no. 10, pp. 4128–4133, 2010.

[111] H. Cao *et al.*, "Large-scale graphitic thin films synthesized on Ni and transferred to insulators: Structural and electronic properties," *J. Appl. Phys.*, vol. 107, no. 4, 2010.

[112] J. Du and H. M. Cheng, "The Fabrication, Properties, and Uses of Graphene/Polymer Composites," *Macromol. Chem. Phys.*, vol. 213, pp. 1060–1077, 2012.

[113] I. Ovid'ko, "Mechanical Properties of Graphene," *Rev. Adv. Mater. Sci.*, vol. 34, pp. 1–11, 2013.

[114] C. Lee, X. Wei, J. W. Kysar, and J. Hone, "Measurement of the elastic properties and intrinsic strength of Monolayer Graphene," *Science (80-.).*, vol. 321, no. July, pp. 385–388, 2008.

[115] F. Liu, P. Ming, and J. Li, "Ab initio calculation of ideal strength and phonon instability of graphene under tension," *Phys. Rev. B - Condens. Matter Mater. Phys.*, vol. 76, no. 6, pp. 1–7, 2007.

[116] C. Lee, X. Wei, Q. Li, R. Carpick, J. W. Kysar, and J. Hone, "Elastic and frictional properties of graphene," *Phys. Status Solidi*, vol. 246, no. 11–12, pp. 2562–2567, 2009.

[117] J. C. Meyer, C. Kisielowski, R. Erin, M. D. Rossell, and M. F. Crommie, "Direct Imaging of Lattice Atoms and Topological Defects in Graphene Membranes," *Nano Lett.*, vol. 8, no. 11, pp. 3582–3586, 2008.

[118] J. H. Warner, E. R. Margine, M. Mukai, A. W. Robertson, F. Giustino, and A. I. Kirkland, "Dislocation-Driven Deformations in Graphene," *Science (80-.).*, vol. 337, no. 6091, pp. 209–212, 2012.

[119] P. Y. Huang *et al.*, "Grains and grain boundaries in single-layer graphene atomic patchwork quilts," *Nature*, vol. 469, no. 7330, pp. 389–392, 2011.

[120] K. Kim, Z. Lee, W. Regan, C. Kisielowski, M. F. Crommie, and A. Zettl, "Grain boundary mapping in polycrystalline graphene," *ACS Nano*, vol. 5, no. 3, pp. 2142–2146, 2011.

[121] A. H. C. Neto, F. Guinea, N. M. R. Peres, K. S. Novoselov, and A. K. Geim, "The electronic properties of graphene," vol. 81, no. March, 2007.

[122] B. Partoens and F. M. Peeters, "From graphene to graphite: Electronic structure around the K point.," *Phys. Rev. B*, vol. 74, no. August, pp. 1–11, 2006.

[123] A. C. Ferrari *et al.*, "Raman spectrum of graphene and graphene layers," *Phys. Rev. Lett.*, vol. 97, no. 18, pp. 1–4, 2006.

[124] M. Sendova, E. Flahaut, and T. Hartsfield, "Temperature dependence of Raman scattering in filled double-walled carbon nanotubes," *J. Appl. Phys.*, vol. 108, no. 4, 2010.

[125] A. Bassil, P. Puech, L. Tubery, W. Bacsa, and E. Flahaut, "Controlled laser heating of carbon nanotubes," *Appl. Phys. Lett.*, vol. 88, no. 17, 2006.

[126] I. Calizo, A. A. Balandin, W. Bao, F. Miao, and C. N. Lau, "Temperature dependence of the raman spectra of graphene and graphene multilayers," *Nano Lett.*, vol. 7, no. 9, pp. 2645–2649, 2007.

[127] A. A. Balandin *et al.*, "Superior Thermal Conductivity of Single-Layer Graphene: geim," *Nano Lett.*, vol. 8, no. 3, pp. 902–907, 2008.

[128] C. T'Joen, Y. Park, Q. Wang, A. Sommers, X. Han, and A. Jacobi, "A review on polymer heat exchangers for HVAC&R applications," *Int. J. Refrig.*, vol. 32, no. 5, pp. 763–779, 2009.

[129] H. S. Tekce, D. Kumlutas, and I. H. Tavman, "Effect of Particle Shape on Thermal Conductivity of Copper Reinforced Polymer Composites," *J. Reinf. Plast. Compos.*, vol. 26, no. 1, pp. 113–121, 2007.

[130] S. Kemaloglu, G. Ozkoc, and A. Aytac, "Properties of thermally conductive micro and nano size boron nitride reinforced silicon rubber

composites," *Thermochim. Acta*, vol. 499, no. 1–2, pp. 40–47, 2010.

[131] P. S. Goh, A. F. Ismail, and B. C. Ng, "Directional alignment of carbon nanotubes in polymer matrices : Contemporary approaches and future advances," *Compos. Part A*, vol. 56, pp. 103–126, 2014.

[132] J. H. Du, J. Bai, and H. M. Cheng, "The present status and key problems of carbon nanotube based polymer composites," *Express Polym. Lett.*, vol. 1, no. 5, pp. 253–273, 2007.

[133] M. Rahmat and P. Hubert, "Carbon nanotube-polymer interactions in nanocomposites: A review," *Compos. Sci. Technol.*, vol. 72, no. 1, pp. 72–84, 2011.

[134] K. S. Ibrahim, "Carbon nanotubes-properties and applications: a review," *Carbon Lett.*, vol. 14, no. 3, pp. 131–144, 2013.

[135] M. O. Khan, S. N. Leung, E. Chan, H. E. Naguib, F. Dawson, and V. Adinkrah, "Effects of Microsized and Nanosized Carbon Fillers on the Thermal and Electrical Properties of Polyphenylene Sulfide Based Composites," *Polym. Eng. Sci.*, no. 53, pp. 2398–2406, 2013.

[136] J. A. King *et al.*, "Characterization of exfoliated graphite nanoplatelets/polycarbonate composites: electrical and thermal conductivity, and tensile, flexural, and rheological properties," *J. Compos. Mater.*, vol. 46, no. 9, pp. 1029–1039, 2011.

[137] K. Kalaitzidou, H. Fukushima, and L. T. Drzal, "A new compounding method for exfoliated graphite-polypropylene nanocomposites with enhanced flexural properties and lower percolation threshold," *Compos. Sci. Technol.*, vol. 38, no. 7, pp. 2045–2051, 2007.

[138] K. Kalaitzidou, H. Fukushima, and L. T. Drzal, "Multifunctional polypropylene composites produced by incorporation of exfoliated graphite nanoplatelets," *Carbon N. Y.*, vol. 45, no. 7, pp. 1446–1452, 2007.

[139] S. Chandrasekaran, C. Seidel, and K. Schulte, "Preparation and characterization of graphite nano-platelet (GNP)/epoxy nano-composite: Mechanical, electrical and thermal properties," *Eur. Polym. J.*, vol. 49, no. 12, pp. 3878–3888, 2013.

[140] B. Ahmadi-Moghadam, M. Sharafimasooleh, S. Shadlou, and F. Taheri, "Effect of functionalization of graphene nanoplatelets on the mechanical response of graphene/epoxy composites," *Mater. Des.*, vol. 66, no. PA, pp. 142–149, 2015.

[141] S. Ganguli, A. K. Roy, and D. P. Anderson, "Improved thermal conductivity for chemically functionalized exfoliated graphite/epoxy composites," *Carbon N. Y.*, vol. 46, no. 5, pp. 806–817, 2008.

[142] C. C. Teng *et al.*, "Thermal conductivity and structure of non-covalent functionalized graphene/epoxy composites," *Carbon N. Y.*, vol. 49, no. 15, pp. 5107–5116, 2011.

[143] F. Conrado and M. Pavese, "A Continuous 3D-Graphene Network to Overcome Threshold Issues and Contact Resistance in Thermally Conductive Graphene Nanocomposites," *J. Nanomater.*, vol. 2017, 2017.

[144] G. Colucci, O. Ostrovskaya, A. Frache, B. Martorana, and C. Badini, "The effect of mechanical recycling on the microstructure and properties of PA66 composites reinforced with carbon fibers," *J. Appl. Polym. Sci.*, vol. 132, no. 29, pp. 1–9, 2015.

[145] L. Vovchenko *et al.*, "Mechanical and electrical properties of the epoxy composites with graphite nanoplatelets and carbon nanotubes," *Phys. Status Solidi*, vol. 211, no. 2, pp. 336–341, 2014.

[146] A. Di Gianni, G. Colucci, A. Priola, L. Conzatti, M. Alessi, and P. Stagnaro, "Exfoliated/intercalated rubber/organo-montmorillonite nanocomposites: Preparation and characterization," *Macromol. Mater. Eng.*, vol. 294, no. 10, pp. 705–710, 2009.

[147] B. B. Marosfoi, A. Szabó, G. Marosi, D. Tabuani, G. Camino, and S. Pagliari, "Thermal and spectroscopic characterization of polypropylene-carbon nanotube composites," *J. Therm. Anal. Calorim.*, vol. 86, no. 3, pp. 669–673, 2006.

[148] S. Bocchini, A. Frache, G. Camino, and M. Claes, "Polyethylene thermal oxidative stabilisation in carbon nanotubes based nanocomposites," *Eur. Polym. J.*, vol. 43, no. 8, pp. 3222–3235, 2007.

[149] M. Herrera, G. Matuschek, and A. Kettrup, "Thermal degradation of thermoplastic polyurethane elastomers (TPU) based on MDI," *Polym. Degrad. Stab.*, vol. 78, no. 2, pp. 323–331, 2002.

[150] S. Ghosh *et al.*, "Extremely high thermal conductivity of graphene: Prospects for thermal management applications in nanoelectronic circuits," *Appl. Phys. Lett.*, vol. 92, no. 15, pp. 1–4, 2008.

[151] A. A. Balandin, D. L. Nika, S. Ghosh, and E. P. Pokatilov, "Lattice thermal conductivity of graphene flakes: Comparison with bulk graphite," *Appl.*

Phys. Lett., vol. 94, no. 20, pp. 1–4, 2009.

[152] M. A. Raza, A. V. K. Westwood, A. P. Brown, and C. Stirling, "Texture, transport and mechanical properties of graphite nanoplatelet/silicone composites produced by three roll mill," *Compos. Sci. Technol.*, vol. 72, no. 3, pp. 467–475, 2012.

[153] K. Salonitis, J. Pandremenos, J. Paralikas, and G. Chryssolouris, "Multifunctional materials: Engineering applications and processing challenges," *Int. J. Adv. Manuf. Technol.*, vol. 49, no. 5–8, pp. 803–826, 2010.

[154] P. M. Ajayan, O. Stephan, C. Colliex, and D. Trauth, "Aligned carbon nanotube arrays formed by cutting a polymer resin--nanotube composite.," *Science (80-.).*, vol. 265, no. 5176, pp. 1212–1214, 1994.

[155] W. Bauhofer and J. Z. Kovacs, "A review and analysis of electrical percolation in carbon nanotube polymer composites," *Compos. Sci. Technol.*, vol. 69, no. 10, pp. 1486–1498, 2009.

[156] K. Sidler *et al.*, "Resistivity measurements of gold wires fabricated by stencil lithography on flexible polymer substrates," *Adv. Mater.*, vol. 85, no. 8–9, pp. 343–345, 2008.

[157] T. H. J. Van Osch, J. Perelaer, A. W. M. De Laat, and U. S. Schubert, "Inkjet printing of narrow conductive tracks on untreated polymeric substrates," *Adv. Mater.*, vol. 20, no. 2, pp. 343–345, 2008.

[158] K. Kordás *et al.*, "Inkjet printing of electrically conductive patterns of carbon nanotubes," *Small*, vol. 2, no. 8–9, pp. 1021–1025, 2006.

[159] M. Gonzalez, F. Axisa, M. Vanden Bulcke, D. Brosteaux, B. Vandevelde, and J. Vanfleteren, "Design of metal interconnects for stretchable electronic circuits," *Microelectron. Reliab.*, vol. 48, no. 6, pp. 825–832, 2008.

[160] A. Islam, H. N. Hansen, P. T. Tang, and J. Sun, "Process chains for the manufacturing of molded interconnect devices," *Int. J. Adv. Manuf. Technol.*, vol. 42, no. 9–10, pp. 831–841, 2009.

[161] D. Benz, T. Botzelmann, H. K??ck, and D. Warkentin, "On low cost inclination sensors made from selectively metallized polymer," *Sensors Actuators, A Phys.*, vol. 123–124, pp. 18–22, 2005.

[162] P. Putsch, "WO 2010/015420 A1, PCT/EP2009/005757."

[163] P. Putsch, "POLYMER MOLDED BODIES AND PRINTED CIRCUIT BOARD ARRANGEMENT AND METHOD FOR THE PRODUCTION THEREOF. US Patent, 2011/0134617 A1," 2011.

[164] F. Cesano *et al.*, "Structure and properties of metal-free conductive tracks on polyethylene/multiwalled carbon nanotube composites as obtained by laser stimulated percolation," *Carbon N. Y.*, vol. 61, pp. 63–71, 2013.

[165] M. Liebscher *et al.*, "Achieving electrical conductive tracks by laser treatment of non-conductive polypropylene/polycarbonate blends filled with MWCNTs," *Macromol. Mater. Eng.*, vol. 299, no. 7, pp. 869–877, 2014.

[166] G. Colucci *et al.*, "A novel approach to obtain conductive tracks on PP/MWCNT nanocomposites by laser printing," *RSC Adv.*, vol. 6, no. 34, pp. 28522–28531, 2016.

[167] A. Zecchina *et al.*, "Process for producing conductive and/or piezoresistive tracks on a polymeric substrate. EP 2 448 383 B1," no. May, 2011.

[168] L. B. Barrentine, *An Introduction to Design of Experiment*. 1999.

[169] K. Nishino, Y. Shindo, T. Takayama, and H. Ito, "Improvement of impact strength and hydrolytic stability of PC/ABS blend using reactive polymer," *J. Appl. Polym. Sci.*, vol. 134, no. 9, pp. 1–6, 2017.

[170] A. Rostami, M. Masoomi, M. J. Fayazi, and M. Vahdati, "Role of multiwalled carbon nanotubes (MWCNTs) on rheological, thermal and electrical properties of PC/ABS blend," *RSC Adv.*, vol. 5, no. 41, pp. 32880–32890, 2015.

[171] J. Antony, *Design of experiments for engineers and scientists*. Elsevier Science, 2014.

[172] Z. Spitalsky, D. Tasis, K. Papagelis, and C. Galiotis, "Carbon nanotube-polymer composites: Chemistry, processing, mechanical and electrical properties," *Prog. Polym. Sci.*, vol. 35, no. 3, pp. 357–401, 2010.

[173] I. B. Sohn, Y. C. Noh, S. C. Choi, D. K. Ko, J. Lee, and Y. J. Choi, "Femtosecond laser ablation of polypropylene for breathable film," *Appl. Surf. Sci.*, vol. 254, no. 16, pp. 4919–4924, 2008.

[174] S. I. Anisimov, N. M. Bityurin, and B. S. Luk, "Models for laser ablation," *Photo-Excited Process. Diagnostics Appl.*, pp. 121–159, 2003.

[175] A. Moisala, Q. Li, I. A. Kinloch, and A. H. Windle, “Thermal and electrical conductivity of single- and multi-walled carbon nanotube-epoxy composites,” *Compos. Sci. Technol.*, vol. 66, no. 10, pp. 1285–1288, 2006.

[176] U. Szeluga, B. Kumanek, and B. Trzebicka, “Composites : Part A Synergy in hybrid polymer / nanocarbon composites . A review,” *Compos. PART A*, vol. 73, pp. 204–231, 2015.

[177] Y. Lei, Q. Wu, F. Yao, and Y. Xu, “Preparation and properties of recycled HDPE/natural fiber composites,” *compoiste Compos. Part A Appl. Sci. Manuf.*, vol. 38, no. 7, pp. 1664–1674, 2007.